CHARACTERIZATION OF THE CASZ1-DEPENDENT MECHANISMS ESSENTIAL FOR CARDIOMYOCYTE DEVELOPMENT

Kerry M. Dorr

A dissertation submitted to the faculty of the University of North Carolina at Chapel Hill in partial fulfillment of the requirements for the degree of Doctor of Philosophy in Genetics and Molecular Biology in the School of Medicine.

Chapel Hill
2015

Approved by:

Frank Conlon

Terry Magnuson

Li Qian

Joan Taylor

Andy Wessels

ABSTRACT

Kerry M. Dorr: Characterization of the Casz1-Dependent Mechanisms Essential for Cardiomyocyte Development
(Under the direction of Frank L. Conlon)

The heart is one of the first structures to form during development and is required for embryonic growth and survival. The four-chambered mammalian heart arises from a series of complex processes during embryonic development that includes the specification and differentiation of the different cardiac cell types within the heart, proliferation, and morphological movements of the early heart fields. Early development of the heart is governed by hyperplastic growth in which cardiac cells undergo mitogen-dependent activation during the G_1-phase of the cell cycle. Though numerous growth factor signals have been shown to be required for cardiomyocyte proliferation, genetic studies have only identified a limited number of transcription factors that act to regulate the entry of cardiomyocytes into S-phase. Casz1 is an evolutionarily conserved transcription factor that is essential for heart development; however, there are vast deficiencies in our understanding of the mechanism by which Casz1 regulates aspects of cardiac development.

Here we report that Casz1 is expressed in, and gives rise to, cardiomyocytes in the first and second heart fields. We show through the generation of a cardiac conditional null mutation that Casz1 is required for the proper development and growth

of the cardiac chambers. We further demonstrate that Casz1 is essential for the proliferation of cardiomyocytes in both heart fields and that loss of Casz1 leads to severe cardiac hypoplasia, ventricular septal defects, and a decrease in cardiomyocyte cell number. Additionally, we report that the loss of Casz1 leads to a prolonged or arrested S-phase, a decrease in DNA synthesis, an increase in phosphorylated-Rb, and a concomitant decrease in the cardiac mitotic index. Taken together these studies establish a role for Casz1 in mammalian heart development and cardiomyocyte cell cycle progression.

To my wonderful boys, I couldn’t have done it without you. Thank you for illuminating my life.

ACKNOWLEDGEMENTS

There are many people that have been critical to the success of my graduate studies. I would first like to thank current and past members of the Conlon Lab for helpful discussions, advice, support, and technical know-how: Kathleen Christine, Chris Showell, Panna Tandon, Erin Kaltenbrun, Lauren Kuchenbrod, Lauren Waldron, Nirav Amin, Stephen Sojka, Kerry Dorr, Marta Charpentier, Chris Slagle, Michelle Villasmil, Leslie Kennedy, and Carrie Wilczewski. Special thanks to Chris Showell for being an excellent mentor and friend my first few years in the lab, and to Erin Kaltenbrun for being my lab BFF. This experience would not have been the same without her sarcastic and charming wit.

I cannot thank or acknowledge Frank Conlon enough. He has been so supportive of my career and of me as a person. Frank has a remarkable ability to build me up when I am down and push me when I need it. He has been enthusiastic throughout this very difficult and time-consuming project, always available when I needed to bounce ideas around, and has allowed me an enormous amount of independence. This mentoring has helped me to grow as a scientist and a professional and for that I am forever grateful. It is also a joy to work for someone that truly cares about the people in his lab, not only from a scientific perspective, but also on a personal level. For this reason, the morale in the Conlon Lab is extremely high and there is a lot of camaraderie, qualities that have made coming to work a pleasure even when science wasn't going so well.

I would also like to thank my committee members Terry Magnuson, Li Qian, Joan Taylor, and Andy Wessels. I am so grateful for the mentorship and support that I have received from each of them. One of the things that drew me to UNC was the faculty commitment to good training, and my committee has demonstrated this commitment throughout my graduate experience. I am extremely appreciative for their insights and helpful discussions on my work.

Finally, I would like to thank my family and friends for their support, encouragement, and friendship. My parents have given me their unwavering support and have always made me feel loved and appreciated. My father is an amazing, well-accomplished scientist and I think it was all of those Saturdays I spent with him at work playing with Eppendorf tubes that made me gain a passion for science. I would especially like to thank my wonderful husband, Mark, whose companionship, wisdom, patience, tolerance, and love have uplifted me every day that we have been together. We rode the bus together our very first day of graduate school and have been inseparable ever since. I also thank our wonderful baby, Maxwell, who has uplifted my life to heights I never thought I would attain and is truly the best developmental biology experiment I ever undertook. Thanks also to our other baby boy, “soon to be named”. I can’t wait to meet you.

TABLE OF CONTENTS

LIST OF FIGURES

LIST OF TABLES

LIST OF ABBREVIATIONS

ACTC	Cardiac Actin
AD	Activation Domain
α/β-MHC	Alpha/Beta-Myosin Heavy Chain
AMPK	AMP-activated protein kinase
APC	Adenomatosis Polyposis Coli
AS	Atrial Septum
ASD	Atrial Septal Defects
Avi	Biotin acceptor peptide
AVSD	Atrioventricular Septal Defects
BAC	Bacterial Artificial Chromosome
bHLH	Basic Helix Loop Helix
BIO	6-bromoindirubin-3′-oxime
BMP	Bone Morphogenetic Protein
BrdU	5’-bromo-2’-deoxyuridine
CAC	Common Atrial Chamber
CC	Cardiac Crescent
CDKs	Cyclin-dependent kinases
CHD	Congenital Heart Disease
ChIP	chromatin immunoprecipitation
CL	Compact Layer
cTNT	Cardiac troponin T
CVC	common ventricular chamber

DAPI	4',6-diamidino-2-phenylindole
DE	Differential Expression
E	Embryonic day or Eye
EC	Endothelial Cells
ECM	Extracellular Matrix
EdU	5-ethynyl-2'deoxyuridine
EGFL7	Epidermal Growth Factor-Like Domain 7
EGFP	Enhanced green fluorescent protein
EN	Endocardium or Endothelial Cells
ESC	Embryonic Stem Cell
EPI	Epicardium
ERK	Extracellular-signal-related kinase
EXE	Extra-embryonic tissue
FACS	Fluorescence activated cell sorting
FG	Foregut
FGF	Fibroblast growth factor
FGFR	Fibroblast growth factor receptor tyrosine kinase
FHF	First heart field
FILA	FilaminA
GSK3	Serine-threonine kinase glycogen synthase kinase 3
GMT	GATA4, MEF2C and TBX5
GO	Gene Ontology
GRB2	Growth factor receptor-bound protein 2

HB	Hindbrain
HCM	Hypertrophic Cardiomyopathy
HDAC	Histone Deacetylase
HOS	Holt-Oram Syndrome
HEK	Human Embryonic Kidney
HT	Heart Tube
HUVECs	Human umbilical vein endothelial cells
IGF	Insulin-like growth factor
iPSCs	induced pluri-potent stem cells
IVS	Interventricular Septum or of intersomitic vessels
JNK	c-Jun N-terminal kinase
LA	Left atria
LB	Limb Bud
LH	Looped Heart
LSC	Laser scanning cytometry
LV	Left ventricle
LEF	Lymphoid Enhancer Binding Factor
miRNA	MicroRNA
MI	Myocardial infarction
MIMS	Multi-isotope Imaging Mass Spectrometry
MTA	Metastasis-associated Protein
MBD3	Methyl-CpG Binding Domain Protein 3
MO	Morpholino

MEF2	Myocyte Enhancer Factor 2
MOI	multiplicity of infection
MP	Myocardial Progenitor Cells
MS	Mass Spectrometry
MV	Mitral valve
MY	Myocardium
MYBPC3	Cardiac myosin-binding protein C
MYH7	Cardiac β-myosin heavy chain
MYL2	Regulatory myosin light chain
MYL3	Essential myosin light chain
N	Neural Tube
^{15}N	Stable Isotope of Nitrogen
NB	Neuroblastoma
NID	NURD interacting domain
NLS	Nuclear Localization Signal
NP	Nasal Placode
NRG1	Neuregulin1
NT	Neural Tube
NuRD	Nucleosome Remodeling and Deacetylase
OFT	Outflow Tract
P	Postnatal day
PBS	Phosphate Buffered Saline
PCV	Posterior Cardinal Vein

PECAM	Platelet endothelial cell adhesion molecule
PFA	Paraformaldehyde
pHH3	phosphorylated Histone H3
PME	Pharyngeal Mesoderm
PML	Promyelocytic Leukemia
R	Restriction Point
RA	Right atria
RAF	Rapidly accelerated fibrosarcoma kinase
RAS	Rat sarcoma kinase
RASIP1	Ras interacting protein 1
RB	Retinoblastoma protein
RLM-RACE	RNA ligase-mediated rapid amplification of cDNA ends
ROCK	Rho kinase
RTKs	Trans-membrane receptor tyrosine kinases
RT-PCR	Reverse transcriptase polymerase chain reaction
RV	Right ventricle
SEM	Standard Error of Measure or Scanning Electron Microscopy
SHF	Second heart field
shRNA	short hairpin RNA
S	Somites or Sarcomere
SOS	Son of Sevenless
SRF	Serum Response Factor
SWI/SNF	SWItch/Sucrose NonFermentable

T	Telencephalon
Tbx	T-box Containing Protein
TGFβ	Transforming Growth Factor Beta
TMY	Tropomyosin
TNNI3	Cardiac Troponin I
TNNT2	Cardiac Troponin T
TPM1	α-Tropomyosin
TR	Trabeculae
TV	Tricuspid Valve
UTR	Untranslated Region
VEGF	Vascular Endothelial Growth Factor
VSD	Ventricular Septal Defect
VVN	Vitelline Vein Network
WT	Wild-type
Z-d	Z-disks

Chapter 1: Introduction

The heart is one of the first structures to form during development, and heart precursor cells are among the first cells of the epiblast to undergo gastrulation (Lawson et al., 1991; DeRuiter et al., 1992; Parameswaran and Tam, 1995; Tam et al., 1997; Saga et al., 1999; Saga et al., 2000; Buckingham et al., 2005; Devine et al., 2014; Lescroart et al., 2014). In murine development, following ingression in the early to mid-primitive streak stages, mesodermal heart precursor cells begin to migrate anterolaterally as a sheet, and by the late primitive streak stages, they are localized as identifiable bilateral fields that lie on either side of the ventral midline forming a structure known as the cardiac crescent (Parameswaran and Tam, 1995; Tam et al., 1997; Saga et al., 2000; Shenje et al., 2014). Heart precursor cells that form the cardiac crescent are derived from two mesodermal populations: termed a first heart field (FHF) and a second heart field (SHF). Cardiac precursors of the first heart field undergo differentiation and assemble into a primitive heart tube by embryonic day 8.5 (E8.5) (Tam et al., 1997; Saga et al., 1999; Meilhac et al., 2004; Buckingham et al., 2005; Tzouanacou et al., 2009; Devine et al., 2014; Lescroart et al., 2014). This tube is lengthened by the addition of newly differentiated myocardium derived from the SHF, giving rise to the arterial and venous poles (Kelly et al., 2001; Mjaatvedt et al., 2001; Waldo et al., 2001; Cai et al., 2003; Meilhac et al., 2003; Meilhac et al., 2004; Zaffran et al., 2004; Buckingham et al., 2005; Tzouanacou et al., 2009).

During the early stages of heart development, cardiomyocytes of the FHF and SHF are highly proliferative, resulting in substantial growth of the embryonic heart (Tam et al., 1997; Buckingham et al., 2005; Tzouanacou et al., 2009; van den Berg et al., 2009; Dominguez et al., 2012; Meilhac et al., 2014). In both rodents and humans, the overall rate of cardiomyocyte proliferation gradually declines concomitant with the onset of terminal cardiomyocyte differentiation (Soonpaa et al., 1996; Christoffels et al., 2000; Pasumarthi and Field, 2002; Sedmera et al., 2003; Toyoda et al., 2003; Walsh et al., 2010; Ikenishi et al., 2012). After this period, the mammalian heart continues to grow, largely through hypertrophy and recruitment of cells from extra-cardiac sources including the neural crest and epicardium (Viragh and Challice, 1981; Gorza et al., 1988; Kirby, 1990; Kirby and Waldo, 1995; Li et al., 1996; Creazzo et al., 1998; Manner et al., 2001; Brown and Baldwin, 2006; Ahuja et al., 2007; Winter and Gittenberger-de Groot, 2007; Zhou and Pu, 2008; van Wijk et al., 2009; Kelly, 2012; Maillet et al., 2013).

All animal life is dependent upon the sustained function of the heart. It is therefore not surprising that genetic and acquired cardiac diseases can result in devastating consequences with congenital heart defects representing the number one type of human birth defect, and cardiovascular disease accounting for the most common cause of adult death worldwide (Hoffman, 1995; Hoffman and Kaplan, 2002; Lopez et al., 2006; Heron et al., 2009; Dolk et al., 2010a; Dolk et al., 2010b; van der Linde et al., 2011; Fahed et al., 2013; Pediatric Cardiac Genomics et al., 2013). The mammalian heart has limited regenerative potential, which is in stark contrast to the fish or amphibian heart, which retains robust capacities for regeneration via the activation of cardiomyocyte proliferation (Oberpriller and Oberpriller, 1974; Poss et al., 2002; Laube

et al., 2006; Jopling et al., 2010; Kikuchi et al., 2010; Jopling et al., 2012; Piatkowski et al., 2013). Cardiomyocyte loss is the causal etiology of many forms of heart disease; therefore, strategies aimed at repopulating the damaged heart with replacement cardiomyocytes could potentially restore cardiac structure and more importantly, cardiac function.

The cardiomyocyte cell cycle

The eukaryotic cell cycle consists of four coordinated processes that include cell growth, DNA replication, distribution of duplicated chromosomes into daughter cells, and cell division. The cycle of most eukaryotic cells is composed of four distinct phases: S-phase, where DNA synthesis occurs; M-phase, where karyokinesis and cytokinesis occur; and G_1-phase and G_2-phases**,** where cells continue to grow and prepare for entry into their respective, subsequent phase. The central core of the cell cycle machinery comprises the cyclin-dependent kinases (Cdks) and cyclins. In most eukaryotes, there are different Cdks that control different stages of the cell cycle. Cdks are activated via complex formation with phase-specific cyclins, leading to changes in the phosphorylation of intracellular proteins that both regulate cell cycle events and advance the cell cycle through the stage that the particular Cdk controls (Mitchison, 1971; Baserga, 1985; Murray and Hunt, 1993; Sherr, 1993; Morgan, 1997; Pavletich, 1999; Nurse, 2000; Hochegger et al., 2008; Lim and Kaldis, 2013; Alberts, 2015). Cdk activity is terminated by either cyclin protein degradation or by Cdk inhibitors, such as INK family members (p15, p16, p18 and p19) and Cip/Kip family members (p21, p27 and p57) (Serrano et al., 1993; Guan et al., 1994; Hannon and Beach, 1994; Polyak et

al., 1994; Roberts et al., 1994; Chan et al., 1995; Hirai et al., 1995; Russo et al., 1996; Brotherton et al., 1998; Russo et al., 1998; Pavletich, 1999; Sherr and Roberts, 1999; Lim and Kaldis, 2013). Cyclin protein synthesis and degradation determine the timing of the activation of the cyclin's partner Cdk. The Cdks are critical for cell cycle progression because their inactivation prevents mitosis (Figure 1.1) (Devault et al., 1991; van den Heuvel and Harlow, 1993; Morgan, 1997; Nurse, 2000; Lim and Kaldis, 2013; Alberts, 2015). There are four classes of cyclins that are defined by the cell cycle stage during which they complex with Cdks: G_1-cyclins, which promote passage through the start of the cell cycle; G_1/S-cyclins, which commit the cell to DNA replication; S-cyclins, which initiate DNA replication; and M-cyclins, which promote mitosis (Sherr, 1993; Morgan, 1997; Hochegger et al., 2008; Alberts, 2015).

Cell cycle activity is an essential component of cardiac differentiation and morphogenesis. Detailed analyses of cyclins and Cdks have revealed dramatic changes in cell cycle patterns during embryonic and postnatal stages of cardiac development. Positive cell cycle regulators are highly expressed in the embryonic heart and downregulated in the adult heart while cell cycle inhibitors show the opposite expression pattern (Soonpaa and Field, 1998; Pasumarthi and Field, 2002; Goetz et al., 2006; Ahuja et al., 2007; Walsh et al., 2010; Ikenishi et al., 2012). Protein expression analyses by western blot for cyclin E, cyclin A, cyclin D1, and cyclin B1 in heart ventricles demonstrate a synchronous change in expression during embryonic and postnatal stages. Cyclin levels are high during early embryonic stages (E12) and gradually decrease as embryogenesis proceeds with minimal levels detected at birth. Interestingly, a surge in expression occurs at postnatal day 5 (P5), followed by a rapid

decline, and cyclins are undetectable in adult ventricles. Concomitant with these data, western blot analyses of the cyclin E-Cdk2, cyclin A-Cdk1/2, and cyclin B1-Cdk1 complexes also demonstrated a similar synchronous pattern with high levels present in early embryogenesis (E12), followed by a gradual decline, a surge at P5, and a rapid decline to undetectable levels in adult ventricles (Ikenishi et al., 2012). Terminally differentiated cardiomyocytes show repression of cell cycle activators such as the Cyclin/Cdk complexes (described above), Myc, and E2F transcription factors. Conversely, negative cell cycle regulators such as INK4, p21, p27, retinoblastoma protein (Rb), and cyclin-dependent kinase inhibitors are increased (Table 1.1) (Kim et al., 1994; Flink et al., 1998; Li et al., 1998; Pasumarthi and Field, 2002).

Cardiomyocyte cell cycle control and growth

Mammalian cardiomyocytes exhibit three developmentally determined forms of cell cycle control and growth: proliferation, binucleation and hypertrophy. During embryonic development, the heart primarily grows via hyperplasia or cell proliferation, which is defined as an increase in cell number by cell division. Shortly after birth, proliferation ceases and cardiomyocytes undergo cell-cycle withdrawal, following an additional round of DNA synthesis and mitosis without cytokinesis, which leads to the formation of binucleated cardiomyocytes. The postnatal heart primarily grows via hypertrophy, or an increase in cell size (Figure 1.2) (Erokhnia, 1968a; Erokhnia, 1968b; Dowell and McManus, 1978; Clubb and Bishop, 1984; Oparil et al., 1984; Goldspink et al., 1986; Li et al., 1996; Soonpaa et al., 1996; Bergmann et al., 2009; Walsh et al., 2010; Maillet et al., 2013). The transition from hyperplastic to hypertrophic growth is

required for normal heart morphogenesis and determines the appropriate heart size necessary for pumping a large volume of blood.

Proliferation

Tritiated thymidine analyses (Erokhnia, 1968a; Erokhnia, 1968b) that measure DNA synthesis demonstrate that cardiomyocyte proliferation is high during early murine embryogenesis at E8, with labeling indices of approximately 70% of precardiac mesodermal cells. These levels start to decrease around E10-12, with labeling indices plunging to 45%. This decrease is concomitant with the onset of cardiomyocyte differentiation (Erokhnia, 1968a; Erokhnia, 1968b). As embryogenesis proceeds, cardiomyocyte proliferation gradually declines (Erokhnia, 1968a; Erokhnia, 1968b; Soonpaa et al., 1996; Toyoda et al., 2003; Walsh et al., 2010; Zeng et al., 2014). Fluorescence-activated cell sorting (FACS) analyses of purified populations of E14 cardiomyocytes treated with 5'-bromo-2'-deoxyuridine (BrdU) revealed cardiomyocyte DNA synthesis levels of 22.95% (Walsh et al., 2010). This work is further supported by 5-ethynyl-2'deoxyuridine (EdU) analyses, an alternative thymidine analog, of sectioned cardiac tissue at E10, E17, P7, P21 and in the adult, demonstrating a decrease in cardiomyocyte proliferation as embryogenesis proceeds, with no EdU incorporation observed after P21 (Zeng et al., 2014).

The proliferative capacity of adult cardiomyocytes is quite limited; the frequency and source of new cardiac cells is somewhat controversial, as different labs have reported dissimilar results, most likely due to differences in experimental techniques and analyses (Li et al., 1996; Soonpaa et al., 1996; Soonpaa and Field, 1997; Soonpaa and

Field, 1998; Bergmann et al., 2009; Walsh et al., 2010; Mollova et al., 2013; Senyo et al., 2013; Ali et al., 2014; Naqvi et al., 2014). Tritiated thymidine analyses of α-cardiac myosin heavy chain-positive ventricular myocardium revealed DNA synthesis levels of 0.0006% in wild-type 12 week-old adult murine cardiomyocytes (Soonpaa and Field, 1997). Additionally, DNA synthesis levels increased to 0.0083% in 12 week old mice subjected to a myocardial injury, in which the myocardium was cauterized midway between the apex and base of the heart (Soonpaa and Field, 1997). FACS analysis of cardiomyocyte populations treated with BrdU revealed DNA synthesis levels of 9.6% for P3 neonates, which dropped to 0.94% by P7, 0.02% at P14, and was undetectable by 3 weeks of age (Walsh et al., 2010). More recently, using genetic fate-mapping with stable isotope labeling and multi-isotope imaging mass spectrometry (MIMS), it was shown that cardiomyocytes proliferate at a low rate by the division of pre-existing cardiomyocytes during normal aging. This process increases 4-fold in areas adjacent to myocardial injury (Senyo et al., 2013). MIMS is a technique that utilizes a rare stable isotope of nitrogen (^{15}N) and allows for high-resolution quantitation (Steinhauser et al., 2012). Treatment with ^{15}N-thymidine for 8 weeks at three different timepoints beginning at P4 (neonates), and in 10 week (young adult) and 22 month-old (old adult) adults followed by MIMS analysis revealed dramatic changes in DNA synthesis throughout aging (Senyo et al., 2013). The percentage of ^{15}N-labeled cardiomyocytes per day in the neonatal heart was 1.00%; percentages in the young adult heart were 0.015% and 0.007% in the old adult heart (Senyo et al., 2013). In line with these observations, recent mouse studies revealed that mammals possess the ability to regenerate heart tissue immediately after birth (by P2), but lose this ability by P7 (Porrello et al., 2011).

Interestingly, a recent mouse study confirmed the previously identified postnatal time window during which cardiomyocyte cell numbers increased during P1-4, and suggested the existence of a second tight, transient, proliferative time window at P15, leading to a 40% increase in predominantly binucleated cardiomyocytes (Naqvi et al., 2014).

In humans, cardiomyocyte proliferation can be observed until 20 years of age, which is much longer than anticipated, based on the data detailed above for mice and rats. Of particular significance and in contrast with mice, myocardial growth in humans occurs through the simultaneous cycles of cardiomyocyte proliferation and cell enlargement. However, similar to mice, cardiomyocyte cycling and division decreases with age (Li et al., 1996; Soonpaa and Field, 1997; Soonpaa and Field, 1998; Bergmann et al., 2009; Mollova et al., 2013). A novel ^{14}C-based, birth-dating technique, which can establish the age of cardiomyocytes based on the integration of ^{14}C into human DNA, demonstrated that cardiomyocytes renew with an annual turnover rate of 1.9% for a 19 year-old individual, decreasing to 1% between the ages of 21 and 40 years, with levels decreasing to 0.45% by 75 years of age (Bergmann et al., 2009). A more recent study supporting these results utilized a combined approach that first determined the percentage of cardiomyocytes in M-phase by laser-scanning cytometry (LSC) of myocardial sections that stained positive for phosphorylated histone H3 (pHH3), an M-phase marker, followed by a stereological quantification technique to quantify the number of cardiomyocytes present in the myocardium. LSC is a highly sensitive, microscopy-based cytofluorometry method that measures fluorescence emitted from individual cells at several wavelength ranges (Pozarowski et al., 2006). The optical

dissection method is a stereological technique that obtains quantitative information about three-dimensional tissues from two-dimensional sections (Muhlfeld et al., 2010). This study identified 0.8–1.1$\times10^9$ newly generated cardiomyocytes during the first year of life; 0.9$\times10^9$ new cardiomyocytes during years 1–10; and 0.6$\times10^9$ new cardiomyocytes during years 10–20 (Mollova et al., 2013). Consistent with these data, morphometric analyses revealed that during physiological hypertrophy, the cardiomyocyte nuclear DNA content remains constant. However, as the heart grows in size and when the weight of the myocardium reaches approximately 210 grams, there appears to be a linear increase in the percentage of cardiomyocyte nuclear DNA content as cardiac mass increases. Because human hearts do not change nuclear number with hypertrophy, this observation indicates that new cardiomyocytes are generated during this period of growth (Adler, 1975; Adler and Costabel, 1975; Adler and Friedburg, 1986; Herget et al., 1997; Laflamme and Murry, 2011).

Binucleation

The cell cycle ends in the division of the cytoplasm by cytokinesis. In a typical cell, cytokinesis accompanies every round of mitosis. However, some cells undergo mitosis without cytokinesis, resulting in a multinucleated cell (Rappaport, 1996; Glotzer, 1997; Field et al., 1999). This type of endoreduplication generally occurs in tissues with high metabolic activity and in cells that are terminally differentiated (MacAuley et al., 1998; Larkins et al., 2001; Gonzalez et al., 2006; Zielke et al., 2013). In the heart, the transition from hyperplastic to hypertrophic growth is associated with the formation of binucleated cardiomyocytes (Oparil et al., 1984), resulting from incomplete cell division in which karyokinesis becomes uncoupled from cytokinesis. During the murine

embryonic burst of proliferation (E10–12), karyokinesis and cytokinesis are matched, resulting in cardiomyocyte proliferation. In contrast, during early neonatal stages (P4–6), karyokinesis occurs in the absence of cytokinesis, resulting in binucleation of cardiomyocytes (Li et al., 1996; Soonpaa et al., 1996; Li, F. et al., 1997b; Walsh et al., 2010). In mice and rats, binucleation begins around P4; by 3 weeks of age, 85–90% of cardiomyocytes are binucleated with normal diploid DNA content in each nucleus (Clubb and Bishop, 1984; Li et al., 1996; Soonpaa et al., 1996; Porrello et al., 2011). In humans, these percentages range from 25–57% (Schmid and Pfitzer, 1985; Olivetti et al., 1996). Notably, humans do not display a transition to predominantly binucleated cardiomyocytes, maintaining relatively high levels (~64%) of mononucleated cardiomyocytes up to 20 years of life. However, cardiomyocyte cytokinesis ceases after this time point, resulting in mononucleated cells with tetraploid (4n) or higher DNA content (Adler and Costabel, 1975; Olivetti et al., 1996; Mollova et al., 2013).

The mechanism by which binucleation occurs remains unclear. However, the actin-myosin contractile ring, the structure that generates the force necessary to separate the daughter cells after mitosis, forms during the binucleation process indicating that the molecules involved in later stages of cytokinesis are responsible for binucleation (Li, F. et al., 1997b; Miller, 2011). One possible explanation is that the presence and incomplete disassembly of myofibrils in the equator region where cleavage furrows normally form could physically impede cytokinesis (Li, F. et al., 1997a). In muscle, for example, contractile myofibrils are organized into sarcomeres. Recent evidence suggests that during karyokinesis, the sarcomeric Z-disks and M-bands disassemble in the midzone region. Interestingly, during cytokinesis, the

sarcomeric structure is absent, indicating that cardiomyocyte division involves sarcomeric disassembly (Figure 1.3) (Bersell et al., 2009). Interestingly, recent studies suggest that multinucleation could result from defects in the recruitment of the contractile ring protein, anillin (Straight et al., 2005; Smith et al., 2013). Anillin binds to myosin II heavy chain and helps to focus myosin at the contractile ring (Straight and Field, 2000). Depletion of anillin leads to disorganized contractility and cytokinesis failure (Field and Alberts, 1995; Straight et al., 2005; Smith et al., 2013).

The physiological significance of possessing binucleated cells also remains to be elucidated. There are few examples of multinucleated cells in higher-level vertebrates; however, most examples of multinucleation occur in highly metabolically active cells such as osteoclasts, hepatocytes and muscle cells (Holtzer et al., 1957; Okazaki and Holtzer, 1966; Kahn and Simmons, 1975; Hall and Ralston, 1989; Manolagas and Jilka, 1995; Rossi et al., 2000; Miyaoka et al., 2012). Multinucleated cells often occur in pathological conditions due to aberrant cell cycle control (Gillespie and Stevens, 1972; Most et al., 1997; Sagona and Stenmark, 2010; Weihua et al., 2011). It has been hypothesized that multinucleation is advantageous, generating twice the amount of RNA for greater protein synthesis. Indeed, transcriptional activity that influences specialized cellular functions has been implicated in other multinucleated cell types (Boissy et al., 2002). Another advantage specific to muscle cells could be adaptation to the physiological process of contraction, which requires myofibrils to maintain their organization along their entire lengths. An increase in cross-sectional area could lead to an increase in the force of contraction (Ahuja et al., 2007).

Hypertrophy

The size of an organ depends both on the number and size of the cells it contains. In mammals, nutritional status, growth factors, and hormones play important roles in the control of organ size (Conlon and Raff, 1999). The heart is an essential pump and its size is tightly regulated across species to ensure proper function. The heart must be large enough to generate a physiological cardiac output, but not so large as to block cardiac output, which is common in cardiomyopathies (Seidman, 2000; Seidman and Seidman, 2001; Heallen et al., 2011). During the postnatal period, the cardiomyocytes of both rodents and humans undergo a period of physiological growth, increasing in size by 30–40-fold (Adler and Costabel, 1975; Li et al., 1996).

Between preadolescence (P10) and puberty (P35), mouse body weight (in grams) increases by 3.8-fold, whereas mouse heart weight (in milligrams) increases by 3.5-fold. At the cellular level, cardiomyocyte length increases by 46 μm with little change in diameter. During this period of growth, the left ventricle increases in weight 3.47-fold, and cardiomyocyte volume increases 1.7-fold (Adler, 1975; Adler and Costabel, 1975; Laflamme and Murry, 2011; Naqvi et al., 2014). This interesting discrepancy, suggests that an increase in cardiomyocyte number also occurs during this time period (Naqvi et al., 2014). A similar trend is observed in humans, where the cellular volume of cardiomyocytes increases by 8.6-fold between birth and 20 years of age; this increase is concomitant with an increase in the number of cardiomyocytes (Mollova et al., 2013) as well as an increase in the number of non-cardiomyocytes including fibroblasts and endothelial cells (Adler and Costabel, 1975). Physiological hypertrophy is initiated by multiple signaling pathways including the vascular endothelial growth factor B (VEGFB)

and receptor (VEGFR1), insulin and insulin-like growth factor 1 (IGF1). These trigger intracellular signalling pathways that regulate protein synthesis, metabolism and energy production (Reiss et al., 1996; Bellomo et al., 2000; Karpanen et al., 2008; Bry et al., 2010). Growth signals are controlled by ERK1/2, PI3K, AKT and mTOR complex 1 (mTORC1), whereas AMP-activated protein kinase (AMPK) governs metabolic adaptive reprogramming (Maillet et al., 2013) (Bueno et al., 2000; Lips et al., 2004; Purcell et al., 2007; Kehat and Molkentin, 2010; Kehat et al., 2011; Horman et al., 2012).

One very important distinction with regard to hypertrophy is to highlight the difference between normal hypertrophy during heart growth and pathological hypertrophy. Cardiomyocytes increase in size in response to biomechanical stress, a process known as pathological hypertrophy (Seidman and Seidman, 2001). Pathological hypertrophy is functionally, mechanistically, and histologically distinguished from normal embryonic and postnatal myocardial growth by characteristic changes in cardiac myocyte shape and volume (Bishop, 1990; Dorn, 2007). In humans, hypertrophic cardiomyopathy (HCM) is a genetic condition caused by mutations in genes that encode sarcomeric proteins, including cardiac β-myosin heavy chain (*MYH7*), cardiac myosin-binding protein C (*MYBPC3*), cardiac troponin T (*TNNT2*), cardiac troponin I (*TNNI3*), essential myosin light chain (*MYL3*), regulatory myosin light chain (*MYL2*), α-tropomyosin (*TPM1*), cardiac actin (*ACTC*), and titin (Bettencourt-Dias et al.) (Poetter et al., 1996; Kimura et al., 1997; Mogensen et al., 1999; Satoh et al., 1999). HCM often presents as sudden death during exertion in a formerly asymptomatic individual. Increased awareness and echocardiographic screening have improved detection and shown that HCM is more common than previously thought. At the cellular

level, the major features of HCM are cardiomyocyte and myofibrillar disarray, hypertrophy, and myocardial fibrosis. Genetic causes of HCM, which are autosomal dominant, are now estimated to account for at least 50% of sporadic childhood onset cases (Seidman, 2000; Seidman and Seidman, 2001; Morita et al., 2008). Consequently, the need for genetic screens for HCM could greatly impact human health.

Adult onset pathological hypertrophy is also induced by acquired cardiac deficiencies such as hypertension, valvular disease, myocardial infarction (MI), and endocrine disorders. In these types of cardiac pathologies, chronic pressure overload results in concentric hypertrophy with a small, thick-walled left ventricle that is associated with significantly increased risk of heart failure and malignant arrhythmia (Grossman et al., 1975; Levy et al., 1990b; Levy et al., 1990a; Koren et al., 1991; Morita et al., 1996; Dorn et al., 2003; Frey et al., 2004; Heineke and Molkentin, 2006; Dorn, 2007; van Berlo et al., 2013). Genes upregulated in adult onset pathological hypertrophy include brain natriuretic peptide, angiotensin-converting enzyme, the endothelin receptor, and the β-adrenergic receptor kinase (Iemitsu et al., 2001; Dorn and Force, 2005). In addition, studies have implicated the calcium–calcineurin–NFAT and protein kinase A pathways in regulating the pathological growth of the heart. Other examples of mediators of pathological cardiac hypertrophy are the p38 and c-Jun N-terminal kinase (JNK) branches of the MAPK cascade. Sustained p38 or JNK activation in the heart leads to cardiomyopathy and heart failure (Heineke and Molkentin, 2006; Maillet et al., 2013; van Berlo et al., 2013).

Growth factors that regulate cardiomyocyte proliferation

Cardiomyocytes from both FHF and SHF undergo hyperplastic growth in response to input from a large network of growth factor signaling pathways; such pathways integrate a suite of transcription factors and microRNAs (miRNAs), which are proposed to directly regulate the cardiac cell cycle (Lavine et al., 2005; Ahuja et al., 2007; Bersell et al., 2009; Heallen et al., 2011; Porrello et al., 2011; Xin et al., 2011; Eulalio et al., 2012; von Gise et al., 2012; Wadugu and Kuhn, 2012; Xin et al., 2013). Many of these growth factors are secreted by the epicardium, an epithelial sheet of cells that forms over the heart, and several lines of evidence suggest that cardiomyocyte proliferation in the developing myocardium is influenced by these secreted factors (Rumyantsev, 1977; Chen et al., 2002; Sengbusch et al., 2002; Kang and Sucov, 2005; Sun et al., 2007; Sucov et al., 2009; Shen et al., 2015). Additionally, in cell culture, many mitogens have been shown to stimulate the proliferation of fetal cardiomyocytes (Figure 1.4) (Armstrong et al., 2000).

Hippo pathway

First identified in *Drosophila melanogaster*, the Hippo signaling pathway is a conserved regulator of organ size (Pan, 2010). Hippo signaling mediates contact inhibition of cell proliferation by cell to cell interactions that control tissue growth (Fagotto and Gumbiner, 1996; Zhao, B. et al., 2007; McClatchey and Yap, 2012). Genetic loss-of-function mutations of Hippo pathway members in *Drosophila* lead to tissue overgrowth, characterized by increased proliferation and decreased cell death (Wu et al., 2003; Wei et al., 2007). The mammalian core Hippo signaling components

include the Ste-20-like protein kinases Mst1 and Mst2, which form a complex with the WW-repeat scaffolding protein Salv that phosphorylates Lats1 and Lats2. These Lats kinases complex with Mob, which phosphorylates and inactivates Yap and Taz. Yap and Taz partner with transcription factors, such as Tead, to regulate gene expression (Chan et al., 2005; Callus et al., 2006; Dong et al., 2007; Zhao, B. et al., 2007; Lei et al., 2008; Praskova et al., 2008; Pan, 2010).

The conditional depletion of the *Salv* gene using *Nkx2.5-Cre* (Moses et al., 2001), an early cardiac marker, leads to perinatal lethality due to heart enlargement (cardiomegaly) (Heallen et al., 2011). Furthermore, phenotypic analysis at E14.5 revealed that cardiac expression of a *Salv* mutant caused expansion of trabecular and subcompact ventricular myocardial layers, thickened ventricular walls, and enlarged ventricular chambers, but showed no change in myocardial cell size (Heallen et al., 2011). In addition, conditional mutants of *Lats2* and *Mst1/2* showed similar myocardial expansion phenotypes in the heart (Heallen et al., 2011).

Yap1 is a major target of the Hippo signaling pathway and is inactivated by Hippo kinase activity (Dong et al., 2007; Zhao, B. et al., 2007). Conditional depletion of the *Yap1* gene in the embryonic heart, utilizing either the *Tnnt2-Cre* (Jiao et al., 2003) or the *Nkx2.5-Cre* driver (Moses et al., 2001), results in cardiac abnormalities and embryonic lethality by E16.5 due to myocardial hypoplasia (Xin et al., 2011; von Gise et al., 2012). *Yap1*-null mutants showed a significant reduction in the cardiomyocyte mitotic index by pHH3 staining as well as reduced DNA synthesis by EdU analysis, indicating that Yap1 is required for cardiomyocyte proliferation (Xin et al., 2011). Conversely, *Yap1* gain-of-function mutants stimulate cardiomyocyte proliferation both in

vitro and in vivo. Treatment of embryos at E8.5 with a doxocycline-inducible *Yap1* transgene results in embryonic lethality by E15.5, with embryos exhibiting cardiomegaly (von Gise et al., 2012). Histological examination revealed dramatic myocardial overgrowth with moderate thickening of the compact myocardium and marked expansion of the trabecular myocardium. Furthermore, *Yap1* gain-of-function mutants showed enhanced cardiomyocyte proliferation (von Gise et al., 2012).

The above-mentioned studies, demonstrate that Hippo signaling inhibits cardiomyocyte proliferation. A recent study found that depletion of Hippo signaling in the adult myocardium is an endogenous repressor of cardiomyocyte renewal and regeneration. Inactivating either the *Salv* or *Lats1/2* genes with a tamoxifen-inducible Cre, the *Myh6*^{CreERT2} transgene (Sohal et al., 2001), in the adult heart leads to cell cycle re-entry and a significant induction of DNA synthesis, measured by EdU and Ki67 analyses (Heallen et al., 2011). Moreover, Hippo deficiency promoted efficient heart regeneration in both postnatal cardiac apex resection and adult myocardial infarction models, revealing a crucial, inhibitory role for Hippo signaling in cardiomyocyte renewal and regeneration (Heallen et al., 2013).

Wnt pathway

Wnt proteins compose a large family of secreted signaling molecules that regulate critical aspects of development, including cell-fate specification, proliferation, survival, migration and adhesion (Cohen et al., 2008). The Wnt signaling pathway is an evolutionarily conserved pathway that encompasses two major signaling branches: the canonical or Wnt-β-catenin-dependent pathway and the noncanonical or β-catenin-

independent pathway (Komiya and Habas, 2008). The canonical Wnt signaling pathway begins with Wnt proteins binding to a coreceptor complex composed of the frizzled (Fzd) family, seven-pass transmembrane proteins and lipoprotein receptor-related 5/6 (Lrp5/6) proteins. Wnt receptor binding activates the intracellular effector protein dishevelled, which in turn inactivates a protein complex that includes the constitutively active serine-threonine kinase glycogen synthase kinase 3 (Gsk3), as well as the scaffolding proteins axin and adenomatosis polyposis coli (APC). This complex normally phosphorylates β-catenin and targets it for degradation (He et al., 2004; Gordon and Nusse, 2006; Komiya and Habas, 2008; MacDonald et al., 2009; Rao and Kuhl, 2010). The hallmark of the canonical Wnt pathway is the accumulation and translocation of the adherens junction associated-protein β-catenin into the nucleus (He, 2004; Gordon and Nusse, 2006). In contrast, the noncanonical pathway is further divided into two distinct branches: the planar cell polarity pathway, known for its role in epithelial cell orientation, and the Wnt/Ca^{2+} pathway, known for its role in cell movement during gastrulation (Strutt, 2002; Klein and Mlodzik, 2005; Barrow, 2006; Green et al., 2008; Komiya and Habas, 2008; De, 2011) .

Wnt signaling is essential for cardiogenesis and regulates many aspects of cardiac morphogenesis as well as the self-renewal and differentiation of cardiac progenitor cells (Cohen et al., 2008). Several components of the canonical Wnt pathway are required for proper heart and vascular formation (Brade et al., 2006; Eisenberg and Eisenberg, 2006; Tzahor, 2007; Cohen et al., 2008; Rochais et al., 2009; Bergmann, 2010; Rao and Kuhl, 2010; Zelarayan et al., 2010). Recently, Wnt signaling was shown to play a critical role in regulating cardiomyocyte proliferation. Treatment of

cardiomyocytes with the small molecule 6-bromoindirubin-3′-oxime (BIO), a specific inhibitor of Gsk3 promoted proliferation in vitro (Meijer et al., 2003). Stimulation of both neonatal and adult rat cardiomyocytes with BIO induced S-phase entry, upregulated positive cell cycle regulators, and increased the cardiomyocyte mitotic index. In addition, BIO treatment elevated β-catenin activity in cardiomyocytes, suggesting that the increase in proliferative ability may be due, in part, to the activation of the canonical Wnt pathway (Tseng et al., 2006).

Interestingly, a recent study (Heallen et al., 2011) revealed that Hippo signaling inhibits Wnt/β-catenin to regulate heart size. Gene expression profiling in *Salv*-cardiac null mice revealed a dramatic upregulation of canonical Wnt target genes, including *Sox2*, *Snai2/Slug*, and *Birc5/Survivin* in the heart (Heallen et al., 2011). Immunostaining using β-catenin-specific antibodies revealed a 4-fold increase in nuclear β-catenin, which is normally localized to the cytosol. Genetic interaction studies with *Salv*-null mice combined with a conditional β-*catenin*-null allele (Hippo-deficient embryos with reduced β-*catenin* dosage) resulted in suppression of the Hippo cardiomyocyte overgrowth phenotype and returned gene expression profiles to wild-type levels (Heallen et al., 2011). These findings indicate that Wnt signaling is required for the upregulation of cardiomyocyte proliferation and cardiomegaly in Hippo mutants. Furthermore, the authors demonstrated by chromatin immunoprecipitation (ChIP) studies that Yap and β-catenin are contained within a common regulatory complex on *Sox2* and *Snai2*. Therefore, in cardiomyocytes, Hippo signaling restricts Yap from the nucleus, resulting in the diminution of Hippo/Wnt–regulated gene expressions. The Yap and β-catenin interaction with *Snai2* and *Sox2* reveals a nuclear mechanism for the antagonistic

control of cardiomyocyte growth by Hippo and canonical Wnt signaling (Heallen et al., 2011).

Insulin-like Growth Factor (IGF) pathway

Insulin-like growth factors 1 and 2 (IGF1 and 2) are secreted ligands that are important for embryonic growth (Le Roith, 1997). IGF2 signaling is mediated by the type-1 IGF receptor (IGF1R), whereas receptor-mediated endocytosis of type-2 IGF receptor (IGF2R) causes the degradation of excess IGF2 (Ludwig et al., 1995). In cell culture, both IGFs stimulate the proliferation of primary fetal ventricular cardiomyocytes (Liu et al., 1996; Hertig et al., 1999), and both are expressed in the epicardium during myocardial compact zone expansion (Fraidenraich et al., 2004; Li et al., 2011). Notably, combined treatment of cultured whole mouse embryos with NRG1 and IGF1 results in a substantial increase in DNA synthesis, as well as the expansion of the ventricular compact zone leading to chamber growth and maturation (Hertig et al., 1999). Interestingly, injection of exogenous IGF1 leads to a partial rescue of cardiac defects observed in *Id*-null embryos (Fraidenraich et al., 2004). Id proteins inhibit cell lineage-specific gene expression and differentiation of several different bHLH transcription factors required for development (Norton and Atherton, 1998; Norton et al., 1998; Sikder et al., 2003). *Id-null* mice exhibit severe cardiac abnormalities leading to embryonic lethality. Treatment of *Id-null* mice with IGF1 results in enhanced myocardial proliferation and a rescue of embryonic lethality (Fraidenraich et al., 2004). The role of IGF1 in cardiomyocyte proliferation is further enhanced by the transgenic overexpression of IGF1 in the postnatal myocardium with the α-myosin-heavy chain

promoter (α-MHC), leading to a significant increase in cardiomyocyte cell number and cardiomegaly (Reiss et al., 1996).

IGF2 is encoded by the imprinted gene *Igf2* and is expressed only from the paternal allele in most tissues (DeChiara et al., 1991). Genomic imprinting affects several mammalian genes and results in the expression of those genes from only one of the two parental chromosomes (Reik and Walter, 2001). Depletion of IGF2R, also encoded by an imprinted gene, in mice leads to excess IGF2, causing severe hyperplasia, with heart size 2–5 times larger than that of a wild-type littermate. In addition to heart failure, these mice exhibit respiratory abnormalities and die at birth (Lau et al., 1994; Wang et al., 1994; Eggenschwiler et al., 1997). *Igf2*-null embryos exhibit a substantial decrease in ventricular wall cardiomyocyte proliferation leading to severe hypoplasia. Furthermore, the conditional depletion of both IGFRs in embryonic hearts also leads to a significant decrease in myocardial compact zone proliferation at E12.5 (Li et al., 2011).

Neuregulin/ErbB pathway

Neuregulin1 (NRG1) is a cell-cell signaling protein that is a ligand for receptor tyrosine kinases (RTKs) of the epidermal growth factor receptor family (ErbB1 – 4) (Falls, 2003). Binding of NRG1 to *ErbB4* leads to heterodimerization with *ErbB2* or homodimerization with ErbB4 (Fuller et al., 2008). Deletion of NRG1, *ErbB2*, or *ErbB4* leads to myocardial hypoplasia and embryonic lethality in mice, indicating that each of these genes is essential for cardiac development (Gassmann et al., 1995; Lee et al., 1995; Meyer and Birchmeier, 1995). Interestingly, NRG1 induces mononucleated

cardiomyocytes to proliferate. Following NRG1 stimulation, cardiomyocytes re-enter the cell cycle from S-phase and disassemble sarcomeres, enabling cytokinesis. Furthermore, the conditional deletion of ErbB4 in the adult myocardium leads to a complete ablation of DNA synthesis as measured by EdU incorporation and a 20% reduction in the number of cardiomyocyte nuclei. Conversely, overexpression of ErbB4 in the adult heart leads to a 3-fold increase in EdU incorporation. Together these data demonstrate that NRG1 induces proliferation of differentiated cardiomyocytes in vivo. Most strikingly, NRG1-treated animals show significant improvements in cardiac function and structure following myocardial infarction (Bersell et al., 2009). However, a recent study contradicted these findings, demonstrating that nine consecutive daily injections of NRG1β1 did not result in an increase in DNA synthesis in either the normal or infarcted adult mouse heart (Reuter et al., 2014). Therefore, the potential for NRG1 to be used as a therapeutic regimen for cardiac regeneration remains unclear. Notably, during embryogenesis NRG1 does not play a role in proliferation, but participates in signaling between the endocardium and myocardium that is required for differentiation and maturation (Grego-Bessa et al., 2007).

Periostin

Cardiomyocytes in the border zone of a myocardial infarction have a transient increase in cell-cycle activity. Based on these findings, it was hypothesized that it may be possible to apply extracellular factors to induce cardiomyocyte proliferation (Kuhn et al., 2007). Periostin (Postn) is a secreted extracellular matrix protein that is associated with the epithelial-to-mesenchymal transition during cardiac development where it is localized to the subendocardial region of atrioventricular cushions and along the

mesenchyme myocardium interface (Norris et al., 2004; Litvin et al., 2005; Butcher et al., 2007). It is re-expressed in adult life following cardiac injury (Stanton et al., 2000; Wang et al., 2003). *Postn*-null mice are viable and show very mild phenotypes, none of which are cardiovascular (Rios et al., 2005). However, following myocardial infarction, *Postn*-null mice show reduced scar formation, but no change in rates of cardiomyocyte proliferation (Shimazaki et al., 2008; Lorts et al., 2009). Overexpression of full-length periostin via the α-MHC promoter in differentiated cardiomyocytes also did not increase cardiomyocyte cell cycle activity (Lorts et al., 2009). Conversely, the local delivery of a periostin peptide in rats immediately after myocardial infarction increased cardiomyocyte proliferation, reduced scar formation, and improved both ventricular remodeling and myocardial function. In addition, periostin stimulates mononucleated cardiomyocytes to enter a full mitotic cell cycle (Kuhn et al., 2007). The discrepancy between these findings has yet to be explained but could be due to either the molecular mechanisms involved (peptide vs. gene) or the timing of delivery (acute vs. chronic overexpression (Senyo et al., 2014).

Fibroblast Growth Factor (FGF) pathway

Fibroblast growth factors (FGFs) encoded by a large family of genes are polypeptide signaling proteins with many important functions during development. FGFs activate cell surface FGF receptors (FGFRs) which are trans-membrane RTKs. During embryonic development, FGFs play diverse roles in regulating cell proliferation, migration, and differentiation. In the adult organism, FGFs are homeostatic factors and function in tissue repair and response to injury. There are at least 22 FGF ligands and 4 FGFRs. Alternative mRNA splicing of FGFRs is tissue specific, producing epithelial

variants (b-splice forms) and mesenchymal variants (c-splice forms) (Miki et al., 1992; Chellaiah et al., 1994; Naski and Ornitz, 1998; Ornitz and Itoh, 2001; Pownall and Isaacs, 2010). Binding of FGF ligands leads to the autophosphorylation of the FGFR, allowing interaction of the FRS2 docking protein, followed by activation of the GRB2/SOS complex. Activated SOS then activates RAS and triggers a phosphorylation cascade leading to the activation of RAF, MEK, and mitogen-activated protein kinase (ERK) (Kouhara et al., 1997; Rochais et al., 2009; Pownall and Isaacs, 2010). FGFR signals are also transduced by the phospholipase C-γ pathway and the phosphoinositide-3 kinase (PI3K) pathway (Bottcher and Niehrs, 2005; Thisse and Thisse, 2005; Beenken and Mohammadi, 2009; Knights and Cook, 2010; Pownall and Isaacs, 2010).

A role for FGF signaling in cardiomyocyte proliferation has been demonstrated from flies to humans (Beiman et al., 1996; Ornitz and Itoh, 2001; Moon, 2006; Lavine and Ornitz, 2008; Moon, 2008). Several studies have demonstrated that FGFs are mitogenic for cardiomyocytes in culture (Speir et al., 1992; Engelmann et al., 1993; Pasumarthi et al., 1996). In addition, overexpression of FGFR1 in rat cardiomyocytes leads to increased proliferation (Sheikh et al., 1999). *Fgf8* depletion in cardiac mesoderm leads to embryonic lethality due to proliferative defects in the SHF and a failure to properly elongate the developing heart tube (Ilagan et al., 2006; Park et al., 2006). *Fgf10* was the first identified marker of the SHF (Kelly et al., 2001). However, embryos lacking *Fgf10* exhibit abnormal ventricular morphogenesis and malpositioning of the heart in the thoracic cavity, but no outflow tract (OFT) alignment defects (Marguerie et al., 2006). Conditional ablation of *Fgfr1* and *Fgfr2* in SHF cells (using

Islet1-Cre) (Srinivas et al., 2001) results in a substantial reduction in proliferation (Park et al., 2008). FGFs can be classified within subfamilies, which share similar receptor-binding properties and overlapping patterns of expression (Ornitz and Itoh, 2001). *Fgf9*, *Fgf16* and *Fgf20* compose one subfamily and are all expressed in the epicardium and endocardium of the developing heart (Colvin et al., 1999; Lavine et al., 2005). *Fgf9*-null mice die at birth due to lung hypoplasia and an enlarged dilated heart (Colvin et al., 2001). However, during embryonic development, *Fgf9*-null hearts are hypoplastic and exhibit decreased cardiomyocyte proliferation (Colvin et al., 2001; Lavine et al., 2005). Interestingly, double-knockout mice for *Fgfr1* and *Fgfr2* also display cardiac hypoplasia and decreased proliferation. Further work has demonstrated that FGF9 signals to the myocardium from the epicardium through *Fgfr1c* and *Fgfr2c* (Lavine et al., 2005). In line with these studies, mice lacking *Fgf16* also show decreased cardiomycoyte proliferation (Hotta et al., 2008).

FGF signaling has also been shown to play a role in adult cardiomyocyte proliferation. Mammalian cardiomyocytes control the cell cycle via p38 MAP kinase, which regulates the expression of genes required for mitosis, including cyclin A and cyclin B. p38 activity is inversely correlated with cardiac growth during development, and its overexpression blocks fetal cardiomyocyte proliferation. Cardiac-specific p38α knockout mice show enhanced cardiomyocyte proliferation and pronounced cytokinesis (Engel et al., 2005; Engel et al., 2006). In contrast, genetic activation of p38 in a dominant-negative transgenic mouse model led to reduced proliferation in the adult heart (Engel et al., 2005). Treatment with a p38 MAP kinase inhibitor coupled with recombinant FGF1 following acute myocardial injury enhanced cardiomyocyte

proliferation and improved cardiac function. The addition of FGF1 alone or in combination with the p38 inhibitor also improved angiogenesis around the scar area, possibly contributing to the survival of newly generated cardiomyocytes (Engel et al., 2006). Furthermore, the apoptosis observed with ischemia-reperfusion injury is attenuated by FGF-1 in the adult myocardium (Cuevas et al., 1997).

MicroRNAs regulate cardiomyocyte proliferation

The regulatory pathways that govern heart development and growth are modulated by several miRNAs. miRNAs, 21–25 nucleotides in length, are noncoding RNAs that play important regulatory roles in biology by targeting mRNAs for cleavage or repressing translation (Bartel, 2004; Liu and Olson, 2010; Small and Olson, 2011; Xin et al., 2013). miRNAs can be classified into three categories: intergenic, intronic, and exonic. Intergenic miRNAs are derived from their own transcriptional units in the intergenic regions of the genome. Intronic and exonic miRNAs are located within the introns and exons of host genes (protein-coding or nonprotein-coding genes) and are usually cotranscribed and coexpressed with their host genes (Bartel, 2004). Nucleotides 2–8 of the miRNA, termed the “seed” sequence located at the 5’ end, are essential for target recognition and binding. Based on the seed sequence, miRNAs can suppress collections of mRNAs that encode proteins participating in similar biological networks (Bartel, 2009).

Many miRNAs are implicated in the regulation of many aspects of cardiovascular biology (Figure 1.5). miR-1 and miR-133 promote mesoderm differentiation early in

development. By contrast, they have opposing roles later in the cardiac lineage when miR-1 promotes and miR-133 inhibits cardiomyocyte differentiation (Zhao, Y. et al., 2007; Ivey et al., 2008; Small and Olson, 2011). However, only a few have been identified that specifically regulate cardiomyocyte proliferation (Liu and Olson, 2010; Xin et al., 2013). To identify pathways involved in cardiomyocyte proliferation, a high-throughput miRNA screen was conducted, and 40 miRNAs were identified that induced DNA synthesis and increased cytokinesis in neonatal rat cardiomyocytes (Eulalio et al., 2012). Of these, miR-590-3p and miR-199a-3p were subsequently implicated in cardiomyocyte proliferation during injury repair (Shin et al., 2002; Kook and Epstein, 2003; Eulalio et al., 2012). Interestingly, these miRNAs contain different seed sequences, but have several of the same predicted targets. Both were found to target the Homer1 gene, which modulates Ca^{2+} signaling in the heart through its interaction with the Ca^{2+} release channel ryanodine receptor (RyR). Also, both target the Hopx gene, which encodes a homeodomain protein that inhibits cardiomyocyte proliferation (Kook and Epstein, 2003; Trivedi et al., 2010; Grubb et al., 2012). In vivo, overexpression of miR-590-3p and miR-199a-3p in neonatal mice results in increased cardiomyocyte proliferation. Of particular note, the presence of these two miRNAs in cardiomyocytes reduces fibrotic scar size and improves cardiac function following myocardial infarction, suggesting a potential therapeutic use. Interestingly, miR-590-3p but not miR-199a-3p, was found to target Clic5, a cell proliferation inhibitor, demonstrating a unique specificity for certain targets (Eulalio et al., 2012). However, despite evidence for roles of the mir-590-3p and mir-199a-3p in cardiomyocyte

proliferation in neonatal mice and rats, what role, if any, they play in embryonic cardiomyocyte proliferation, remains to be established.

In addition, miR-15 and miR-195 (members of the miR-15 family) have been shown to regulate the cardiomyocyte cell cycle. miR-195 is highly upregulated in neonatal mouse ventricles at P10 after cardiomyocytes have exited the cell cycle (Porrello et al., 2011; Porrello et al., 2013). Overexpression of miR-195 in the developing heart leads to severe hypoplasia and cell cycle arrest during G_2-phase. Further work showed that miR-195 targets Chek1*,* a cell cycle checkpoint kinase that promotes G_2-to-M-phase transition and thus mitotic progression (Porrello et al., 2011). Conversely, inhibition of miR-15 leads to an increase in cardiomyocyte proliferation in neonatal and adult mice, and improved cardiac function following injury (Hullinger et al., 2012; Porrello et al., 2013).

Transcription factors that regulate cardiomyocyte proliferation

Cardiomyocyte proliferation is an intrinsic component of normal cardiac morphogenesis and is dependent upon cardiac-specific transcriptional regulators as well as exogenous signals, as described above (Dunwoodie, 2007; Smith and Bader, 2007; Lavine and Ornitz, 2008; Ikenishi et al., 2012).

Foxp1

Foxp1 is a transcriptional repressor protein that binds to DNA via its highly conserved forkhead DNA-binding domain (Li and Tucker, 1993; Shu et al., 2001; Li et

al., 2004). Foxp1 is expressed in cardiomyocytes, in the endocardium, and in cells underlying the cushion mesenchyme (Lu et al., 2002; Wang et al., 2004). Global loss of the *Foxp1* gene results in a complex, and slightly confusing, cardiac phenotype characterized by defects in outflow tract septation, increased myocardial proliferation, and thinning of ventricular myocardium (Wang et al., 2004). The observations of increased cell proliferation and loss of ventricular mass in *Foxp1* mutants suggest that Foxp1 may regulate cardiomyocyte proliferation in a complex manner. Loss of *Foxp1* in endothelial cells using *Tie2-Cre* (Kisanuki et al., 2001) results in embryonic lethality that correlates with decreased ventricular mass and reduced cardiomyocyte proliferation. This finding contrasts with the increased proliferation observed in global loss-of-function mice (Zhang et al., 2010), which is the result of decreased *Fgf3/16/17/20* expression in the endocardium. Loss of *Foxp1* specifically in the myocardium using the *Nkx2.5-Cre* (Moses et al., 2001) leads to increased proliferation (particularly in the trabecular zone) increased ventricular wall thickness, and ventricular septation defects. Interestingly, Foxp1 directly represses Nkx2.5 in the myocardium, and loss of *Foxp1* leads to increased *Nkx2.5* expression (Zhang et al., 2010). Moreover, transgenic overexpression of *Nkx2.5* results in increased cardiomyocyte proliferation and ventricular wall thickness, similar to that in myocardial-deficient *Foxp1* mutants. Together, these data indicate that Foxp1 regulates the balance of myocardial growth in development, resulting in the controlled exit of cardiomyocytes from the cell cycle (Zhang et al., 2010).

Jumonji

Jumonji is a member of the JMJ transcription factor family that features an AT-rich interaction domain and is highly expressed in the myocardium throughout

embryonic development (Gregory et al., 1996; Kortschak et al., 2000; Jung et al., 2005a). *Jumonji* mutant mice exhibit hyperproliferation and overexpression of cyclin D1 (Takeuchi et al., 1995; Takeuchi et al., 1999; Toyoda et al., 2003; Jung et al., 2005b; Jung et al., 2005a). Interestingly, jumonji downregulates growth via an interaction with the cell cycle regulator, retinoblastoma protein (Rb) (Jung et al., 2005b). Further studies, revealed that enhanced expression of *cyclin D1* in mutant mice decreased GATA4 protein levels and inhibited the differentiation of cardiomyocytes in a Cdk4/6-dependent manner (Nakajima et al., 2011).

Hopx

Hopx is a transcriptional corepressor that is essential for the normal development of the mammalian heart. It is expressed in the embryonic and postnatal myocardium, and functions downstream of the early cardiac-specific transcription factor, Nkx2-5. Hopx modifies the expression of cardiac-specific genes and thereby finely regulates heart development (Kook and Epstein, 2003; Kook et al., 2006). Hopx inhibits the transcriptional activity of serum response factor (SRF) in cardiomyocytes, and, by doing so, modulates cardiac growth and proliferation. Hopx inhibits SRF-dependent transcriptional activation by recruiting and forming a complex with histone deacetylase (HDAC), forming a complex that includes HDAC2. Transgenic mice that overexpress Hopx develop severe cardiac hypertrophy, cardiac fibrosis, and premature death due to a shift in the balance of pro and antihypertrophic pathways. Conversely, a mutant form of the Hopx gene, which does not recruit HDAC, does not induce hypertrophy (Kook et al., 2003). Furthermore, HDAC2 and Hopx mediate the deacetylation of GATA4, a critical cardiac transcription factor. In the absence of Hopx and HDAC2 in mouse

embryos, GATA4 hyperacetylation is associated with a substantial increase in cardiomyocyte proliferation, upregulation of GATA4 target genes, and subsequent lethality. These data suggest that HDAC2, Hopx and GATA4 coordinately regulate cardiomyocyte proliferation during embryonic development (Trivedi et al., 2010).

Meis1

Meis1 is a homeodomain transcription factor that is required for normal cardiac development and hematopoiesis (Imamura et al., 2002; Hisa et al., 2004; Azcoitia et al., 2005). siRNA-mediated knockdown of *Meis1* in neonatal rat cardiomyocytes results in a 3-fold increase in cardiomyocyte proliferation. Cardiac-specific deletion of Meis1 induces cardiomyocyte proliferation and most notably, extends the postnatal proliferative time window without any deleterious effects on cardiac function. Conversely, the overexpression of Meis1 in cardiomyocytes decreases proliferation. Furthermore, Meis1 is required for the transcriptional activation of the Cdk inhibitors $p15^{ink4b}$, $p16^{ink4a}$, and $p21^{Cip1}$, suggesting that Meis1 is a critical regulator of the cardiomyocyte cell cycle, prompting cell cycle exit (Mahmoud et al., 2013).

T-box genes

T-box (Tbx) transcription factors are highly conserved across species, expressed in a wide variety of tissue types, and are required for the development of several organs and tissues (Agulnik et al., 1996; Kiefer, 2004; Showell et al., 2004; Naiche et al., 2005). Tbx genes regulate patterning and cell fate, cell survival and/or proliferation (Kispert and Herrmann, 1993; Chapman et al., 1996; Bruneau et al., 2001; Papaioannou, 2001; Takeuchi et al., 2003; Kiefer, 2004; Showell et al., 2004; Cai et al., 2005; Naiche et al.,

2005; Singh et al., 2005; Stennard et al., 2005; Stennard and Harvey, 2005). They are also of great clinical relevance as mutations in Tbx genes cause a number of human disorders, such as DiGeorge syndrome (Tbx1) and Holt-Oram syndrome (Tbx5) (Basson et al., 1994; Li, Q. Y. et al., 1997; Bruneau et al., 2001; Jerome and Papaioannou, 2001; Lindsay et al., 2001; Packham and Brook, 2003; Naiche et al., 2005; Baban et al., 2014).

The pharyngeal mesodermal progenitor cells of the SHF are situated medially to the FHF, that gives rise to the linear heart tube and are distinguished by the expression of genes encoding the transcription factors Isl1 and Tbx1 (Kelly et al., 2001; Mjaatvedt et al., 2001; Waldo et al., 2001; Cai et al., 2003; Xu et al., 2004). Conditional depletion of *Tbx1* results in a shortened and narrow outflow tract and severe hypoplasia of the SHF due to the requirement for Tbx1 in the pharyngeal mesoderm during cardiac looping. Furthermore, Tbx1 positively regulates proliferation in the SHF through the transcriptional regulation of Fgf8, Fgf10, and Fgfr1 (Garg et al., 2001; Hu et al., 2004; Xu et al., 2004; Zhang et al., 2006; Liao et al., 2008).

Tbx5 is expressed very early in heart development in the cardiac crescent and the early heart tube. As the tube develops, Tbx5 expression becomes restricted to the cardiac regions that will form the sinus venosus, atria, and left ventricle (Bruneau et al., 1999; Liberatore et al., 2000). Tbx5 is required for normal heart development and *Tbx5*-null mice arrest around E10.5 due to severe cardiac defects (Bruneau et al., 2001). Furthermore, mice heterozygous for the *Tbx5* gene display many of the same cardiac abnormalities associated with human patients suffering from Holt-Oram syndrome (HOS), an autosomal-dominant condition associated with upper limb and cardiac

malformations (Basson et al., 1997; Li, Q. Y. et al., 1997; Bruneau et al., 2001). In *Xenopus* embryos, depletion of the *Tbx5* gene results in a dramatic decrease in cardiomyocyte number due to defects in cell proliferation. Furthermore, *Tbx5* gene depletion leads to G_1/S-phase arrest and a decrease in the embryonic cardiac mitotic index. In contrast, overexpression of Tbx5, which we show also leads to heart-specific defects, results in an increase in the cardiac mitotic index and has an inverse effect on the timing of the cardiac differentiation program. Collectively, these studies demonstrate that Tbx5 is both necessary and sufficient to determine the length of cardiac G_1/S-phase and the timing of the cardiac differentiation program (Brown et al., 2005; Goetz et al., 2006).

Tbx20 is expressed throughout the early cardiac crescent, and later in both the myocardium and the endocardium (Iio et al., 2001; Kraus et al., 2001; Cai et al., 2005). *Tbx20*-null mutants exhibit severe cardiac hypoplasia and show embryonic lethality due to defects in cardiac morphogenesis. Tbx20 directly represses Tbx2 in the developing heart; furthermore, Tbx2 itself directly represses Nmyc1 activity (Cai et al., 2005). Nmyc1 is required for myocardial proliferation, and *Nmyc1*-null mice show pronounced cardiac hypoplasia (Davis and Bradley, 1993). Together, these data demonstrate that Tbx20 is a key component of a genetic network that regulates cell proliferation and morphogenesis.

Casz1-dependent mechanisms

Studies investigating the transcriptional regulation of cardiogenesis reveal a role for the para-zinc finger transcription factor Casz1 in vertebrate heart development. Depletion of Casz1 in *Xenopus* embryos results in the failure of a subset of progenitor cells to differentiate into cardiomyocytes, resulting in aberrant cardiac morphogenesis (Christine and Conlon, 2008). There have been relatively few studies of Casz1 in mammals. In one of these studies, however, a partial murine Casz1 cDNA was shown to be expressed in the developing heart (Vacalla and Theil, 2002), whereas another study showed that CASZ1 is expressed in adult human heart tissue (Liu et al., 2006).

Recently, I demonstrated that Casz1 is expressed in cardiomyocytes during the earliest stages of mammalian heart development and used genetic fate mapping to show that Casz1-positive cells give rise to derivatives of both the FHF and SHF, including cardiomyocytes in the left and right ventricles, and in the left and right atria (Dorr et al., in review). Cardiac-specific depletion of *Casz1* using both the *Nkx2.5-Cre* driver (Moses et al., 2001) and the *Islet1-Cre* driver (Srinivas et al., 2001) results in embryonic lethality due to severe cardiac hypoplasia. Furthermore, Casz1 plays an essential role in the cardiomyocyte cell cycle. Loss of Casz1 leads to a prolonged or arrested G_1-phase that is associated with a marked reduction in DNA synthesis, an increase in phosphorylated Rb, and a decrease in the cardiac mitotic index. Taken together, these results demonstrate a role for Casz1 in the G_1-to-S-phase progression of cardiomyocytes (Dorr et al., in review).

DISSERTATION GOALS

Our findings in *Xenopus* imply that cardiomyocytes do not differentiate in a uniform manner and suggest that cells located in the ventral region of the heart differentiate in response to localized signals. Although those studies demonstrated a requirement for Casz1 during development, the genetic requirement for Casz1 remains unclear. *Xenopus* is an excellent model organism for developmental studies. However, it is not a genetic model organism, and morpholino knockdown is not suitable for tissue-specific investigations. Furthermore, unlike the mammalian heart, the *Xenopus* heart is three chambered, featuring two atria and one common ventricle. The laboratory mouse is an ideal model organism for cardiovascular genetic studies. Murine cardiac development is well characterized and quite similar to that of humans. In addition, the mouse genome is quite amenable to modification using the techniques of classical transgenesis, gene targeting, and site-specific recombination. For these reasons, I sought to determine the genetic requirement for Casz1 during murine cardiac development. In chapter 2, I show that cardiac-specific depletion of the *Casz1* gene results in severe cardiac hypoplasia, and ventricular septal defects leading to embryonic lethality. Here, I show that Casz1 regulates cardiomyocyte proliferation and is necessary for proper G_1-to-S-phase transition of the embryonic cardiac cell cycle. Next, I demonstrate using RNA sequencing technologies that pathways involved in cell growth and proliferation are misregulated in hearts depleted of *Casz1*. Collectively, this work will enhance the understanding of *Casz1* and provide further insight into the cardiac transcriptional network required for proper heart growth.

Figure 1.1 The Cardiomyocyte Cell Cycle. Factors involved in cardiomyocyte cell cycle progression.

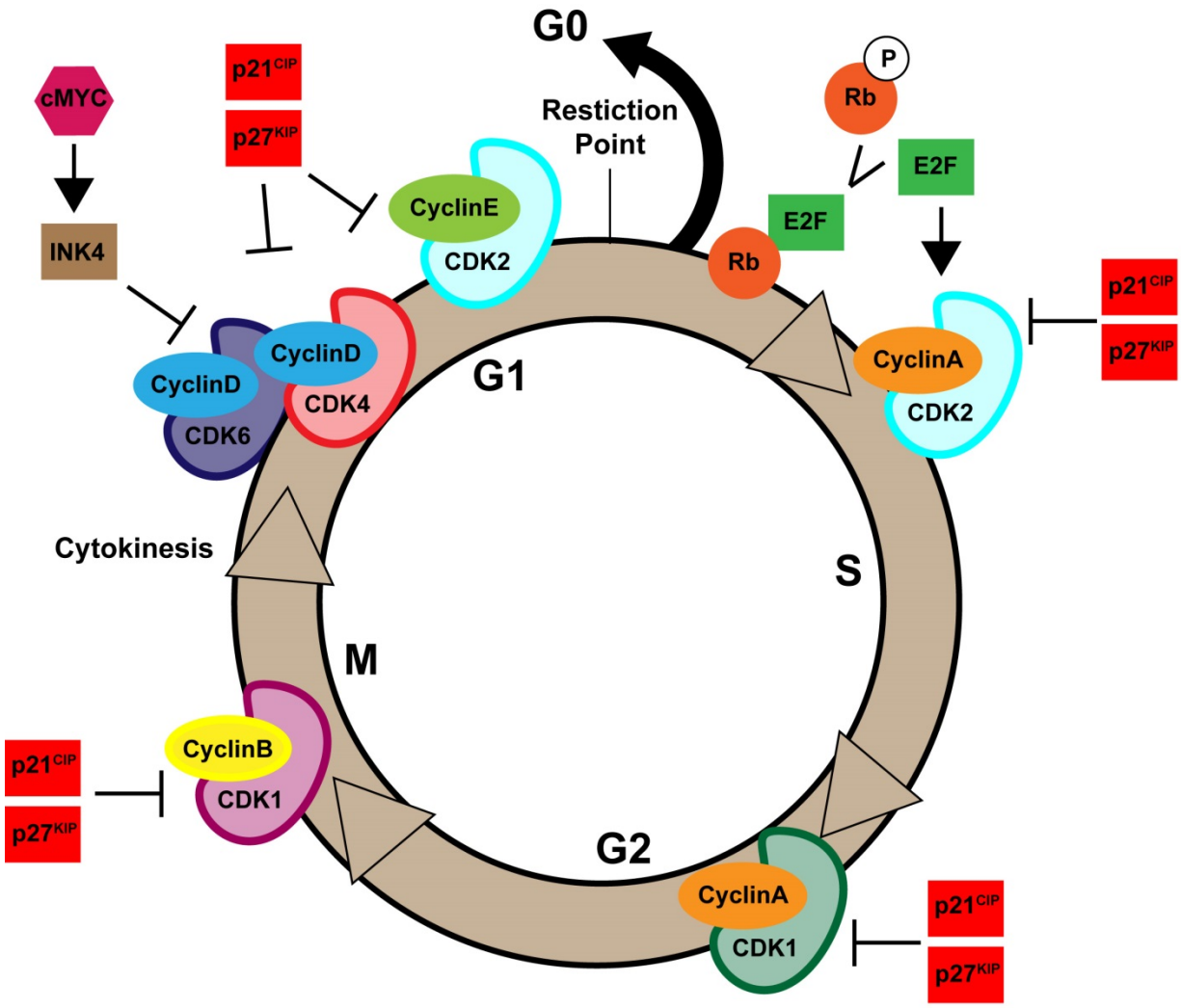

Figure 1.2 Control of Cardiomyocyte Growth. Schematic representation of the developmentally determined forms of cell cycle control and growth at different developmental stages.

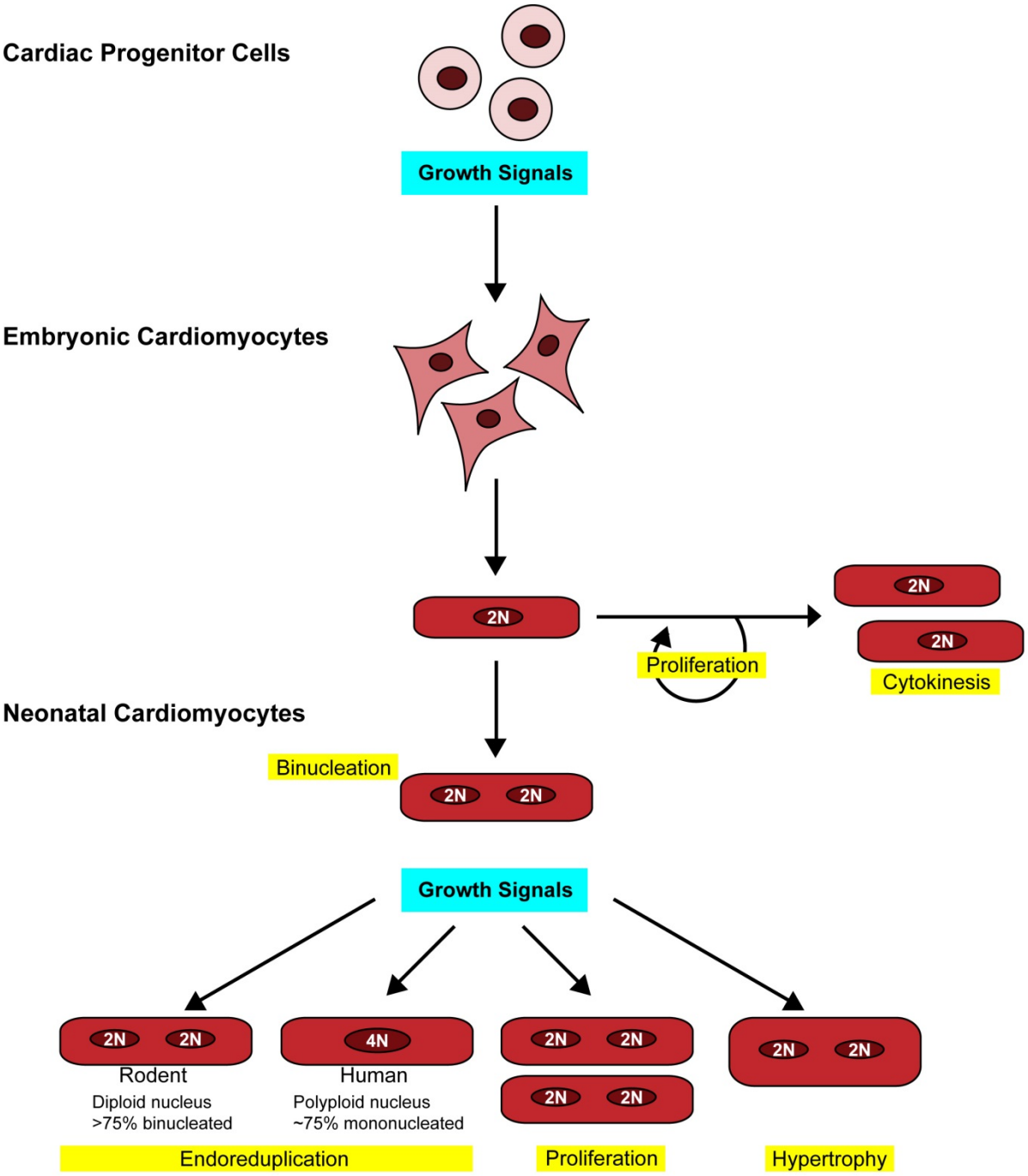

Figure 1.3. Cardiomyocyte Structure. In muscle cells, contractile myofibrils are organized into sarcomeres. During karyokinesis, the sarcomeric Z-disks and M-bands disassemble in the midzone region.

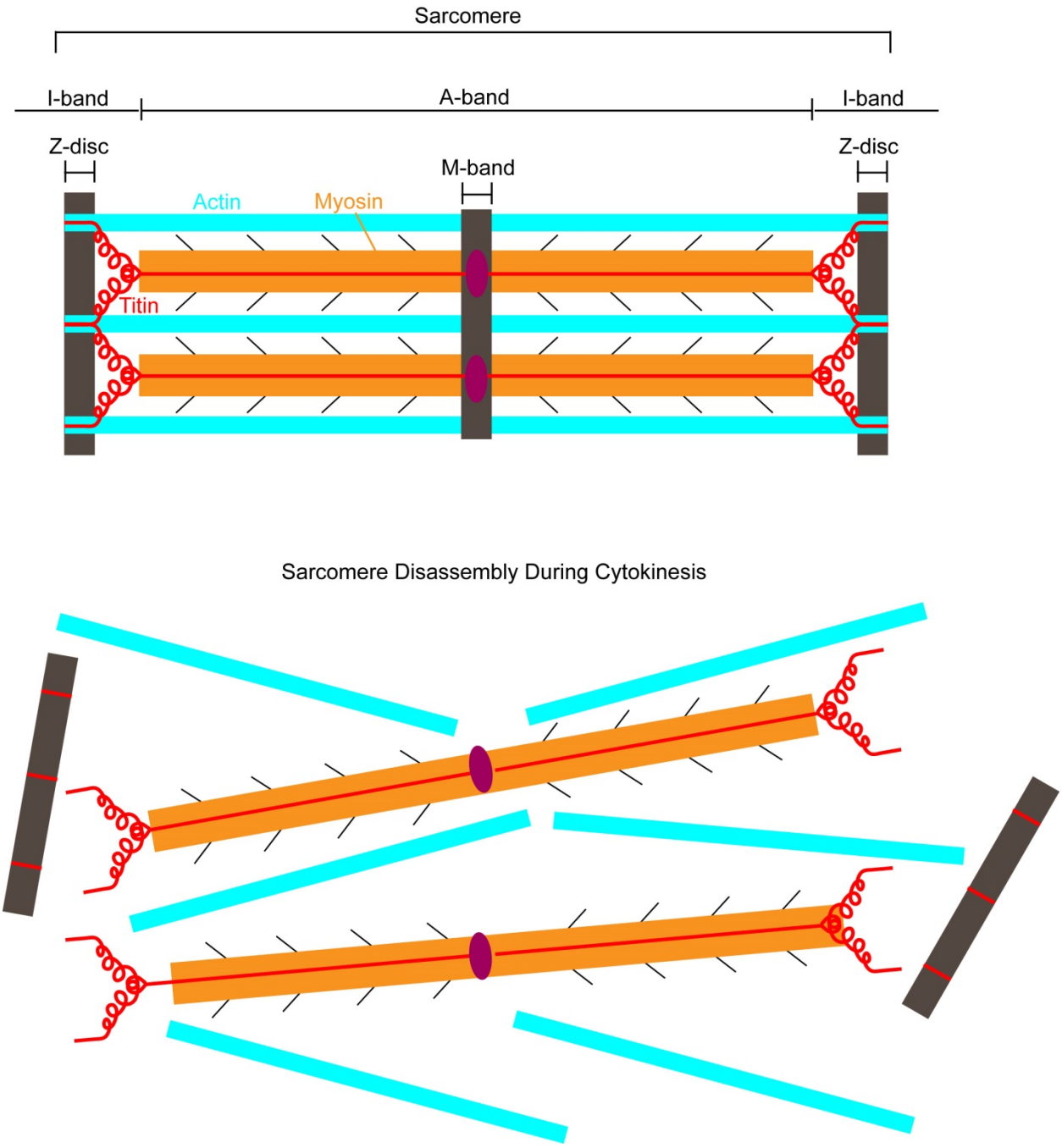

Figure 1.4. Growth Factors that Regulate Cardiomyocyte Proliferation . Illustration showing the core features of the Hippo, Wnt, Igf, Fgf, Periostin, and Nrg signaling pathways. This simplified schematic summarizes the key steps from ligand binding to target gene transcription for each pathway.

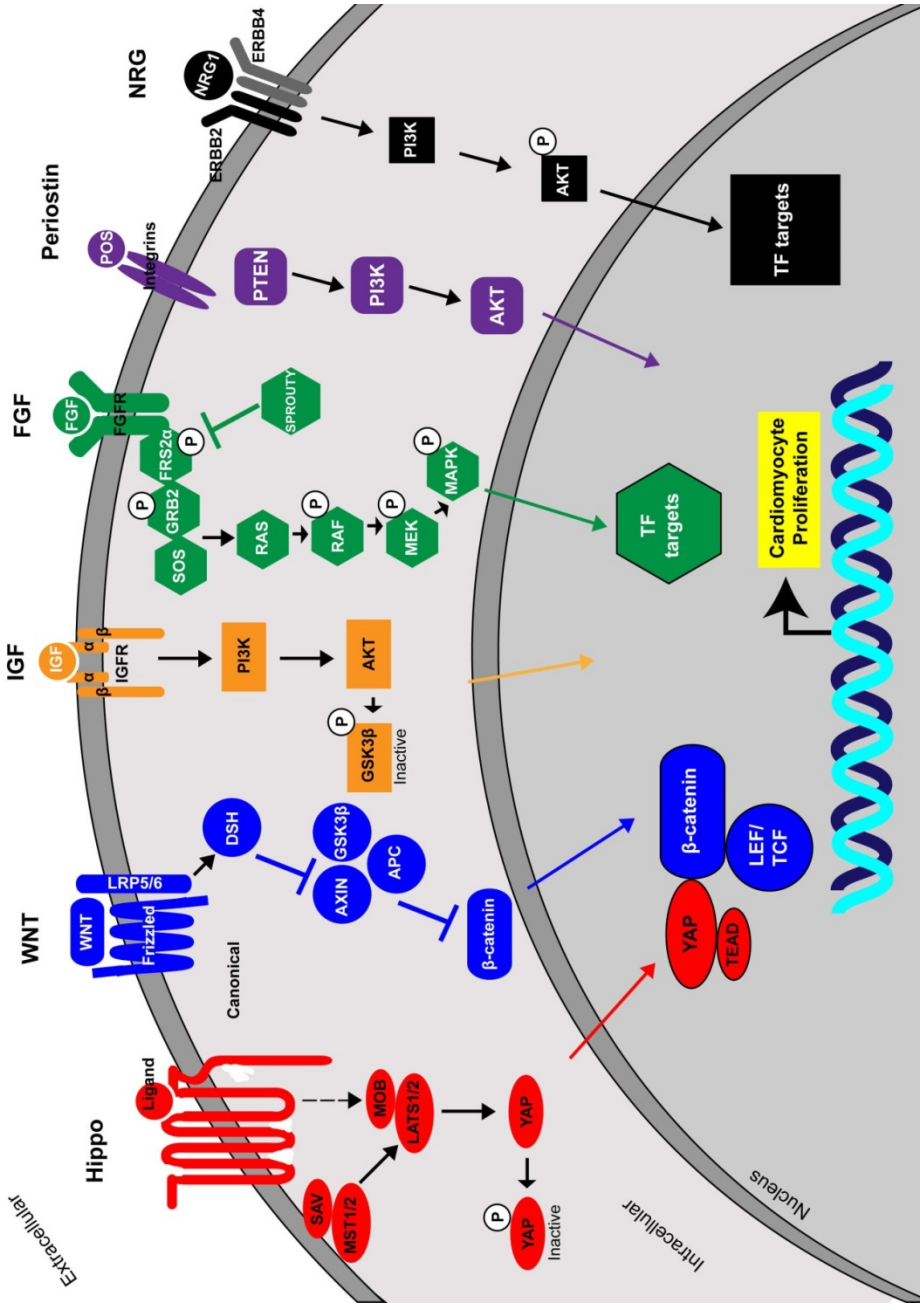

Figure 1.5. miRNAs Involved in Cardiomyocyte Proliferation. Regulation of cardiomyocyte proliferation by microRNAS (miRNAs). miRNAs can positively or negatively regulated cardiomyocyte proliferation.

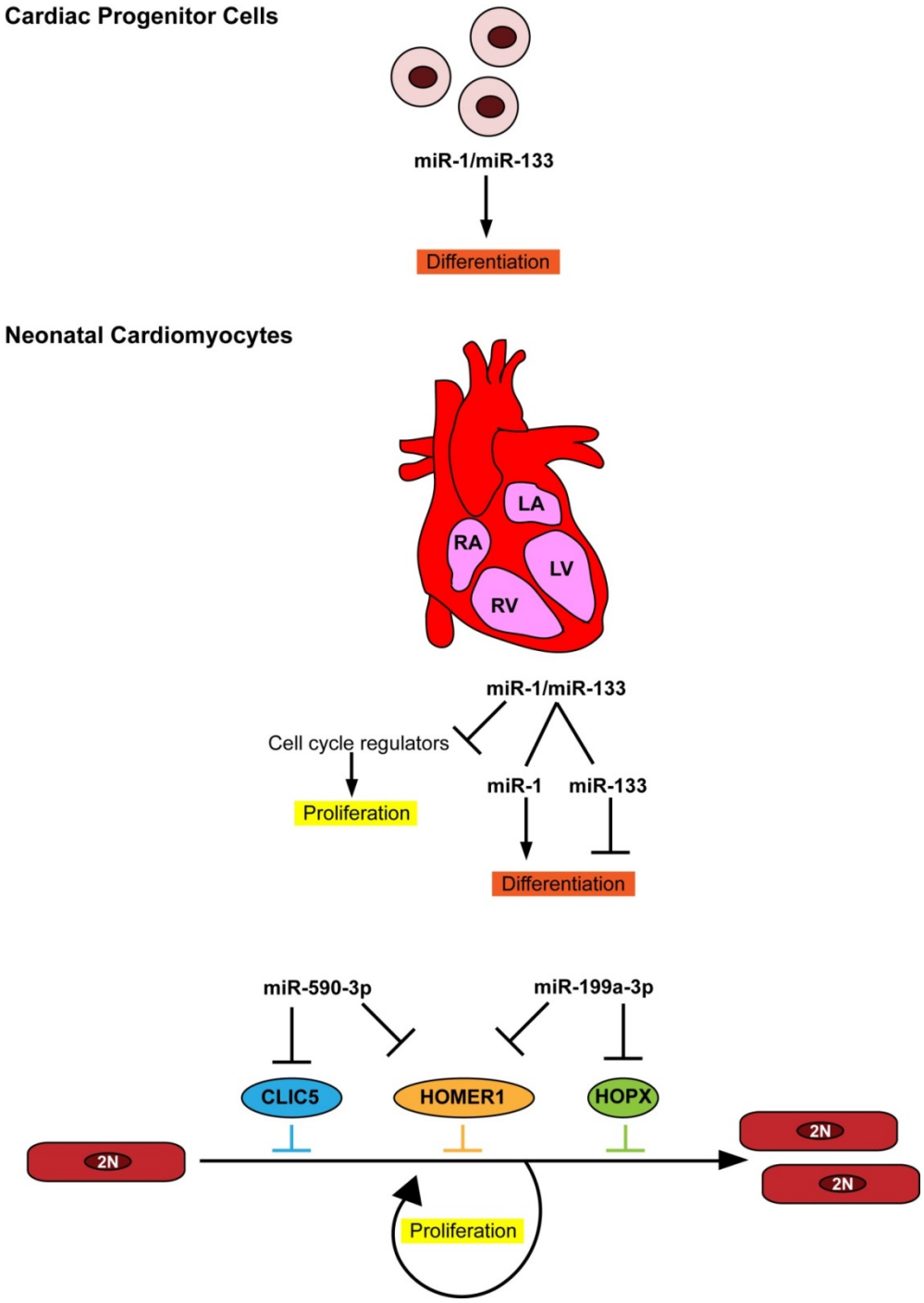

Table 1.1. The Major Cyclins and Cyclin-Dependent Kinases Involved in The Cardiomyocyte Cell Cycle

GENE	FUNCTION	CELL CYCLE PHASE
CELL CYCLE MEDIATORS		
Cyclin D1	Cdk4/6 cofactor; positive regulator of restriction point transit	G1/S
Cyclin D2	Cdk4/6 cofactor; positive regulator of restriction point transit	G1/S
Cyclin D3	Cdk4/6 cofactor; positive regulator of restriction point transit	G1/S
Cyclin E	Cdk2 cofactor; promotes G1-S transition	G1/S
Cyclin A	Cdk1/2 cofactor; positive regulator of S and G2-M transition	G2/M
Cyclin B	Cdk1 cofactor; promotes G2-M transition	G2/M
Cdk1	Promotes G2-M transition	G2/M
Cdk2	Phosphorylates Rb family members; promotes G1-S transition	G1/S
Cdk4	Phosphorylates Rb family members; promotes restriction point transit	G1/S
Cdk6	Phosphorylates Rb family members	G1/S
CELL CYCLE INHIBITORS		
INK4	Inhibits Cdk2,4,6 activity; blocks restriction point and G1-S transition	G1/S
p21	Inhibits Cdk2,4,6 activity; blocks restriction point and G1-S transition	G1/S
p27	Inhibits Cdk2,4,6 activity; blocks restriction point and G1-S transition	G1/S
RB	Regulates G1-S transition by inhibiting E2F activity	G1/S
TRANSCRIPTION FACTORS		
E2F	Activates cell cycle transcription	G1-S-G2/M

REFERENCES

Adler, C. P. (1975). Relationship between deoxyribonucleic acid content and nucleoli in human heart muscle cells and estimation of cell number during cardiac growth and hyperfunction. *Recent advances in studies on cardiac structure and metabolism* **8**, 373-386.

Adler, C. P. and Costabel, U. (1975). Cell number in human heart in atrophy, hypertrophy, and under the influence of cytostatics. *Recent advances in studies on cardiac structure and metabolism* **6**, 343-355.

Adler, C. P. and Friedburg, H. (1986). Myocardial DNA content, ploidy level and cell number in geriatric hearts: post-mortem examinations of human myocardium in old age. *Journal of molecular and cellular cardiology* **18**, 39-53.

Agulnik, S. I., Garvey, N., Hancock, S., Ruvinsky, I., Chapman, D. L., Agulnik, I., Bollag, R., Papaioannou, V. and Silver, L. M. (1996). Evolution of mouse T-box genes by tandem duplication and cluster dispersion. *Genetics* **144**, 249-254.

Ahuja, P., Sdek, P. and MacLellan, W. R. (2007). Cardiac myocyte cell cycle control in development, disease, and regeneration. *Physiological reviews* **87**, 521-544.

Alberts, B. (2015). Molecular biology of the cell. New York, NY: Garland Science, Taylor and Francis Group.

Ali, S. R., Hippenmeyer, S., Saadat, L. V., Luo, L., Weissman, I. L. and Ardehali, R. (2014). Existing cardiomyocytes generate cardiomyocytes at a low rate after birth in mice. *Proceedings of the National Academy of Sciences of the United States of America* **111**, 8850-8855.

Armstrong, M. T., Lee, D. Y. and Armstrong, P. B. (2000). Regulation of proliferation of the fetal myocardium. *Developmental dynamics : an official publication of the American Association of Anatomists* **219**, 226-236.

Azcoitia, V., Aracil, M., Martinez, A. C. and Torres, M. (2005). The homeodomain protein Meis1 is essential for definitive hematopoiesis and vascular patterning in the mouse embryo. *Developmental biology* **280**, 307-320.

Baban, A., Pitto, L., Pulignani, S., Cresci, M., Mariani, L., Gambacciani, C., Digilio, M. C., Pongiglione, G. and Albanese, S. (2014). Holt-Oram syndrome with

intermediate atrioventricular canal defect, and aortic coarctation: functional characterization of a de novo TBX5 mutation. *American journal of medical genetics. Part A* **164A**, 1419-1424.

Barrow, J. R. (2006). Wnt/PCP signaling: a veritable polar star in establishing patterns of polarity in embryonic tissues. *Seminars in cell & developmental biology* **17**, 185-193.

Bartel, D. P. (2004). MicroRNAs: genomics, biogenesis, mechanism, and function. *Cell* **116**, 281-297.

Bartel, D. P. (2009). MicroRNAs: target recognition and regulatory functions. *Cell* **136**, 215-233.

Baserga, R. (1985). The biology of cell reproduction. Cambridge, Mass.: Harvard University Press.

Basson, C. T., Cowley, G. S., Solomon, S. D., Weissman, B., Poznanski, A. K., Traill, T. A., Seidman, J. G. and Seidman, C. E. (1994). The clinical and genetic spectrum of the Holt-Oram syndrome (heart-hand syndrome). *The New England journal of medicine* **330**, 885-891.

Basson, C. T., Bachinsky, D. R., Lin, R. C., Levi, T., Elkins, J. A., Soults, J., Grayzel, D., Kroumpouzou, E., Traill, T. A., Leblanc-Straceski, J. et al. (1997). Mutations in human TBX5 [corrected] cause limb and cardiac malformation in Holt-Oram syndrome. *Nature genetics* **15**, 30-35.

Beenken, A. and Mohammadi, M. (2009). The FGF family: biology, pathophysiology and therapy. *Nature reviews. Drug discovery* **8**, 235-253.

Beiman, M., Shilo, B. Z. and Volk, T. (1996). Heartless, a Drosophila FGF receptor homolog, is essential for cell migration and establishment of several mesodermal lineages. *Genes & development* **10**, 2993-3002.

Bellomo, D., Headrick, J. P., Silins, G. U., Paterson, C. A., Thomas, P. S., Gartside, M., Mould, A., Cahill, M. M., Tonks, I. D., Grimmond, S. M. et al. (2000). Mice lacking the vascular endothelial growth factor-B gene (Vegfb) have smaller hearts, dysfunctional coronary vasculature, and impaired recovery from cardiac ischemia. *Circulation research* **86**, E29-35.

Bergmann, M. W. (2010). WNT signaling in adult cardiac hypertrophy and remodeling: lessons learned from cardiac development. *Circulation research* **107**, 1198-1208.

Bergmann, O., Bhardwaj, R. D., Bernard, S., Zdunek, S., Barnabe-Heider, F., Walsh, S., Zupicich, J., Alkass, K., Buchholz, B. A., Druid, H. et al. (2009). Evidence for cardiomyocyte renewal in humans. *Science* **324**, 98-102.

Bersell, K., Arab, S., Haring, B. and Kuhn, B. (2009). Neuregulin1/ErbB4 signaling induces cardiomyocyte proliferation and repair of heart injury. *Cell* **138**, 257-270.

Bettencourt-Dias, M., Mittnacht, S. and Brockes, J. P. (2003). Heterogeneous proliferative potential in regenerative adult newt cardiomyocytes. *Journal of cell science* **116**, 4001-4009.

Bishop, S. P. (1990). The myocardial cell: normal growth, cardiac hypertrophy and response to injury. *Toxicologic pathology* **18**, 438-453.

Boissy, P., Saltel, F., Bouniol, C., Jurdic, P. and Machuca-Gayet, I. (2002). Transcriptional activity of nuclei in multinucleated osteoclasts and its modulation by calcitonin. *Endocrinology* **143**, 1913-1921.

Bottcher, R. T. and Niehrs, C. (2005). Fibroblast growth factor signaling during early vertebrate development. *Endocrine reviews* **26**, 63-77.

Brade, T., Manner, J. and Kuhl, M. (2006). The role of Wnt signalling in cardiac development and tissue remodelling in the mature heart. *Cardiovascular research* **72**, 198-209.

Brotherton, D. H., Dhanaraj, V., Wick, S., Brizuela, L., Domaille, P. J., Volyanik, E., Xu, X., Parisini, E., Smith, B. O., Archer, S. J. et al. (1998). Crystal structure of the complex of the cyclin D-dependent kinase Cdk6 bound to the cell-cycle inhibitor p19INK4d. *Nature* **395**, 244-250.

Brown, C. B. and Baldwin, H. S. (2006). Neural crest contribution to the cardiovascular system. *Advances in experimental medicine and biology* **589**, 134-154.

Brown, D. D., Martz, S. N., Binder, O., Goetz, S. C., Price, B. M., Smith, J. C. and Conlon, F. L. (2005). Tbx5 and Tbx20 act synergistically to control vertebrate heart morphogenesis. *Development* **132**, 553-563.

Bruneau, B. G., Logan, M., Davis, N., Levi, T., Tabin, C. J., Seidman, J. G. and Seidman, C. E. (1999). Chamber-specific cardiac expression of Tbx5 and heart defects in Holt-Oram syndrome. *Developmental biology* **211**, 100-108.

Bruneau, B. G., Nemer, G., Schmitt, J. P., Charron, F., Robitaille, L., Caron, S., Conner, D. A., Gessler, M., Nemer, M., Seidman, C. E. et al. (2001). A murine model of Holt-Oram syndrome defines roles of the T-box transcription factor Tbx5 in cardiogenesis and disease. *Cell* **106**, 709-721.

Bry, M., Kivela, R., Holopainen, T., Anisimov, A., Tammela, T., Soronen, J., Silvola, J., Saraste, A., Jeltsch, M., Korpisalo, P. et al. (2010). Vascular endothelial growth factor-B acts as a coronary growth factor in transgenic rats without inducing angiogenesis, vascular leak, or inflammation. *Circulation* **122**, 1725-1733.

Buckingham, M., Meilhac, S. and Zaffran, S. (2005). Building the mammalian heart from two sources of myocardial cells. *Nature reviews. Genetics* **6**, 826-835.

Bueno, O. F., De Windt, L. J., Tymitz, K. M., Witt, S. A., Kimball, T. R., Klevitsky, R., Hewett, T. E., Jones, S. P., Lefer, D. J., Peng, C. F. et al. (2000). The MEK1-ERK1/2 signaling pathway promotes compensated cardiac hypertrophy in transgenic mice. *The EMBO journal* **19**, 6341-6350.

Butcher, J. T., Norris, R. A., Hoffman, S., Mjaatvedt, C. H. and Markwald, R. R. (2007). Periostin promotes atrioventricular mesenchyme matrix invasion and remodeling mediated by integrin signaling through Rho/PI 3-kinase. *Developmental biology* **302**, 256-266.

Cai, C. L., Liang, X., Shi, Y., Chu, P. H., Pfaff, S. L., Chen, J. and Evans, S. (2003). Isl1 identifies a cardiac progenitor population that proliferates prior to differentiation and contributes a majority of cells to the heart. *Developmental cell* **5**, 877-889.

Cai, C. L., Zhou, W., Yang, L., Bu, L., Qyang, Y., Zhang, X., Li, X., Rosenfeld, M. G., Chen, J. and Evans, S. (2005). T-box genes coordinate regional rates of proliferation and regional specification during cardiogenesis. *Development* **132**, 2475-2487.

Callus, B. A., Verhagen, A. M. and Vaux, D. L. (2006). Association of mammalian sterile twenty kinases, Mst1 and Mst2, with hSalvador via C-terminal coiled-coil domains, leads to its stabilization and phosphorylation. *The FEBS journal* **273**, 4264-4276.

Chan, E. H., Nousiainen, M., Chalamalasetty, R. B., Schafer, A., Nigg, E. A. and Sillje, H. H. (2005). The Ste20-like kinase Mst2 activates the human large tumor suppressor kinase Lats1. *Oncogene* **24**, 2076-2086.

Chan, F. K., Zhang, J., Cheng, L., Shapiro, D. N. and Winoto, A. (1995). Identification of human and mouse p19, a novel CDK4 and CDK6 inhibitor with homology to p16ink4. *Molecular and cellular biology* **15**, 2682-2688.

Chapman, D. L., Garvey, N., Hancock, S., Alexiou, M., Agulnik, S. I., Gibson-Brown, J. J., Cebra-Thomas, J., Bollag, R. J., Silver, L. M. and Papaioannou, V. E. (1996). Expression of the T-box family genes, Tbx1-Tbx5, during early mouse development. *Developmental dynamics : an official publication of the American Association of Anatomists* **206**, 379-390.

Chellaiah, A. T., McEwen, D. G., Werner, S., Xu, J. and Ornitz, D. M. (1994). Fibroblast growth factor receptor (FGFR) 3. Alternative splicing in immunoglobulin-like domain III creates a receptor highly specific for acidic FGF/FGF-1. *The Journal of biological chemistry* **269**, 11620-11627.

Chen, T., Chang, T. C., Kang, J. O., Choudhary, B., Makita, T., Tran, C. M., Burch, J. B., Eid, H. and Sucov, H. M. (2002). Epicardial induction of fetal cardiomyocyte proliferation via a retinoic acid-inducible trophic factor. *Developmental biology* **250**, 198-207.

Christine, K. S. and Conlon, F. L. (2008). Vertebrate CASTOR is required for differentiation of cardiac precursor cells at the ventral midline. *Developmental cell* **14**, 616-623.

Christoffels, V. M., Habets, P. E., Franco, D., Campione, M., de Jong, F., Lamers, W. H., Bao, Z. Z., Palmer, S., Biben, C., Harvey, R. P. et al. (2000). Chamber formation and morphogenesis in the developing mammalian heart. *Developmental biology* **223**, 266-278.

Clubb, F. J., Jr. and Bishop, S. P. (1984). Formation of binucleated myocardial cells in the neonatal rat. An index for growth hypertrophy. *Laboratory investigation; a journal of technical methods and pathology* **50**, 571-577.

Cohen, E. D., Tian, Y. and Morrisey, E. E. (2008). Wnt signaling: an essential regulator of cardiovascular differentiation, morphogenesis and progenitor self-renewal. *Development* **135**, 789-798.

Colvin, J. S., White, A. C., Pratt, S. J. and Ornitz, D. M. (2001). Lung hypoplasia and neonatal death in Fgf9-null mice identify this gene as an essential regulator of lung mesenchyme. *Development* **128**, 2095-2106.

Colvin, J. S., Feldman, B., Nadeau, J. H., Goldfarb, M. and Ornitz, D. M. (1999). Genomic organization and embryonic expression of the mouse fibroblast growth factor 9 gene. *Developmental dynamics : an official publication of the American Association of Anatomists* **216**, 72-88.

Conlon, I. and Raff, M. (1999). Size control in animal development. *Cell* **96**, 235-244.

Creazzo, T. L., Godt, R. E., Leatherbury, L., Conway, S. J. and Kirby, M. L. (1998). Role of cardiac neural crest cells in cardiovascular development. *Annual review of physiology* **60**, 267-286.

Cuevas, P., Reimers, D., Carceller, F., Martinez-Coso, V., Redondo-Horcajo, M., Saenz de Tejada, I. and Gimenez-Gallego, G. (1997). Fibroblast growth factor-1 prevents myocardial apoptosis triggered by ischemia reperfusion injury. *European journal of medical research* **2**, 465-468.

Davis, A. and Bradley, A. (1993). Mutation of N-myc in mice: what does the phenotype tell us? *BioEssays : news and reviews in molecular, cellular and developmental biology* **15**, 273-275.

De, A. (2011). Wnt/Ca2+ signaling pathway: a brief overview. *Acta biochimica et biophysica Sinica* **43**, 745-756.

DeChiara, T. M., Robertson, E. J. and Efstratiadis, A. (1991). Parental imprinting of the mouse insulin-like growth factor II gene. *Cell* **64**, 849-859.

DeRuiter, M. C., Poelmann, R. E., VanderPlas-de Vries, I., Mentink, M. M. and Gittenberger-de Groot, A. C. (1992). The development of the myocardium and endocardium in mouse embryos. Fusion of two heart tubes? *Anatomy and embryology* **185**, 461-473.

Devault, A., Cavadore, J. C., Fesquet, D., Labbe, J. C., Lorca, T., Picard, A., Strausfeld, U. and Doree, M. (1991). Concerted roles of cyclin A, cdc25+ mitotic inducer, and type 2A phosphatase in activating the cyclin B/cdc2 protein kinase at the G2/M phase transition. *Cold Spring Harbor symposia on quantitative biology* **56**, 503-513.

Devine, W. P., Wythe, J. D., George, M., Koshiba-Takeuchi, K. and Bruneau, B. G. (2014). Early patterning and specification of cardiac progenitors in gastrulating mesoderm. *eLife* **3**.

Dolk, H., Loane, M. and Garne, E. (2010a). The prevalence of congenital anomalies in Europe. *Advances in experimental medicine and biology* **686**, 349-364.

Dolk, H., Loane, M. A., Abramsky, L., de Walle, H. and Garne, E. (2010b). Birth prevalence of congenital heart disease. *Epidemiology* **21**, 275-277; author reply 277.

Dominguez, J. N., Meilhac, S. M., Bland, Y. S., Buckingham, M. E. and Brown, N. A. (2012). Asymmetric fate of the posterior part of the second heart field results in unexpected left/right contributions to both poles of the heart. *Circulation research* **111**, 1323-1335.

Dong, J., Feldmann, G., Huang, J., Wu, S., Zhang, N., Comerford, S. A., Gayyed, M. F., Anders, R. A., Maitra, A. and Pan, D. (2007). Elucidation of a universal size-control mechanism in Drosophila and mammals. *Cell* **130**, 1120-1133.

Dorn, G. W., 2nd. (2007). The fuzzy logic of physiological cardiac hypertrophy. *Hypertension* **49**, 962-970.

Dorn, G. W., 2nd and Force, T. (2005). Protein kinase cascades in the regulation of cardiac hypertrophy. *The Journal of clinical investigation* **115**, 527-537.

Dorn, G. W., 2nd, Robbins, J. and Sugden, P. H. (2003). Phenotyping hypertrophy: eschew obfuscation. *Circulation research* **92**, 1171-1175.

Dowell, R. T. and McManus, R. E., 3rd. (1978). Pressure-induced cardiac enlargement in neonatal and adult rats. Left ventricular functional characteristics and evidence of cardiac muscle cell proliferation in the neonate. *Circulation research* **42**, 303-310.

Dunwoodie, S. L. (2007). Combinatorial signaling in the heart orchestrates cardiac induction, lineage specification and chamber formation. *Seminars in cell & developmental biology* **18**, 54-66.

Eggenschwiler, J., Ludwig, T., Fisher, P., Leighton, P. A., Tilghman, S. M. and Efstratiadis, A. (1997). Mouse mutant embryos overexpressing IGF-II exhibit

phenotypic features of the Beckwith-Wiedemann and Simpson-Golabi-Behmel syndromes. *Genes & development* **11**, 3128-3142.

Eisenberg, L. M. and Eisenberg, C. A. (2006). Wnt signal transduction and the formation of the myocardium. *Developmental biology* **293**, 305-315.

Engel, F. B., Hsieh, P. C., Lee, R. T. and Keating, M. T. (2006). FGF1/p38 MAP kinase inhibitor therapy induces cardiomyocyte mitosis, reduces scarring, and rescues function after myocardial infarction. *Proceedings of the National Academy of Sciences of the United States of America* **103**, 15546-15551.

Engel, F. B., Schebesta, M., Duong, M. T., Lu, G., Ren, S., Madwed, J. B., Jiang, H., Wang, Y. and Keating, M. T. (2005). p38 MAP kinase inhibition enables proliferation of adult mammalian cardiomyocytes. *Genes & development* **19**, 1175-1187.

Engelmann, G. L., Dionne, C. A. and Jaye, M. C. (1993). Acidic fibroblast growth factor and heart development. Role in myocyte proliferation and capillary angiogenesis. *Circulation research* **72**, 7-19.

Erokhnia, I. L. (1968a). The proliferation and DNA synthesis during early stages of myocardial development. *Tsiotologiya* **10**, 162-172.

Erokhnia, I. L. (1968b). Proliferation dynamics of cellular elements in the differentiating mouse myocardium. *Tsiotologiya* **10**, 1391-1409.

Eulalio, A., Mano, M., Dal Ferro, M., Zentilin, L., Sinagra, G., Zacchigna, S. and Giacca, M. (2012). Functional screening identifies miRNAs inducing cardiac regeneration. *Nature* **492**, 376-381.

Fagotto, F. and Gumbiner, B. M. (1996). Cell contact-dependent signaling. *Developmental biology* **180**, 445-454.

Fahed, A. C., Gelb, B. D., Seidman, J. G. and Seidman, C. E. (2013). Genetics of congenital heart disease: the glass half empty. *Circulation research* **112**, 707-720.

Falls, D. L. (2003). Neuregulins: functions, forms, and signaling strategies. *Experimental cell research* **284**, 14-30.

Field, C., Li, R. and Oegema, K. (1999). Cytokinesis in eukaryotes: a mechanistic comparison. *Current opinion in cell biology* **11**, 68-80.

Field, C. M. and Alberts, B. M. (1995). Anillin, a contractile ring protein that cycles from the nucleus to the cell cortex. *The Journal of cell biology* **131**, 165-178.

Flink, I. L., Oana, S., Maitra, N., Bahl, J. J. and Morkin, E. (1998). Changes in E2F complexes containing retinoblastoma protein family members and increased cyclin-dependent kinase inhibitor activities during terminal differentiation of cardiomyocytes. *Journal of molecular and cellular cardiology* **30**, 563-578.

Fraidenraich, D., Stillwell, E., Romero, E., Wilkes, D., Manova, K., Basson, C. T. and Benezra, R. (2004). Rescue of cardiac defects in id knockout embryos by injection of embryonic stem cells. *Science* **306**, 247-252.

Frey, N., Katus, H. A., Olson, E. N. and Hill, J. A. (2004). Hypertrophy of the heart: a new therapeutic target? *Circulation* **109**, 1580-1589.

Fuller, S. J., Sivarajah, K. and Sugden, P. H. (2008). ErbB receptors, their ligands, and the consequences of their activation and inhibition in the myocardium. *Journal of molecular and cellular cardiology* **44**, 831-854.

Garg, V., Yamagishi, C., Hu, T., Kathiriya, I. S., Yamagishi, H. and Srivastava, D. (2001). Tbx1, a DiGeorge syndrome candidate gene, is regulated by sonic hedgehog during pharyngeal arch development. *Developmental biology* **235**, 62-73.

Gassmann, M., Casagranda, F., Orioli, D., Simon, H., Lai, C., Klein, R. and Lemke, G. (1995). Aberrant neural and cardiac development in mice lacking the ErbB4 neuregulin receptor. *Nature* **378**, 390-394.

Gillespie, D. M. and Stevens, D. F. (1972). A study of multinucleated tumor cells demonstrating the effect of transplant duration on serum changes in cancer-bearing hamsters. *Cancer research* **32**, 1577-1579.

Glotzer, M. (1997). The mechanism and control of cytokinesis. *Current opinion in cell biology* **9**, 815-823.

Goetz, S. C., Brown, D. D. and Conlon, F. L. (2006). TBX5 is required for embryonic cardiac cell cycle progression. *Development* **133**, 2575-2584.

Goldspink, D. F., Lewis, S. E. and Merry, B. J. (1986). Effects of aging and long term dietary intervention on protein turnover and growth of ventricular muscle in the rat heart. *Cardiovascular research* **20**, 672-678.

Gonzalez, M. A., Tachibana, K. E., Adams, D. J., van der Weyden, L., Hemberger, M., Coleman, N., Bradley, A. and Laskey, R. A. (2006). Geminin is essential to prevent endoreduplication and to form pluripotent cells during mammalian development. *Genes & development* **20**, 1880-1884.

Gordon, M. D. and Nusse, R. (2006). Wnt signaling: multiple pathways, multiple receptors, and multiple transcription factors. *The Journal of biological chemistry* **281**, 22429-22433.

Gorza, L., Schiaffino, S. and Vitadello, M. (1988). Heart conduction system: a neural crest derivative? *Brain research* **457**, 360-366.

Green, J. L., Inoue, T. and Sternberg, P. W. (2008). Opposing Wnt pathways orient cell polarity during organogenesis. *Cell* **134**, 646-656.

Grego-Bessa, J., Luna-Zurita, L., del Monte, G., Bolos, V., Melgar, P., Arandilla, A., Garratt, A. N., Zang, H., Mukouyama, Y. S., Chen, H. et al. (2007). Notch signaling is essential for ventricular chamber development. *Developmental cell* **12**, 415-429.

Gregory, S. L., Kortschak, R. D., Kalionis, B. and Saint, R. (1996). Characterization of the dead ringer gene identifies a novel, highly conserved family of sequence-specific DNA-binding proteins. *Molecular and cellular biology* **16**, 792-799.

Grossman, W., Jones, D. and McLaurin, L. P. (1975). Wall stress and patterns of hypertrophy in the human left ventricle. *The Journal of clinical investigation* **56**, 56-64.

Grubb, D. R., Luo, J., Yu, Y. L. and Woodcock, E. A. (2012). Scaffolding protein Homer 1c mediates hypertrophic responses downstream of Gq in cardiomyocytes. *FASEB journal : official publication of the Federation of American Societies for Experimental Biology* **26**, 596-603.

Guan, K. L., Jenkins, C. W., Li, Y., Nichols, M. A., Wu, X., O'Keefe, C. L., Matera, A. G. and Xiong, Y. (1994). Growth suppression by p18, a p16INK4/MTS1- and p14INK4B/MTS2-related CDK6 inhibitor, correlates with wild-type pRb function. *Genes & development* **8**, 2939-2952.

Hall, Z. W. and Ralston, E. (1989). Nuclear domains in muscle cells. *Cell* **59**, 771-772.

Hannon, G. J. and Beach, D. (1994). p15INK4B is a potential effector of TGF-beta-induced cell cycle arrest. *Nature* **371**, 257-261.

He, X. (2004). Wnt signaling went derailed again: a new track via the LIN-18 receptor? *Cell* **118**, 668-670.

He, X., Semenov, M., Tamai, K. and Zeng, X. (2004). LDL receptor-related proteins 5 and 6 in Wnt/beta-catenin signaling: arrows point the way. *Development* **131**, 1663-1677.

Heallen, T., Zhang, M., Wang, J., Bonilla-Claudio, M., Klysik, E., Johnson, R. L. and Martin, J. F. (2011). Hippo pathway inhibits Wnt signaling to restrain cardiomyocyte proliferation and heart size. *Science* **332**, 458-461.

Heallen, T., Morikawa, Y., Leach, J., Tao, G., Willerson, J. T., Johnson, R. L. and Martin, J. F. (2013). Hippo signaling impedes adult heart regeneration. *Development* **140**, 4683-4690.

Heineke, J. and Molkentin, J. D. (2006). Regulation of cardiac hypertrophy by intracellular signalling pathways. *Nature reviews. Molecular cell biology* **7**, 589-600.

Herget, G. W., Neuburger, M., Plagwitz, R. and Adler, C. P. (1997). DNA content, ploidy level and number of nuclei in the human heart after myocardial infarction. *Cardiovascular research* **36**, 45-51.

Heron, M., Hoyert, D. L., Murphy, S. L., Xu, J., Kochanek, K. D. and Tejada-Vera, B. (2009). Deaths: final data for 2006. *National vital statistics reports : from the Centers for Disease Control and Prevention, National Center for Health Statistics, National Vital Statistics System* **57**, 1-134.

Hertig, C. M., Kubalak, S. W., Wang, Y. and Chien, K. R. (1999). Synergistic roles of neuregulin-1 and insulin-like growth factor-I in activation of the phosphatidylinositol 3-kinase pathway and cardiac chamber morphogenesis. *The Journal of biological chemistry* **274**, 37362-37369.

Hirai, H., Roussel, M. F., Kato, J. Y., Ashmun, R. A. and Sherr, C. J. (1995). Novel INK4 proteins, p19 and p18, are specific inhibitors of the cyclin D-dependent kinases CDK4 and CDK6. *Molecular and cellular biology* **15**, 2672-2681.

Hisa, T., Spence, S. E., Rachel, R. A., Fujita, M., Nakamura, T., Ward, J. M., Devor-Henneman, D. E., Saiki, Y., Kutsuna, H., Tessarollo, L. et al. (2004). Hematopoietic, angiogenic and eye defects in Meis1 mutant animals. *The EMBO journal* **23**, 450-459.

Hochegger, H., Takeda, S. and Hunt, T. (2008). Cyclin-dependent kinases and cell-cycle transitions: does one fit all? *Nature reviews. Molecular cell biology* **9**, 910-916.

Hoffman, J. I. (1995). Incidence of congenital heart disease: I. Postnatal incidence. *Pediatric cardiology* **16**, 103-113.

Hoffman, J. I. and Kaplan, S. (2002). The incidence of congenital heart disease. *Journal of the American College of Cardiology* **39**, 1890-1900.

Holtzer, H., Marshall, J. M., Jr. and Finck, H. (1957). An analysis of myogenesis by the use of fluorescent antimyosin. *The Journal of biophysical and biochemical cytology* **3**, 705-724.

Horman, S., Beauloye, C., Vanoverschelde, J. L. and Bertrand, L. (2012). AMP-activated protein kinase in the control of cardiac metabolism and remodeling. *Current heart failure reports* **9**, 164-173.

Hotta, Y., Sasaki, S., Konishi, M., Kinoshita, H., Kuwahara, K., Nakao, K. and Itoh, N. (2008). Fgf16 is required for cardiomyocyte proliferation in the mouse embryonic heart. *Developmental dynamics : an official publication of the American Association of Anatomists* **237**, 2947-2954.

Hu, T., Yamagishi, H., Maeda, J., McAnally, J., Yamagishi, C. and Srivastava, D. (2004). Tbx1 regulates fibroblast growth factors in the anterior heart field through a reinforcing autoregulatory loop involving forkhead transcription factors. *Development* **131**, 5491-5502.

Hullinger, T. G., Montgomery, R. L., Seto, A. G., Dickinson, B. A., Semus, H. M., Lynch, J. M., Dalby, C. M., Robinson, K., Stack, C., Latimer, P. A. et al. (2012). Inhibition of miR-15 protects against cardiac ischemic injury. *Circulation research* **110**, 71-81.

Iemitsu, M., Miyauchi, T., Maeda, S., Sakai, S., Kobayashi, T., Fujii, N., Miyazaki, H., Matsuda, M. and Yamaguchi, I. (2001). Physiological and pathological cardiac hypertrophy induce different molecular phenotypes in the rat. *American journal of physiology. Regulatory, integrative and comparative physiology* **281**, R2029-2036.

Iio, A., Koide, M., Hidaka, K. and Morisaki, T. (2001). Expression pattern of novel chick T-box gene, Tbx20. *Development genes and evolution* **211**, 559-562.

Ikenishi, A., Okayama, H., Iwamoto, N., Yoshitome, S., Tane, S., Nakamura, K., Obayashi, T., Hayashi, T. and Takeuchi, T. (2012). Cell cycle regulation in mouse heart during embryonic and postnatal stages. *Development, growth & differentiation* **54**, 731-738.

Ilagan, R., Abu-Issa, R., Brown, D., Yang, Y. P., Jiao, K., Schwartz, R. J., Klingensmith, J. and Meyers, E. N. (2006). Fgf8 is required for anterior heart field development. *Development* **133**, 2435-2445.

Imamura, T., Morimoto, A., Takanashi, M., Hibi, S., Sugimoto, T., Ishii, E. and Imashuku, S. (2002). Frequent co-expression of HoxA9 and Meis1 genes in infant acute lymphoblastic leukaemia with MLL rearrangement. *British journal of haematology* **119**, 119-121.

Ivey, K. N., Muth, A., Arnold, J., King, F. W., Yeh, R. F., Fish, J. E., Hsiao, E. C., Schwartz, R. J., Conklin, B. R., Bernstein, H. S. et al. (2008). MicroRNA regulation of cell lineages in mouse and human embryonic stem cells. *Cell stem cell* **2**, 219-229.

Jerome, L. A. and Papaioannou, V. E. (2001). DiGeorge syndrome phenotype in mice mutant for the T-box gene, Tbx1. *Nature genetics* **27**, 286-291.

Jiao, K., Kulessa, H., Tompkins, K., Zhou, Y., Batts, L., Baldwin, H. S. and Hogan, B. L. (2003). An essential role of Bmp4 in the atrioventricular septation of the mouse heart. *Genes & development* **17**, 2362-2367.

Jopling, C., Sune, G., Faucherre, A., Fabregat, C. and Izpisua Belmonte, J. C. (2012). Hypoxia induces myocardial regeneration in zebrafish. *Circulation* **126**, 3017-3027.

Jopling, C., Sleep, E., Raya, M., Marti, M., Raya, A. and Izpisua Belmonte, J. C. (2010). Zebrafish heart regeneration occurs by cardiomyocyte dedifferentiation and proliferation. *Nature* **464**, 606-609.

Jung, J., Mysliwiec, M. R. and Lee, Y. (2005a). Roles of JUMONJI in mouse embryonic development. *Developmental dynamics : an official publication of the American Association of Anatomists* **232**, 21-32.

Jung, J., Kim, T. G., Lyons, G. E., Kim, H. R. and Lee, Y. (2005b). Jumonji regulates cardiomyocyte proliferation via interaction with retinoblastoma protein. *The Journal of biological chemistry* **280**, 30916-30923.

Kahn, A. J. and Simmons, D. J. (1975). Investigation of cell lineage in bone using a chimaera of chick and quial embryonic tissue. *Nature* **258**, 325-327.

Kang, J. O. and Sucov, H. M. (2005). Convergent proliferative response and divergent morphogenic pathways induced by epicardial and endocardial signaling in fetal heart development. *Mechanisms of development* **122**, 57-65.

Karpanen, T., Bry, M., Ollila, H. M., Seppanen-Laakso, T., Liimatta, E., Leskinen, H., Kivela, R., Helkamaa, T., Merentie, M., Jeltsch, M. et al. (2008). Overexpression of vascular endothelial growth factor-B in mouse heart alters cardiac lipid metabolism and induces myocardial hypertrophy. *Circulation research* **103**, 1018-1026.

Kehat, I. and Molkentin, J. D. (2010). Extracellular signal-regulated kinase 1/2 (ERK1/2) signaling in cardiac hypertrophy. *Annals of the New York Academy of Sciences* **1188**, 96-102.

Kehat, I., Davis, J., Tiburcy, M., Accornero, F., Saba-El-Leil, M. K., Maillet, M., York, A. J., Lorenz, J. N., Zimmermann, W. H., Meloche, S. et al. (2011). Extracellular signal-regulated kinases 1 and 2 regulate the balance between eccentric and concentric cardiac growth. *Circulation research* **108**, 176-183.

Kelly, R. G. (2012). The second heart field. *Current topics in developmental biology* **100**, 33-65.

Kelly, R. G., Brown, N. A. and Buckingham, M. E. (2001). The arterial pole of the mouse heart forms from Fgf10-expressing cells in pharyngeal mesoderm. *Developmental cell* **1**, 435-440.

Kiefer, J. C. (2004). The Tbx-files: the truth is out there. *Developmental dynamics : an official publication of the American Association of Anatomists* **231**, 232-236.

Kikuchi, K., Holdway, J. E., Werdich, A. A., Anderson, R. M., Fang, Y., Egnaczyk, G. F., Evans, T., Macrae, C. A., Stainier, D. Y. and Poss, K. D. (2010). Primary contribution to zebrafish heart regeneration by gata4(+) cardiomyocytes. *Nature* **464**, 601-605.

Kim, K. K., Soonpaa, M. H., Daud, A. I., Koh, G. Y., Kim, J. S. and Field, L. J. (1994). Tumor suppressor gene expression during normal and pathologic myocardial growth. *The Journal of biological chemistry* **269**, 22607-22613.

Kimura, A., Harada, H., Park, J. E., Nishi, H., Satoh, M., Takahashi, M., Hiroi, S., Sasaoka, T., Ohbuchi, N., Nakamura, T. et al. (1997). Mutations in the cardiac troponin I gene associated with hypertrophic cardiomyopathy. *Nature genetics* **16**, 379-382.

Kirby, M. L. (1990). Alteration of cardiogenesis after neural crest ablation. *Annals of the New York Academy of Sciences* **588**, 289-295.

Kirby, M. L. and Waldo, K. L. (1995). Neural crest and cardiovascular patterning. *Circulation research* **77**, 211-215.

Kisanuki, Y. Y., Hammer, R. E., Miyazaki, J., Williams, S. C., Richardson, J. A. and Yanagisawa, M. (2001). Tie2-Cre transgenic mice: a new model for endothelial cell-lineage analysis in vivo. *Developmental biology* **230**, 230-242.

Kispert, A. and Herrmann, B. G. (1993). The Brachyury gene encodes a novel DNA binding protein. *The EMBO journal* **12**, 3211-3220.

Klein, T. J. and Mlodzik, M. (2005). Planar cell polarization: an emerging model points in the right direction. *Annual review of cell and developmental biology* **21**, 155-176.

Knights, V. and Cook, S. J. (2010). De-regulated FGF receptors as therapeutic targets in cancer. *Pharmacology & therapeutics* **125**, 105-117.

Komiya, Y. and Habas, R. (2008). Wnt signal transduction pathways. *Organogenesis* **4**, 68-75.

Kook, H. and Epstein, J. A. (2003). Hopping to the beat. Hop regulation of cardiac gene expression. *Trends in cardiovascular medicine* **13**, 261-264.

Kook, H., Lepore, J. J., Gitler, A. D., Lu, M. M., Wing-Man Yung, W., Mackay, J., Zhou, R., Ferrari, V., Gruber, P. and Epstein, J. A. (2003). Cardiac hypertrophy and histone deacetylase-dependent transcriptional repression mediated by the atypical homeodomain protein Hop. *The Journal of clinical investigation* **112**, 863-871.

Kook, H., Yung, W. W., Simpson, R. J., Kee, H. J., Shin, S., Lowry, J. A., Loughlin, F. E., Yin, Z., Epstein, J. A. and Mackay, J. P. (2006). Analysis of the structure and function of the transcriptional coregulator HOP. *Biochemistry* **45**, 10584-10590.

Koren, M. J., Devereux, R. B., Casale, P. N., Savage, D. D. and Laragh, J. H. (1991). Relation of left ventricular mass and geometry to morbidity and mortality in uncomplicated essential hypertension. *Annals of internal medicine* **114**, 345-352.

Kortschak, R. D., Tucker, P. W. and Saint, R. (2000). ARID proteins come in from the desert. *Trends in biochemical sciences* **25**, 294-299.

Kouhara, H., Hadari, Y. R., Spivak-Kroizman, T., Schilling, J., Bar-Sagi, D., Lax, I. and Schlessinger, J. (1997). A lipid-anchored Grb2-binding protein that links FGF-receptor activation to the Ras/MAPK signaling pathway. *Cell* **89**, 693-702.

Kraus, F., Haenig, B. and Kispert, A. (2001). Cloning and expression analysis of the mouse T-box gene tbx20. *Mechanisms of development* **100**, 87-91.

Kuhn, B., del Monte, F., Hajjar, R. J., Chang, Y. S., Lebeche, D., Arab, S. and Keating, M. T. (2007). Periostin induces proliferation of differentiated cardiomyocytes and promotes cardiac repair. *Nature medicine* **13**, 962-969.

Laflamme, M. A. and Murry, C. E. (2011). Heart regeneration. *Nature* **473**, 326-335.

Larkins, B. A., Dilkes, B. P., Dante, R. A., Coelho, C. M., Woo, Y. M. and Liu, Y. (2001). Investigating the hows and whys of DNA endoreduplication. *Journal of experimental botany* **52**, 183-192.

Lau, M. M., Stewart, C. E., Liu, Z., Bhatt, H., Rotwein, P. and Stewart, C. L. (1994). Loss of the imprinted IGF2/cation-independent mannose 6-phosphate receptor results in fetal overgrowth and perinatal lethality. *Genes & development* **8**, 2953-2963.

Laube, F., Heister, M., Scholz, C., Borchardt, T. and Braun, T. (2006). Re-programming of newt cardiomyocytes is induced by tissue regeneration. *Journal of cell science* **119**, 4719-4729.

Lavine, K. J. and Ornitz, D. M. (2008). Fibroblast growth factors and Hedgehogs: at the heart of the epicardial signaling center. *Trends in genetics : TIG* **24**, 33-40.

Lavine, K. J., Yu, K., White, A. C., Zhang, X., Smith, C., Partanen, J. and Ornitz, D. M. (2005). Endocardial and epicardial derived FGF signals regulate myocardial proliferation and differentiation in vivo. *Developmental cell* **8**, 85-95.

Lawson, K. A., Meneses, J. J. and Pedersen, R. A. (1991). Clonal analysis of epiblast fate during germ layer formation in the mouse embryo. *Development* **113**, 891-911.

Le Roith, D. (1997). Seminars in medicine of the Beth Israel Deaconess Medical Center. Insulin-like growth factors. *The New England journal of medicine* **336**, 633-640.

Lee, K. F., Simon, H., Chen, H., Bates, B., Hung, M. C. and Hauser, C. (1995). Requirement for neuregulin receptor erbB2 in neural and cardiac development. *Nature* **378**, 394-398.

Lei, Q. Y., Zhang, H., Zhao, B., Zha, Z. Y., Bai, F., Pei, X. H., Zhao, S., Xiong, Y. and Guan, K. L. (2008). TAZ promotes cell proliferation and epithelial-mesenchymal transition and is inhibited by the hippo pathway. *Molecular and cellular biology* **28**, 2426-2436.

Lescroart, F., Chabab, S., Lin, X., Rulands, S., Paulissen, C., Rodolosse, A., Auer, H., Achouri, Y., Dubois, C., Bondue, A. et al. (2014). Early lineage restriction in temporally distinct populations of Mesp1 progenitors during mammalian heart development. *Nature cell biology* **16**, 829-840.

Levy, D., Wilson, P. W., Anderson, K. M. and Castelli, W. P. (1990a). Stratifying the patient at risk from coronary disease: new insights from the Framingham Heart Study. *American heart journal* **119**, 712-717; discussion 717.

Levy, D., Garrison, R. J., Savage, D. D., Kannel, W. B. and Castelli, W. P. (1990b). Prognostic implications of echocardiographically determined left ventricular mass in the Framingham Heart Study. *The New England journal of medicine* **322**, 1561-1566.

Li, C. and Tucker, P. W. (1993). DNA-binding properties and secondary structural model of the hepatocyte nuclear factor 3/fork head domain. *Proceedings of the National Academy of Sciences of the United States of America* **90**, 11583-11587.

Li, F., Wang, X. and Gerdes, A. M. (1997a). Formation of binucleated cardiac myocytes in rat heart: II. Cytoskeletal organisation. *Journal of molecular and cellular cardiology* **29**, 1553-1565.

Li, F., Wang, X., Capasso, J. M. and Gerdes, A. M. (1996). Rapid transition of cardiac myocytes from hyperplasia to hypertrophy during postnatal development. *Journal of molecular and cellular cardiology* **28**, 1737-1746.

Li, F., Wang, X., Bunger, P. C. and Gerdes, A. M. (1997b). Formation of binucleated cardiac myocytes in rat heart: I. Role of actin-myosin contractile ring. *Journal of molecular and cellular cardiology* **29**, 1541-1551.

Li, J. M., Poolman, R. A. and Brooks, G. (1998). Role of G1 phase cyclins and cyclin-dependent kinases during cardiomyocyte hypertrophic growth in rats. *The American journal of physiology* **275**, H814-822.

Li, P., Cavallero, S., Gu, Y., Chen, T. H., Hughes, J., Hassan, A. B., Bruning, J. C., Pashmforoush, M. and Sucov, H. M. (2011). IGF signaling directs ventricular cardiomyocyte proliferation during embryonic heart development. *Development* **138**, 1795-1805.

Li, Q. Y., Newbury-Ecob, R. A., Terrett, J. A., Wilson, D. I., Curtis, A. R., Yi, C. H., Gebuhr, T., Bullen, P. J., Robson, S. C., Strachan, T. et al. (1997). Holt-Oram syndrome is caused by mutations in TBX5, a member of the Brachyury (T) gene family. *Nature genetics* **15**, 21-29.

Li, S., Weidenfeld, J. and Morrisey, E. E. (2004). Transcriptional and DNA binding activity of the Foxp1/2/4 family is modulated by heterotypic and homotypic protein interactions. *Molecular and cellular biology* **24**, 809-822.

Liao, J., Aggarwal, V. S., Nowotschin, S., Bondarev, A., Lipner, S. and Morrow, B. E. (2008). Identification of downstream genetic pathways of Tbx1 in the second heart field. *Developmental biology* **316**, 524-537.

Liberatore, C. M., Searcy-Schrick, R. D. and Yutzey, K. E. (2000). Ventricular expression of tbx5 inhibits normal heart chamber development. *Developmental biology* **223**, 169-180.

Lim, S. and Kaldis, P. (2013). Cdks, cyclins and CKIs: roles beyond cell cycle regulation. *Development* **140**, 3079-3093.

Lindsay, E. A., Vitelli, F., Su, H., Morishima, M., Huynh, T., Pramparo, T., Jurecic, V., Ogunrinu, G., Sutherland, H. F., Scambler, P. J. et al. (2001). Tbx1 haploinsufficieny in the DiGeorge syndrome region causes aortic arch defects in mice. *Nature* **410**, 97-101.

Lips, D. J., Bueno, O. F., Wilkins, B. J., Purcell, N. H., Kaiser, R. A., Lorenz, J. N., Voisin, L., Saba-El-Leil, M. K., Meloche, S., Pouyssegur, J. et al. (2004). MEK1-ERK2 signaling pathway protects myocardium from ischemic injury in vivo. *Circulation* **109**, 1938-1941.

Litvin, J., Zhu, S., Norris, R. and Markwald, R. (2005). Periostin family of proteins: therapeutic targets for heart disease. *The anatomical record. Part A, Discoveries in molecular, cellular, and evolutionary biology* **287**, 1205-1212.

Liu, N. and Olson, E. N. (2010). MicroRNA regulatory networks in cardiovascular development. *Developmental cell* **18**, 510-525.

Liu, Q., Yan, H., Dawes, N. J., Mottino, G. A., Frank, J. S. and Zhu, H. (1996). Insulin-like growth factor II induces DNA synthesis in fetal ventricular myocytes in vitro. *Circulation research* **79**, 716-726.

Liu, Z., Yang, X., Tan, F., Cullion, K. and Thiele, C. J. (2006). Molecular cloning and characterization of human Castor, a novel human gene upregulated during cell differentiation. *Biochemical and biophysical research communications* **344**, 834-844.

Lopez, A. D., Mathers, C. D., Ezzati, M., Jamison, D. T. and Murray, C. J. L. (2006). Measuring the Global Burden of Disease and Risk Factors, 1990-2001. In *Global Burden of Disease and Risk Factors* (eds A. D. Lopez C. D. Mathers M. Ezzati D. T. Jamison and C. J. L. Murray). Washington (DC).

Lorts, A., Schwanekamp, J. A., Elrod, J. W., Sargent, M. A. and Molkentin, J. D. (2009). Genetic manipulation of periostin expression in the heart does not affect myocyte content, cell cycle activity, or cardiac repair. *Circulation research* **104**, e1-7.

Lu, M. M., Li, S., Yang, H. and Morrisey, E. E. (2002). Foxp4: a novel member of the Foxp subfamily of winged-helix genes co-expressed with Foxp1 and Foxp2 in pulmonary and gut tissues. *Gene expression patterns : GEP* **2**, 223-228.

Ludwig, T., Le Borgne, R. and Hoflack, B. (1995). Roles for mannose-6-phosphate receptors in lysosomal enzyme sorting, IGF-II binding and clathrin-coat assembly. *Trends in cell biology* **5**, 202-206.

MacAuley, A., Cross, J. C. and Werb, Z. (1998). Reprogramming the cell cycle for endoreduplication in rodent trophoblast cells. *Molecular biology of the cell* **9**, 795-807.

MacDonald, B. T., Tamai, K. and He, X. (2009). Wnt/beta-catenin signaling: components, mechanisms, and diseases. *Developmental cell* **17**, 9-26.

Mahmoud, A. I., Kocabas, F., Muralidhar, S. A., Kimura, W., Koura, A. S., Thet, S., Porrello, E. R. and Sadek, H. A. (2013). Meis1 regulates postnatal cardiomyocyte cell cycle arrest. *Nature* **497**, 249-253.

Maillet, M., van Berlo, J. H. and Molkentin, J. D. (2013). Molecular basis of physiological heart growth: fundamental concepts and new players. *Nature reviews. Molecular cell biology* **14**, 38-48.

Manner, J., Perez-Pomares, J. M., Macias, D. and Munoz-Chapuli, R. (2001). The origin, formation and developmental significance of the epicardium: a review. *Cells, tissues, organs* **169**, 89-103.

Manolagas, S. C. and Jilka, R. L. (1995). Bone marrow, cytokines, and bone remodeling. Emerging insights into the pathophysiology of osteoporosis. *The New England journal of medicine* **332**, 305-311.

Marguerie, A., Bajolle, F., Zaffran, S., Brown, N. A., Dickson, C., Buckingham, M. E. and Kelly, R. G. (2006). Congenital heart defects in Fgfr2-IIIb and Fgf10 mutant mice. *Cardiovascular research* **71**, 50-60.

McClatchey, A. I. and Yap, A. S. (2012). Contact inhibition (of proliferation) redux. *Current opinion in cell biology* **24**, 685-694.

Meijer, L., Skaltsounis, A. L., Magiatis, P., Polychronopoulos, P., Knockaert, M., Leost, M., Ryan, X. P., Vonica, C. A., Brivanlou, A., Dajani, R. et al. (2003). GSK-3-

selective inhibitors derived from Tyrian purple indirubins. *Chemistry & biology* **10**, 1255-1266.

Meilhac, S. M., Lescroart, F., Blanpain, C. and Buckingham, M. E. (2014). Cardiac cell lineages that form the heart. *Cold Spring Harbor perspectives in medicine* **4**, a013888.

Meilhac, S. M., Esner, M., Kelly, R. G., Nicolas, J. F. and Buckingham, M. E. (2004). The clonal origin of myocardial cells in different regions of the embryonic mouse heart. *Developmental cell* **6**, 685-698.

Meilhac, S. M., Kelly, R. G., Rocancourt, D., Eloy-Trinquet, S., Nicolas, J. F. and Buckingham, M. E. (2003). A retrospective clonal analysis of the myocardium reveals two phases of clonal growth in the developing mouse heart. *Development* **130**, 3877-3889.

Meyer, D. and Birchmeier, C. (1995). Multiple essential functions of neuregulin in development. *Nature* **378**, 386-390.

Miki, T., Bottaro, D. P., Fleming, T. P., Smith, C. L., Burgess, W. H., Chan, A. M. and Aaronson, S. A. (1992). Determination of ligand-binding specificity by alternative splicing: two distinct growth factor receptors encoded by a single gene. *Proceedings of the National Academy of Sciences of the United States of America* **89**, 246-250.

Miller, A. L. (2011). The contractile ring. *Current biology : CB* **21**, R976-978.

Mitchison, J. M. (1971). The biology of the cell cycle. Cambridge Eng.: University Press.

Miyaoka, Y., Ebato, K., Kato, H., Arakawa, S., Shimizu, S. and Miyajima, A. (2012). Hypertrophy and unconventional cell division of hepatocytes underlie liver regeneration. *Current biology : CB* **22**, 1166-1175.

Mjaatvedt, C. H., Nakaoka, T., Moreno-Rodriguez, R., Norris, R. A., Kern, M. J., Eisenberg, C. A., Turner, D. and Markwald, R. R. (2001). The outflow tract of the heart is recruited from a novel heart-forming field. *Developmental biology* **238**, 97-109.

Mogensen, J., Klausen, I. C., Pedersen, A. K., Egeblad, H., Bross, P., Kruse, T. A., Gregersen, N., Hansen, P. S., Baandrup, U. and Borglum, A. D. (1999). Alpha-

cardiac actin is a novel disease gene in familial hypertrophic cardiomyopathy. *The Journal of clinical investigation* **103**, R39-43.

Mollova, M., Bersell, K., Walsh, S., Savla, J., Das, L. T., Park, S. Y., Silberstein, L. E., Dos Remedios, C. G., Graham, D., Colan, S. et al. (2013). Cardiomyocyte proliferation contributes to heart growth in young humans. *Proceedings of the National Academy of Sciences of the United States of America* **110**, 1446-1451.

Moon, A. (2008). Mouse models of congenital cardiovascular disease. *Current topics in developmental biology* **84**, 171-248.

Moon, A. M. (2006). Mouse models for investigating the developmental basis of human birth defects. *Pediatric research* **59**, 749-755.

Morgan, D. O. (1997). Cyclin-dependent kinases: engines, clocks, and microprocessors. *Annual review of cell and developmental biology* **13**, 261-291.

Morita, H., Rehm, H. L., Menesses, A., McDonough, B., Roberts, A. E., Kucherlapati, R., Towbin, J. A., Seidman, J. G. and Seidman, C. E. (2008). Shared genetic causes of cardiac hypertrophy in children and adults. *The New England journal of medicine* **358**, 1899-1908.

Morita, M., Kawashima, S., Ikeoka, K. and Iwasaki, T. (1996). Effects of chronic hypertension and left ventricular hypertrophy on the extent of infarct expansion in rats. *American journal of hypertension* **9**, 753-759.

Moses, K. A., DeMayo, F., Braun, R. M., Reecy, J. L. and Schwartz, R. J. (2001). Embryonic expression of an Nkx2-5/Cre gene using ROSA26 reporter mice. *Genesis* **31**, 176-180.

Most, J., Spotl, L., Mayr, G., Gasser, A., Sarti, A. and Dierich, M. P. (1997). Formation of multinucleated giant cells in vitro is dependent on the stage of monocyte to macrophage maturation. *Blood* **89**, 662-671.

Muhlfeld, C., Nyengaard, J. R. and Mayhew, T. M. (2010). A review of state-of-the-art stereology for better quantitative 3D morphology in cardiac research. *Cardiovascular pathology : the official journal of the Society for Cardiovascular Pathology* **19**, 65-82.

Murray, A. W. and Hunt, T. (1993). The cell cycle : an introduction. New York: W.H. Freeman.

Naiche, L. A., Harrelson, Z., Kelly, R. G. and Papaioannou, V. E. (2005). T-box genes in vertebrate development. *Annual review of genetics* **39**, 219-239.

Nakajima, K., Inagawa, M., Uchida, C., Okada, K., Tane, S., Kojima, M., Kubota, M., Noda, M., Ogawa, S., Shirato, H. et al. (2011). Coordinated regulation of differentiation and proliferation of embryonic cardiomyocytes by a jumonji (Jarid2)-cyclin D1 pathway. *Development* **138**, 1771-1782.

Naqvi, N., Li, M., Calvert, J. W., Tejada, T., Lambert, J. P., Wu, J., Kesteven, S. H., Holman, S. R., Matsuda, T., Lovelock, J. D. et al. (2014). A proliferative burst during preadolescence establishes the final cardiomyocyte number. *Cell* **157**, 795-807.

Naski, M. C. and Ornitz, D. M. (1998). FGF signaling in skeletal development. *Frontiers in bioscience : a journal and virtual library* **3**, d781-794.

Norris, R. A., Kern, C. B., Wessels, A., Moralez, E. I., Markwald, R. R. and Mjaatvedt, C. H. (2004). Identification and detection of the periostin gene in cardiac development. *The anatomical record. Part A, Discoveries in molecular, cellular, and evolutionary biology* **281**, 1227-1233.

Norton, J. D. and Atherton, G. T. (1998). Coupling of cell growth control and apoptosis functions of Id proteins. *Molecular and cellular biology* **18**, 2371-2381.

Norton, J. D., Deed, R. W., Craggs, G. and Sablitzky, F. (1998). Id helix-loop-helix proteins in cell growth and differentiation. *Trends in cell biology* **8**, 58-65.

Nurse, P. (2000). A long twentieth century of the cell cycle and beyond. *Cell* **100**, 71-78.

Oberpriller, J. O. and Oberpriller, J. C. (1974). Response of the adult newt ventricle to injury. *The Journal of experimental zoology* **187**, 249-253.

Okazaki, K. and Holtzer, H. (1966). Myogenesis: fusion, myosin synthesis, and the mitotic cycle. *Proceedings of the National Academy of Sciences of the United States of America* **56**, 1484-1490.

Olivetti, G., Cigola, E., Maestri, R., Corradi, D., Lagrasta, C., Gambert, S. R. and Anversa, P. (1996). Aging, cardiac hypertrophy and ischemic cardiomyopathy do not affect the proportion of mononucleated and multinucleated myocytes in the human heart. *Journal of molecular and cellular cardiology* **28**, 1463-1477.

Oparil, S., Bishop, S. P. and Clubb, F. J., Jr. (1984). Myocardial cell hypertrophy or hyperplasia. *Hypertension* **6**, III38-43.

Ornitz, D. M. and Itoh, N. (2001). Fibroblast growth factors. *Genome biology* **2**, REVIEWS3005.

Packham, E. A. and Brook, J. D. (2003). T-box genes in human disorders. *Human molecular genetics* **12 Spec No 1**, R37-44.

Pan, D. (2010). The hippo signaling pathway in development and cancer. *Developmental cell* **19**, 491-505.

Papaioannou, V. E. (2001). T-box genes in development: from hydra to humans. *International review of cytology* **207**, 1-70.

Parameswaran, M. and Tam, P. P. (1995). Regionalisation of cell fate and morphogenetic movement of the mesoderm during mouse gastrulation. *Developmental genetics* **17**, 16-28.

Park, E. J., Ogden, L. A., Talbot, A., Evans, S., Cai, C. L., Black, B. L., Frank, D. U. and Moon, A. M. (2006). Required, tissue-specific roles for Fgf8 in outflow tract formation and remodeling. *Development* **133**, 2419-2433.

Park, E. J., Watanabe, Y., Smyth, G., Miyagawa-Tomita, S., Meyers, E., Klingensmith, J., Camenisch, T., Buckingham, M. and Moon, A. M. (2008). An FGF autocrine loop initiated in second heart field mesoderm regulates morphogenesis at the arterial pole of the heart. *Development* **135**, 3599-3610.

Pasumarthi, K. B. and Field, L. J. (2002). Cardiomyocyte cell cycle regulation. *Circulation research* **90**, 1044-1054.

Pasumarthi, K. B., Kardami, E. and Cattini, P. A. (1996). High and low molecular weight fibroblast growth factor-2 increase proliferation of neonatal rat cardiac myocytes but have differential effects on binucleation and nuclear morphology. Evidence for both

paracrine and intracrine actions of fibroblast growth factor-2. *Circulation research* **78**, 126-136.

Pavletich, N. P. (1999). Mechanisms of cyclin-dependent kinase regulation: structures of Cdks, their cyclin activators, and Cip and INK4 inhibitors. *Journal of molecular biology* **287**, 821-828.

Pediatric Cardiac Genomics, C., Gelb, B., Brueckner, M., Chung, W., Goldmuntz, E., Kaltman, J., Kaski, J. P., Kim, R., Kline, J., Mercer-Rosa, L. et al. (2013). The Congenital Heart Disease Genetic Network Study: rationale, design, and early results. *Circulation research* **112**, 698-706.

Piatkowski, T., Muhlfeld, C., Borchardt, T. and Braun, T. (2013). Reconstitution of the myocardium in regenerating newt hearts is preceded by transient deposition of extracellular matrix components. *Stem cells and development* **22**, 1921-1931.

Poetter, K., Jiang, H., Hassanzadeh, S., Master, S. R., Chang, A., Dalakas, M. C., Rayment, I., Sellers, J. R., Fananapazir, L. and Epstein, N. D. (1996). Mutations in either the essential or regulatory light chains of myosin are associated with a rare myopathy in human heart and skeletal muscle. *Nature genetics* **13**, 63-69.

Polyak, K., Lee, M. H., Erdjument-Bromage, H., Koff, A., Roberts, J. M., Tempst, P. and Massague, J. (1994). Cloning of p27Kip1, a cyclin-dependent kinase inhibitor and a potential mediator of extracellular antimitogenic signals. *Cell* **78**, 59-66.

Porrello, E. R., Johnson, B. A., Aurora, A. B., Simpson, E., Nam, Y. J., Matkovich, S. J., Dorn, G. W., 2nd, van Rooij, E. and Olson, E. N. (2011). MiR-15 family regulates postnatal mitotic arrest of cardiomyocytes. *Circulation research* **109**, 670-679.

Porrello, E. R., Mahmoud, A. I., Simpson, E., Johnson, B. A., Grinsfelder, D., Canseco, D., Mammen, P. P., Rothermel, B. A., Olson, E. N. and Sadek, H. A. (2013). Regulation of neonatal and adult mammalian heart regeneration by the miR-15 family. *Proceedings of the National Academy of Sciences of the United States of America* **110**, 187-192.

Poss, K. D., Wilson, L. G. and Keating, M. T. (2002). Heart regeneration in zebrafish. *Science* **298**, 2188-2190.

Pownall, M. E. and Isaacs, H. V. (2010). In *FGF Signalling in Vertebrate Development*. San Rafael (CA).

Pozarowski, P., Holden, E. and Darzynkiewicz, Z. (2006). Laser scanning cytometry: principles and applications. *Methods in molecular biology* **319**, 165-192.

Praskova, M., Xia, F. and Avruch, J. (2008). MOBKL1A/MOBKL1B phosphorylation by MST1 and MST2 inhibits cell proliferation. *Current biology : CB* **18**, 311-321.

Purcell, N. H., Wilkins, B. J., York, A., Saba-El-Leil, M. K., Meloche, S., Robbins, J. and Molkentin, J. D. (2007). Genetic inhibition of cardiac ERK1/2 promotes stress-induced apoptosis and heart failure but has no effect on hypertrophy in vivo. *Proceedings of the National Academy of Sciences of the United States of America* **104**, 14074-14079.

Rao, T. P. and Kuhl, M. (2010). An updated overview on Wnt signaling pathways: a prelude for more. *Circulation research* **106**, 1798-1806.

Rappaport, R. (1996). Cytokinesis in animal cells. Cambridge ; New York, NY, USA: Cambridge University Press.

Reik, W. and Walter, J. (2001). Genomic imprinting: parental influence on the genome. *Nature reviews. Genetics* **2**, 21-32.

Reiss, K., Cheng, W., Ferber, A., Kajstura, J., Li, P., Li, B., Olivetti, G., Homcy, C. J., Baserga, R. and Anversa, P. (1996). Overexpression of insulin-like growth factor-1 in the heart is coupled with myocyte proliferation in transgenic mice. *Proceedings of the National Academy of Sciences of the United States of America* **93**, 8630-8635.

Reuter, S., Soonpaa, M. H., Firulli, A. B., Chang, A. N. and Field, L. J. (2014). Recombinant neuregulin 1 does not activate cardiomyocyte DNA synthesis in normal or infarcted adult mice. *PloS one* **9**, e115871.

Rios, H., Koushik, S. V., Wang, H., Wang, J., Zhou, H. M., Lindsley, A., Rogers, R., Chen, Z., Maeda, M., Kruzynska-Frejtag, A. et al. (2005). periostin null mice exhibit dwarfism, incisor enamel defects, and an early-onset periodontal disease-like phenotype. *Molecular and cellular biology* **25**, 11131-11144.

Roberts, J. M., Koff, A., Polyak, K., Firpo, E., Collins, S., Ohtsubo, M. and Massague, J. (1994). Cyclins, Cdks, and cyclin kinase inhibitors. *Cold Spring Harbor symposia on quantitative biology* **59**, 31-38.

Rochais, F., Mesbah, K. and Kelly, R. G. (2009). Signaling pathways controlling second heart field development. *Circulation research* **104**, 933-942.

Rossi, S. G., Vazquez, A. E. and Rotundo, R. L. (2000). Local control of acetylcholinesterase gene expression in multinucleated skeletal muscle fibers: individual nuclei respond to signals from the overlying plasma membrane. *The Journal of neuroscience : the official journal of the Society for Neuroscience* **20**, 919-928.

Rumyantsev, P. P. (1977). Interrelations of the proliferation and differentiation processes during cardiact myogenesis and regeneration. *International review of cytology* **51**, 186-273.

Russo, A. A., Jeffrey, P. D., Patten, A. K., Massague, J. and Pavletich, N. P. (1996). Crystal structure of the p27Kip1 cyclin-dependent-kinase inhibitor bound to the cyclin A-Cdk2 complex. *Nature* **382**, 325-331.

Russo, A. A., Tong, L., Lee, J. O., Jeffrey, P. D. and Pavletich, N. P. (1998). Structural basis for inhibition of the cyclin-dependent kinase Cdk6 by the tumour suppressor p16INK4a. *Nature* **395**, 237-243.

Saga, Y., Kitajima, S. and Miyagawa-Tomita, S. (2000). Mesp1 expression is the earliest sign of cardiovascular development. *Trends in cardiovascular medicine* **10**, 345-352.

Saga, Y., Miyagawa-Tomita, S., Takagi, A., Kitajima, S., Miyazaki, J. and Inoue, T. (1999). MesP1 is expressed in the heart precursor cells and required for the formation of a single heart tube. *Development* **126**, 3437-3447.

Sagona, A. P. and Stenmark, H. (2010). Cytokinesis and cancer. *FEBS letters* **584**, 2652-2661.

Satoh, M., Takahashi, M., Sakamoto, T., Hiroe, M., Marumo, F. and Kimura, A. (1999). Structural analysis of the titin gene in hypertrophic cardiomyopathy: identification of a novel disease gene. *Biochemical and biophysical research communications* **262**, 411-417.

Schmid, G. and Pfitzer, P. (1985). Mitoses and binucleated cells in perinatal human hearts. *Virchows Archiv. B, Cell pathology including molecular pathology* **48**, 59-67.

Sedmera, D., Reckova, M., DeAlmeida, A., Coppen, S. R., Kubalak, S. W., Gourdie, R. G. and Thompson, R. P. (2003). Spatiotemporal pattern of commitment to slowed proliferation in the embryonic mouse heart indicates progressive differentiation of the cardiac conduction system. *The anatomical record. Part A, Discoveries in molecular, cellular, and evolutionary biology* **274**, 773-777.

Seidman, C. (2000). Hypertrophic cardiomyopathy: from man to mouse. *Journal of Clinical Investigation* **106**, S9-S13.

Seidman, J. G. and Seidman, C. (2001). The genetic basis for cardiomyopathy: from mutation identification to mechanistic paradigms. *Cell* **104**, 557-567.

Sengbusch, J. K., He, W., Pinco, K. A. and Yang, J. T. (2002). Dual functions of [alpha]4[beta]1 integrin in epicardial development: initial migration and long-term attachment. *The Journal of cell biology* **157**, 873-882.

Senyo, S. E., Lee, R. T. and Kuhn, B. (2014). Cardiac regeneration based on mechanisms of cardiomyocyte proliferation and differentiation. *Stem cell research* **13**, 532-541.

Senyo, S. E., Steinhauser, M. L., Pizzimenti, C. L., Yang, V. K., Cai, L., Wang, M., Wu, T. D., Guerquin-Kern, J. L., Lechene, C. P. and Lee, R. T. (2013). Mammalian heart renewal by pre-existing cardiomyocytes. *Nature* **493**, 433-436.

Serrano, M., Hannon, G. J. and Beach, D. (1993). A new regulatory motif in cell-cycle control causing specific inhibition of cyclin D/CDK4. *Nature* **366**, 704-707.

Sheikh, F., Fandrich, R. R., Kardami, E. and Cattini, P. A. (1999). Overexpression of long or short FGFR-1 results in FGF-2-mediated proliferation in neonatal cardiac myocyte cultures. *Cardiovascular research* **42**, 696-705.

Shen, H., Cavallero, S., Estrada, K. D., Sandovici, I., Kumar, S. R., Makita, T., Lien, C. L., Constancia, M. and Sucov, H. M. (2015). Extracardiac control of embryonic cardiomyocyte proliferation and ventricular wall expansion. *Cardiovascular research* **105**, 271-278.

Shenje, L. T., Andersen, P., Uosaki, H., Fernandez, L., Rainer, P. P., Cho, G. S., Lee, D. I., Zhong, W., Harvey, R. P., Kass, D. A. et al. (2014). Precardiac deletion of Numb and Numblike reveals renewal of cardiac progenitors. *eLife* **3**, e02164.

Sherr, C. J. (1993). Mammalian G1 cyclins. *Cell* **73**, 1059-1065.

Sherr, C. J. and Roberts, J. M. (1999). CDK inhibitors: positive and negative regulators of G1-phase progression. *Genes & development* **13**, 1501-1512.

Shimazaki, M., Nakamura, K., Kii, I., Kashima, T., Amizuka, N., Li, M., Saito, M., Fukuda, K., Nishiyama, T., Kitajima, S. et al. (2008). Periostin is essential for cardiac healing after acute myocardial infarction. *The Journal of experimental medicine* **205**, 295-303.

Shin, C. H., Liu, Z. P., Passier, R., Zhang, C. L., Wang, D. Z., Harris, T. M., Yamagishi, H., Richardson, J. A., Childs, G. and Olson, E. N. (2002). Modulation of cardiac growth and development by HOP, an unusual homeodomain protein. *Cell* **110**, 725-735.

Showell, C., Binder, O. and Conlon, F. L. (2004). T-box genes in early embryogenesis. *Developmental dynamics : an official publication of the American Association of Anatomists* **229**, 201-218.

Shu, W., Yang, H., Zhang, L., Lu, M. M. and Morrisey, E. E. (2001). Characterization of a new subfamily of winged-helix/forkhead (Fox) genes that are expressed in the lung and act as transcriptional repressors. *The Journal of biological chemistry* **276**, 27488-27497.

Sikder, H. A., Devlin, M. K., Dunlap, S., Ryu, B. and Alani, R. M. (2003). Id proteins in cell growth and tumorigenesis. *Cancer cell* **3**, 525-530.

Singh, M. K., Christoffels, V. M., Dias, J. M., Trowe, M. O., Petry, M., Schuster-Gossler, K., Burger, A., Ericson, J. and Kispert, A. (2005). Tbx20 is essential for cardiac chamber differentiation and repression of Tbx2. *Development* **132**, 2697-2707.

Small, E. M. and Olson, E. N. (2011). Pervasive roles of microRNAs in cardiovascular biology. *Nature* **469**, 336-342.

Smith, T. C., Fridy, P. C., Li, Y., Basil, S., Arjun, S., Friesen, R. M., Leszyk, J., Chait, B. T., Rout, M. P. and Luna, E. J. (2013). Supervillin binding to myosin II and synergism with anillin are required for cytokinesis. *Molecular biology of the cell* **24**, 3603-3619.

Smith, T. K. and Bader, D. M. (2007). Signals from both sides: Control of cardiac development by the endocardium and epicardium. *Seminars in cell & developmental biology* **18**, 84-89.

Sohal, D. S., Nghiem, M., Crackower, M. A., Witt, S. A., Kimball, T. R., Tymitz, K. M., Penninger, J. M. and Molkentin, J. D. (2001). Temporally regulated and tissue-specific gene manipulations in the adult and embryonic heart using a tamoxifen-inducible Cre protein. *Circulation research* **89**, 20-25.

Soonpaa, M. H. and Field, L. J. (1997). Assessment of cardiomyocyte DNA synthesis in normal and injured adult mouse hearts. *The American journal of physiology* **272**, H220-226.

Soonpaa, M. H. and Field, L. J. (1998). Survey of studies examining mammalian cardiomyocyte DNA synthesis. *Circulation research* **83**, 15-26.

Soonpaa, M. H., Kim, K. K., Pajak, L., Franklin, M. and Field, L. J. (1996). Cardiomyocyte DNA synthesis and binucleation during murine development. *The American journal of physiology* **271**, H2183-2189.

Speir, E., Tanner, V., Gonzalez, A. M., Farris, J., Baird, A. and Casscells, W. (1992). Acidic and basic fibroblast growth factors in adult rat heart myocytes. Localization, regulation in culture, and effects on DNA synthesis. *Circulation research* **71**, 251-259.

Srinivas, S., Watanabe, T., Lin, C. S., William, C. M., Tanabe, Y., Jessell, T. M. and Costantini, F. (2001). Cre reporter strains produced by targeted insertion of EYFP and ECFP into the ROSA26 locus. *BMC developmental biology* **1**, 4.

Stanton, L. W., Garrard, L. J., Damm, D., Garrick, B. L., Lam, A., Kapoun, A. M., Zheng, Q., Protter, A. A., Schreiner, G. F. and White, R. T. (2000). Altered patterns of gene expression in response to myocardial infarction. *Circulation research* **86**, 939-945.

Steinhauser, M. L., Bailey, A. P., Senyo, S. E., Guillermier, C., Perlstein, T. S., Gould, A. P., Lee, R. T. and Lechene, C. P. (2012). Multi-isotope imaging mass spectrometry quantifies stem cell division and metabolism. *Nature* **481**, 516-519.

Stennard, F. A. and Harvey, R. P. (2005). T-box transcription factors and their roles in regulatory hierarchies in the developing heart. *Development* **132**, 4897-4910.

Stennard, F. A., Costa, M. W., Lai, D., Biben, C., Furtado, M. B., Solloway, M. J., McCulley, D. J., Leimena, C., Preis, J. I., Dunwoodie, S. L. et al. (2005). Murine T-box transcription factor Tbx20 acts as a repressor during heart development, and is essential for adult heart integrity, function and adaptation. *Development* **132**, 2451-2462.

Straight, A. F. and Field, C. M. (2000). Microtubules, membranes and cytokinesis. *Current biology : CB* **10**, R760-770.

Straight, A. F., Field, C. M. and Mitchison, T. J. (2005). Anillin binds nonmuscle myosin II and regulates the contractile ring. *Molecular biology of the cell* **16**, 193-201.

Strutt, D. I. (2002). The asymmetric subcellular localisation of components of the planar polarity pathway. *Seminars in cell & developmental biology* **13**, 225-231.

Sucov, H. M., Gu, Y., Thomas, S., Li, P. and Pashmforoush, M. (2009). Epicardial control of myocardial proliferation and morphogenesis. *Pediatric cardiology* **30**, 617-625.

Sun, Y., Liang, X., Najafi, N., Cass, M., Lin, L., Cai, C. L., Chen, J. and Evans, S. M. (2007). Islet 1 is expressed in distinct cardiovascular lineages, including pacemaker and coronary vascular cells. *Developmental biology* **304**, 286-296.

Takeuchi, J. K., Ohgi, M., Koshiba-Takeuchi, K., Shiratori, H., Sakaki, I., Ogura, K., Saijoh, Y. and Ogura, T. (2003). Tbx5 specifies the left/right ventricles and ventricular septum position during cardiogenesis. *Development* **130**, 5953-5964.

Takeuchi, T., Kojima, M., Nakajima, K. and Kondo, S. (1999). jumonji gene is essential for the neurulation and cardiac development of mouse embryos with a C3H/He background. *Mechanisms of development* **86**, 29-38.

Takeuchi, T., Yamazaki, Y., Katoh-Fukui, Y., Tsuchiya, R., Kondo, S., Motoyama, J. and Higashinakagawa, T. (1995). Gene trap capture of a novel mouse gene, jumonji, required for neural tube formation. *Genes & development* **9**, 1211-1222.

Tam, P. P., Parameswaran, M., Kinder, S. J. and Weinberger, R. P. (1997). The allocation of epiblast cells to the embryonic heart and other mesodermal lineages: the role of ingression and tissue movement during gastrulation. *Development* **124**, 1631-1642.

Thisse, B. and Thisse, C. (2005). Functions and regulations of fibroblast growth factor signaling during embryonic development. *Developmental biology* **287**, 390-402.

Toyoda, M., Shirato, H., Nakajima, K., Kojima, M., Takahashi, M., Kubota, M., Suzuki-Migishima, R., Motegi, Y., Yokoyama, M. and Takeuchi, T. (2003). jumonji downregulates cardiac cell proliferation by repressing cyclin D1 expression. *Developmental cell* **5**, 85-97.

Trivedi, C. M., Zhu, W., Wang, Q., Jia, C., Kee, H. J., Li, L., Hannenhalli, S. and Epstein, J. A. (2010). Hopx and Hdac2 interact to modulate Gata4 acetylation and embryonic cardiac myocyte proliferation. *Developmental cell* **19**, 450-459.

Tseng, A. S., Engel, F. B. and Keating, M. T. (2006). The GSK-3 inhibitor BIO promotes proliferation in mammalian cardiomyocytes. *Chemistry & biology* **13**, 957-963.

Tzahor, E. (2007). Wnt/beta-catenin signaling and cardiogenesis: timing does matter. *Developmental cell* **13**, 10-13.

Tzouanacou, E., Wegener, A., Wymeersch, F. J., Wilson, V. and Nicolas, J. F. (2009). Redefining the progression of lineage segregations during mammalian embryogenesis by clonal analysis. *Developmental cell* **17**, 365-376.

Vacalla, C. M. and Theil, T. (2002). Cst, a novel mouse gene related to Drosophila Castor, exhibits dynamic expression patterns during neurogenesis and heart development. *Mech Dev* **118**, 265-268.

van Berlo, J. H., Maillet, M. and Molkentin, J. D. (2013). Signaling effectors underlying pathologic growth and remodeling of the heart. *The Journal of clinical investigation* **123**, 37-45.

van den Berg, G., Abu-Issa, R., de Boer, B. A., Hutson, M. R., de Boer, P. A., Soufan, A. T., Ruijter, J. M., Kirby, M. L., van den Hoff, M. J. and Moorman, A. F. (2009). A caudal proliferating growth center contributes to both poles of the forming heart tube. *Circulation research* **104**, 179-188.

van den Heuvel, S. and Harlow, E. (1993). Distinct roles for cyclin-dependent kinases in cell cycle control. *Science* **262**, 2050-2054.

van der Linde, D., Konings, E. E., Slager, M. A., Witsenburg, M., Helbing, W. A., Takkenberg, J. J. and Roos-Hesselink, J. W. (2011). Birth prevalence of congenital heart disease worldwide: a systematic review and meta-analysis. *Journal of the American College of Cardiology* **58**, 2241-2247.

van Wijk, B., van den Berg, G., Abu-Issa, R., Barnett, P., van der Velden, S., Schmidt, M., Ruijter, J. M., Kirby, M. L., Moorman, A. F. and van den Hoff, M. J. (2009). Epicardium and myocardium separate from a common precursor pool by crosstalk between bone morphogenetic protein- and fibroblast growth factor-signaling pathways. *Circulation research* **105**, 431-441.

Viragh, S. and Challice, C. E. (1981). The origin of the epicardium and the embryonic myocardial circulation in the mouse. *The Anatomical record* **201**, 157-168.

von Gise, A., Lin, Z., Schlegelmilch, K., Honor, L. B., Pan, G. M., Buck, J. N., Ma, Q., Ishiwata, T., Zhou, B., Camargo, F. D. et al. (2012). YAP1, the nuclear target of Hippo signaling, stimulates heart growth through cardiomyocyte proliferation but not hypertrophy. *Proceedings of the National Academy of Sciences of the United States of America* **109**, 2394-2399.

Wadugu, B. and Kuhn, B. (2012). The role of neuregulin/ErbB2/ErbB4 signaling in the heart with special focus on effects on cardiomyocyte proliferation. *American journal of physiology. Heart and circulatory physiology* **302**, H2139-2147.

Waldo, K. L., Kumiski, D. H., Wallis, K. T., Stadt, H. A., Hutson, M. R., Platt, D. H. and Kirby, M. L. (2001). Conotruncal myocardium arises from a secondary heart field. *Development* **128**, 3179-3188.

Walsh, S., Ponten, A., Fleischmann, B. K. and Jovinge, S. (2010). Cardiomyocyte cell cycle control and growth estimation in vivo--an analysis based on cardiomyocyte nuclei. *Cardiovascular research* **86**, 365-373.

Wang, B., Weidenfeld, J., Lu, M. M., Maika, S., Kuziel, W. A., Morrisey, E. E. and Tucker, P. W. (2004). Foxp1 regulates cardiac outflow tract, endocardial cushion morphogenesis and myocyte proliferation and maturation. *Development* **131**, 4477-4487.

Wang, D., Oparil, S., Feng, J. A., Li, P., Perry, G., Chen, L. B., Dai, M., John, S. W. and Chen, Y. F. (2003). Effects of pressure overload on extracellular matrix expression in the heart of the atrial natriuretic peptide-null mouse. *Hypertension* **42**, 88-95.

Wang, Z. Q., Fung, M. R., Barlow, D. P. and Wagner, E. F. (1994). Regulation of embryonic growth and lysosomal targeting by the imprinted Igf2/Mpr gene. *Nature* **372**, 464-467.

Wei, X., Shimizu, T. and Lai, Z. C. (2007). Mob as tumor suppressor is activated by Hippo kinase for growth inhibition in Drosophila. *The EMBO journal* **26**, 1772-1781.

Weihua, Z., Lin, Q., Ramoth, A. J., Fan, D. and Fidler, I. J. (2011). Formation of solid tumors by a single multinucleated cancer cell. *Cancer* **117**, 4092-4099.

Winter, E. M. and Gittenberger-de Groot, A. C. (2007). Epicardium-derived cells in cardiogenesis and cardiac regeneration. *Cellular and molecular life sciences : CMLS* **64**, 692-703.

Wu, S., Huang, J., Dong, J. and Pan, D. (2003). hippo encodes a Ste-20 family protein kinase that restricts cell proliferation and promotes apoptosis in conjunction with salvador and warts. *Cell* **114**, 445-456.

Xin, M., Olson, E. N. and Bassel-Duby, R. (2013). Mending broken hearts: cardiac development as a basis for adult heart regeneration and repair. *Nature reviews. Molecular cell biology* **14**, 529-541.

Xin, M., Kim, Y., Sutherland, L. B., Qi, X., McAnally, J., Schwartz, R. J., Richardson, J. A., Bassel-Duby, R. and Olson, E. N. (2011). Regulation of insulin-like growth factor signaling by Yap governs cardiomyocyte proliferation and embryonic heart size. *Science signaling* **4**, ra70.

Xu, H., Morishima, M., Wylie, J. N., Schwartz, R. J., Bruneau, B. G., Lindsay, E. A. and Baldini, A. (2004). Tbx1 has a dual role in the morphogenesis of the cardiac outflow tract. *Development* **131**, 3217-3227.

Zaffran, S., Kelly, R. G., Meilhac, S. M., Buckingham, M. E. and Brown, N. A. (2004). Right ventricular myocardium derives from the anterior heart field. *Circulation research* **95**, 261-268.

Zelarayan, L. C., Noack, C., Zafiriou, M. P., Renger, A. and Bergmann, M. W. (2010). Wnt signaling molecules in left ventricular remodeling: focus on dishevelled 1. *Hypertension* **55**, 852-854.

Zeng, B., Tong, S., Ren, X. and Xia, H. (2014). Cardiac cell proliferation assessed by EdU, a novel analysis of cardiac regeneration. *Cytotechnology*.

Zhang, Y., Li, S., Yuan, L., Tian, Y., Weidenfeld, J., Yang, J., Liu, F., Chokas, A. L. and Morrisey, E. E. (2010). Foxp1 coordinates cardiomyocyte proliferation through both cell-autonomous and nonautonomous mechanisms. *Genes & development* **24**, 1746-1757.

Zhang, Z., Huynh, T. and Baldini, A. (2006). Mesodermal expression of Tbx1 is necessary and sufficient for pharyngeal arch and cardiac outflow tract development. *Development* **133**, 3587-3595.

Zhao, B., Wei, X., Li, W., Udan, R. S., Yang, Q., Kim, J., Xie, J., Ikenoue, T., Yu, J., Li, L. et al. (2007). Inactivation of YAP oncoprotein by the Hippo pathway is involved in cell contact inhibition and tissue growth control. *Genes & development* **21**, 2747-2761.

Zhao, Y., Ransom, J. F., Li, A., Vedantham, V., von Drehle, M., Muth, A. N., Tsuchihashi, T., McManus, M. T., Schwartz, R. J. and Srivastava, D. (2007). Dysregulation of cardiogenesis, cardiac conduction, and cell cycle in mice lacking miRNA-1-2. *Cell* **129**, 303-317.

Zhou, B. and Pu, W. T. (2008). More than a cover: epicardium as a novel source of cardiac progenitor cells. *Regenerative medicine* **3**, 633-635.

Zielke, N., Edgar, B. A. and DePamphilis, M. L. (2013). Endoreplication. *Cold Spring Harbor perspectives in biology* **5**, a012948.

CHAPTER 2: *Casz1* is required for cardiomyocyte G1-to-S progression during mammalian cardiac development[1]

INTRODUCTION

Early development of the heart is governed by hyperplastic growth in which cardiac cells undergo mitogen-dependent activation during the G1 phase of the cell cycle (Ahuja et al., 2007). During early stages of heart development cardiomyocytes of the first and second heart fields are highly proliferative, resulting in substantial growth of the embryonic heart. The overall rate of cardiomyocyte proliferation gradually declines concomitant with the onset of terminal cardiomyocyte differentiation (Soonpaa et al., 1996; Christoffels et al., 2000; Pasumarthi and Field, 2002; Sedmera et al., 2003; Ikenishi et al., 2012). After this period, the vertebrate heart continues to grow largely through hypertrophy and by recruitment and proliferation of cells from the neural crest and the epicardium (Li et al., 1996; Creazzo et al., 1998; Manner et al., 2001; Ahuja et al., 2007; Kelly, 2012; Maillet et al., 2013).

---

[1]This chapter is an article in press in the journal *Development*. The citation is as follows: Dorr, K.M., Amin, N.M., Kuchenbrod, L.M., Labiner, H., Charpentier, M.S., Pevny, L.H., Wessels, A., Conlon, F.L. *Casz1* is required for cardiomyocyte G1-to-S progression during mammalian cardiac development. *Development* (2015).

Understanding the transcriptional mechanisms of cardiomyocyte proliferation is critical for uncovering pathologies and treatments for congenital heart disease. Past studies have shown that cardiomyocyctes hyperplastic growth occurs in response to input from a large network of growth factor signaling pathways (Lavine et al., 2005; Ahuja et al., 2007; Bersell et al., 2009; Heallen et al., 2011; Porrello et al., 2011; Xin et al., 2011; Eulalio et al., 2012; von Gise et al., 2012; Wadugu and Kuhn, 2012; Xin et al., 2013). However, many basic questions regarding the mechanisms underlying how these growth factors regulate the cardiomyocyte cell cycle remain unanswered. Central to this issue, it is unknown which cardiac-specific transcription factors act to drive or commit cardiomyocytes into the next round of division.

Casz1 is a para-zinc finger transcription factor that has been shown to be expressed in and required for vertebrate heart development, with depletion of *Casz1* in *Xenopus* embryos leading to a failure of a small subset of progenitor cells to differentiate into cardiomyocytes resulting in aberrant cardiac morphogenesis and eventual death (Vacalla and Theil, 2002; Liu et al., 2006; Christine and Conlon, 2008; Amin et al., 2014; Sojka et al., 2014). The evolutionary role of *Casz1* in heart development is further emphasized by genome-wide association studies showing genetic association of the CASZ1 locus with blood pressure and hypertension (Levy et al., 2009; Takeuchi et al., 2010; Lu et al., 2014). Consistently, it has been demonstrated that CASZ1 has an essential role in blood vessel assembly and lumen formation (Charpentier et al., 2013b; Charpentier et al., 2013a). Together, these studies implicate a potential link between *Casz1* and

cardiovascular dysfunction. However, the genetic requirement and endogenous role for *Casz1* in mammalian cardiac development remains to be established.

Here we report that *Casz1* is expressed in cardiomyocytes during the earliest stages of mammalian heart development, and using genetic fate mapping show *Casz1*-positive cells give rise to derivatives of both the first and second heart field including cardiomyocytes in the left and right ventricles and the left and right atria. Through the generation of a conditional null allele, we demonstrate that *Casz1* is essential for early mammalian heart development and define a role for *Casz1* in the proliferation of cardiomyocytes during chamber formation. We go on to demonstrate an essential role for *Casz1* in the cardiomyocyte cell cycle demonstrating that loss of *Casz1* leads to a prolonged or arrested G1 phase that is associated with a marked reduction in DNA synthesis, an increase in phospho-RB, and a decrease in cardiac mitotic index. Taken together, our results demonstrate a role for *Casz1* in the G1-to-S phase progression of cardiomyocytes.

MATERIALS AND METHODS

Generation of *Casz1* Mutant Mice

BAC clones containing *Casz1* genomic DNA from mouse strain 129 were isolated by established methods (Testa et al., 2003). A plasmid, pBS-DTRX-Casz1Exon6CKO, was constructed that contains the PGKneo expression cassette flanked by two FRT sites, and containing a loxP site was inserted into intron 5. *loxP*

sites were introduced into the *Casz1* locus flanking exon 6 (Liu et al., 2003). Deletion of exon 6 introduces a +2 frameshift in the translational reading frame leading to premature stop codons, resulting in the elimination of CASZ1 protein expression. Furthermore, alternate splicing to the next three exons all result in proteins that are out of frame. The targeting vector contained 2.2 kb of homologous DNA upstream of the first loxP and 1.8 kb of homologous DNA (right arm) downstream of the PGKneo cassette (Liu et al., 2003). The targeting vector was linearized with NotI and electroporated into 1292/Ola embryonic stem cells. G418-resistant colonies were picked, expanded, and screened for homologous recombination by Southern blot analysis of HindIII digested ES cell gDNA using 5' and 3' probes respectively containing sequences outside of those in the targeting vector. Homologous recombinant ES cells were injected into C57BL6/J blastocysts and chimeric male mice were obtained. Male chimeras were mated to C57BL6/J females to establish a mouse line carrying the $Casz1^{flox\text{-}neo/+}$ allele. The frt-flanked PGKneo cassette was removed by mating F1 heterozygous mice to mice expressing the FlpE recombinase (Jackson Labs stock #003800) (Rodriguez et al., 2000). The resulting $Casz1^{flox/flox}$ allele was bred to homozygosity on a C57BL6 background. *Casz1* conditional knockout mice and their control littermates were obtained by breeding female $Casz1^{flox/flox}$ mice to male $Casz1^{flox/+}$ mice expressing $Nkx2.5^{Cre/+}$. $Nkx2.5^{Cre/+}$ mice were obtained from Robert Schwartz (Moses et al., 2001). $Sox2^{Cre/+}$ mice were obtained from Larysa Pevny (Hayashi et al., 2002). $Isl1^{Cre/+}$ mice were obtained from Li Qian (Srinivas et al., 2001).

In Situ Hybridization

In situ hybridization was carried out as previously described (Wilkinson, 1992). Specifically, sense and antisense probes were generated using a digoxigenin (DIG) RNA labeling kit (Roche). Probes were hybridized overnight at 65°C onto E8.5 – E10.5 embryos. DIG-labeled probes were detected by anti-digoxigenin-AP Fab fragments (Roche) and precipitated by BM Purple AP substrate (Roche). Embryos and embryonic hearts were dissected free from surrounding tissues in PBS. Specimens were fixed overnight at 4°C in 4% paraformaldehyde/PBS. In situ probes used were *Nkx2.5* (gift from Benoit Bruneau), and *Casz1* (See primer table for sequences). Tissues were photographed, embedded in 4% low melt agarose (Promega) and sectioned by a Leica VT1200S vibratome to 30μm thickness. Vibratome sections were mounted on slides and imaged on an Olympus BX61 microscope.

RLM-RACE

5’ RLM-RACE was performed according to the manufacturer's instructions (First Choice RLM-RACE kit, Ambion #AM1700). Mouse adult heart RNA was isolated using standard Trizol extraction.

Histologic sectioning and Immunohistochemistry

Embryos were fixed in 4% paraformaldehyde and either paraffin embedded or frozen in OCT. Paraffin sections (8 μm) were dewaxed, rehydrated, and stained with hematoxylin and eosin using standard methodology. Histology sections were imaged on an Olympus BX61 fluorescent microscope. Digital images were utilized for

measurement using Image J software. Paraffin sections and cryosections (10 μm) were washed in PBS+1% Triton X-100 (PBS-T), blocked in PBS-T+10% FBS, and incubated overnight at 4°C with primary antibodies against a series of antigens: rabbit anti-CASZ1 (Santa Cruz #SC-135453) 1:500, mouse anti-cardiac tropomyosin (TMY) (DSHB, clone CH1) 1:50, mouse anti-Islet1 (DSHB, clone 39.4D5) 1:50, rabbit anti-FilaminA (Epitomics #2242-1) 1:100, mouse anti-GFP (Clontech #632381) 1:1000, rabbit anti-phospho histone H3 (Millipore #06-570) 1:200, mouse anti-cardiac troponin T (DSHB, clone RV-C2) 1:50, mouse anti-sarcomeric myosin (DSHB, clone MF20) 1:50, rabbit anti-caspase 3 (Cell Signaling #9661) 1:100, Alexa Fluor 488 – Phalloidin (Molecular Probes #A12379) 1:100, rabbit anti-phosphoRb (Cell Signaling #9308) 1:100, mouse anti-PML (Santa Cruz, #SC-966) 1:500, rabbit anti-cleaved caspase 3 (Asp175) (Cell Signaling #9661) 1:50. CASZ1 antibody staining required antigen retrieval. Briefly, sections were steamed in 10 mM Sodium Citrate pH 6.0/0.05% Tween-20 for 20 minutes, washed in 1X PBS and subjected to processing as detailed above. The following day, sections were washed in PBS-T then incubated for 1 hour at room temperature with secondary antibodies: Alexa 488 goat anti-mouse IgG, H+L (Molecular Probes #A11001) 1:1000, Alexa 488 donkey anti-rabbit IgG (Molecular Probes #A21206) 1:1000, Alexa 546 goat anti-rabbit IgG (Molecular Probes #A11010) 1:1000, Alexa 546 goat anti-mouse IgG (Molecular Probes #A11030) 1:1000. Sections were washed in PBS-T, incubated with 200ng/mL DAPI (Sigma) and mounted with Fluoromount. Stained sections were imaged on Zeiss 700 confocal microscope and ImageJ was used for analysis.

Cell culture

HUVECS (Lonza) were maintained and immunostained as previously described (Charpentier et al., 2013b).

Reporter crosses

Tie2-Cre (Kisanuki et al., 2001) mice were crossed to $R26R^{eGFP}$ reporter mice. *Wt1/IRES/GFP-Cre* mice were previously reported (Wessels et al., 2012). Time-mated females were harvested at E14.5 and processed for immunostaining with anti-GFP as detailed above. *Nkx2.5-Cre* mice (Moses et al., 2001) were crossed to $R26R^{tdT}$ reporter mice (Madisen et al., 2010). Time-mated females were harvested at E7.5, E9.5, E12.5 and E14.5. *Sox2-Cre* mice (Hayashi et al., 2002) were crossed to $R26R^{LacZ}$ reporter mice (Soriano, 1999) and time-mated females were harvested at E10.5. All embryos were imaged with a Leica MZ 16F dissection microscope.

β-Galactosidase Staining

Embryos were fixed in X-gal fixative (0.2% glutaraldehyde, 2mM $MgCl_2$, 5mM EGTA, 0.1M phosphate buffer) for 40 minutes on ice, washed in detergent (0.1M phosphate buffer, 2mM $MgCl_2$, 0.01% sodium deoxycholate, 0.02% NP-40), and incubated in X-gal staining solution (1mg/ml X-gal in DMF, 5mM potassium ferricyanide, 5mM potassium ferrocyanide, 0.1M phosphate buffer, 2mM $MgCl_2$, 0.01% sodium deoxycholate, 0.02% NP-40, 20mM Tris) at 37°C overnight.

Tamoxifen Injections

Tamoxifen (Sigma#T5648) was dissolved in 1/10 volume 200 proof ethanol and 9/10 volume sunflower oil to make a 0.03mg/µl solution. Time-mated females were injected IP with 3 mg of tamoxifen at E8.5 and embryos were harvested at E12.5. No reporter activity was observed in the absence of tamoxifen. Embryos were fixed in 4% paraformaldehyde, incubated in Scale U2 solution (Hama et al., 2011) at 4°C for 3 weeks, imaged with a Leica MZ 16F dissection microscope, washed in 1X PBS, sunk in 30% sucrose and frozen in OCT. Cryosections were processed and immunostained as detailed above.

Imaging and statistical analysis

A Leica MZ 16F dissection microscope with a Retiga 4000RV camera was used for whole-mount imaging and an Olympus BX61 with a Retiga 4000R camera for color imaging. Higher magnification images were captured using a Zeiss 700 laser scanning confocal microscope. All images and figures were edited and created in either Image J or Photoshop CS4. All statistical calculations were performed using Prism 5 (Graph Pad). P values for statistical significance were obtained using a Student's t-test for single variable between control and test samples.

Cardiomyocyte counting assay

Embryos from time-mated females were recovered at E10.5 and E12.5, fixed in 4% PFA and embedded for cryosection. Sections were stained with tropomyosin (TMY) and DAPI. For statistical analysis, 9 transverse sections were analyzed, 3 sections

(representing the anterior, mid, and posterior heart) from 3 difference embryos per genotype. The number of TMY-positive and DAPI-positive cardiomyocytes were counted from six 40X fields per section. Cell counts of total cells positive for TMY and DAPI were averaged from 54 sections. Data shown as mean ±SEM. ImageJ was used for analysis and cell counts. Data were compared for statistical significance using a student t-test.

Proliferation assays

For EdU analysis, time-mated females were injected IP with 250 µg EdU (5-ethynyl-2′deoxyuridine, Click-iT EdU Imaging Kit, Invitrogen C10338) three hours prior to sacrifice. Embryos were recovered at E12.5, fixed with PFA and embedded for cryosections (n=3/3). EdU staining was performed according to the manufacturer's instructions. For statistical analysis, 9 transverse sections were analyzed, 3 sections (representing the anterior, mid, and posterior heart) from 3 different wild-type embryos and two *Casz1*$^{f/f}$*;Nkx2.5*$^{Cre/+}$ embryos. The number of EdU-positive cardiomyocytes relative to the total number of cardiomyocytes (TMY-positive cells) was counted from four 40X fields per section (2 fields per ventricle). For mitotic index analysis, cell counts of total cells positive for TMY and total cells positive for phospho-histone H3 (pHH3) expression were performed on transverse sections using the same statistical analysis of wild-type and *Casz1* mutant hearts at E12.5 (n=3/3) from four 63X fields per sections (2 fields per ventricle). Mitotic index was calculated by dividing total cells positive for TMY and pHH3 expression by total cells positive for TMY. All sections were processed for immunostaining as detailed above. Data shown as mean ±SEM. ImageJ was used for

analysis and cell counts. Data were compared for statistical significance using a student t-test.

Scanning Electron Microscopy

A standardized procedure for scanning electron microscopy (Hullinger et al.) of the heart was utilized (Pexieder, 1986). Briefly, the pericardial cavity membrane was excised in embryos before being fixed in 2.5% glutaraldehyde (EM grade, Electron Microscopy Science, PA) as previously reported (Tandon et al., 2013) in 1X PBS at 4°C overnight. Embryos were washed in 1X PBS, dehydrated into 100% ethanol dehydration and subject to critical point drying. Dried specimens were mounted ventral side up and ion sputtered with Gold Palladium to approximately 40 nm thickness before being scanned with a Zeiss Supra 25 FESEM microscope. SEM photomicrographs were taken in standard orientations and magnifications.

RNA-Seq

E10.5 hearts were collected from three *Casz1*$^{f/f}$*;Nkx2.5*$^{Cre/+}$and three *Casz1*$^{f/+}$*;Nkx2.5*$^{+/+}$ embryos. RNA was isolated using standard Trizol extraction. RNA-seq libraries were generated with TruSeq adaptor barcodes from these six samples using standard library preparation protocols (Illumina) by the Vanderbilt Genomic Core. Samples were run over three lanes of a HiSeq2500 (Illumina) to generate on average 103.7 million 50 base pair single-end reads per sample by the Vanderbilt Genomic Core. Samples were assessed for quality using Fastqc 0.10.1 and then mapped to the mouse genome (build mm10) using TopHat, version 2.0.8 with default parameters

(Trapnell et al., 2009; Trapnell et al., 2012). Aligned reads were then tallied per annotated gene (RefSeq genes downloaded from www.genome.ucsc.edu July 24, 2013) were then normalized using RPKM values and analyzed for differential expression via Cufflinks, version 2.1.1 (Trapnell et al., 2012). For Gene Ontology Analysis, genes tested for differential expression that had a *p* value of less than 0.05 were considered differentially expressed. These genes were split into two classes, upregulated and downregulated in *Casz1* mutant hearts. These genes were assessed for Gene Ontology (GO) biological process enrichment using Gorilla (Eden et al., 2009), with the annotated gene list provided as a background. GO terms enriched in either class with an FDR q-value of less than 0.05 were consolidated based on similar processes to generate a more manageable set of GO terms for visualization using REVIGO (Supek et al., 2011).

Embryonic Cardiac Nuclei Isolation and Flow Cytometry

Embryos from time-mated females were recovered at E12.5. Hearts were dissected in PBS and atria were removed. Ventricles were placed in liquid nitrogen and stored at -80°C. Similar genotypes were pooled (n=4 wild-type/4 cardiac nulls) and homogenized in liquid nitrogen following a modified cardiac nuclei extraction protocol (Franklin et al., 2011). Briefly, ventricle powder was resuspended in homogenization buffer (10mM Tris pH 7.4, 250mM sucrose, 1mM EDTA, 0.1% NP-40, 10mM sodium butyrate, 0.1mM PMSF, 1X protease inhibitors) and subjected to 10 strokes with a dounce homogenizer on ice. Nuclei were passed through a cell strainer, centrifuged at 1000g for 10 minutes at 4°C and pellets were resuspended in PBS, and fixed with 70%

ETOH for 30 minutes on ice. Nuclei were washed and resuspended in FACS Buffer (PBS, 7.5% BSA, 2mM EDTA). Nuclei were and treated with 100 µg/ml RNaseA and stained with 50 µg/ml propidium iodide (Sigma #P4170) and analyzed on a flow cytometer. All samples were analyzed on an Accuri Flowcytometer using CFlowPlus Analysis Software. DNA content was determined using at least 100,000 cardiac nuclei.

RESULTS

Casz1 is expressed in the developing myocardium

To address the role of *Casz1* in mammalian heart development, we cloned full-length *Casz1* from adult mouse heart tissue and conducted a detailed expression analysis. We found that *Casz1* is first expressed in the cardiac crescent (E7.5, Figure 2.1A) and continues to be expressed in the heart during cardiac looping (E8, Figure 2.1B,F; E8.5 – E9.5, Figure 2.1C,D,G,H), when we observed *Casz1* expression in the future left and right ventricles, in both the compact layer and the trabeculae, and in the primitive atria (E9.5, Figure 2.1D,H). Sectioning of heart tissue at these stages further revealed *Casz1* to be expressed in both the myocardium and endocardium (E8.5; Figure 2.1G). By E11.5 we found expression of *Casz1* in the heart but also in other tissue types including the limb bud, nasal placode, somites, telencephalon, hindbrain, and consistent with recent reports the eye (Konstantinides et al., 2015; Mattar et al., 2015) (Figure 2.1E).

We observed that CASZ1 protein is expressed in a pattern similar to that of *Casz1* mRNA. Our data demonstrates that CASZ1 is expressed in defined subdomains of the nucleus (Figure 2.1I-L). Given that it is not technically possible to investigate nuclear domains in cardiac tissue in vivo, we examined the compartmentalization of CASZ1 in human primary endothelial cells (HUVECS), a cell type previously shown to express CASZ1 (Charpentier et al., 2013b). From these studies we demonstrate that CASZ1 co-localizes with promyelocytic leukemia (PML), a defining protein of PML bodies (Figure S2.1). PML bodies are well-defined nuclear subdomains found to associate with a distinct set of genomic loci however, these loci are undefined and moreover, there is no known function for PML in cardiovascular development in disease (Matera et al., 2009).

Expression analysis demonstrated that CASZ1 protein is expressed in the tropomyosin (TMY)-positive cardiomyocytes (Fig. 1I-L), while its expression is mutually exclusive to that of *Tie2*-positive derived endothelial cells (Figure 2.1M) and *Wt1*-positive derived epicardial cells (Figure 2.1N). We further find that CASZ1 is co-expressed in second heart field cells with the second heart field marker ISL1 (Cai et al., 2003; Sun et al., 2007) (Figure 2.1O-P). Collectively, this data demonstrates that CASZ1 is expressed in the nucleus of cardiomyocytes, and by inference in PML bodies, of the first and second heart fields during the early stages of cardiogenesis.

Casz1-expressing cells give rise to first and second heart field derivatives

To determine if cardiomyocytes that express *Casz1* contribute to derivatives of the first and second heart field, we performed genetic lineage tracing of *Casz1*-expressing cells. To permanently label this population of cells and its descendants, we generated a tamoxifen-inducible "CreERT2" allele (*Casz1*^{CreERT2}) by homologous recombination in embryonic stem cells (ESCs) and subsequently passed the *Casz1*^{CreERT2} through the germline (Figure S2.2). Treatment with tamoxifen results in Cre recombination and in the presence of a tomato reporter (*R26R*^{tdT}), identification of *Casz1*-expressing cells and their progeny. Co-staining with the cardiomyocyte marker, tropomyosin (TMY), enabled lineage identification of tagged cell populations. From this lineage analysis we identified cardiomyocytes derived from *Casz1*-expressing cells (Figure S2.2C-D, Figure 2.2A-J) at E12.5 in the left (Figure 2.2I,J) and right ventricular walls (Figure 2.2A,B,G,H), the interventricular septum (Figure 2.2C,D), the compact layer (Figure 2.2G,H) and the trabeculae (Figure 2.2E,F). We found no evidence that *Casz1*-expressing cells can give rise to cardiac fibroblasts or cardiac endothelium however, we note that the recombination frequency of the *Casz1*^{CreERT2} allele with the present tamoxifen regime is low and therefore we cannot formally rule out this possibility. Collectively, our studies show that E8.5 *Casz1*-expressing cells give rise to cardiomyocytes derived from both the first and second heart fields.

Casz1 is essential for cardiac development

To determine the requirement for *Casz1* in cardiac development, we mapped the cardiac transcriptional start site(s) of *Casz1* (Figure S2.3B). Our analysis identified two transcriptional start sites in embryonic hearts: one 275 bp upstream and the other 139 bp upstream from the predicted translational start site. Using this data we went on to generate a conditional "floxed" null allele (*Casz1*$^{flox\text{-}neo}$) by homologous recombination in ESCs. Successful targeting of the selection cassette generated a *Casz1*$^{flox\text{-}neo}$ allele, which flanks exon 6 with loxP sites (Figure S2.3A). Exon 6 was chosen because it is a critical coding exon located downstream of both *Casz1* transcriptional start sites. Furthermore, alternate splicing to the next three exons all result in proteins that are out of frame.

The presence of the *Casz1*$^{flox\text{-}neo}$ allele in ESCs was confirmed by Southern blot, PCR and genomic sequence analysis (Figure S2.3C,D, data not shown). ESCs harboring *Casz1*$^{flox\text{-}neo}$ were used to generate chimeric mice which passed the *Casz1*$^{flox\text{-}neo}$ through the germline. The PGKneo cassette (Liu et al., 2003) was removed by mating F1 heterozygous mice to mice expressing FlpE recombinase (Rodriguez et al., 2000) and *Casz1*$^{f/+}$ progeny were mated to an *Nkx2.5-Cre* line to generate *Casz1*$^{f/+}$*;Nkx2.5*$^{Cre/+}$ (Moses et al., 2001). The resulting *Casz1*$^{f/+}$*;Nkx2.5*$^{Cre/+}$ mice were mated to *Casz1*$^{f/f}$ mice to generate a cardiac specific conditional *Casz1* mutation: *Casz1*$^{f/f}$*;Nkx2.5*$^{Cre/+}$. Expression of Cre from the *Nkx2.5-Cre* allele was confirmed by mating to R26R^{tdT} reporter mice (Madisen et al., 2010) (Figure S2.4) and loss of *Casz1*

in *Casz1*$^{f/f}$*;Nkx2.5*$^{Cre/+}$ in cardiac but not neural tissue (dorsal root ganglia) confirmed by immuno-histochemistry (Figure S2.3E-H).

We observed that heterozygotes containing the *Casz1*$^{f/+}$*;Nkx2.5*$^{Cre/+}$ alleles are viable, fertile, and display no obvious phenotypic abnormalities. In contrast, no homozygous mice for the floxed allele, *Casz1*$^{f/f}$*;Nkx2.5*$^{Cre/+}$, were recovered postnatally, indicating that loss of *Casz1* in the developing heart is embryonic lethal.

Analysis of timed intercrosses of *Casz1*$^{f/+}$*;Nkx2.5*$^{Cre/+}$ mice failed to identify viable homozygous *Casz1*$^{f/f}$*;Nkx2.5*$^{Cre/+}$embryos subsequent to E14.5 (Figure 2.3). Gross examination of *Casz1*$^{f/f}$*;Nkx2.5*$^{Cre/+}$embryos demonstrated that E12.5 mutants are indistinguishable from their wild-type littermates (Figure 2.3A,B). However, at E13.5 *Casz1*$^{f/f}$*;Nkx2.5*$^{Cre/+}$embryos exhibit inflated pericardial sacs, severe edema and blood hemorrhaging, consistently indicative of circulatory distress (Figure 2.3C,D) (Conway et al., 2003).

Ultrastructural analysis using Scanning Electron Microscopy (Hullinger et al.) of *Casz1*$^{f/f}$*;Nkx2.5*$^{Cre/+}$ hearts at E12.5, showed detectable cardiac malformations including an enlarged right atrium and an malformed left ventricle (Figure 2.3E,F). These defects are more pronounced by E13.5 (Figure 2.3G,H) with ballooning of the right atria indicative of blood pooling in the right ventricle (Deng et al., 1996). Collectively, these results demonstrate an essential requirement for *Casz1* in mammalian heart development between E10.5 and E12.5.

Casz1 is required for growth of the cardiac chambers

Histological examination showed that *Casz1$^{f/f}$;Nkx2.5$^{Cre/+}$* and wild-type hearts were indistinguishable at E10.5 (mean ventricular wall thickness of 15.4±0.44 μm versus 16.1±0.70 μm respectively, n=3, p0.42) (Figure 2.3I-J',O). However by E12.5, severe thinning of the myocardium and associated decreased wall thickness was observed in *Casz1$^{f/f}$;Nkx2.5$^{Cre/+}$* embryos as compared to wild-type littermate controls (mean of 22.6±1.2 μm; n=2 versus 14.3±0.91 μm; n=4, p<0.005), indicating that *Casz1* is required in the ventricular myocardium. In addition, we observed an underdeveloped interventricular septum and decreased trabeculation (Figure 2.3K-L',P). By E13.5, *Casz1$^{f/f}$;Nkx2.5$^{Cre/+}$* hearts were hypoplastic, with narrower ventricular lumens and membranous ventricular septal defects (Figure S2.5). Together these results demonstrate that *Casz1* is essential for development of the cardiac chambers and further imply that *Casz1* is essential for cardiomyocyte growth.

Casz1 embryonic nulls phenocopy Casz1$^{f/f}$;Nkx2.5$^{Cre/+}$ embryos

To test if *Casz1* is required for embryogenesis prior to E12.5 we generated a complete embryonic null allele of *Casz1* by mating *Casz1$^{f/f}$* mice to a *Sox2-Cre* driver: *Casz1$^{f/f}$;Sox2$^{Cre/+}$* (Hayashi et al., 2002). Extensive studies have established that *Sox2-Cre* is expressed and functions in all cells of the epiblast (Figure 2.4A,B) (Hayashi et al., 2002; Barrow et al., 2007; Arnold et al., 2009; Delgado-Esteban et al., 2013). We found that *Casz1$^{f/f}$;Sox2$^{Cre/+}$* mice, as with *Casz1$^{f/f}$;Nkx2.5$^{Cre/+}$*, do not survive beyond E14.5. Histological examination at E12.5 confirmed that *Casz1$^{f/f}$;Sox2$^{Cre/+}$* homozygotes have a

cardiac phenotype indistinguishable from that of *Casz1*$^{f/f}$*;Nkx2.5*$^{Cre/+}$mice (ventricular wall thickness mean of 41.2±2.1 μm versus 25.8±1.6 μm respectively, n=2, p<0.0005) (Figure 2.3I-P,4E-I). These results demonstrate that an initial and essential requirement for *Casz1* in the mouse embryo is in the developing heart and confirm that loss of *Casz1* in cardiac tissue leads to hypoplastic growth and embryonic lethality.

Casz1 is essential in the second heart field

Cells from the second heart field give rise to the right ventricle, the interventricular septum, the outflow tract, both atria, and the atrial septum (Kelly, 2012). Our data demonstrated that CASZ1 is co-expressed with the second heart field marker ISL1 at E10.5 (Figure 2.1O,P), and our fate mapping studies identified descendants of *Casz1* expressing cells within second heart field derivatives (Figure 2.2A,B,G,H). We further observed that loss of *Casz1* in *Nkx2.5*-positive cells leads to a hypoplastic right ventricle. Based on these observations we hypothesize that *Casz1* is required for second heart field development. To test this hypothesis we generated mice that lack *Casz1* in the second heart field by crossing *Casz1*$^{f/f}$ mice to an *Isl1-Cre* driver, *Casz1*$^{f/f}$*;Isl1*$^{Cre/+}$ (Srinivas et al., 2001). Gross examination of *Casz1*$^{f/f}$*;Isl1*$^{Cre/+}$ embryos showed that they are viable and indistinguishable from heterozygous and wild-type littermates at least until E14.5 (Figure 2.5G,H). Examination showed that at E14.5 *Casz1*$^{f/f}$*;Isl1*$^{Cre/+}$ hearts have a normal left ventricle (mean=82.6±3.7 μm versus 79.7±5.4 μm, n=2, p-value=0.66) (Figure 2.5J) while displaying reduced thickness in the right (mean=64.5±1.7 μm versus 37.9±4.3 μm, n=2, p-value<0.005) (Figure 2.5I). Though there were significant differences in thickness of the ventricular free wall, we did not

detect any observable ventricular septal defects (Figure 2.5A-F). Consistently with right ventricular hypoplasia, no *Casz1*$^{f/f}$;*Isl1*$^{Cre/+}$ mice were recovered postnatally, indicating that *Casz1* is required for the growth of the second heart field.

Regulation of cell growth by Casz1

The observations that the loss of *Casz1* in cardiac tissue leads to a hypoplastic heart and a concomitant decrease in chamber wall thickness led us to hypothesize that *Casz1* functions to regulate cardiomyocyte proliferation. To test this hypothesis, we determined the number of cardiomyocytes in wild-type and *Casz1*$^{f/f}$;*Nkx2.5*$^{Cre/+}$ mice. From this analysis, we find cardiomyocytes, as marked by expression of tropomyosin (TMY), were significantly reduced in *Casz1* cardiac null versus wild-type ventricles at E12.5 (Figures 2.6A-F, S2.6), and further found a striking reduction in cardiomyocyte number within the ventricular walls of the heart at E12.5 (mean of 868±69 versus 638±60 cardiomyocytes, $n \geq 3$, $p < 0.05$). We note that the cardiac hypoplasia observed in *Casz1*cardiac null hearts is specific to the cardiomyocytes and does not affect the epicardium or the endothelial cells at E12.5 (Figure 2.6P,Q). Furthermore, the reduction in cell number is not associated with programmed cell death (Figure S2.8). Consistently, cardiomyocytes in *Casz1* cardiac null hearts continue to express the cardiomyocyte markers TMY and cardiac troponin T (cTNT) and we can detect higher order structures including sarcomeres with Z-disks (Figure 2.6R-U). Together, these studies support a role for *Casz1* in cardiomyocyte growth.

To validate our findings, we performed a comparative expression analysis of the developing heart using RNA isolated from E10.5 hearts (n = 3, cardiac null; n = 3, controls), a period before we can detect any cardiac abnormalities in *Casz1*$^{f/f}$*;Nkx2.5*$^{Cre/+}$ embryos. RNA-seq data was processed for differential expression (DE) analysis using Cufflinks (Trapnell et al., 2012) (Raw data and full analysis is available at the NCBI Gene Expression Omnibus (accession #GSE55394)). We used unbiased gene ontology and from this analysis determined the three largest categories of genes downregulated as a result of the loss of *Casz1* were “Regulation of growth”, Regulation of systems processes” and “Cardiac muscle development” (Figure S2.7). Thus, these analyses suggest that *Casz1* functions to regulate the growth of the cardiac chambers.

Casz1 is required for cardiomyocyte G1-to-S phase transition

Our phenotypic analysis, cell quantification, and transcriptional profiling are all consistent with a role for *Casz1* in cardiomyocyte cell division. To gain insight into the mechanisms of *Casz1*-mediated cardiomyocyte growth, we conducted a detailed analysis of cell proliferation. Our results show a significant reduction in EdU incorporation in myocardial cells in the developing myocardium in *Casz1* cardiac null ventricles versus controls (mean of 19.5±0.9%; n=3 versus 13.6±0.8%; n=3, $p<0.0001$) (Figure 2.6G-J,M). The cardiomyocyte mitotic index in E12.5 *Casz1*$^{f/f}$*;Nkx2.5*$^{Cre/+}$ ventricles (mean of 19.6±1.1% versus 13.7±0.98%, n=3, $p<0.005$) and *Casz1*$^{f/f}$*;Isl1*$^{Cre/+}$ right ventricles (mean of 19.3±1.1% versus 13.5±2.1%, n=2, $p<0.05$) was also reduced as assessed by phospho-histone H3 (pHH3) (Figure 2.6K-L,N,O). Thus, *Casz1* acts to control cardiomyocyte proliferation in both the first and second heart fields.

To further define the mechanism by which *Casz1* functions in cardiomyocyte cell division, we conducted cell cycle profiling of cardiac nuclei from control and *Casz1* cardiac null heart tissue (Figure 2.7A). Our results indicate that cardiac nuclei null for *Casz1* display a significant increase in cells in G1-phase (52.3% versus 60.1%) and a concomitant decrease of cells in S-phase (26.1% versus 19.4%) while displaying no alteration of the percent of cells in G2-phase (21.5% versus 20.5%). Consistently, we observe a significant increase in *Casz1* cardiac null cardiomyocytes expressing the phosphorylated form of the tumour suppressor protein RB, a highly effective inhibitor of the G1-to-S transition (mean of 3.5±0.3% versus 5.3±0.7%, $p<0.05$) (Figure 2.7B-D) (Mulligan and Jacks, 1998). Taken together, our results show that a loss of *Casz1* leads to a prolonged or arrested S-phase, a decrease in DNA synthesis, an increase in phospho-RB, and a decrease in the cardiac mitotic index. Thus, these results support a role for *Casz1* in the cardiomyocyte G1-to-S cell cycle transition.

DISCUSSION

Here we report that *Casz1* is expressed in mammalian cardiomyocytes and by genetic fate mapping studies demonstrate that *Casz1*-positive cells give rise to cardiomyocytes in the first and second heart field. We show through our phenotypic analysis of cardiac conditional null *Casz1* embryos, that *Casz1* is essential for proliferation of cardiomyocytes in both heart fields and define a role of *Casz1* in cardiomyocyte proliferation.

We note that these findings differ from those reported for a *Casz1* gene trap line of mice that were generated from an ESC line carrying a βgeo cassette integrated into the 9th intron of *Casz1* (Liu et al., 2014). Mice homozygous for the insertion led to embryonic arrest at E16.5, a time point in development much later than those reported here in mice in which *Casz1* was depleted in both the primary and secondary heart fields (*Casz1*$^{f/f}$*;Nkx2.5*$^{Cre/+}$), in those mice depleted of *Casz1* in the second heart field (*Casz1*$^{f/f}$*;Isl1*$^{Cre/+}$) or in a complete embryonic null (*Casz1*$^{f/f}$*;Sox2*$^{Cre/+}$). Since the trapped allele and our panel of *Casz1* mutants are in the same genetic background, it is unclear why the trapped allele is less penetrant though it remains formally possible that the allele disrupted by the βgeo insertion occurs in an alternatively spliced form of *Casz1* and/or is hypomorphic.

CASZ1 and the G1-to-S phase transition

During early G1, cells respond to mitotic signals to pause or initiate DNA replication (Bertoli et al., 2013). Our analysis of the cardiomyocyte mitotic index coupled with our cell cycle profiling demonstrates a decrease in *Casz1* cardiac null cells progressing through S-phase. The failure to progress through S-phase, and the decrease in cardiomyocyte number in *Casz1*-null hearts, is not associated with programmed cell death, and we show that at the period when we observe decreased cardiomyocyte numbers, *Casz1*-null cardiomyocytes maintain their structural integrity and higher ordered structure (Figure 2.6). Given that we observe a decrease in DNA

replication in *Casz1* null hearts, as shown by EdU, and a concomitant increase in phospho-RB, our data strongly imply that *Casz1* acts at the G1-to-S phase transition.

We note in our cell cycle profiling that an appreciable number of cells pass through the G1-to-S phase. Since it is not possible to isolate pure cardiomyocyte population from our *Casz1* null embryos these cells most likely represent other cardiac cell populations including cardiac fibroblasts and endothelial cells. However, it is formally possible that some of these cells may represent cardiomyocytes that have not reached the G1-to-S transition; i.e. a period after which they require *Casz1*.

One the major checkpoint controls of cell cycle is the ‘commitment point’ or ‘restriction point’ associated with the G1-to-S phase transition. This point in the cycle, also known as ‘start’ in yeast, is the point beyond which a cell will pass through the cycle without external input (Bertoli et al., 2013). Based on our findings, we presently favor a model by which *Casz1* is necessary but not sufficient for cardiomyocytes to pass the restriction point and commit to the next round of division. We note this role of *Casz1* must be stage specific as we fail to see any phenotypic consequences of removing *Casz1* during the initial stages of cardiac specification and determination (E6-E8). This observation would imply that this checkpoint control is under a separate, as of yet unidentified mechanism in the early stages of heart development. In the future, it will be of importance to identify the *Casz1*-dependent pathway during these early stages of cardiac development and determine what role, if any, CASZ1 plays in adult homoeostasis and injury repair.

Figure 2.1. *Casz1* is expressed in the developing heart

Whole mount in situ hybridization at E7.5 (A), E8.0 (B) and (F), E8.5 (C) and (G), E9.5 (D) and (H), and E11.5 (E). *Casz1* is first expressed in myocardial precursors cells beginning at embryonic day e7.5 (A). At E8.0, *Casz1* transcripts are found in the linear heart tube (B) and as the heart undergoes looping (C, D). (E) *Casz1* is also expressed in the eye, the nasal placode, somites, telencephalon, hindbrain, and the developing limb bud. (F-H) Vibratome sections of whole mount embryos reveal that *Casz1* is expressed specifically in the first heart field at early stages of heart development (F). *Casz1* is expressed in the myocardium and the endocardium (G) and in the trabeculae (H). (I- L) CASZ1 colocalizes with the cardiomyocyte marker tropomyosin (TMY) in the myocardium of an E14.5 left ventricle. CASZ1 is not expressed at E14.5 in *Tie2*-positive endothelial cells (M) nor *Wt1*-positive epicardial cells (N). (M,N) Sections of *Tie2-Cre*;*R26R-EGFP* reporters were used to mark endothelial cells (M) and a *Wt1-Cre*;*R26R-EGFP* reporters to mark epicardial cells. (L) Enlarged image (white box in Fig. 1K) of the left ventricular myocardium highlights the expression of CASZ1 within the nuclear bodies of the nucleus. (O-P) Immunofluorescent staining for CASZ1 and ISL1shows coexpression in OFT myocardium at E10.5. (P) Enlarged images of OFT myocardium depicted in (O). MP, myocardial progenitor cells; HT, developing heart tube; LH, looped heart; N, neural tube; E, eye; HB, hindbrain; NP, nasal placode; T, telencephalon; LB, limb bud; S, somites; PME, pharyngeal mesoderm; MY, myocardium; EN, endocardium; TR, trabeculae; CAC, common atrial chamber; CVC, common ventricular chamber; CL, compact layer; EPI, epicardium; LV, left ventricle; OFT, outflow tract; FG, foregut. Scale bars indicate 20 μm (I – K, M, N), 5 μm (L), 10 μm (P), 20 μm (O).

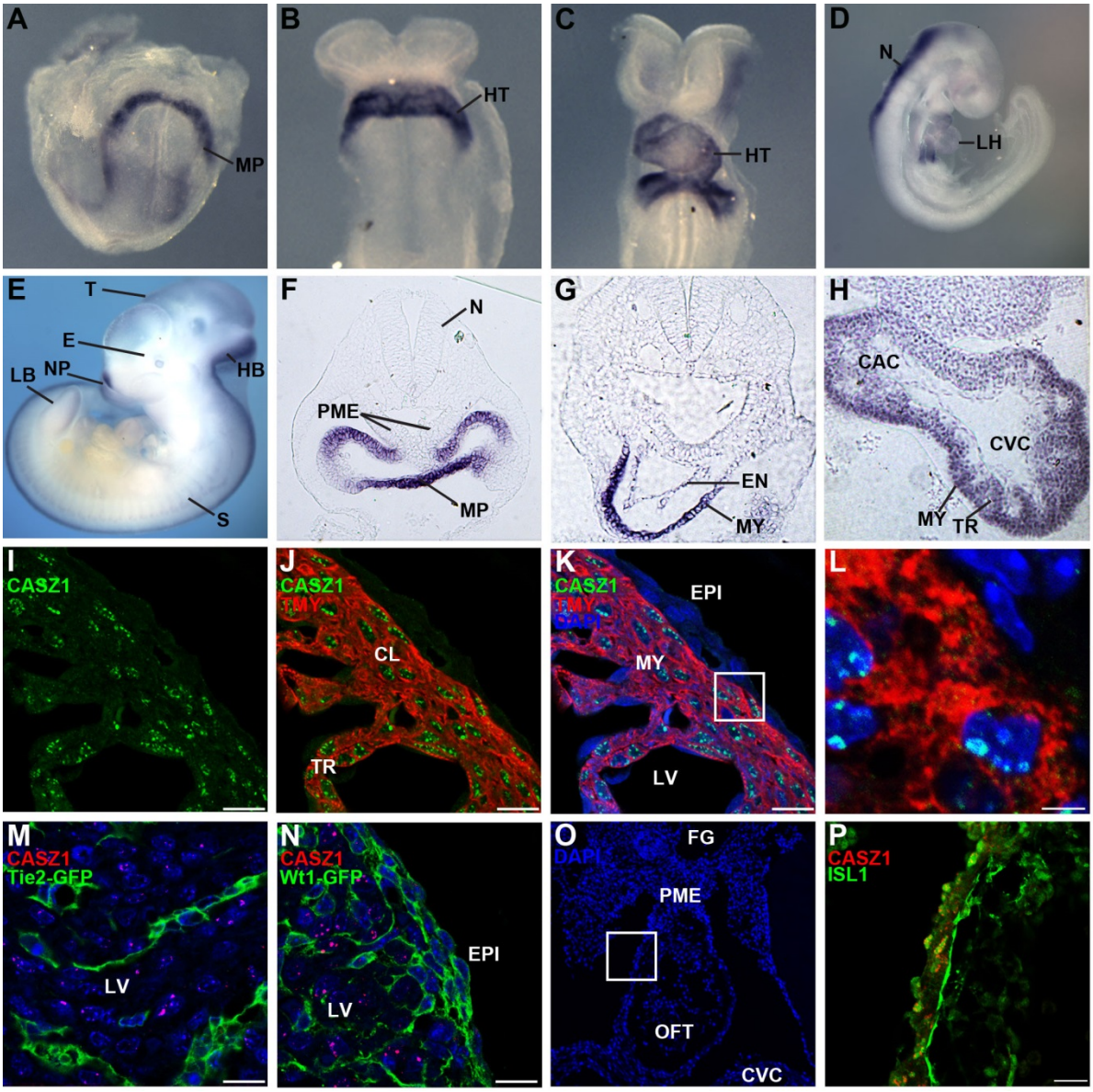
A
MP
B
HT
C
HT
D
N
LH
E
T
E
LB
NP
HB
S
F
N
PME
MP
G
EN
MY
H
CAC
CVC
MY
TR
I
CASZ1
J
CASZ1
CL
TR
K
CASZ1
EPI
MY
LV
L
M
CASZ1
Tie2-GFP
LV
N
CASZ1
Wt1-GFP
EPI
LV
O
DAPI
FG
PME
OFT
CVC
P
CASZ1
ISL1

Figure 2.2. Lineage tracing with *Casz1*$^{CreERT2\text{-}neo}$ labels cardiomyocytes in first and second heart field derivatives

(A-J) Immunofluorescent staining for cardiac tropomyosin and DAPI (blue) of *Casz1*$^{CreERT2/+}$;*R26R*$^{tdT/+}$ embryo depicted in (Fig.S2) shows *Casz1*-expressing cells give rise to cardiomyocytes located in the walls of the left (I,J) and right ventricles (A,B,G,H) the interventricular septum (C,D), and the trabeculae (E,F). Scale bars indicate 20 μm. RV, right ventricle; LV, left ventricle; IVS, interventricular septum; TR, trabeculae; CL, compact layer.

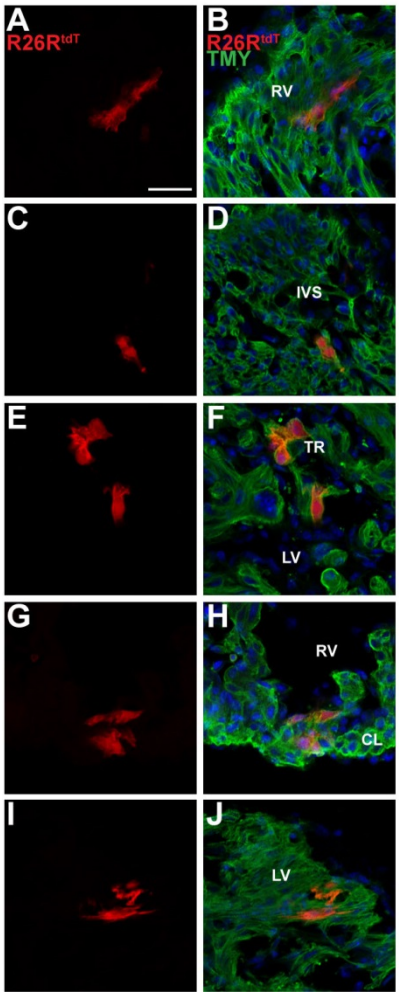

Figure 2.3. *Casz1* is required for cardiac development

(A – D) Gross morphology of *Casz1*$^{f/+}$;*Nkx2.5*$^{+/+}$ wild-type (WT) and C*asz1*$^{f/f}$;*Nkx2.5*$^{Cre/+}$ embryos. By E13.5 *Casz1*$^{f/f}$;*Nkx2.5*$^{Cre/+}$ embryos are beginning to exhibit edema and have decreased blood flow throughout the vasculature. (E – H) SEM analysis of wild-type and *Casz1*$^{f/f}$;*Nkx2.5*$^{Cre/+}$ hearts at E12.5 and E13.5 highlights cardiac defects. At E12.5, *Casz1*$^{f/f}$;*Nkx2.5*$^{Cre/+}$ embryos have cardiac malformations including an enlarged right atria and an aberrant left ventricle. These defects are more pronounced at E13.5. (I – P) Histological analysis of WT and *Casz1*$^{f/f}$;*Nkx2.5*$^{Cre/+}$ hearts. *Casz1*$^{f/f}$;*Nkx2.5*$^{Cre/+}$ embryos exhibit severe cardiac hypoplasia and ventral septal defects. Hematoxylin & Eosin staining of transverse sections shows thinning of the ventricular walls beginning at E12.5 leading to severe cardiac hypoplasia. Boxed areas represent enlarged images shown to the right of the corresponding section. (L) Arrow highlights the ventricular septal defect. (O – P) Quantification of ventricular wall thickness in WT and *Casz1*$^{f/f}$;*Nkx2.5*$^{Cre/+}$ embryos at E10.5 (O), E12.5 (P). Data shown as mean ±SEM and * denotes a statistically significant difference (at $P<0.05$) between WT and *Casz1*$^{f/f}$;*Nkx2.5*$^{Cre/+}$ embryos and NS denotes not significant. Scale bars indicate 60μm (I, J, K, L) and 15μm (I', J', K', L'). RV, right ventricle; LV, left ventricle; RA, right atria; LA, left atria; OFT, outflow tract; IVS, interventricular septum; CL, compact layer; TR, trabeculae.

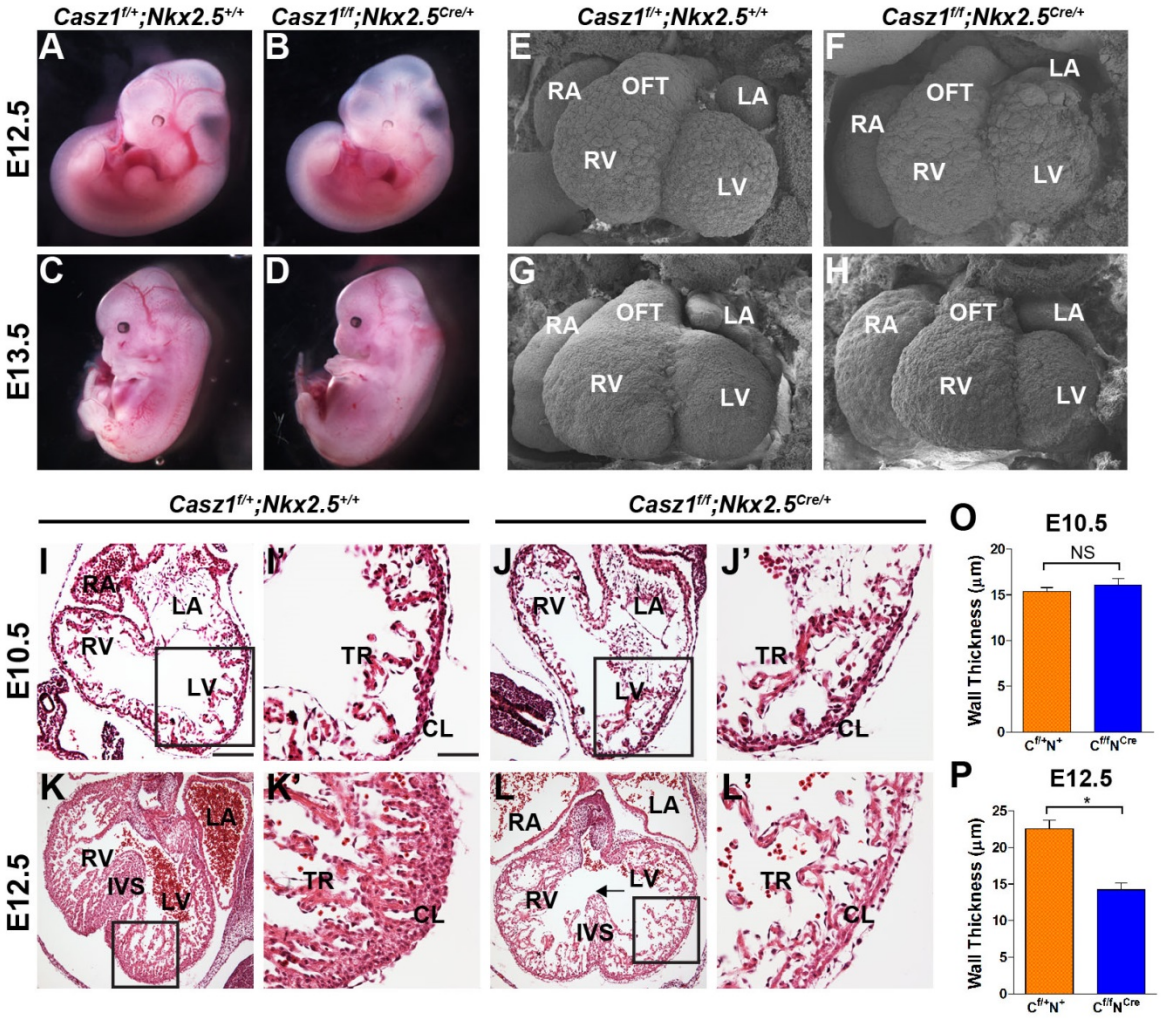
Casz1f/+;Nkx2.5+/+
Casz1f/f;Nkx2.5Cre/+
Casz1f/+;Nkx2.5+/+
Casz1f/f;Nkx2.5Cre/+
E12.5
E13.5
A
B
C
D
E
F
G
H
RA
OFT
LA
RV
LV
Casz1f/+;Nkx2.5+/+
Casz1f/f;Nkx2.5Cre/+
E10.5
E12.5
I
I'
J
J'
K
K'
L
L'
TR
CL
IVS
O
E10.5
NS
P
E12.5
*
Wall Thickness (μm)
Cf/+N+
Cf/fNCre

Figure 2.4. *Casz1* null embryos phenocopy *Casz1* cardiac null embryos

(A-B) Whole mount LacZ staining of *Sox2*$^{+/+}$;*R26R*$^{LacZ/+}$ and *Sox2*$^{Cre/+}$;*R26R*$^{LacZ/+}$ E10.5 embryos demonstrates that *Sox2-Cre* is ubiquitously expressed. (C-D) Gross morphology of E12.5 *Casz1*$^{f/+.Sox2+}$ wild-type (WT) and *Casz1*$^{f/f}$;*Sox2*$^{Cre/+}$embryos. (E-I) Histological analysis of WT and *Casz1*$^{f/f}$;*Sox2*$^{Cre/+}$ hearts. *Casz1*$^{f/f}$;*Sox2*$^{Cre/+}$ embryos exhibit severe cardiac hypoplasia and ventral septal defects. H & E staining of transverse sections shows cardiac hypoplasia at E12.5 Boxed areas represent enlarged images shown to the right of the corresponding section. (G) Arrow highlights the ventricular septal defect. (I) Quantification of ventricular wall thickness in WT and *Casz1*$^{f/f}$;*Sox2*$^{Cre/+}$ embryos at E12.5. Data shown as mean ±SEM and and *** denotes a statistically significant difference (at P<0.0005) between WT and *Casz1*$^{f/f}$;*Sox2*$^{Cre/+}$ embryos and NS denotes not significant. RV, right ventricle; LV, left ventricle; RA, right atria; LA, left atria; OFT, outflow tract. Scale bars indicate 60μm (E,G) and 15μm (F,H).

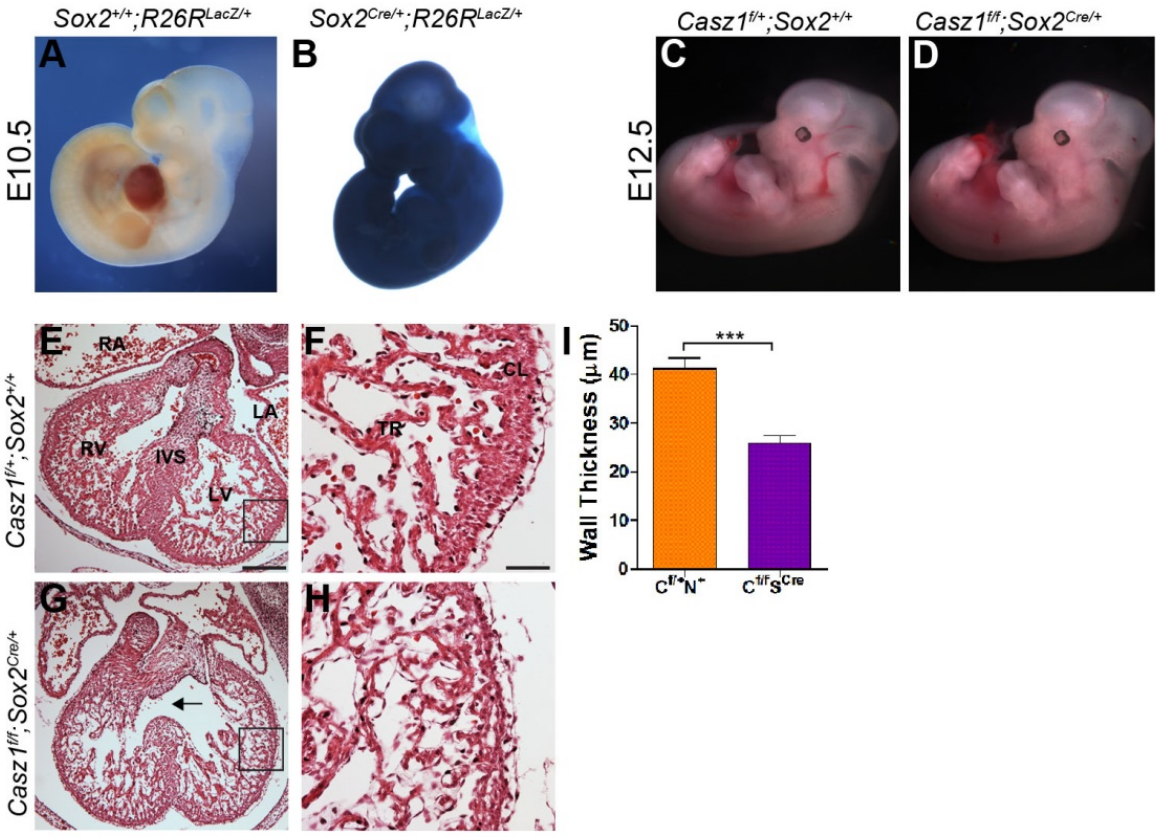
Sox2+/+;R26RLacZ/+
Sox2Cre/+;R26RLacZ/+
Casz1f/+;Sox2+/+
Casz1f/f;Sox2Cre/+
E10.5
E12.5
A
B
C
D
E
F
G
H
I
RA
LA
RV
IVS
LV
CL
TR
Casz1f/+;Sox2+/+
Casz1f/f;Sox2Cre/+
Wall Thickness (μm)
50
40
30
20
10
0
***
Cf/+N+
Cf/fSCre

Figure 2.5. *Casz1* is required in the second heart field

Histological analysis of WT and *Casz1*$^{f/f}$;*Isl1*$^{Cre/+}$ hearts at E14.5 demonstrates that *Casz1*$^{f/f}$;*Isl1*$^{Cre/+}$ hearts are misshapen and have a thin right ventricle. Boxed areas represent enlarged images shown to the right of the corresponding section. (G-H) Gross morphology of E14.5 *Casz1*$^{f/+}$;*Isl1*$^{+}$ wild-type (WT) and *Casz1*$^{f/f}$;*Isl1*$^{Cre/+}$ embryos. (I,J) Quantification of right (I) and left (J) ventricular wall thickness in WT and *Casz1*$^{f/f}$;*Isl1*$^{Cre/+}$ embryos at E14.5. Data shown as mean ±SEM and *** denotes a statistically significant difference (at $P<0.0005$) between WT and *Casz1*$^{f/f}$;*Isl1*$^{Cre/+}$ embryos. Scale bars indicate 60μm (A,D) and 15μm (B,C,E,F).

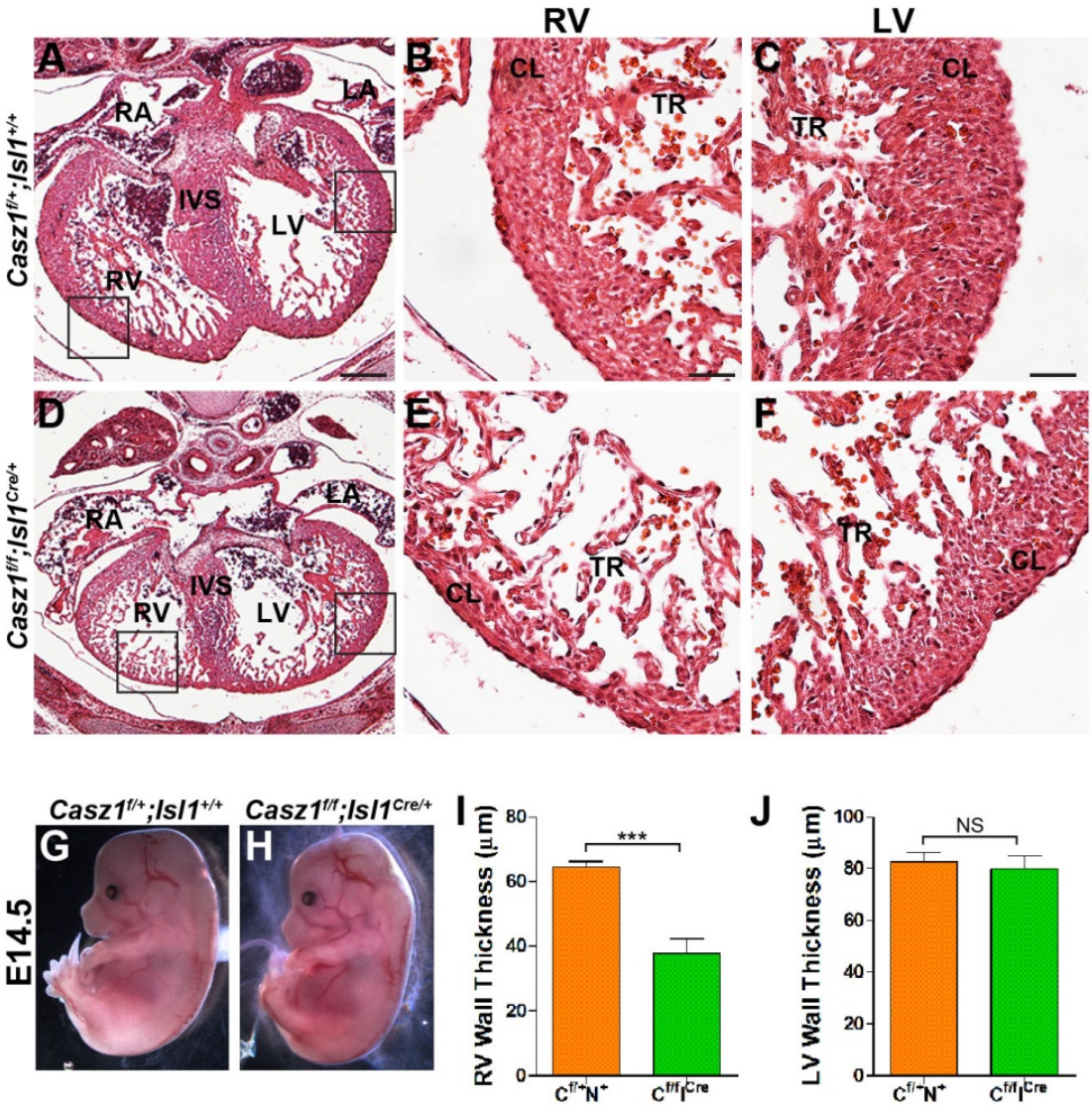
RV
LV
A
B
C
D
E
F
RA
LA
IVS
LV
RV
CL
TR
Casz1f/+;Isl1+/+
Casz1f/f;Isl1Cre/+
Casz1f/+;Isl1+/+
Casz1f/f;Isl1Cre/+
E14.5
G
H
I
J
RV Wall Thickness (μm)
LV Wall Thickness (μm)
***
NS
0
20
40
60
80
100
Cf/+N+
Cf/fCre

Figure 2.6. *Casz1* regulates cardiomyocyte proliferation

(A-D') Immunofluorescent staining for TMY and DAPI (blue) highlights a decrease in the number of differentiated cardiomyocytes at E12.5. (E,F) Quantification of results from cardiomyocyte cell numbers counted per field at E10.5 (E) and E12.5 (F). In all cases, data shown as mean ±SEM of three embryos, and * denotes a statistically significant difference (at $P<0.05$) between WT and *Casz1*$^{f/f}$;*Nkx2.5*$^{Cre/+}$ embryos and NS denotes not significant. (G-J) Immunofluorescent staining for EdU and TMY shows a reduction in proliferation in *Casz1*$^{f/f}$;*Nkx2.5*$^{Cre/+}$ ventricles at E12.5. Zoomed images of boxed area in WT (I) and *Casz1*$^{f/f}$;*Nkx2.5*$^{Cre/+}$ left ventricles (J). (K,L) Immunofluorescent staining for phospho-histone H3 along with TMY demonstrates a decreased cardiomyocyte mitotic index in *Casz1*$^{f/f}$;*Nkx2.5*$^{Cre/+}$ embryos as compared to WT in sections of E12.5 hearts. (M) Quantitative evaluation of reduced proliferation of cardiomocytes in *Casz1*$^{f/f}$;*Nkx2.5*$^{Cre/+}$ ventricles at E12.5 by EdU incorporation and (N) reduced cardiomyocyte mitotic index in *Casz1*$^{f/f}$;*Nkx2.5*$^{Cre/+}$ ventricles and (O) *Casz1*$^{f/f}$;*Isl1*$^{Cre/+}$right ventricles at E12.5. In all cases, data shown as mean ±SEM of three embryos, and *** denotes a statistically significant difference (at $P<0.0005$) between WT and *Casz1*$^{f/f}$;*Nkx2.5*$^{Cre/+}$ embryos at a given stage. (P,Q) Immunofluorescent staining for cTNT to mark cardiomyocytes and FILA to mark the epicardium and endothelial cells demonstrates a reduction in cardiomyocytes while FILA expression within the epicardium and endothelial cells is comparable to WT at E12.5. (R-U) Immunofluorescent staining for phallodin demonstrates that actin filaments are intact in *Casz1*$^{f/f}$;*Nkx2.5*$^{Cre/+}$ E12.5 hearts. (T,U) Boxed areas represent enlarged images shown below the corresponding section. Scale bars indicate 10μm (A'-

D’,K,L,T,U), 20 μm (P-R), 50μm (I,J), 100μm (A,B), and 200μm (C,D,G,H). RV, right ventricle; LV, left ventricle; RA, right atria; LA, left atria; OFT, outflow tract, EPI, epicardium, MY, myocardium; EN, endothelial cells; S, sarcomere; Z-d, Z-disks.

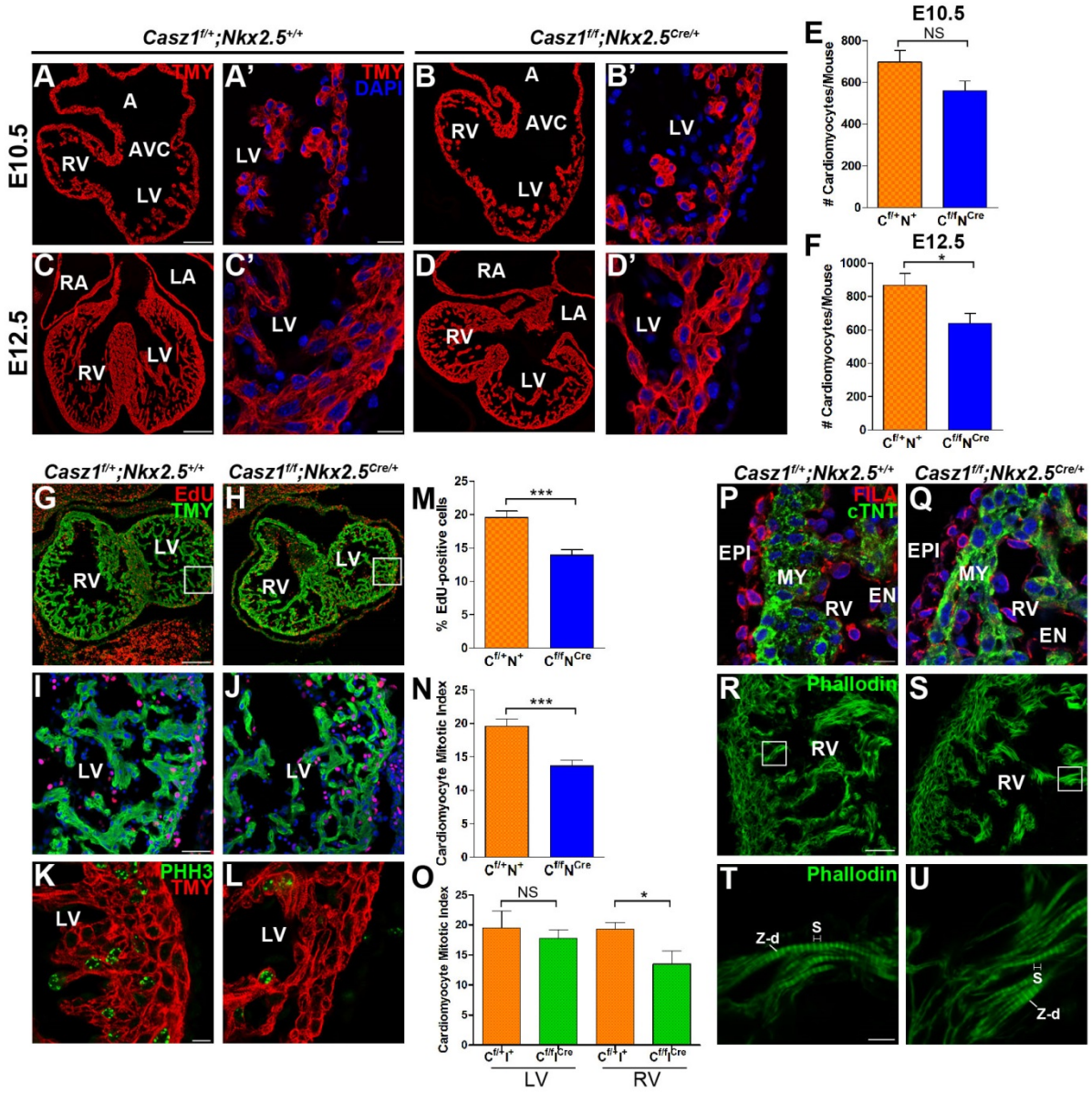

Figure 2.7 – *Casz1* is essential for cardiac G1 to S cell cycle transition

(A) Cell cycle profiles of E12.5 PI-stained cardiac nuclei for *Casz1*$^{f/+}$;*Nkx2.5*$^{+/+}$ and *Casz1*$^{f/f}$;*Nkx2.5*$^{Cre/+}$ and quantitation of cells with G1, S, or G2/M DNA content, showed an increase in G1-phase cells and decrease in S-phase cells in *Casz1* null heart tissue. (B-C) Immunofluorescent staining for phospho-RB (pRB) and TMY demonstrates an increase in the number of pRB-positive cardiomyocytes in *Casz1* cardiac null hearts versus controls at E12.5. (D) Quantification of results and * denotes a statistically significant difference (at P<0.05) between WT and *Casz1*$^{f/f}$;*Nkx2.5*$^{Cre/+}$ embryos.

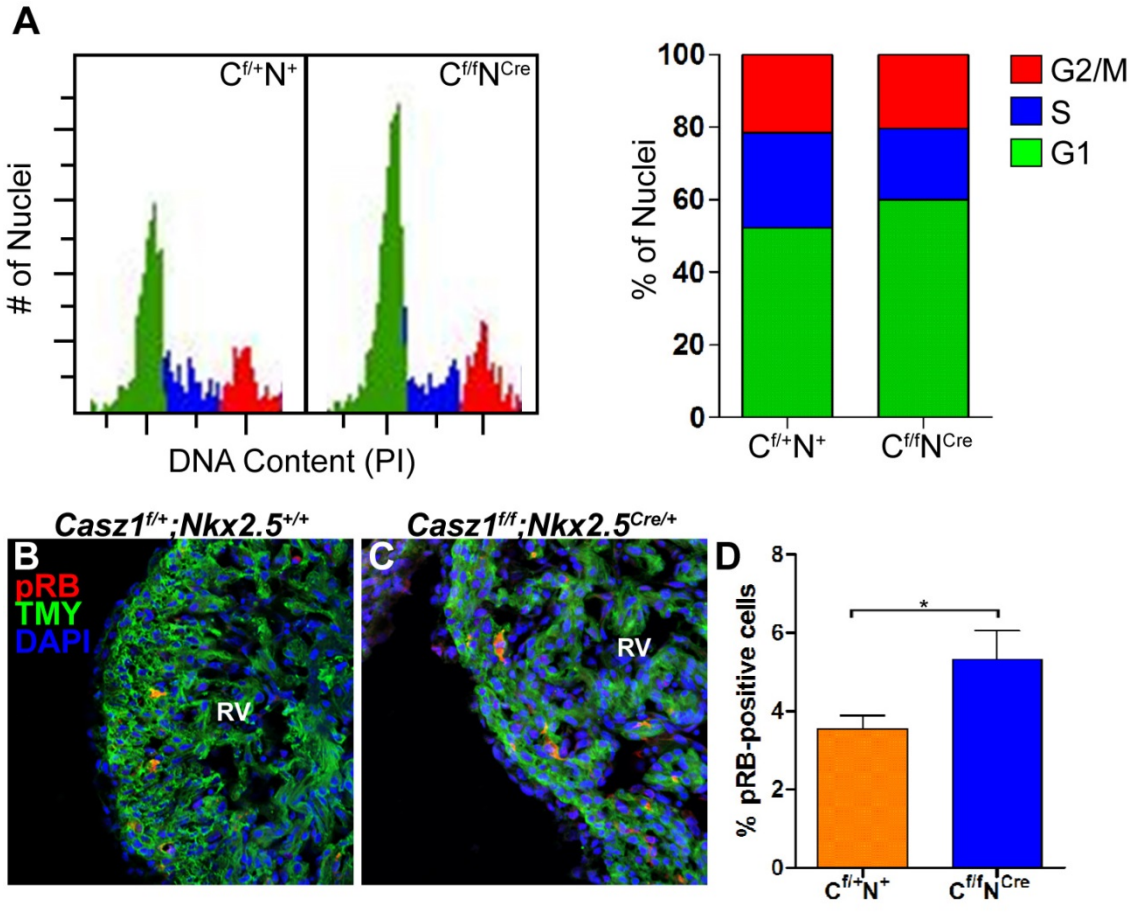

Supplemental Figure 2.1. CASZ1 is expressed in PML bodies

Immunofluorescent staining reveals that CASZ1 is co-expressed with PML in the nucleus of HUVECS.

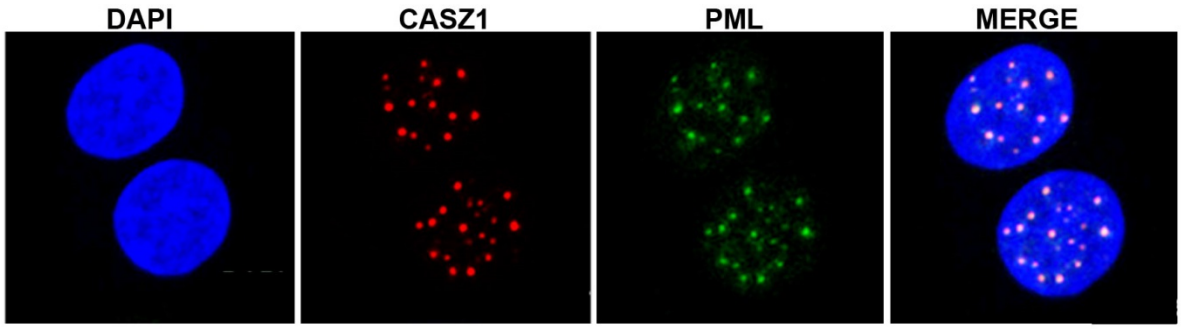

Supplemental Figure 2.2. Generation of a *Casz1*$^{CreERT2\text{-}neo}$ lineage tracing allele

(A) Gene targeting strategy for *Casz1*^{CreERT2} allele. (B) Germline transmission was validated by Southern blot using a 5' external probe. Heterozygous mice containing the *Casz1*^{CreERT2} allele are viable, fertile, and display no obvious phenotypic abnormalities. (C) Fate mapping experimental design – pregnant females were injected with a single dose of tamoxifen at E8.5 and embryos were harvested at E12.5. (D) Image of an E12.5 *Casz1*$^{CreERT2/+}$;*R26R*$^{tdT/+}$ embryo. (E) Enlarged image of the heart in (D) shows *Casz1*-expressing cells in the embryonic heart. E – EcoRI cut sites; FRT sites – white triangles; loxP sites – black triangles.

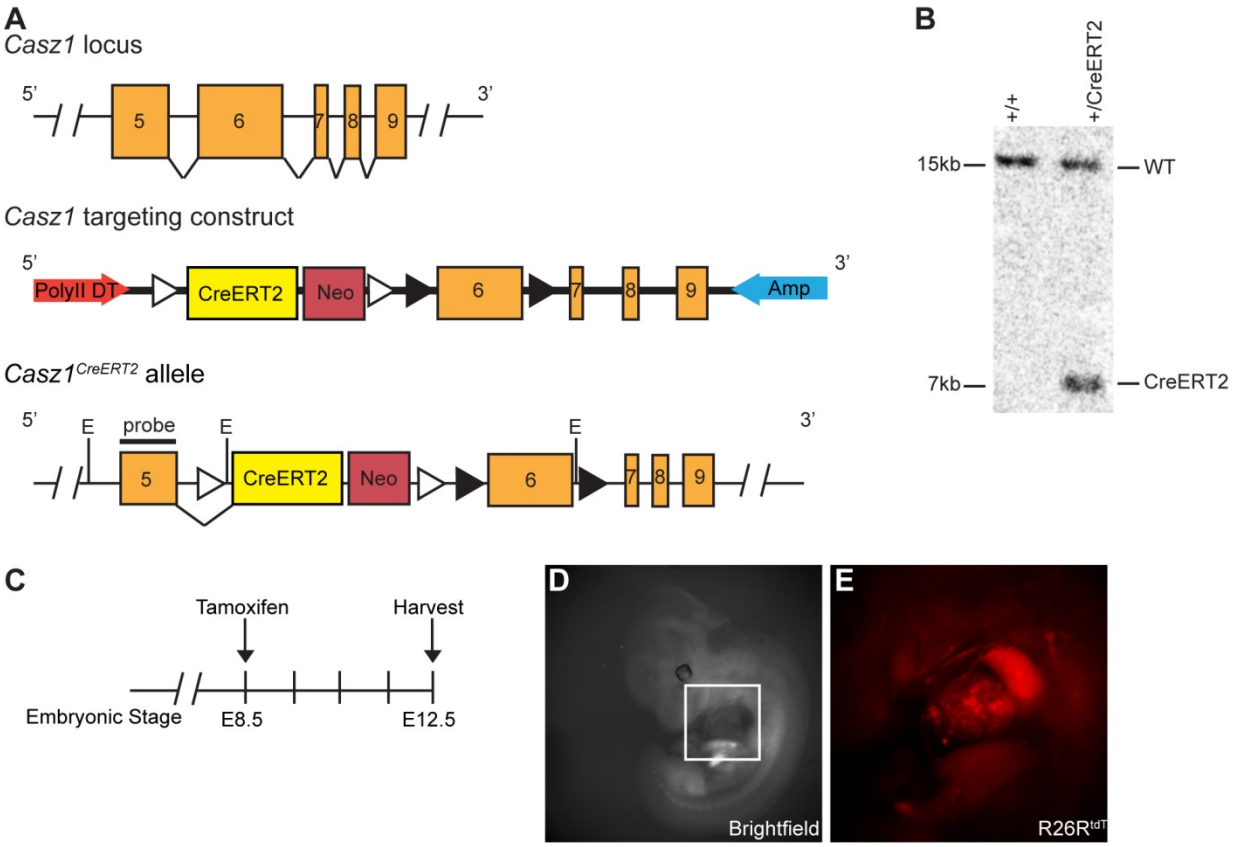
A
Casz1 locus
5'
3'
5
6
7
8
9
Casz1 targeting construct
5'
PolyII DT
CreERT2
Neo
6
7
8
9
Amp
3'
Casz1CreERT2 allele
5'
E
probe
E
E
3'
5
CreERT2
Neo
6
7
8
9
B
+/+
+/CreERT2
15kb
WT
7kb
CreERT2
C
Tamoxifen
Harvest
Embryonic Stage
E8.5
E12.5
D
Brightfield
E
R26RtdT

Supplemental Figure 2.3. Generation of a conditional *Casz1* allele

(A) Conditional gene targeting strategy for *Casz1*^{flox} allele. *loxP* sites were introduced into the *Casz1* locus flanking exon 6. (B) 5' RLM-RACE identified 2 transcription start sites in the murine heart. +RT indicates cDNA sample treated with reverse transcriptase (RT); -RT indicates control cDNA sample not treated with RT. (C) Germline transmission was validated by Southern blot using a 5' external probe. (D) Mice were genotyped by PCR for the presence of the flox allele. Immunofluorescent staining for CASZ1, TMY and DAPI confirms depletion of CASZ1 in the myocardium in *Casz1*$^{f/f}$*;Nkx2.5*$^{Cre/+}$ E13.5 hearts (E,F), but is maintained in the dorsal root ganglia (DRG) (G,H). H – HindIII cut site; FRT sites – white triangles; loxP sites – black triangles; blue bar represents location of a nuclear localization signal; green bars indicate location of C_2H_2 zinc-fingers; red stop sign indicates the location of a premature stop codon subsequent to the frameshift following exon6 removal. Scale bars indicate 20 μm (Bergmann et al.).

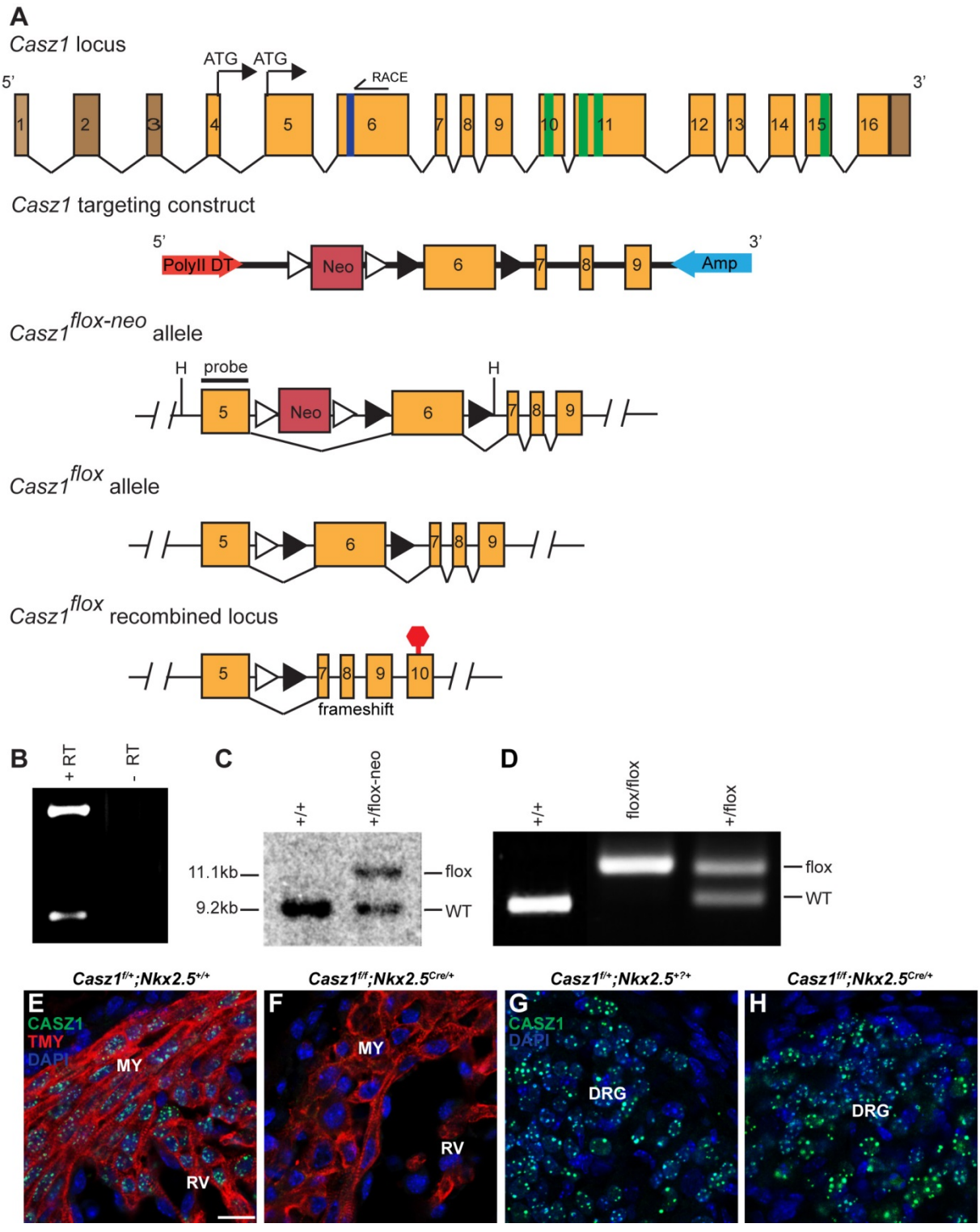
A
Casz1 locus
ATG
ATG
RACE
5'
3'
1
2
3
4
5
6
7
8
9
10
11
12
13
14
15
16
Casz1 targeting construct
5'
3'
PolyII DT
Neo
6
7
8
9
Amp
Casz1flox-neo allele
H
probe
H
5
Neo
6
7
8
9
Casz1flox allele
5
6
7
8
9
Casz1flox recombined locus
5
7
8
9
10
frameshift
B
+ RT
- RT
C
+/+
+/flox-neo
11.1kb
9.2kb
flox
WT
D
+/+
flox/flox
+/flox
flox
WT
Casz1f/+;Nkx2.5+/+
Casz1f/f;Nkx2.5Cre/+
Casz1f/+;Nkx2.5+?+
Casz1f/f;Nkx2.5Cre/+
E
CASZ1
TMY
DAPI
MY
RV
F
MY
RV
G
CASZ1
DAPI
DRG
H
DRG

Supplemental Figure 2.4. *Nkx2.5*^{Cre} Lineage analysis

Gross morphology of *Nkx2.5*$^{Cre/+}$*;R26R*$^{tdT/+}$ embryos at E7.5 (A,E) and E9.5 (B,F), and hearts at E12.5 (C,G) and E14.5 (D,H). Cre recombination is observed in the cardiac crescent at E7.5 (E), the looped heart at E9.5 (F), the ventricles, the OFT and the atria of the four-chambered heart at E12.5 (G) and similarly in the fetal heart at E14.5 (H). EXE, extraembryonic tissue; CC, cardiac crescent; LH, looped heart; PME, pharyngeal mesoderm; LV, left ventricle; LA, left atria; RV, right ventricle; RA, right atria; OFT, outflow tract.

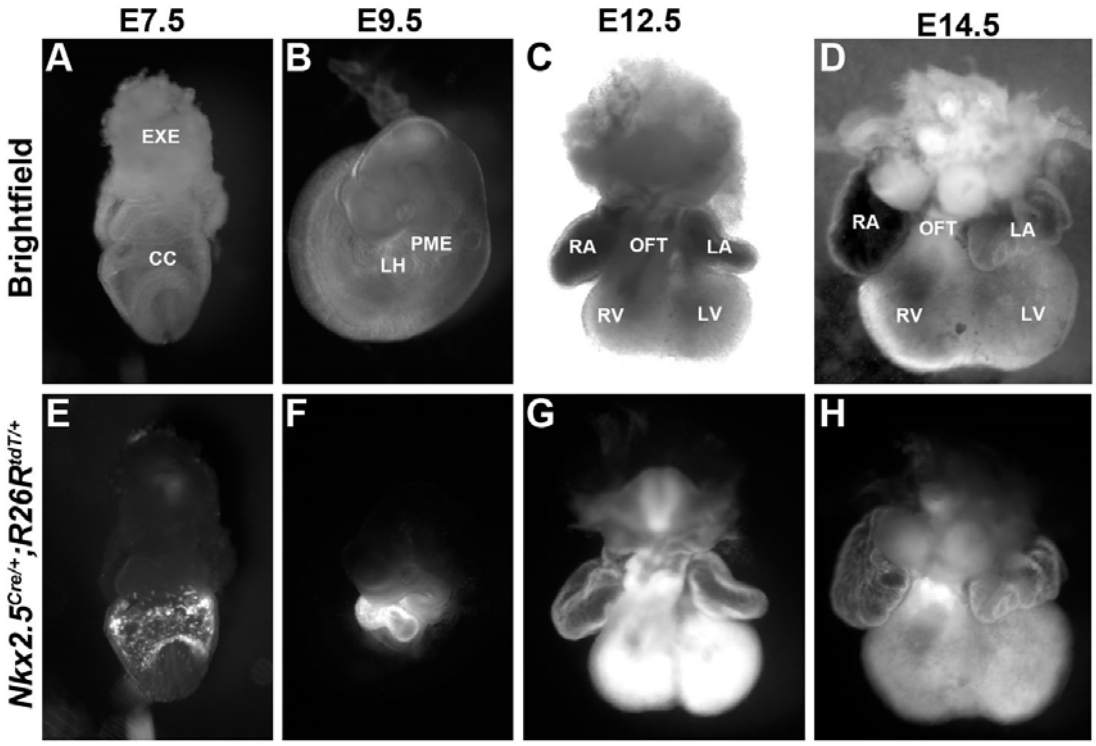

Supplemental Figure 2.5. *Casz1* cardiac null embryos exhibit severe cardiac defects

Histological analysis of WT (A) and *Casz1*$^{f/f}$;*Nkx2.5*$^{Cre/+}$ (B) hearts at E13.5 highlights the enlarged right atria observed in the SEM data. At E13.5, the cardiac hypoplasia and ventricular septal defect is more pronounced and further shows that the *Casz1*$^{f/f}$;*Nkx2.5*$^{Cre/+}$ heart is misshapen and does not form an apex for either the left or the right ventricle as seen in the wild-type (highlighted by the arrows in each panel).

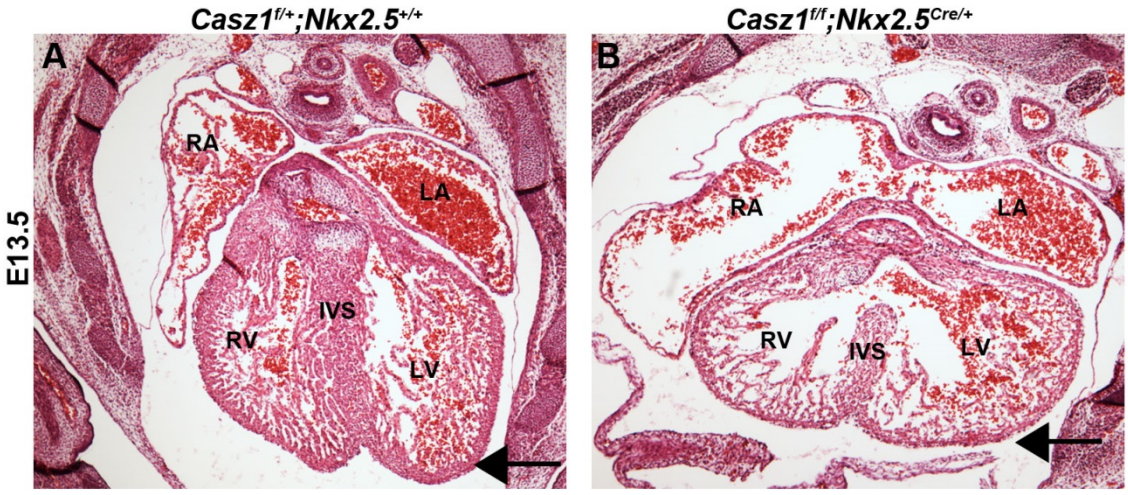

Supplemental Figure 2.6. *Casz1* is required for myocardial development

(A-L) Immunofluorescent staining for TMY of anterior, mid and posterior sections highlights a decrease in differentiated cardiomyocytes in *Casz1*$^{f/f}$;*Nkx2.5*$^{Cre/+}$ hearts at E10.5 (A,B,E,F,I,J) and E12.5 (C,D,G,H,K,L). A, anterior; P, posterior.

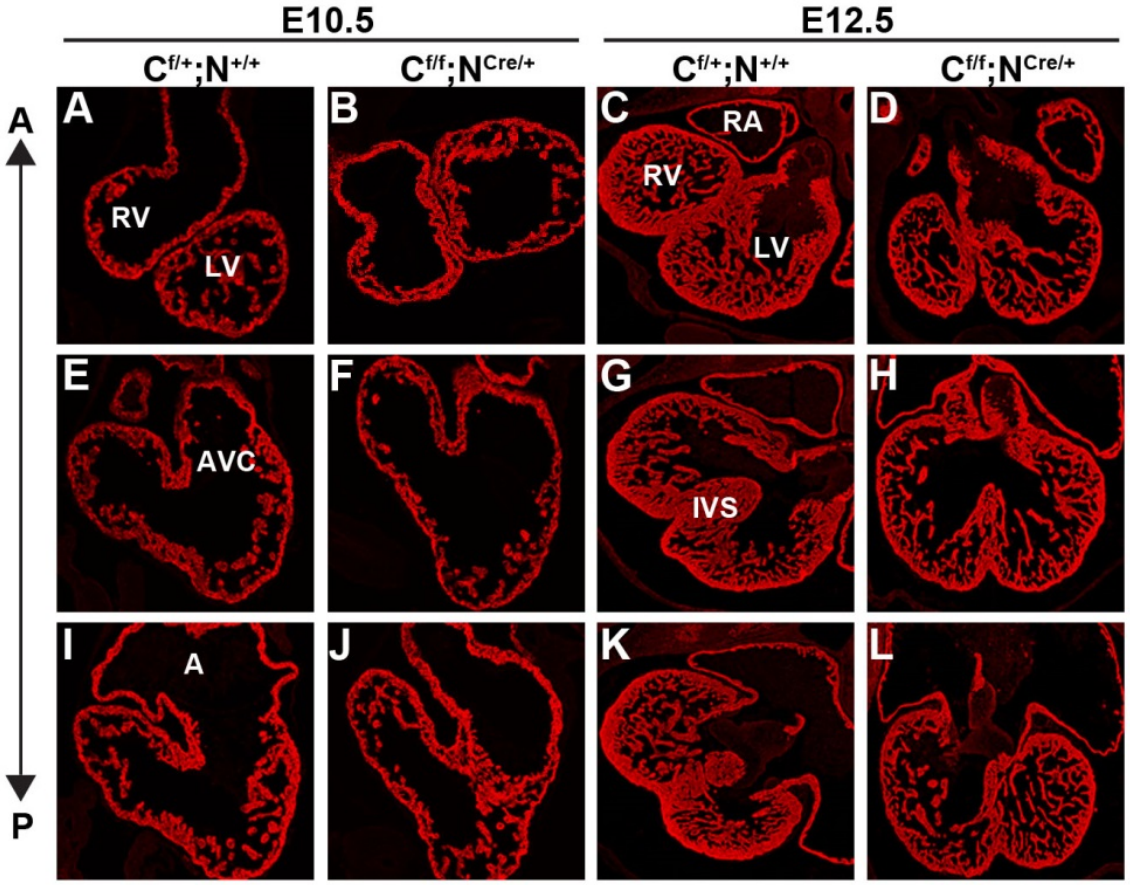

Supplemental Figure 2.7. RNA-Seq Analysis

(A) Gene Ontology (GO) Analysis – significant cellular processes downregulated in *Casz1*$^{f/f}$;*Nkx2.5*$^{Cre/+}$ E10.5 hearts. (B) Cell growth genes downregulated in *Casz1*$^{f/f}$;*Nkx2.5*$^{Cre/+}$ hearts.

A

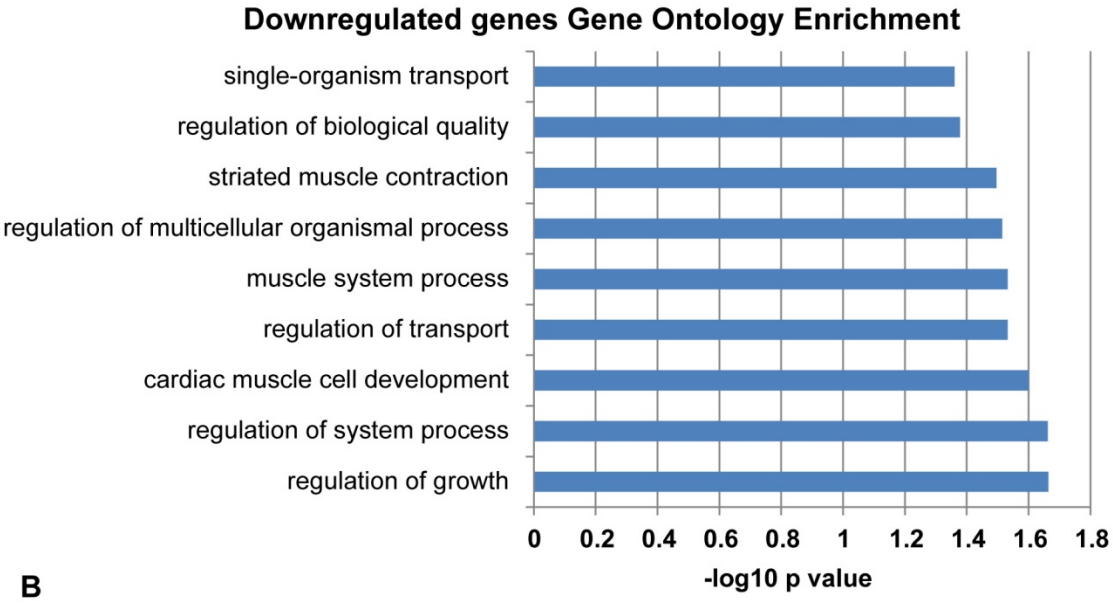

B

Cell Growth Genes Downregulated in *Casz1*^{CKO} Hearts

Gene	log2 Fold Change	Adjusted p-value	Best Blastx hit
Alox12	-0.966	0.017	arachidonate 12-lipoxygenase
Lpar3	-0.85711	0.003	lysophosphatidic acid receptor 3
Fgf9	-1.46448	0.009	fibroblast growth factor 9
Mndal	-1.95735	0.016	myeloid nuclear differentiation antigen like
Alox8	-1.12568	0.028	arachidonate 8-lipoxygenase
P2rx5	-1.23956	0.036	purinergic receptor ligand-gated ion channel, 5
Zc3h12d	-1.58106	0.039	zinc finger ccch type containing 12d
Pou3f2	-1.76676	0.005	pou domain, class 3, transcription factor 2
Hey2	-0.67981	0.0165	hairy/enhancer-of-split related with yrpw motif 2
Ntn1	-1.41721	7.19E-07	netrin 1
Nkx2-5	-0.78714	0.007	nk2 transcription factor related, locus 5 (drosophila)
Nppa	-0.98232	0.012	natriuretic peptide type a
Cav3	-0.7795	0.014	caveolin
Igfbpl1	-1.45848	7.17E-07	insulin-like growth factor binding protein-like 1

Supplemental Figure 2.8. Loss of *Casz1* does not lead to programmed cell death. Immunofluorescent staining for cleaved caspase-3, TMY and DAPI (blue) to identify apoptotic cells shows that *Casz1*$^{f/f}$*;Nkx2.5*$^{Cre/+}$ hearts do not have an increase in programmed cell death compared to controls. As a positive control, sections of the neural tube (NT) were also analyzed. Data represents 2 independent experiements. LV, left ventricle; RV, right ventricle; IVS, interventricular septum.

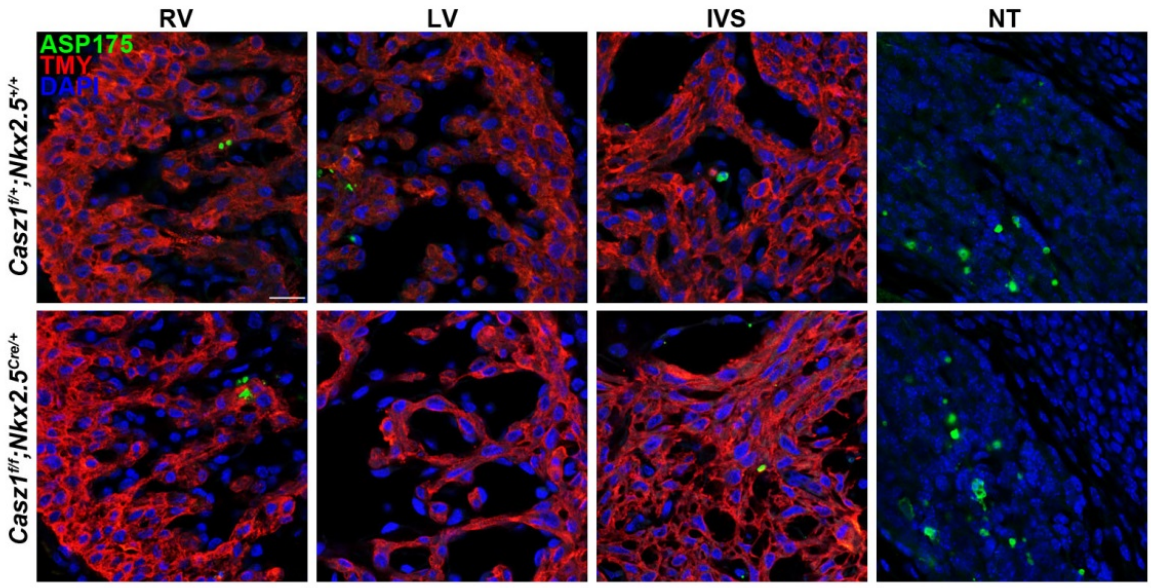

Supplemental Table 2.1. Primer sequences

Gene	Primer Sequence	Size
Casz1 Genotyping	Forward: 5’ – CACAGGAACTGTCTCCACTGTC – 3’ Reverse: 5’ – GTTTCTGTTGCTGGGTTAGGTT – 3’	Flox: 571 bp WT: 471 bp
Cre Genotyping	Forward: 5’ – TGGGCCAGCTAAACATGCTT – 3’ Reverse: 5’ – GGTGTTATAAGCAATCCCCAGA – 3’	236 bp
R26R^{tdT} Genotyping	Forward: 5’ – GGCATTAAAGCAGCGTATCC – 3’ Reverse: 5’ – CTGTTCCTGTACGGCATGG – 3’	126 bp
Casz1 5’ RACE Outer Primer	Reverse: 5’ – GGATGTATTCCTCGTATTTGGAGA – 3’	N/A
Casz1 5’ RACE Inner Primer	Reverse: 5’ – AGCTGATCTTCTTGGCCAGCTCAT – 3’	N/A
Casz1 5’ Southern Probe	Forward: 5’ – CTGAAAGCACCCGGTGCACCGACC – 3’ Reverse: 5’ – CTGAAGCCTGCCTGGTGCTGGGGC – 3’	486 bp
Casz1 In Situ Probe	Forward: 5’ – GAGAAACCTCCTCTCTGAGGGACT – 3’ Reverse: 5’ – CTGGCAATATATTTCTGGTAAATG – 3’	904 bp

REFERENCES

Ahuja, P., Sdek, P. and MacLellan, W. R. (2007). Cardiac myocyte cell cycle control in development, disease, and regeneration. *Physiological reviews* **87**, 521-544.

Amin, N. M., Gibbs, D. and Conlon, F. L. (2014). Differential regulation of CASZ1 protein expression during cardiac and skeletal muscle development. *Developmental dynamics : an official publication of the American Association of Anatomists* **243**, 948-956.

Arnold, S. J., Sugnaseelan, J., Groszer, M., Srinivas, S. and Robertson, E. J. (2009). Generation and analysis of a mouse line harboring GFP in the Eomes/Tbr2 locus. *Genesis* **47**, 775-781.

Barrow, J. R., Howell, W. D., Rule, M., Hayashi, S., Thomas, K. R., Capecchi, M. R. and McMahon, A. P. (2007). Wnt3 signaling in the epiblast is required for proper orientation of the anteroposterior axis. *Developmental biology* **312**, 312-320.

Bergmann, O., Bhardwaj, R. D., Bernard, S., Zdunek, S., Barnabe-Heider, F., Walsh, S., Zupicich, J., Alkass, K., Buchholz, B. A., Druid, H. et al. (2009). Evidence for cardiomyocyte renewal in humans. *Science* **324**, 98-102.

Bersell, K., Arab, S., Haring, B. and Kuhn, B. (2009). Neuregulin1/ErbB4 signaling induces cardiomyocyte proliferation and repair of heart injury. *Cell* **138**, 257-270.

Bertoli, C., Skotheim, J. M. and de Bruin, R. A. (2013). Control of cell cycle transcription during G1 and S phases. *Nature reviews. Molecular cell biology* **14**, 518-528.

Cai, C. L., Liang, X., Shi, Y., Chu, P. H., Pfaff, S. L., Chen, J. and Evans, S. (2003). Isl1 identifies a cardiac progenitor population that proliferates prior to differentiation and contributes a majority of cells to the heart. *Developmental cell* **5**, 877-889.

Charpentier, M. S., Dorr, K. M. and Conlon, F. L. (2013a). Transcriptional regulation of blood vessel formation: The role of the CASZ1/Egfl7/RhoA pathway. *Cell cycle* **12**.

Charpentier, M. S., Christine, K. S., Amin, N. M., Dorr, K. M., Kushner, E. J., Bautch, V. L., Taylor, J. M. and Conlon, F. L. (2013b). CASZ1 promotes vascular assembly and morphogenesis through the direct regulation of an EGFL7/RhoA-mediated pathway. *Developmental cell* **25**, 132-143.

Christine, K. S. and Conlon, F. L. (2008). Vertebrate CASTOR is required for differentiation of cardiac precursor cells at the ventral midline. *Developmental cell* **14**, 616-623.

Christoffels, V. M., Habets, P. E., Franco, D., Campione, M., de Jong, F., Lamers, W. H., Bao, Z. Z., Palmer, S., Biben, C., Harvey, R. P. et al. (2000). Chamber

formation and morphogenesis in the developing mammalian heart. *Developmental biology* **223**, 266-278.

Conway, S. J., Kruzynska-Frejtag, A., Kneer, P. L., Machnicki, M. and Koushik, S. V. (2003). What cardiovascular defect does my prenatal mouse mutant have, and why? *Genesis* **35**, 1-21.

Creazzo, T. L., Godt, R. E., Leatherbury, L., Conway, S. J. and Kirby, M. L. (1998). Role of cardiac neural crest cells in cardiovascular development. *Annual review of physiology* **60**, 267-286.

Delgado-Esteban, M., Garcia-Higuera, I., Maestre, C., Moreno, S. and Almeida, A. (2013). APC/C-Cdh1 coordinates neurogenesis and cortical size during development. *Nature communications* **4**, 2879.

Deng, M. C., Dasch, B., Erren, M., Mollhoff, T. and Scheld, H. H. (1996). Impact of left ventricular dysfunction on cytokines, hemodynamics, and outcome in bypass grafting. *The Annals of thoracic surgery* **62**, 184-190.

Eden, E., Navon, R., Steinfeld, I., Lipson, D. and Yakhini, Z. (2009). GOrilla: a tool for discovery and visualization of enriched GO terms in ranked gene lists. *BMC bioinformatics* **10**, 48.

Eulalio, A., Mano, M., Dal Ferro, M., Zentilin, L., Sinagra, G., Zacchigna, S. and Giacca, M. (2012). Functional screening identifies miRNAs inducing cardiac regeneration. *Nature* **492**, 376-381.

Franklin, S., Zhang, M. J., Chen, H., Paulsson, A. K., Mitchell-Jordan, S. A., Li, Y., Ping, P. and Vondriska, T. M. (2011). Specialized compartments of cardiac nuclei exhibit distinct proteomic anatomy. *Molecular & cellular proteomics : MCP* **10**, M110 000703.

Hama, H., Kurokawa, H., Kawano, H., Ando, R., Shimogori, T., Noda, H., Fukami, K., Sakaue-Sawano, A. and Miyawaki, A. (2011). Scale: a chemical approach for fluorescence imaging and reconstruction of transparent mouse brain. *Nature neuroscience* **14**, 1481-1488.

Hayashi, S., Lewis, P., Pevny, L. and McMahon, A. P. (2002). Efficient gene modulation in mouse epiblast using a Sox2Cre transgenic mouse strain. *Mechanisms of development* **119 Suppl 1**, S97-S101.

Heallen, T., Zhang, M., Wang, J., Bonilla-Claudio, M., Klysik, E., Johnson, R. L. and Martin, J. F. (2011). Hippo pathway inhibits Wnt signaling to restrain cardiomyocyte proliferation and heart size. *Science* **332**, 458-461.

Hullinger, T. G., Montgomery, R. L., Seto, A. G., Dickinson, B. A., Semus, H. M., Lynch, J. M., Dalby, C. M., Robinson, K., Stack, C., Latimer, P. A. et al. (2012).

Inhibition of miR-15 protects against cardiac ischemic injury. *Circulation research* **110**, 71-81.

Ikenishi, A., Okayama, H., Iwamoto, N., Yoshitome, S., Tane, S., Nakamura, K., Obayashi, T., Hayashi, T. and Takeuchi, T. (2012). Cell cycle regulation in mouse heart during embryonic and postnatal stages. *Development, growth & differentiation* **54**, 731-738.

Kelly, R. G. (2012). The second heart field. *Current topics in developmental biology* **100**, 33-65.

Kisanuki, Y. Y., Hammer, R. E., Miyazaki, J., Williams, S. C., Richardson, J. A. and Yanagisawa, M. (2001). Tie2-Cre transgenic mice: a new model for endothelial cell-lineage analysis in vivo. *Developmental biology* **230**, 230-242.

Konstantinides, N., Rossi, A. M. and Desplan, C. (2015). Common temporal identity factors regulate neuronal diversity in fly ventral nerve cord and mouse retina. *Neuron* **85**, 447-449.

Lavine, K. J., Yu, K., White, A. C., Zhang, X., Smith, C., Partanen, J. and Ornitz, D. M. (2005). Endocardial and epicardial derived FGF signals regulate myocardial proliferation and differentiation in vivo. *Developmental cell* **8**, 85-95.

Levy, D., Ehret, G. B., Rice, K., Verwoert, G. C., Launer, L. J., Dehghan, A., Glazer, N. L., Morrison, A. C., Johnson, A. D., Aspelund, T. et al. (2009). Genome-wide association study of blood pressure and hypertension. *Nature genetics* **41**, 677-687.

Li, F., Wang, X., Capasso, J. M. and Gerdes, A. M. (1996). Rapid transition of cardiac myocytes from hyperplasia to hypertrophy during postnatal development. *Journal of molecular and cellular cardiology* **28**, 1737-1746.

Liu, P., Jenkins, N. A. and Copeland, N. G. (2003). A highly efficient recombineering-based method for generating conditional knockout mutations. *Genome research* **13**, 476-484.

Liu, Z., Yang, X., Tan, F., Cullion, K. and Thiele, C. J. (2006). Molecular cloning and characterization of human Castor, a novel human gene upregulated during cell differentiation. *Biochemical and biophysical research communications* **344**, 834-844.

Liu, Z., Li, W., Ma, X., Ding, N., Spallotta, F., Southon, E., Tessarollo, L., Gaetano, C., Mukoyama, Y. S. and Thiele, C. J. (2014). Essential Role of the Zinc Finger Transcription Factor Casz1 for Mammalian Cardiac Morphogenesis and Development. *The Journal of biological chemistry*.

Lu, X., Wang, L., Lin, X., Huang, J., Charles Gu, C., He, M., Shen, H., He, J., Zhu, J., Li, H. et al. (2014). Genome-wide association study in Chinese identifies novel loci for blood pressure and hypertension. *Human molecular genetics*.

Madisen, L., Zwingman, T. A., Sunkin, S. M., Oh, S. W., Zariwala, H. A., Gu, H., Ng, L. L., Palmiter, R. D., Hawrylycz, M. J., Jones, A. R. et al. (2010). A robust and high-throughput Cre reporting and characterization system for the whole mouse brain. *Nature neuroscience* **13**, 133-140.

Maillet, M., van Berlo, J. H. and Molkentin, J. D. (2013). Molecular basis of physiological heart growth: fundamental concepts and new players. *Nature reviews. Molecular cell biology* **14**, 38-48.

Manner, J., Perez-Pomares, J. M., Macias, D. and Munoz-Chapuli, R. (2001). The origin, formation and developmental significance of the epicardium: a review. *Cells, tissues, organs* **169**, 89-103.

Matera, A. G., Izaguire-Sierra, M., Praveen, K. and Rajendra, T. K. (2009). Nuclear bodies: random aggregates of sticky proteins or crucibles of macromolecular assembly? *Developmental cell* **17**, 639-647.

Mattar, P., Ericson, J., Blackshaw, S. and Cayouette, M. (2015). A conserved regulatory logic controls temporal identity in mouse neural progenitors. *Neuron* **85**, 497-504.

Moses, K. A., DeMayo, F., Braun, R. M., Reecy, J. L. and Schwartz, R. J. (2001). Embryonic expression of an Nkx2-5/Cre gene using ROSA26 reporter mice. *Genesis* **31**, 176-180.

Mulligan, G. and Jacks, T. (1998). The retinoblastoma gene family: cousins with overlapping interests. *Trends in genetics : TIG* **14**, 223-229.

Pasumarthi, K. B. and Field, L. J. (2002). Cardiomyocyte cell cycle regulation. *Circulation research* **90**, 1044-1054.

Porrello, E. R., Johnson, B. A., Aurora, A. B., Simpson, E., Nam, Y. J., Matkovich, S. J., Dorn, G. W., 2nd, van Rooij, E. and Olson, E. N. (2011). MiR-15 family regulates postnatal mitotic arrest of cardiomyocytes. *Circulation research* **109**, 670-679.

Rodriguez, C. I., Buchholz, F., Galloway, J., Sequerra, R., Kasper, J., Ayala, R., Stewart, A. F. and Dymecki, S. M. (2000). High-efficiency deleter mice show that FLPe is an alternative to Cre-loxP. *Nature genetics* **25**, 139-140.

Sedmera, D., Reckova, M., DeAlmeida, A., Coppen, S. R., Kubalak, S. W., Gourdie, R. G. and Thompson, R. P. (2003). Spatiotemporal pattern of commitment to slowed proliferation in the embryonic mouse heart indicates progressive differentiation of the cardiac conduction system. *The anatomical record. Part A, Discoveries in molecular, cellular, and evolutionary biology* **274**, 773-777.

Sojka, S., Amin, N. M., Gibbs, D., Christine, K. S., Charpentier, M. S. and Conlon, F. L. (2014). Congenital heart disease protein 5 associates with CASZ1 to maintain myocardial tissue integrity. *Development* **141**, 3040-3049.

Soonpaa, M. H., Kim, K. K., Pajak, L., Franklin, M. and Field, L. J. (1996). Cardiomyocyte DNA synthesis and binucleation during murine development. *The American journal of physiology* **271**, H2183-2189.

Soriano, P. (1999). Generalized lacZ expression with the ROSA26 Cre reporter strain. *Nature genetics* **21**, 70-71.

Srinivas, S., Watanabe, T., Lin, C. S., William, C. M., Tanabe, Y., Jessell, T. M. and Costantini, F. (2001). Cre reporter strains produced by targeted insertion of EYFP and ECFP into the ROSA26 locus. *BMC developmental biology* **1**, 4.

Sun, Y., Liang, X., Najafi, N., Cass, M., Lin, L., Cai, C. L., Chen, J. and Evans, S. M. (2007). Islet 1 is expressed in distinct cardiovascular lineages, including pacemaker and coronary vascular cells. *Developmental biology* **304**, 286-296.

Supek, F., Bosnjak, M., Skunca, N. and Smuc, T. (2011). REVIGO summarizes and visualizes long lists of gene ontology terms. *PloS one* **6**, e21800.

Takeuchi, F., Isono, M., Katsuya, T., Yamamoto, K., Yokota, M., Sugiyama, T., Nabika, T., Fujioka, A., Ohnaka, K., Asano, H. et al. (2010). Blood pressure and hypertension are associated with 7 loci in the Japanese population. *Circulation* **121**, 2302-2309.

Testa, G., Zhang, Y., Vintersten, K., Benes, V., Pijnappel, W. W., Chambers, I., Smith, A. J., Smith, A. G. and Stewart, A. F. (2003). Engineering the mouse genome with bacterial artificial chromosomes to create multipurpose alleles. *Nature biotechnology* **21**, 443-447.

Trapnell, C., Pachter, L. and Salzberg, S. L. (2009). TopHat: discovering splice junctions with RNA-Seq. *Bioinformatics* **25**, 1105-1111.

Trapnell, C., Roberts, A., Goff, L., Pertea, G., Kim, D., Kelley, D. R., Pimentel, H., Salzberg, S. L., Rinn, J. L. and Pachter, L. (2012). Differential gene and transcript expression analysis of RNA-seq experiments with TopHat and Cufflinks. *Nature protocols* **7**, 562-578.

Vacalla, C. M. and Theil, T. (2002). Cst, a novel mouse gene related to Drosophila Castor, exhibits dynamic expression patterns during neurogenesis and heart development. *Mech Dev* **118**, 265-268.

von Gise, A., Lin, Z., Schlegelmilch, K., Honor, L. B., Pan, G. M., Buck, J. N., Ma, Q., Ishiwata, T., Zhou, B., Camargo, F. D. et al. (2012). YAP1, the nuclear target of Hippo signaling, stimulates heart growth through cardiomyocyte proliferation but not hypertrophy. *Proceedings of the National Academy of Sciences of the United States of America* **109**, 2394-2399.

Wadugu, B. and Kuhn, B. (2012). The role of neuregulin/ErbB2/ErbB4 signaling in the heart with special focus on effects on cardiomyocyte proliferation. *American journal of physiology. Heart and circulatory physiology* **302**, H2139-2147.

Wessels, A., van den Hoff, M. J., Adamo, R. F., Phelps, A. L., Lockhart, M. M., Sauls, K., Briggs, L. E., Norris, R. A., van Wijk, B., Perez-Pomares, J. M. et al. (2012). Epicardially derived fibroblasts preferentially contribute to the parietal leaflets of the atrioventricular valves in the murine heart. *Developmental biology* **366**, 111-124.

Xin, M., Olson, E. N. and Bassel-Duby, R. (2013). Mending broken hearts: cardiac development as a basis for adult heart regeneration and repair. *Nature reviews. Molecular cell biology* **14**, 529-541.

Xin, M., Kim, Y., Sutherland, L. B., Qi, X., McAnally, J., Schwartz, R. J., Richardson, J. A., Bassel-Duby, R. and Olson, E. N. (2011). Regulation of insulin-like growth factor signaling by Yap governs cardiomyocyte proliferation and embryonic heart size. *Science signaling* **4**, ra70.

Chapter 3: Discussion and Future Directions

The four-chambered vertebrate heart arises from a series of complex processes during embryonic development that includes the specification and differentiation of the different cardiac cell types within the heart, proliferation, and morphological movements of the early heart fields (Parameswaran and Tam, 1995; Tam et al., 1997; Christoffels et al., 2000; Harvey, 2002; Buckingham et al., 2005; Tzouanacou et al., 2009; van den Berg et al., 2009; Evans et al., 2010; Meilhac et al., 2014). These processes are closely associated with the onset in expression of a number of critical cardiogenic transcriptional factors, which function combinatorally to activate the appropriate cardiogenic gene program and promote proper heart growth. Studies on the progression of cardiogenesis all support the idea that there is no master regulator of cardiac development that is necessary and sufficient to activate the cardiac program. Instead the transcriptional control of heart development occurs by the combinatorial activity of a number of critical cardiogenic transcription factors (Sepulveda et al., 1998; Morin et al., 2000; Hiroi et al., 2001; Buckingham et al., 2005; Stennard et al., 2005; Stennard and Harvey, 2005; Abu-Issa and Kirby, 2007; Abu-Issa and Kirby, 2008; Vincentz et al., 2008; Junion et al., 2012; Meilhac et al., 2014). One of these factors, Casz1, is critical for heart development; however, there are huge deficiencies in our understanding of the

mechanism by which Casz1 regulates aspects of cardiac development. This dissertation comprises a set of studies that investigates the role of Casz1 during cardiac development. In an effort to identify the requirement for Casz1 during cardiac development, we generated a *Casz1* conditional "floxed" allele and a *Casz1* tamoxifen-inducible allele and subsequently produced mice harboring these constructs. In addition, we developed an embryonic cardiac nuclei extraction protocol and determined cell cycle profiles of wild-type hearts and hearts depleted of Casz1. From these studies, we determined that Casz1 is required for cardiac development. Furthermore, we show that Casz1 is a critical regulator of cardiomyocyte proliferation and is necessary for proper G_1-to-S-phase cell cycle progression, thus identifying Casz1 as a key cardiogenic transcription factor required for proper heart growth.

Casz1 is an essential cardiac transcription factor required for development

In Chapter 2, we demonstrated that Casz1 is required for cardiac development, and is specifically required for the growth and proper development of the cardiac chambers. *Casz1*-null mice exhibit severe ventricular hypoplasia and ventricular septal defects (VSDs) (Dorr et al., in review). In normal mammalian development, the wall between the left and right ventricle, termed the interventricular septum (IVS), closes before birth. This separation of the chambers is critical to separate oxygen-rich blood from oxygen-low blood. A VSD is congenital heart defect (CHD) defined as a hole in the interventricular septum, which leads to a higher work load for the heart, higher pressure in the heart and/or reduced oxygen to the body. Normally, the left ventricular chamber

only pumps blood to the body, and the right ventricular chamber only pumps blood to the lungs. However, in a patient with VSD, blood can travel across the hole from the left to the right ventricle and be pumped into the lung arteries, leading to lung congestion and labored breathing. VSDs are the most common type of human congenital heart defects. Currently, VSDs are treated primarily through surgical repair and the patient can enjoy a high quality of life. However, if untreated, VSDs can lead to heart failure, pulmonary hypertension and subsequent death. As such, early detection of these malformations in the newborn is critical to avoid mortality, morbidity, and handicap (Hoffman, 1995; Richmond and Wren, 2001; Hoffman and Kaplan, 2002; van der Linde et al., 2011; Fahed et al., 2013; Pediatric Cardiac Genomics et al., 2013). Despite this, heart disease goes unrecognized in newborn babies in more than half of those with congenital cardiac malformations due to the fact that many infants with heart defects are asymptomatic at birth (Richmond and Wren, 2001).

Studies that identify essential cardiac transcription factors and their gene targets and protein interaction partners will lead to an even more comprehensive list of potential risk factors for CHD. Contemporary genomic methodologies provide opportunities for comprehensive genomic analyses of all CHD patients. The NIH Heart, Lung, and Blood Institute are leading the effort to study genetic pathogenesis in thousands of CHD patients (Pediatric Cardiac Genomics et al., 2013). Deciphering the contributions of genetic and nongenetic causes of CHD has benefited from extensive model organism studies that have provided a wealth of insights into cardiac development. Molecular pathways have been identified that orchestrate formation of the cardiogenic fields, and which drive atrial, ventricular, inflow, and outflow tract morphogenesis. Within these

pathways, details have emerged about molecules that promote lineage specification, differentiation, cell growth and proliferation, migration, and that orchestrate temporal and spatial patterns of gene expression (Fishman and Olson, 1997; Srivastava and Olson, 2000; Buckingham et al., 2005; Srivastava, 2006; Evans et al., 2010; Vincent and Buckingham, 2010; Singh et al., 2011; Boettger and Braun, 2012; Kim et al., 2012; Munshi, 2012; von Gise and Pu, 2012; Fahed et al., 2013; Meilhac et al., 2014). Positioning previously discovered and novel CHD genes onto this blueprint presents extraordinary opportunities to enhance our knowledge of cardiac development and to fully understand the causes and mechanisms of CHD. The studies outlined in this thesis, focused on the role of Casz1 during murine cardiac development. Interestingly, the human ortholog of CASZ1 localizes to chromosome 1p36. Deletion of this region of the genome is quite common and leads to a myriad of genetic abnormalities including cardiac structural defects and cardiomyopathy (Heilstedt et al., 2003a; Heilstedt et al., 2003b; Battaglia et al., 2008). Of the structural defects observed, VSDs and ASDs (atrial septal defects) are the most common (Battaglia et al., 2008). Here, we have identified a novel CHD gene, Casz1, in mice, and demonstrated that cardiac-specific as well as complete loss of Casz1 gives rise to a VSD phenotype, providing further knowledge about the causes and mechanisms giving rise to CHD.

Casz1 regulates G_1-to-S-phase cardiomyocyte cell cycle progression

Our studies demonstrated an essential requirement for Casz1 in regulating cardiomyocyte proliferation in both the first and second heart fields. Specifically, we

showed that loss of *Casz1* in the embryonic heart leads to a prolonged or arrested S-phase, a decrease in DNA synthesis, an increase in phosphorylated-Rb and an associated decrease in the cardiomyocyte mitotic index, suggesting that Casz1 is required for G_1-to-S-phase cell cycle progression. This leads to a severely hypoplastic heart, characterized by a dramatic decrease in the number of cardiomyocytes and eventual embryonic lethality.

The identification of the molecules and signals that regulate cardiomyocyte cell cycle progression is critical to understanding cardiac growth and regeneration potential. As described in Chapter 1, the embryonic heart is characterized by a burst of cardiomyocyte proliferation that decreases as development proceeds. Conversely, the adult heart shows limited ability to proliferate (Erokhnia, 1968a; Erokhnia, 1968b; Dowell and McManus, 1978; Clubb and Bishop, 1984; Oparil et al., 1984; Goldspink et al., 1986; Li et al., 1996; Soonpaa et al., 1996; Soonpaa and Field, 1997; Bergmann et al., 2009; Walsh et al., 2010; Laflamme and Murry, 2011; Maillet et al., 2013; Mollova et al., 2013). Although much is known about the cardiac transcription factors and pathways that are required for proper heart development, very little is known about the cardiac transcription factors that regulate the cardiomyocyte cell cycle. In addition, the stage specific transcriptional requirements for cardiomyocyte cell cycle regulators are unknown. Furthermore, the length of the cell cycle remains elusive; however, studies suggest that it is extremely long, with estimates of greater than 24 hours (Bersell et al., 2009; Mollova et al., 2013). With all of this in mind, the demonstration that Casz1 plays a role in regulating the G_1-to-S-phase transition of the cardiomyocyte cell cycle is a significant finding and worth further exploration.

In Chapter 2, we demonstrated, using a novel cardiac nuclei isolation technique followed by cell cycle analysis, that *Casz1*-cardiac-null hearts show a significant increase in number of cells in G_1-phase combined with a significant decrease in the number of cells in S-phase. This indicated that a proportion of the cells were either arrested in G_1-phase, or had undergone cell death. To validate these findings, we further showed an increase in the number of cardiomyocytes expressing the G_1-phase marker, phophosphorylated-Rb protein. Rb is a well-established negative regulator of the cell cycle and is responsible for a major G_1-phase checkpoint, which blocks S-phase entry (Figure 1.1) (Pardee, 1989; Weinberg, 1995; Foster et al., 2010; Bertoli et al., 2013). Subsequent programmed cell death analysis did not show an alteration indicating that cell cycle arrest occurred instead of death. The mammalian cell cycle consists of 2 main parts: mitosis and interphase. During interphase or S-phase (for synthesis), the genome is duplicated. During mitosis (M-phase) cell division occurs. G_1- and G_2-phases are gaps between mitosis and S phase and between S phase and mitosis, respectively. G_1-phase is usually where decisions are made as to whether to enter a resting quiescent stage known as G_0 or to continue cycling and commit to replicating the genome and mitosis. The point in G_1-phase where this growth factor–dependent decision is made is known as the restriction point (R) (Morgan, 1997; Foster et al., 2010; Lim and Kaldis, 2013; Alberts, 2015). Based on our findings, we presently favor a model by which Casz1 is necessary but not sufficient for cardiomyocytes to pass the restriction point and commit to the next round of division. We note this role of Casz1 must be stage specific as we fail to see any phenotypic consequences of removing *Casz1* during the initial stages of cardiac specification and determination (E6-E8). This

observation would imply that this checkpoint control is under a separate, as of yet unidentified mechanism in the early stages of heart development. In the future, it will be of importance to identify the Casz1-dependent pathway during these early stages of cardiac development and determine what role, if any, Casz1 plays in adult homoeostasis and injury repair.

Future Directions

To date, our Casz1 studies have focused on the role of Casz1 during embryonic development. Going forward, our efforts will be aimed towards an in-depth phenotypic analysis to determine what role, if any, Casz1 plays in adult homeostasis and injury repair. I have previously shown by RT-PCR analysis that Casz1 is expressed in the adult heart. Furthermore, *Casz1*^{CreERT2} adult mice treated with a diet of tamoxifen chow for 3 weeks identified *Casz1*-expressing cells in the cardiomyocytes of the adult myocardium (Dorr et al, unpublished). Together this data suggests that Casz1 plays a role in the adult heart. To elucidate the genetic requirement for Casz1 in the postnatal heart, the *Casz1*$^{flox/flox}$ mice will be crossed first to the tamoxifen inducible *α–MHC-MerCreMer* driver (Sohal et al., 2001). The α-MHC promoter drives expression exclusively in cardiomyocytes and has been used extensively in studies of cardiac gene function. The promoter drives expression in embryonic and adult atrial cardiomyocytes. Expression in ventricular cardiomyocytes is observed mainly after birth (Ng et al., 1991; Palermo et al., 1996; Buerger et al., 2006). The main advantage to the tamoxifen-inducible system is the temporal control of Cre activation (Nagy, 2000). Six-week old

adult mice will be given a single dose of tamoxifen via intraperitoneal injection for 5 sequential days (Sohal et al., 2001). First, it will be essential to determine if any overt phenotype is displayed and if so, to determine if it leads to lethality. Observable phenotypes include: lethargy, labored breathing, weight loss, and sudden death. Next, a detailed phenotypic analysis will be necessary and include: histology to identify structural defects, echocardiograms to measure cardiac function, and Picrosirius red staining to measure fibrosis.

Having established in Chapter 2 that Casz1 is a critical regulator of embryonic cardiomyocyte proliferation with links to the cardiomyocyte cell cycle, identifying the role of Casz1 in the adult myocardium is of utmost importance. Many questions arise that need to be addressed: 1) Is Casz1 upregulated during myocardial injury? 2) Do hearts depleted of Casz1 show any defects in injury repair? 3) If so, are these defects related to the cardiomyocyte cell cycle – do we observe dramatic changes in proliferation levels when compared to controls? 4) What genes does Casz1 regulate and what genes does *Casz1* interact with in the adult heart? Preliminary evidence in neonatal cardiomyocytes indicates that Casz1 does play a role in regulating the cardiomyocyte cell cycle. We generated a human CASZ1 shRNA knockdown lentivirus and a mouse *Casz1* overexpression adenovirus for in vitro analyses (Charpentier et al., 2013)(Dorr et al., unpublished). Next, we treated P1 wild-type neonatal cardiomyocytes with each virus and subsequently performed cell cycle analsysis to reveal a significant increase of cardiomyocytes in G_1-phase and a concomitant decrease of cardiomyocytes in S-phase. This data recapitulates what we observed in embryonic cardiomyocytes and indicates that Casz1 plays a role in postnatal cardiomyocyte cell cycle regulation (Dorr

et al., unpublished). To address these issues in vivo and to complement the adult *Casz1*-cardiac-null mice detailed above, we must first examine Casz1 gene expression levels in myocardial injured wild-type adult hearts. Next, it will be critical to determine if our *Casz1$^{flox/flox}$;α-MHC-MerCreMer* mice show defects in cardiomyocyte proliferation as assessed by EdU and pHH3 analyses. If we see alterations in cardiomyocyte proliferation, then we will perform myocardial injury experiments on *Casz1* cardiac null adult hearts. Studies in mice have demonstrated that adult cardiomyocytes proliferate at a low rate by division of pre-existing cardiomyocytes during normal aging and this process increases by four-fold in areas adjacent to myocardial injury (Li et al., 1996; Soonpaa et al., 1996; Soonpaa and Field, 1997; Soonpaa and Field, 1998; Walsh et al., 2010; Maillet et al., 2013; Porrello et al., 2013; Senyo et al., 2013). If Casz1 is required for adult cardiomyocyte proliferation, then we would expect to see a decrease in the proliferation rate of cardiomyocytes in response to injury.

To date, all genetic manipulations of Casz1 have been done via loss-of-functions studies. Casz1 gain-of-function studies have been limited to cell culture experiments and RNA injection techniques in *Xenopus* embryos. We generated a *Casz1*-overexpression adenovirus and seen successful incorporation and enhanced expression of Casz1 in neonatal cardiomyocytes (See above). We have gone on to show that overexpression of Casz1 in these cells leads to cell cycle defects further demonstrating that Casz1 is necessary to regulate the cardiomyocyte cell cycle and suggesting that it could be sufficient as well. In *Xenopus*, overexpression of *Casz1* also results in abnormal cardiac morphogenesis (Sojka et al., 2014). To determine if Casz1 is necessary and sufficient for cardiomyocyte cell cycle progression and to further define

the role of Casz1 during cardiac development, we aim to generate a transgenic mouse that overexpresses *Casz1*. To overexpress Casz1 in the embryonic heart, we will clone the full-length mouse Casz1 cDNA (utilized for the neonatal studies detailed above) into the *Nkx2.5* promoter, which is expressed in early cardiac progenitor cells beginning at E7.5 (Moses et al., 2001). To overexpress Casz1 in the adult heart, we will clone this construct into the α-MHC promoter which is expressed in the adult myocardium (Ng et al., 1991; Palermo et al., 1996; Buerger et al., 2006). Our phenotypic analysis will include a detailed characterization of any proliferation and cell cycle defects in addition to a thorough histological analysis.

The regulatory architecture of the Casz1 locus in vertebrates remains largely unknown. Therefore, the identification of a cardiac-specific enhancer of Casz1 would reveal further insights into the Casz1 gene as a whole. This is long term project goal. To complete it, we will utilize in vivo bacterial artificial chromosome (BAC) recombination to generate a *Casz1-EGFP* BAC that recapitulates the endogenous pattern of *Casz1* expression in transgenic embryos (Liu et al., 2003). We will need to include several of the first exons of the mouse gene as well as a large piece upstream and downstream of the translational start site. Next, we will look for areas of high sequence conservation in noncoding regions between human and mouse. To be able to visualize expression, we will clone an EGFP gene into the Casz1 locus such that the start codon is deleted, but exon boundaries are preserved. This strategy allows translational initiation from EGFP instead of from Casz1 but allows transcriptional initiation to occur from the endogenous Casz1 start sites present in the BAC.

We have established that Casz1 is an essential cardiac transcription factor that regulates cardiomyocyte proliferation. Nevertheless, only one direct target of Casz1 has been identified: the extracellular matrix protein Egfl7, which is required for endothelial cell development and angiogenesis (Charpentier et al., 2013). It is critical to identify the mechanism(s) by which Casz1 regulates cardiomyocyte proliferation in the adult heart. To do this, an in-depth whole genome analysis of Casz1 is vital. First, we need to perform RNA-Seq on *Casz1*-depleted adult hearts to identify genes and pathways misregulated by the loss of Casz1. Bioinformatics analysis of cell-cycle related genes and genes involved in cardiomyocyte cell growth will be prioritized. Going forward, it is absolutely essential to identify the genes that Casz1 directly regulates in the heart. To address this, we need to perform chromatin immunoprecipitation followed by high-throughput DNA sequencing (ChIP-Seq) for Casz1 in embryonic and adult hearts. ChIP-Seq is a genome-wide method to map the binding sites of a target protein (CASZ1) (Landt et al., 2012). The analysis of Casz1 binding sites at these two time points is critical not only for elucidating the mechanism by which Casz1 regulates cardiomyocyte proliferation, but also can provide insight into the cardiomyocyte cell cycle regulation in general.

Many mammalian tissues respond to injury by activating committed progenitor cells or through proliferation of differentiated cells such as skin, endothelial, and liver cells (Brockes and Kumar, 2005; Horky et al., 2006; Lai et al., 2012; McDonough and Martinez-Cerdeno, 2012). In addition, lower level vertebrates like fish and amphibians are capable of regenerating myocardium after injury via the activation of proliferation pathways in differentiated cells (Nag et al., 1979; Oberpriller et al., 1995; Matz et al.,

1998; Bettencourt-Dias et al., 2003). In contrast, the adult mammalian heart has limited potential for regeneration and repair (Soonpaa et al., 1996; Soonpaa and Field, 1997; Soonpaa and Field, 1998; Bergmann et al., 2009; Walsh et al., 2010; Laflamme and Murry, 2011; Mollova et al., 2013; Porrello et al., 2013; Senyo et al., 2013; Senyo et al., 2014). Moreover, the biological explanations underlying cell cycle exit leading to the dramatic proliferative decreases in the adult heart remain poorly understood. Why is it that terminally differentiated cardiomyocytes have such limited potential to reactivate the cardiomyocyte cell cycle following injury? This is the question that has plagued cardiovascular biologists for many years and it is an area of intense investigation as the loss of cardiomyocytes during injury and disease proves to be so fatal, making cardiovascular disease the leading cause of death worldwide (Seidman and Seidman, 2001; Lopez et al., 2006). Furthermore, congenital heart defects represent the most common type of human birth defect worldwide (Hoffman, 1995; Hoffman and Kaplan, 2002; Dolk et al., 2010a; Dolk et al., 2010b; van der Linde et al., 2011). Insults to the heart, including ischaemic coronary artery disease, hypertension, and genetic mutations can cause heart disease, which is associated with loss or dysfunction of cardiac muscle cells, diminished pump function, arrhythmias and oftentimes subsequent death (Seidman, 2000; Seidman and Seidman, 2001; Lopez et al., 2006; Hill and Olson, 2008; Morita et al., 2008). Congenital malformations and certain types of cardiac injury can be surgically repaired to modest success depending on the condition. Also, there are numerous drugs and mechanical devices that provide temporary improvements to cardiac function, but most results are transient because they do not replace damaged or lost cardiac muscle. Efforts are now focused on identifying and exploiting the molecular

and cellular processes and regulatory mechanisms involved in heart growth to repair the adult injured heart by reviving pathways that are active during embryogenesis.

Extensive efforts towards cardiac repair have gone into the development of 3 major strategies to enhance cardiac regeneration: 1) stem-cell based therapies, 2) reprogramming of non-muscle cells into a cardiac fate, and 3) the induction of cardiomyocyte cell cycle activity. Studies in both rodents and humans have shown that the injection of stem cells directly into the injured heart or into the circulation system can result in modest benefits to cardiac function. However, these results appear to be transient as little evidence exists that the transplanted cells are actually retained in the heart (Passier et al., 2008; Segers and Lee, 2008; Wollert and Drexler, 2010; Laflamme and Murry, 2011; Ptaszek et al., 2012; Anversa et al., 2013). Fibroblasts can be reprogrammed into induced pluri-potent stem cells (iPSCs) through the expression of four pluirpotency genes: OCT4, SOX2, KLF4, and MYC (Takahashi and Yamanaka, 2006; Yamanaka and Takahashi, 2006; Takahashi et al., 2007a; Takahashi et al., 2007b). iPS cells generated from human fibroblasts have been successfully differentiated into beating cardiomyocytes (Yoshida and Yamanaka, 2011; Qian et al., 2012; Fu et al., 2013; Nakamura et al., 2013; Priori et al., 2013; Qian et al., 2013; Qian and Srivastava, 2013). Caridac fibroblasts account for the majority of all heart cells (Jugdutt, 2003). Recent studies have demonstrated that a combination of three transcription factors, namely GATA4, myocyte-specific enhancer factor 2C (MEF2C) and TBX5 (collectively referred to as GMT factors), can reprogram both mice cardiac and dermal fibroblasts into induced cardiac-like myocytes. Further work demonstrated that the inclusion of the cardiac transcription factor, HAND2, (GHMT factors) enhanced

the reprogramming efficiency (Ieda et al., 2010; Chen et al., 2012; Qian et al., 2012; Song et al., 2012; Addis et al., 2013; Fu et al., 2013; Qian et al., 2013; Qian and Srivastava, 2013; Wang et al., 2015). Current work is focused on improving the efficiency of this process to convert more fibroblasts into cardiac-like myocytes. An alternative approach for cardiac repair is to reactivate the proliferative potential of existing cardiomyocytes as observed in lower vertebrates. Studies have focused on overexpressing cell cycle regulatory factors, such as c-Myc, Cyclins D1-D3, Cyclin A2, and SV40 large T antigen, to promote cell cycle progression in injured adult hearts. The results of these studies were variable. However, increases in cardiomyocyte DNA synthesis did occur in many cases, but none were able to induce cytokinesis and so it is unclear as to whether true heart regeneration took place (Field, 1988; Sen et al., 1988; Jackson et al., 1990; Chaudhry et al., 2004; Pasumarthi et al., 2005).

In conclusion, an understanding of the regulation of the cardiac cell cycle is essential for the advancement of the cardiac regeneration field. The studies outlined in this thesis, have identified Casz1 as a critical regulator of the embryonic cardiomyocyte cell cycle. The role of Casz1 in regulating the adult cardiomyocyte cell cycle is unknown, but provides an exciting research avenue to pursue in the context of heart regeneration. Regardless of whether it is to therapeutically reactivate the cell cycle in existing cardiomyocytes, to establish methodologies to expand current cardiac stem cells from losing their differentiation potential in vivo, or to more efficiently reprogram fibroblasts into cardiomyocytes, the ultimate goal is to improve human health and survival. To do so, it is essential to identify the molecules and signals that regulate cardiac growth and homeostasis. These efforts not only hold the potential to benefit cardiovascular patients,

but encompass much broader implications to advance the scientific field in general thereby improving the lives of patients suffering from other cell cycle related diseases, such as cancer. CASZ1, in particular, has many broad clinical implications beyond just congenital heart defects and cardiovascular disease. It has also been identified as a tumor-suppressor gene implicated in Neuroblastoma (NB), a neural crest derived malignant brain tumor (Liu et al., 2011; Henrich et al., 2012). Loss of CASZ1 is associated with poor prognosis in human NB patients. Interestingly, restoration of CASZ1 in a NB cell line induced cell differentiation, enhanced cell adhesion, inhibited migration and suppressed tumorigenicity, but showed no effect on proliferation (Liu et al., 2011). A follow-up in vitro study using NB cells found that CASZ1 inhibits cell cycle progression by restoring pRB activity, leading to decreased proliferation (Liu et al., 2013). Furthermore, a recent study demonstrated that Casz1 controls the production of mid-/late-born neurons in the murine retina, thus suggesting that Casz1 is a temporal identity factor for retina progenitor cells. Moreover, Casz1 does not regulate the proliferation of these progenitor cells, implying that it does not determine a specific cell identity (Mattar et al., 2015). In Chapter 2, I described the broad expression of Casz1 in multiple tissues, including the neural tube and the eye. Together, this data suggests that Casz1 is a critical modulator of neural development. Of particular interest is the contrast between the proliferation requirement in heart tissue that I demonstrated in Chapter 2 and is described above versus the lack of proliferative defects illustrated in these two neuronal cell populations. This difference highlights the dynamic function of Casz1 during development and further emphasizes the need to explore the requirement for Casz1 in a cell-type and tissue-specific manner.

The studies I have conducted in this thesis have generated many of the necessary biological tools to investigate this very issue. The two novel mouse lines that I generated and described in this thesis can be used to explore the role of Casz1 in neural development or cancer. The *Casz1*$^{flox/flox}$ mouse affords the ability to delete *Casz1* in a tissue-specific manner with alternate Cre drivers. Additionally, the *Casz1*^{CreERT2} tamoxifen-inducible mouse can be used to identify neuronal cell types and structures that *Casz1*-expressing cells give rise to during development and in the adult. Most importantly, Casz1 has been identified as a critical cardiac transcription factor. This, combined with the future studies I have proposed here will yield additional information about the genes associated with human congenital heart defects and lead to a great understanding of how Casz1 contributes to cardiovascular development and disease.

REFERENCES

Abu-Issa, R. and Kirby, M. L. (2007). Heart field: from mesoderm to heart tube. *Annual review of cell and developmental biology* **23**, 45-68.

Abu-Issa, R. and Kirby, M. L. (2008). Patterning of the heart field in the chick. *Developmental biology* **319**, 223-233.

Addis, R. C., Ifkovits, J. L., Pinto, F., Kellam, L. D., Esteso, P., Rentschler, S., Christoforou, N., Epstein, J. A. and Gearhart, J. D. (2013). Optimization of direct fibroblast reprogramming to cardiomyocytes using calcium activity as a functional measure of success. *Journal of molecular and cellular cardiology* **60**, 97-106.

Alberts, B. (2015). Molecular biology of the cell. New York, NY: Garland Science, Taylor and Francis Group.

Anversa, P., Kajstura, J., Rota, M. and Leri, A. (2013). Regenerating new heart with stem cells. *The Journal of clinical investigation* **123**, 62-70.

Battaglia, A., Hoyme, H. E., Dallapiccola, B., Zackai, E., Hudgins, L., McDonald-McGinn, D., Bahi-Buisson, N., Romano, C., Williams, C. A., Brailey, L. L. et al. (2008). Further delineation of deletion 1p36 syndrome in 60 patients: a recognizable phenotype and common cause of developmental delay and mental retardation. *Pediatrics* **121**, 404-410.

Bergmann, O., Bhardwaj, R. D., Bernard, S., Zdunek, S., Barnabe-Heider, F., Walsh, S., Zupicich, J., Alkass, K., Buchholz, B. A., Druid, H. et al. (2009). Evidence for cardiomyocyte renewal in humans. *Science* **324**, 98-102.

Bersell, K., Arab, S., Haring, B. and Kuhn, B. (2009). Neuregulin1/ErbB4 signaling induces cardiomyocyte proliferation and repair of heart injury. *Cell* **138**, 257-270.

Bertoli, C., Skotheim, J. M. and de Bruin, R. A. (2013). Control of cell cycle transcription during G1 and S phases. *Nature reviews. Molecular cell biology* **14**, 518-528.

Bettencourt-Dias, M., Mittnacht, S. and Brockes, J. P. (2003). Heterogeneous proliferative potential in regenerative adult newt cardiomyocytes. *Journal of cell science* **116**, 4001-4009.

Boettger, T. and Braun, T. (2012). A new level of complexity: the role of microRNAs in cardiovascular development. *Circulation research* **110**, 1000-1013.

Brockes, J. P. and Kumar, A. (2005). Appendage regeneration in adult vertebrates and implications for regenerative medicine. *Science* **310**, 1919-1923.

Buckingham, M., Meilhac, S. and Zaffran, S. (2005). Building the mammalian heart from two sources of myocardial cells. *Nature reviews. Genetics* **6**, 826-835.

Buerger, A., Rozhitskaya, O., Sherwood, M. C., Dorfman, A. L., Bisping, E., Abel, E. D., Pu, W. T., Izumo, S. and Jay, P. Y. (2006). Dilated cardiomyopathy resulting from high-level myocardial expression of Cre-recombinase. *Journal of cardiac failure* **12**, 392-398.

Charpentier, M. S., Christine, K. S., Amin, N. M., Dorr, K. M., Kushner, E. J., Bautch, V. L., Taylor, J. M. and Conlon, F. L. (2013). CASZ1 promotes vascular assembly and morphogenesis through the direct regulation of an EGFL7/RhoA-mediated pathway. *Developmental cell* **25**, 132-143.

Chaudhry, H. W., Dashoush, N. H., Tang, H., Zhang, L., Wang, X., Wu, E. X. and Wolgemuth, D. J. (2004). Cyclin A2 mediates cardiomyocyte mitosis in the postmitotic myocardium. *The Journal of biological chemistry* **279**, 35858-35866.

Chen, J. X., Krane, M., Deutsch, M. A., Wang, L., Rav-Acha, M., Gregoire, S., Engels, M. C., Rajarajan, K., Karra, R., Abel, E. D. et al. (2012). Inefficient reprogramming of fibroblasts into cardiomyocytes using Gata4, Mef2c, and Tbx5. *Circulation research* **111**, 50-55.

Christoffels, V. M., Habets, P. E., Franco, D., Campione, M., de Jong, F., Lamers, W. H., Bao, Z. Z., Palmer, S., Biben, C., Harvey, R. P. et al. (2000). Chamber formation and morphogenesis in the developing mammalian heart. *Developmental biology* **223**, 266-278.

Clubb, F. J., Jr. and Bishop, S. P. (1984). Formation of binucleated myocardial cells in the neonatal rat. An index for growth hypertrophy. *Laboratory investigation; a journal of technical methods and pathology* **50**, 571-577.

Dolk, H., Loane, M. and Garne, E. (2010a). The prevalence of congenital anomalies in Europe. *Advances in experimental medicine and biology* **686**, 349-364.

Dolk, H., Loane, M. A., Abramsky, L., de Walle, H. and Garne, E. (2010b). Birth prevalence of congenital heart disease. *Epidemiology* **21**, 275-277; author reply 277.

Dowell, R. T. and McManus, R. E., 3rd. (1978). Pressure-induced cardiac enlargement in neonatal and adult rats. Left ventricular functional characteristics and evidence of cardiac muscle cell proliferation in the neonate. *Circulation research* **42**, 303-310.

Erokhnia, I. L. (1968a). The proliferation and DNA synthesis during early stages of myocardial development. *Tsiotologiya* **10**, 162-172.

Erokhnia, I. L. (1968b). Proliferation dynamics of cellular elements in the differentiating mouse myocardium. *Tsiotologiya* **10**, 1391-1409.

Evans, S. M., Yelon, D., Conlon, F. L. and Kirby, M. L. (2010). Myocardial lineage development. *Circulation research* **107**, 1428-1444.

Fahed, A. C., Gelb, B. D., Seidman, J. G. and Seidman, C. E. (2013). Genetics of congenital heart disease: the glass half empty. *Circulation research* **112**, 707-720.

Field, L. J. (1988). Atrial natriuretic factor-SV40 T antigen transgenes produce tumors and cardiac arrhythmias in mice. *Science* **239**, 1029-1033.

Fishman, M. C. and Olson, E. N. (1997). Parsing the heart: genetic modules for organ assembly. *Cell* **91**, 153-156.

Foster, D. A., Yellen, P., Xu, L. and Saqcena, M. (2010). Regulation of G1 Cell Cycle Progression: Distinguishing the Restriction Point from a Nutrient-Sensing Cell Growth Checkpoint(s). *Genes & cancer* **1**, 1124-1131.

Fu, J. D., Stone, N. R., Liu, L., Spencer, C. I., Qian, L., Hayashi, Y., Delgado-Olguin, P., Ding, S., Bruneau, B. G. and Srivastava, D. (2013). Direct reprogramming of human fibroblasts toward a cardiomyocyte-like state. *Stem cell reports* **1**, 235-247.

Goldspink, D. F., Lewis, S. E. and Merry, B. J. (1986). Effects of aging and long term dietary intervention on protein turnover and growth of ventricular muscle in the rat heart. *Cardiovascular research* **20**, 672-678.

Harvey, R. P. (2002). Patterning the vertebrate heart. *Nature reviews. Genetics* **3**, 544-556.

Heilstedt, H. A., Ballif, B. C., Howard, L. A., Kashork, C. D. and Shaffer, L. G. (2003a). Population data suggest that deletions of 1p36 are a relatively common chromosome abnormality. *Clinical genetics* **64**, 310-316.

Heilstedt, H. A., Ballif, B. C., Howard, L. A., Lewis, R. A., Stal, S., Kashork, C. D., Bacino, C. A., Shapira, S. K. and Shaffer, L. G. (2003b). Physical map of 1p36, placement of breakpoints in monosomy 1p36, and clinical characterization of the syndrome. *American journal of human genetics* **72**, 1200-1212.

Henrich, K. O., Schwab, M. and Westermann, F. (2012). 1p36 tumor suppression--a matter of dosage? *Cancer research* **72**, 6079-6088.

Hill, J. A. and Olson, E. N. (2008). Cardiac plasticity. *The New England journal of medicine* **358**, 1370-1380.

Hiroi, Y., Kudoh, S., Monzen, K., Ikeda, Y., Yazaki, Y., Nagai, R. and Komuro, I. (2001). Tbx5 associates with Nkx2-5 and synergistically promotes cardiomyocyte differentiation. *Nature genetics* **28**, 276-280.

Hoffman, J. I. (1995). Incidence of congenital heart disease: I. Postnatal incidence. *Pediatric cardiology* **16**, 103-113.

Hoffman, J. I. and Kaplan, S. (2002). The incidence of congenital heart disease. *Journal of the American College of Cardiology* **39**, 1890-1900.

Horky, L. L., Galimi, F., Gage, F. H. and Horner, P. J. (2006). Fate of endogenous stem/progenitor cells following spinal cord injury. *J Comp Neurol* **498**, 525-538.

Ieda, M., Fu, J. D., Delgado-Olguin, P., Vedantham, V., Hayashi, Y., Bruneau, B. G. and Srivastava, D. (2010). Direct reprogramming of fibroblasts into functional cardiomyocytes by defined factors. *Cell* **142**, 375-386.

Jackson, T., Allard, M. F., Sreenan, C. M., Doss, L. K., Bishop, S. P. and Swain, J. L. (1990). The c-myc proto-oncogene regulates cardiac development in transgenic mice. *Molecular and cellular biology* **10**, 3709-3716.

Jugdutt, B. I. (2003). Ventricular remodeling after infarction and the extracellular collagen matrix: when is enough enough? *Circulation* **108**, 1395-1403.

Junion, G., Spivakov, M., Girardot, C., Braun, M., Gustafson, E. H., Birney, E. and Furlong, E. E. (2012). A transcription factor collective defines cardiac cell fate and reflects lineage history. *Cell* **148**, 473-486.

Kim, K. H., Rosen, A., Bruneau, B. G., Hui, C. C. and Backx, P. H. (2012). Iroquois homeodomain transcription factors in heart development and function. *Circulation research* **110**, 1513-1524.

Laflamme, M. A. and Murry, C. E. (2011). Heart regeneration. *Nature* **473**, 326-335.

Lai, Y. P., Li, D. Q., Li, C. W., Muehleisen, B., Radek, K. A., Park, H. J., Jiang, Z. W., Li, Z. H., Lei, H., Quan, Y. C. et al. (2012). The Antimicrobial Protein REG3A Regulates Keratinocyte Proliferation and Differentiation after Skin Injury. *Immunity* **37**, 74-84.

Landt, S. G., Marinov, G. K., Kundaje, A., Kheradpour, P., Pauli, F., Batzoglou, S., Bernstein, B. E., Bickel, P., Brown, J. B., Cayting, P. et al. (2012). ChIP-seq guidelines and practices of the ENCODE and modENCODE consortia. *Genome research* **22**, 1813-1831.

Li, F., Wang, X., Capasso, J. M. and Gerdes, A. M. (1996). Rapid transition of cardiac myocytes from hyperplasia to hypertrophy during postnatal development. *Journal of molecular and cellular cardiology* **28**, 1737-1746.

Lim, S. and Kaldis, P. (2013). Cdks, cyclins and CKIs: roles beyond cell cycle regulation. *Development* **140**, 3079-3093.

Liu, P., Jenkins, N. A. and Copeland, N. G. (2003). A highly efficient recombineering-based method for generating conditional knockout mutations. *Genome research* **13**, 476-484.

Liu, Z., Rader, J., He, S., Phung, T. and Thiele, C. J. (2013). CASZ1 inhibits cell cycle progression in neuroblastoma by restoring pRb activity. *Cell cycle* **12**, 2210-2218.

Liu, Z., Yang, X., Li, Z., McMahon, C., Sizer, C., Barenboim-Stapleton, L., Bliskovsky, V., Mock, B., Ried, T., London, W. B. et al. (2011). CASZ1, a candidate

tumor-suppressor gene, suppresses neuroblastoma tumor growth through reprogramming gene expression. *Cell death and differentiation* **18**, 1174-1183.

Lopez, A. D., Mathers, C. D., Ezzati, M., Jamison, D. T. and Murray, C. J. L. (2006). Measuring the Global Burden of Disease and Risk Factors, 1990-2001. In *Global Burden of Disease and Risk Factors* (eds A. D. Lopez C. D. Mathers M. Ezzati D. T. Jamison and C. J. L. Murray). Washington (DC).

Maillet, M., van Berlo, J. H. and Molkentin, J. D. (2013). Molecular basis of physiological heart growth: fundamental concepts and new players. *Nature reviews. Molecular cell biology* **14**, 38-48.

Mattar, P., Ericson, J., Blackshaw, S. and Cayouette, M. (2015). A conserved regulatory logic controls temporal identity in mouse neural progenitors. *Neuron* **85**, 497-504.

Matz, D. G., Oberpriller, J. O. and Oberpriller, J. C. (1998). Comparison of mitosis in binucleated and mononucleated newt cardiac myocytes. *The Anatomical record* **251**, 245-255.

McDonough, A. and Martinez-Cerdeno, V. (2012). Endogenous Proliferation after Spinal Cord Injury in Animal Models. *Stem Cells Int*.

Meilhac, S. M., Lescroart, F., Blanpain, C. and Buckingham, M. E. (2014). Cardiac cell lineages that form the heart. *Cold Spring Harbor perspectives in medicine* **4**, a013888.

Mollova, M., Bersell, K., Walsh, S., Savla, J., Das, L. T., Park, S. Y., Silberstein, L. E., Dos Remedios, C. G., Graham, D., Colan, S. et al. (2013). Cardiomyocyte proliferation contributes to heart growth in young humans. *Proceedings of the National Academy of Sciences of the United States of America* **110**, 1446-1451.

Morgan, D. O. (1997). Cyclin-dependent kinases: engines, clocks, and microprocessors. *Annual review of cell and developmental biology* **13**, 261-291.

Morin, S., Charron, F., Robitaille, L. and Nemer, M. (2000). GATA-dependent recruitment of MEF2 proteins to target promoters. *The EMBO journal* **19**, 2046-2055.

Morita, H., Rehm, H. L., Menesses, A., McDonough, B., Roberts, A. E., Kucherlapati, R., Towbin, J. A., Seidman, J. G. and Seidman, C. E. (2008). Shared genetic causes of cardiac hypertrophy in children and adults. *The New England journal of medicine* **358**, 1899-1908.

Moses, K. A., DeMayo, F., Braun, R. M., Reecy, J. L. and Schwartz, R. J. (2001). Embryonic expression of an Nkx2-5/Cre gene using ROSA26 reporter mice. *Genesis* **31**, 176-180.

Munshi, N. V. (2012). Gene regulatory networks in cardiac conduction system development. *Circulation research* **110**, 1525-1537.

Nag, A. C., Healy, C. J. and Cheng, M. (1979). DNA synthesis and mitosis in adult amphibian cardiac muscle cells in vitro. *Science* **205**, 1281-1282.

Nagy, A. (2000). Cre recombinase: the universal reagent for genome tailoring. *Genesis* **26**, 99-109.

Nakamura, K., Hirano, K. and Wu, S. M. (2013). iPS cell modeling of cardiometabolic diseases. *Journal of cardiovascular translational research* **6**, 46-53.

Ng, W. A., Grupp, I. L., Subramaniam, A. and Robbins, J. (1991). Cardiac myosin heavy chain mRNA expression and myocardial function in the mouse heart. *Circulation research* **68**, 1742-1750.

Oberpriller, J. O., Oberpriller, J. C., Matz, D. G. and Soonpaa, M. H. (1995). Stimulation of proliferative events in the adult amphibian cardiac myocyte. *Annals of the New York Academy of Sciences* **752**, 30-46.

Oparil, S., Bishop, S. P. and Clubb, F. J., Jr. (1984). Myocardial cell hypertrophy or hyperplasia. *Hypertension* **6**, III38-43.

Palermo, J., Gulick, J., Colbert, M., Fewell, J. and Robbins, J. (1996). Transgenic remodeling of the contractile apparatus in the mammalian heart. *Circulation research* **78**, 504-509.

Parameswaran, M. and Tam, P. P. (1995). Regionalisation of cell fate and morphogenetic movement of the mesoderm during mouse gastrulation. *Developmental genetics* **17**, 16-28.

Pardee, A. B. (1989). G1 events and regulation of cell proliferation. *Science* **246**, 603-608.

Passier, R., van Laake, L. W. and Mummery, C. L. (2008). Stem-cell-based therapy and lessons from the heart. *Nature* **453**, 322-329.

Pasumarthi, K. B., Nakajima, H., Nakajima, H. O., Soonpaa, M. H. and Field, L. J. (2005). Targeted expression of cyclin D2 results in cardiomyocyte DNA synthesis and infarct regression in transgenic mice. *Circulation research* **96**, 110-118.

Pediatric Cardiac Genomics, C., Gelb, B., Brueckner, M., Chung, W., Goldmuntz, E., Kaltman, J., Kaski, J. P., Kim, R., Kline, J., Mercer-Rosa, L. et al. (2013). The Congenital Heart Disease Genetic Network Study: rationale, design, and early results. *Circulation research* **112**, 698-706.

Porrello, E. R., Mahmoud, A. I., Simpson, E., Johnson, B. A., Grinsfelder, D., Canseco, D., Mammen, P. P., Rothermel, B. A., Olson, E. N. and Sadek, H. A. (2013). Regulation of neonatal and adult mammalian heart regeneration by the miR-15 family. *Proceedings of the National Academy of Sciences of the United States of America* **110**, 187-192.

Priori, S. G., Napolitano, C., Di Pasquale, E. and Condorelli, G. (2013). Induced pluripotent stem cell-derived cardiomyocytes in studies of inherited arrhythmias. *The Journal of clinical investigation* **123**, 84-91.

Ptaszek, L. M., Mansour, M., Ruskin, J. N. and Chien, K. R. (2012). Towards regenerative therapy for cardiac disease. *Lancet* **379**, 933-942.

Qian, L. and Srivastava, D. (2013). Direct cardiac reprogramming: from developmental biology to cardiac regeneration. *Circulation research* **113**, 915-921.

Qian, L., Berry, E. C., Fu, J. D., Ieda, M. and Srivastava, D. (2013). Reprogramming of mouse fibroblasts into cardiomyocyte-like cells in vitro. *Nature protocols* **8**, 1204-1215.

Qian, L., Huang, Y., Spencer, C. I., Foley, A., Vedantham, V., Liu, L., Conway, S. J., Fu, J. D. and Srivastava, D. (2012). In vivo reprogramming of murine cardiac fibroblasts into induced cardiomyocytes. *Nature* **485**, 593-598.

Richmond, S. and Wren, C. (2001). Early diagnosis of congenital heart disease. *Seminars in neonatology : SN* **6**, 27-35.

Segers, V. F. and Lee, R. T. (2008). Stem-cell therapy for cardiac disease. *Nature* **451**, 937-942.

Seidman, C. (2000). Hypertrophic cardiomyopathy: from man to mouse. *Journal of Clinical Investigation* **106**, S9-S13.

Seidman, J. G. and Seidman, C. (2001). The genetic basis for cardiomyopathy: from mutation identification to mechanistic paradigms. *Cell* **104**, 557-567.

Sen, A., Dunnmon, P., Henderson, S. A., Gerard, R. D. and Chien, K. R. (1988). Terminally differentiated neonatal rat myocardial cells proliferate and maintain specific differentiated functions following expression of SV40 large T antigen. *The Journal of biological chemistry* **263**, 19132-19136.

Senyo, S. E., Lee, R. T. and Kuhn, B. (2014). Cardiac regeneration based on mechanisms of cardiomyocyte proliferation and differentiation. *Stem cell research* **13**, 532-541.

Senyo, S. E., Steinhauser, M. L., Pizzimenti, C. L., Yang, V. K., Cai, L., Wang, M., Wu, T. D., Guerquin-Kern, J. L., Lechene, C. P. and Lee, R. T. (2013). Mammalian heart renewal by pre-existing cardiomyocytes. *Nature* **493**, 433-436.

Sepulveda, J. L., Belaguli, N., Nigam, V., Chen, C. Y., Nemer, M. and Schwartz, R. J. (1998). GATA-4 and Nkx-2.5 coactivate Nkx-2 DNA binding targets: role for regulating early cardiac gene expression. *Molecular and cellular biology* **18**, 3405-3415.

Singh, N., Trivedi, C. M., Lu, M., Mullican, S. E., Lazar, M. A. and Epstein, J. A. (2011). Histone deacetylase 3 regulates smooth muscle differentiation in neural crest cells and development of the cardiac outflow tract. *Circulation research* **109**, 1240-1249.

Sohal, D. S., Nghiem, M., Crackower, M. A., Witt, S. A., Kimball, T. R., Tymitz, K. M., Penninger, J. M. and Molkentin, J. D. (2001). Temporally regulated and tissue-specific gene manipulations in the adult and embryonic heart using a tamoxifen-inducible Cre protein. *Circulation research* **89**, 20-25.

Sojka, S., Amin, N. M., Gibbs, D., Christine, K. S., Charpentier, M. S. and Conlon, F. L. (2014). Congenital heart disease protein 5 associates with CASZ1 to maintain myocardial tissue integrity. *Development* **141**, 3040-3049.

Song, K., Nam, Y. J., Luo, X., Qi, X., Tan, W., Huang, G. N., Acharya, A., Smith, C. L., Tallquist, M. D., Neilson, E. G. et al. (2012). Heart repair by reprogramming non-myocytes with cardiac transcription factors. *Nature* **485**, 599-604.

Soonpaa, M. H. and Field, L. J. (1997). Assessment of cardiomyocyte DNA synthesis in normal and injured adult mouse hearts. *The American journal of physiology* **272**, H220-226.

Soonpaa, M. H. and Field, L. J. (1998). Survey of studies examining mammalian cardiomyocyte DNA synthesis. *Circulation research* **83**, 15-26.

Soonpaa, M. H., Kim, K. K., Pajak, L., Franklin, M. and Field, L. J. (1996). Cardiomyocyte DNA synthesis and binucleation during murine development. *The American journal of physiology* **271**, H2183-2189.

Srivastava, D. (2006). Making or breaking the heart: from lineage determination to morphogenesis. *Cell* **126**, 1037-1048.

Srivastava, D. and Olson, E. N. (2000). A genetic blueprint for cardiac development. *Nature* **407**, 221-226.

Stennard, F. A. and Harvey, R. P. (2005). T-box transcription factors and their roles in regulatory hierarchies in the developing heart. *Development* **132**, 4897-4910.

Stennard, F. A., Costa, M. W., Lai, D., Biben, C., Furtado, M. B., Solloway, M. J., McCulley, D. J., Leimena, C., Preis, J. I., Dunwoodie, S. L. et al. (2005). Murine T-box transcription factor Tbx20 acts as a repressor during heart development, and is essential for adult heart integrity, function and adaptation. *Development* **132**, 2451-2462.

Takahashi, K. and Yamanaka, S. (2006). Induction of pluripotent stem cells from mouse embryonic and adult fibroblast cultures by defined factors. *Cell* **126**, 663-676.

Takahashi, K., Okita, K., Nakagawa, M. and Yamanaka, S. (2007a). Induction of pluripotent stem cells from fibroblast cultures. *Nature protocols* **2**, 3081-3089.

Takahashi, K., Tanabe, K., Ohnuki, M., Narita, M., Ichisaka, T., Tomoda, K. and Yamanaka, S. (2007b). Induction of pluripotent stem cells from adult human fibroblasts by defined factors. *Cell* **131**, 861-872.

Tam, P. P., Parameswaran, M., Kinder, S. J. and Weinberger, R. P. (1997). The allocation of epiblast cells to the embryonic heart and other mesodermal lineages: the role of ingression and tissue movement during gastrulation. *Development* **124**, 1631-1642.

Tzouanacou, E., Wegener, A., Wymeersch, F. J., Wilson, V. and Nicolas, J. F. (2009). Redefining the progression of lineage segregations during mammalian embryogenesis by clonal analysis. *Developmental cell* **17**, 365-376.

van den Berg, G., Abu-Issa, R., de Boer, B. A., Hutson, M. R., de Boer, P. A., Soufan, A. T., Ruijter, J. M., Kirby, M. L., van den Hoff, M. J. and Moorman, A. F. (2009). A caudal proliferating growth center contributes to both poles of the forming heart tube. *Circulation research* **104**, 179-188.

van der Linde, D., Konings, E. E., Slager, M. A., Witsenburg, M., Helbing, W. A., Takkenberg, J. J. and Roos-Hesselink, J. W. (2011). Birth prevalence of congenital heart disease worldwide: a systematic review and meta-analysis. *Journal of the American College of Cardiology* **58**, 2241-2247.

Vincent, S. D. and Buckingham, M. E. (2010). How to make a heart: the origin and regulation of cardiac progenitor cells. *Current topics in developmental biology* **90**, 1-41.

Vincentz, J. W., Barnes, R. M., Firulli, B. A., Conway, S. J. and Firulli, A. B. (2008). Cooperative interaction of Nkx2.5 and Mef2c transcription factors during heart development. *Developmental dynamics : an official publication of the American Association of Anatomists* **237**, 3809-3819.

von Gise, A. and Pu, W. T. (2012). Endocardial and epicardial epithelial to mesenchymal transitions in heart development and disease. *Circulation research* **110**, 1628-1645.

Walsh, S., Ponten, A., Fleischmann, B. K. and Jovinge, S. (2010). Cardiomyocyte cell cycle control and growth estimation in vivo--an analysis based on cardiomyocyte nuclei. *Cardiovascular research* **86**, 365-373.

Wang, L., Liu, Z., Yin, C., Asfour, H., Chen, O., Li, Y., Bursac, N., Liu, J. and Qian, L. (2015). Stoichiometry of Gata4, Mef2c, and Tbx5 influences the efficiency and quality of induced cardiac myocyte reprogramming. *Circulation research* **116**, 237-244.

Weinberg, R. A. (1995). The retinoblastoma protein and cell cycle control. *Cell* **81**, 323-330.

Wollert, K. C. and Drexler, H. (2010). Cell therapy for the treatment of coronary heart disease: a critical appraisal. *Nature reviews. Cardiology* **7**, 204-215.

Yamanaka, S. and Takahashi, K. (2006). [Induction of pluripotent stem cells from mouse fibroblast cultures]. *Tanpakushitsu kakusan koso. Protein, nucleic acid, enzyme* **51**, 2346-2351.

Yoshida, Y. and Yamanaka, S. (2011). iPS cells: a source of cardiac regeneration. *Journal of molecular and cellular cardiology* **50**, 327-332.

Appendix 1: CASZ1 Promotes Vascular Assembly and Morphogenesis Through the Direct Regulation of an EGFL7/RhoA-mediated Pathway[2]

INTRODUCTION

Endothelial cells (ECs) are building blocks for the formation of a functional vascular system during embryonic development. Early stages of blood vessel development occur via vasculogenesis whereby mesodermal cells differentiate into EC progenitors that subsequently proliferate, migrate, and assemble into vascular cords. Cords then undergo tubulogenesis, or lumen formation, continuing to mature by angiogenesis where vessels sprout, branch, and remodel. Vessels then become surrounded and stabilized by pericytes and smooth muscle cells that provide structural support (Patan, 2000; De Val, 2011). The critical nature of these events is emphasized by observations that disruption of these processes is associated with human disease states including cancer, stroke, and atherosclerosis, therefore necessitating a better understanding of transcriptional networks that regulate these key developmental steps (Carmeliet, 2003; Carmeliet and Jain, 2011; Potente et al., 2011).

While numerous transcription factors have been discovered to regulate endothelial gene expression, relatively few factors are necessary for development. Deletions or mutations of a number of single genes, especially members of Ets and

---

[2]This chapter previously appeared as an article in the journal *Developmental Cell*. The original citation is as follows: Charpentier, M.S.[#], Christine, K.S.[#], Amin, N.M., Dorr, K.M., Kushner, E.J., Bautch, V.L., Taylor, J.M., and Conlon, F.L. CASZ1 promotes vascular assembly and morphogenesis through the direct regulation of an EGFL7/RhoA-mediated pathway. *Dev Cell* 25, no.2 (April 2013): 132. [#]These authors contributed equally to this work.

forkhead families, result in moderate to no vascular phenotypes likely due to functional redundancy (Barton et al., 1998; Lelievre et al., 2001; De Val and Black, 2009; De Val, 2011). Previous studies have implicated the zinc finger transcription factor CASZ1 in cardiovascular development with depletion of CASZ1 in *Xenopus* embryos resulting in failure of a subset of progenitor cells to differentiate into cardiomyocytes (Christine and Conlon, 2008). Recent genome-wide association studies have shown a genetic link between human *Casz1* and high blood pressure and hypertension, suggesting a possible role for CASZ1 in EC biology (Levy et al., 2009; Takeuchi et al., 2010). However, no studies have addressed expression, function, or transcriptional targets of CASZ1 in vascular tissue.

Despite an essential role for the vasculature in development and disease, our knowledge of molecular mechanisms controlling these events remains incomplete (De Val and Black, 2009). One protein recently shown to play a role in EC morphogenesis is *Epidermal Growth Factor-Like Domain 7* (*Egfl7*), an extracellular matrix (ECM) protein expressed exclusively in EC progenitors and vessels during embryonic and neonatal development. EGFL7 is also expressed in highly vascularized adult organs and is upregulated upon injury (Fitch et al., 2004; Parker et al., 2004; Campagnolo et al., 2005). Depletion studies in zebrafish have defined a role for EGFL7 in tubulogenesis likely through modulation of cell-matrix interactions (Parker et al., 2004; Nikolic et al., 2010). In addition, overexpression of *Egfl7* in mouse results in abnormal patterning of embryonic and postnatal vasculature (Nichol et al., 2010). However, the specific function of EGFL7 has been complicated by recent discovery of microRNA miR-126, the only EC-specific microRNA, within intron 7 of the *Egfl7* locus. While *Egfl7* and miR-126

are co-expressed, the function of miR-126 has indicated a distinct role from its host gene in maintaining vessel integrity and modulating angiogenesis through repression of targets *Spred1* and *PIK3R2* (Fish et al., 2008; Kuhnert et al., 2008; Wang et al., 2008).

In this study, we demonstrate CASZ1 is required for angiogenic sprouting and lumen morphogenesis. CASZ1 regulates EC contractility, adhesion, and sprouting promoting assembly and tubulogenesis of blood vessels. Furthermore, we demonstrate CASZ1 activates *Egfl7*/miR-126 in mammals and *Xenopus* by directly binding to an intronic element but does not regulate miR-126 in *Xenopus*. Moreover, defects associated with CASZ1-depletion can be phenocopied by EGFL7-depletion, and importantly, rescued by restoration of *Egfl7* levels. We further show CASZ1 transcriptional control of EGFL7 modulates EC behavior through RhoA. Collectively, our studies point to a network whereby CASZ1 regulates an EGFL7/RhoA-mediated pathway to promote vessel assembly and morphogenesis.

MATERIALS AND METHODS

Xenopus Embryo Collection and Morpholino Design

Preparation and collection of *Xenopus* embryos was performed as described (Showell et al., 2006). Embryos were staged according to Nieuwkoop and Faber (Nieuwkoop and Faber, 1967). MOs were obtained from Gene Tools, LLC. *Casz1*-specific MOs used as reported (Christine and Conlon, 2008). *Egfl7*-specific MO designed against acceptor region of *X. laevis* exon 6 and miR-126-specific MO designed against guide dicer region of *X. laevis* (Supplemental information).

In Situ Hybridization

Whole mount *in situ* analysis was carried out as described (Harland, 1991) using probes of *Casz1* (Christine and Conlon, 2008), *Msr* (Devic, 1996), *Ami* (Inui and Asashima, 2006), *Erg* (cloned from st. 39 *X. laevis* cDNA), *Egfl7* (cloned from st. 33-38 *X. tropicalis* cDNA), and *EphrinB2* (cloned from st. 39 *X. laevis* cDNA). miR-126 locked nucleic acid probe from Exiqon (38523-05) and hybridization was performed according to manufacturer's instructions at 51°C.

Chromatin Immunoprecipitation (ChIP)

Four hundred cardiovascular-enriched regions were dissected from st. 29 *X. tropicalis* embryos and processed for ChIP as reported (Weinmann and Farnham, 2002) (Taranova et al., 2006) with following exceptions: (1)Sonication was carried out with Branson Digital Sonifier at 20% amplitude (2.5 cycles, 30s [1s on/0.5s off]) to yield 4kb DNA fragments. (Porrello et al.)Affinity-purified rabbit anti-CASZ1 polyclonal antibody was added and incubated overnight at 4°C. (Dowell and McManus)DNA was digested with *NlaIII* (NEB) and ligated into *SphI*-digested (NEB) pUC19 using DNA ligation kit (Stratagene). Ligated DNA was transformed into NEB10β electrocompetent cells. Transformants were selected by blue/white screening, cultured, and isolated plasmids were sequenced. CASZ1 target DNA sequences were assessed by BLAT analysis using UCSC *X. tropicalis* Genome Browser (http://genome.ucsc.edu, August 2005 assembly). DNA scaffold location coordinates were imported into the annotated Joint Genome Institute. v4.1 database (http://genome.jgi-psf.org/Xentr4/Xentr4.home.html). Validation of targets by ChIP PCR was performed as above with following exceptions:

(1)Thirty st. 32 *X. tropicalis* embryos were collected and processed as described. (Porrello et al.)Nuclear samples were sonicated at 20% amplitude (5 cycles, 30s [1s on/0.5s off]) to generate ~300bp DNA fragments.

In vivo Transcriptional Assays

Egfl7 intronic regions (introns 2,3,4,5) were subcloned into pGL3-Promoter firefly luciferase vector (Promega). *X. laevis* embryos were injected at 1-cell stage with 300 pg reporter plasmid and 10 pg Renilla reporter plasmid in presence or absence of CASZ1 mRNA. Injected embryos were cultured until st. 11.5. Ten injected embryos were lysed in 50 μl Passive Lysis Buffer (Promega) in triplicate. 20 μl of cleared lysates were assayed using Dual-Luciferase Reporter Assay System (Promega).

Cell Culture

Pooled population of HUVEC (Lonza) were maintained in Complete EBM-2 (Lonza) containing 10% fetal bovine serum, 100 U/mL penicillin and streptomycin and used between passages 1-6. hCASZ1 was IP'ed from HUVECs using polyclonal rabbit anti-human CASZ1 (LifeSpan Biosciences) and probed by western blot with same antibody.

shRNA

shRNA viral constructs specific to human *Casz1* and *Egfl7* were obtained from Open Biosystems TRC1 shRNA library. *Casz1, Egfl7,* and control scrambled sequence (Addgene) shRNA lentiviral particles were prepared by UNC Lentiviral Core Facility. 40-

50% confluent HUVECs were infected with $1x10^6$ IU lentivirus combined with 10 μg/mL polybrene (Sigma) for 7.5 hr. Infected cells were placed under 1.5 μg/mL puromycin selection for 3 days and processed for further analysis.

Live Time-Lapse Imaging

Cells seeded on uncoated or Fibronectin-coated (10 μg/mL) 12-well dishes, or embedded in fibrin gel were imaged over 24 hr using Olympus IX70 inverted microscope encased in Plexiglas housing to control internal environment (37°C, 5% CO_2 and relative humidity of 60%). Images were collected by Volocity 5.4.1 software.

Immunofluorescence

Cells seeded in chamber slides (BD Falcon) were fixed with cold methanol/acetone, blocked, and incubated with phospho-histone H3 (Millipore) or cleaved caspase-3 (Cell Signaling) overnight. Cells were incubated with rabbit anti-Cy3 (Sigma), stained with DAPI, and mounted (DakoCytomation). For cytoskeletal staining, cells were serum-starved (EBM-2+0.75% FBS) overnight, half of the cells were treated with 10μM Y-27632 (Sigma). Cells were fixed in 4% PFA, permeabilized with 0.1% Triton X-100, and incubated overnight with anti-vinculin (Sigma), and anti-phospho-paxillin (pY118, Invitrogen). Cells were incubated with fluorescent secondary antibodies, stained with FITC-conjugated phalloidin (Invitrogen) and DAPI, mounted and imaged (Zeiss 710 or 700 microscope).

Sprouting Angiogenesis Assay

Sprouting assays were performed as described (Nakatsu et al., 2003; Sweet et al., 2012). Cells were stained with phalloidin (FITC) to visualize actin and with DRAQ5 to mark EC nuclei, and imaged (Olympus FLV500 inverted confocal microscope, 20x objective). Assay quantified measuring total length of protruding sprouts and number of branch points.

Western Blotting

Western blots were performed with 50 μg protein using RhoA (Santa Cruz), phospho-myosin light chain 2 (Cell Signaling [Ser 19]), RhoC (Santa Cruz [K-12]).

Statistical Analysis

Data are expressed as means ± SEM as indicated. Statistical analysis was done by Student's *t*-test and $p<0.05$ was considered significant.

RESULTS

EC Expression of CASZ1 is Evolutionarily Conserved

Analysis of *Casz1* expression in *Xenopus* embryos showed transcripts in the vitelline vein network (vvn) at a stage when the network is primarily made up of vascular ECs and devoid of smooth muscle cells (Figure A1.1A) (Warkman et al., 2005; Cox et al., 2006; Christine and Conlon, 2008) suggesting *Casz1* is expressed in vascular ECs. Furthermore, RT-PCR on vascular explants from late tailbud stage embryos (stage 32)

demonstrated that *Casz1* is co-expressed in the vitelline vein region with vascular markers, *Msr* and *Erg* (Figure SA1.1A). Consistently, we found CASZ1 co-localizes with the EC-specific marker PECAM in blood vessels of mouse embryos (Figure A1.1B). We have also cloned human *Casz1* and showed, as in *Xenopus* and mouse, *Casz1* is expressed in primary human umbilical vein ECs (HUVEC)(Figures A1.1C and A1.1D). These results taken together with sequence homology and synteny of CASZ1 across vertebrates (Christine and Conlon, 2008) demonstrate CASZ1 is an evolutionarily conserved transcription factor expressed in ECs.

CASZ1 is Required for Vascular Patterning and Lumen Morphogenesis

To ascertain the function of CASZ1 in vascular development, we depleted CASZ1 in *Xenopus* embryos using a morpholino-based approach (Christine and Conlon, 2008). Whole-mount *in situ* hybridization using a panel of EC markers such as *Msr* and *Erg* (Devic, 1996; Baltzinger et al., 1999) demonstrated that at stages when ECs begin to migrate dorsally from ventral blood islands within the trunk region, there were no noticeable differences between control and CASZ1-depleted embryos (stage 29, Figures SA1.1B, SA1.1C, SA1.1J, SA1.1K). However, when ECs begin to assemble into cords (stage 32), defects became apparent whereby CASZ1-depleted embryos displayed a dramatically reduced vascular plexus (Figures A1.2A-2D, SA1.1D—SA1.1E). Extension of intersomitic vessels from posterior cardinal veins, which is known to occur in *Xenopus* via sprouting angiogenesis in an anterior-to-posterior direction (Cleaver et al., 1997; Levine et al., 2003), was also absent or significantly delayed in

CASZ1-depleted embryos (Figures A1.2A, 2C, 2E, 2G). By mid- to late tadpole stages (stages 36 and 39), vascular networks of CASZ1-depleted embryos were comprised of cords which ran predominately in a dorsal-to-ventral pattern and underwent little to no branching or remodeling (Figures A1.2E-2H, SA1.1F-SA1.1I, SA1.1L-SA1.1M). Overall, at stage 36, total length of the vitelline vein vasculature and number of branch points and intersomitic vessels were all significantly decreased in CASZ1-depleted embryos implying a role for CASZ1 in sprouting and remodeling of the vasculature (Figure A1.2I). While our studies focused on vein-derived sprouts, CASZ1-depletion unlikely disrupts arterial/venous differentiation due to proper specification and localization of the aortic arches (arterial) and posterior cardinal veins as well as due to the lack of arterial marker expression in veins (data not shown).

Noting the posterior cardinal veins of CASZ1-depleted embryos appeared thickened (stage 36), we sought to determine the time course of lumen formation in *Xenopus*. At stage 29, control and CASZ1-depleted ECs, as marked by *Msr*, were localized to positions of the future veins but had not yet undergone lumen formation (Figures A1.2J, 2N). By stage 32, ECs separated in control embryos but remained as aggregates in CASZ1-depleted embryos (Figures A1.2K, 2O). By stages 36 and 39, the veins of control embryos exhibited well-formed lumens surrounded by *Msr*-positive ECs while CASZ1-depleted veins remained closed and failed to open even at late stages (Figures A1.2L, 2M, 2P, 2Q). Collectively, these studies demonstrate CASZ1 is required for angiogenic remodeling and lumen morphogenesis during vertebrate vascular development.

Since we have previously established CASZ1 is required for heart development (Christine and Conlon, 2008), we determined if the vascular requirements for CASZ1 were secondary to its role in cardiac tissue. Taking advantage of the amenability of *Xenopus* embryos to organotypic culture (Mandel et al., 2010), we removed anterior regions of embryos, including all cardiac tissue at a stage prior to heart formation. Culture of explants showed in the absence of cardiac tissue, control explants formed vascular networks, as marked by the EC-specific gene *Ami* (Inui and Asashima, 2006), that were indistinguishable from un-manipulated embryos, demonstrating blood flow is not essential for correct patterning of the early vasculature (Figures SA1.1N, SA1.1P). Critically, we observed severe defects in vascular networks of CASZ1-depleted explants, strongly suggesting the role of CASZ1 in vascular development is independent of its role in cardiogenesis (Figures SA1.1O, SA1.1Q).

CASZ1 Regulates EC Behavior

To examine vascular development in more detail and determine if the function of CASZ1 is evolutionarily conserved, we depleted CASZ1 in HUVECs by lentiviral-mediated short hairpin RNA (shRNA, 16-fold decrease in *Casz1* mRNA; Figure A1.3A). CASZ1-depleted cells displayed a thin and elongated morphology in stark contrast to characteristic cobblestone appearance of uninfected HUVECs or HUVECs infected with control shRNA (Figure A1.3B).

To determine the precise requirement for CASZ1 and to characterize the dynamics of CASZ1-depleted HUVECs in real time, we coupled time-lapse imaging with

quantitative analysis. Time-lapse movies showed that CASZ1-depleted cells initially adhered to plastic or fibronectin-coated substrates but a proportion of cells rounded up and detached (33%, Figure A1.3C, Movie SA1.1, data not shown). Of CASZ1-depleted HUVECs that adhered, live imaging demonstrated the elongated morphology resulted from defects in contractility whereby the leading edge of CASZ1-depleted cells moved forward without retraction of the trailing edge (Figure A1.3C, Movie SA1.1). CASZ1-depleted cells also stopped dividing (0% shCasz1 vs. 20% control) and consistently, we failed to detect any phospho-histone H3 (pH3)-positive CASZ1-depleted cells (vs. 3% control cells; Figure SA1.2A). Using fluorescence-activated cell sorting (FACS), we determined CASZ1-depleted ECs were blocked at the G1/S transition as seen by the significantly reduced number of cells in S-phase (Figure SA1.2B). Blockage in G1/S progression was not associated with programmed cell death as determined by cleaved caspase-3 staining (Figure SA1.2C). Furthermore, inability of CASZ1-depleted cells to maintain adhesion to the substrate was not a secondary consequence of cell cycle arrest as wildtype HUVECs chemically treated with mitomycin C did not divide yet remained attached (data not shown). Taken together, these results indicate CASZ1 has a conserved role in vascular development and is required for EC adhesion, contractility, and G1/S cell cycle progression.

To assess how adhesive and morphological defects of CASZ1-depleted cells manifested themselves in vessel assembly, we assessed sprouting using a sprouting angiogenesis assay in which HUVEC-coated beads were placed in fibrin. While control cells displayed elongated sprouts with multiple branch points, similar to our findings in *Xenopus*, CASZ1-depleted HUVECs had strikingly few sprouts and branches (Figure

A1.3D). Live time-lapse imaging further showed that CASZ1-depleted cells extended out from beads to initiate sprout formation but then abruptly detached, indicating that CASZ1 is required for proper EC adhesion to promote angiogenic sprouting (Movie SA1.4).

Isolation of *Egfl7*/miR-126 Locus by CASZ1 Chromatin Immunoprecipitation

To identify direct cardiac and endothelial transcriptional targets of CASZ1, we generated a CASZ1-specific antibody and performed cloning chromatin immunoprecipitation (ChIP) from dissected cardiovascular *Xenopus* tissue (stages 27-29, i.e. same time and tissue requiring CASZ1)(Figure A1.4A). We identified 110 putative transcriptional targets including *Egfl7*, an ECM protein specifically secreted by ECs shown to be associated with similar cellular processes as we observe for CASZ1; EC adhesion and vessel tubulogenesis (Figure A1.4B, Table S1)(Parker et al., 2004; Nichol et al., 2010; Nikolic et al., 2010).

Recently, studies in mouse and zebrafish identified the evolutionarily conserved miR-126 contained within intron 7 of *Egfl7* (Fish et al., 2008; Kuhnert et al., 2008; Wang et al., 2008). We cloned *Egfl7* and miR-126 from *Xenopus* and showed EGFL7 is 47% identical to human and 45% identical to mouse EGFL7, while *Xenopus* miR-126 is completely (100%) conserved between mouse and human (Fitch et al., 2004)(Figure SA1.3A). Genome analysis and characterization of *Xenopus* BACs corresponding to the *Egfl7*/miR-126 locus confirmed that like other model systems, miR-126 is located within intron 7 of the *Xenopus Egfl7* locus (Figure A1.4B).

Expression analysis revealed *Egfl7* is expressed in all major vessels at all stages of vasculogenesis in *Xenopus*, as reported for zebrafish, mouse, and human (Figures 4C, 4E, 4G, 4I)(Fitch et al., 2004; Parker et al., 2004). Though *Egfl7* and miR-126 have been reported to be co-transcribed and co-expressed in the vasculature, we found *Xenopus* miR-126 has an expression pattern distinct from *Egfl7* as well as that reported in other species (Fish et al., 2008; Wang et al., 2008). Most notably, miR-126 expression is initiated in ECs at stage 32, slightly later than *Egfl7* (stage 29), and we observed strong expression of miR-126, but not *Egfl7*, in the developing somites (Figure SA1.3B-SA1.3I). Taken together these data show that the sequence, genomic arrangement, and vascular expression of *Egfl7* and miR-126 are evolutionarily conserved, however in *Xenopus,* miR-126 has developed additional levels of regulation distinct from *Egfl7*.

Consistent with *Egfl7* being a direct target of CASZ1, analysis in CASZ1-depleted embryos showed *Egfl7* was initiated but not maintained in vascular tissues at all stages analyzed (Figures A1.4D, 4F, 4H, 4J). Consistently, *Egfl7* levels were significantly reduced in CASZ1-depleted HUVEC (3-fold; Figure A1.4K). We further observed a dramatic reduction in miR-126 (9-fold) in CASZ1-depleted HUVECs (Figure A1.4K). These effects were specific as the EC marker *Flk1* was unaltered (Figure A1.4K). However, we did not observe reduction in miR-126 in CASZ1-depleted *Xenopus* embryos at mid- and late-tadpole stages (stages 32-39, Figures S3E, S3G, S3I). Collectively, these studies demonstrate regulation of *Egfl7* and miR-126 expression in human ECs is dependent on CASZ1 while *Xenopus* miR-126 appears to have evolved a CASZ1-independent mechanism of regulation.

Egfl7 is a Direct Transcriptional Target of CASZ1

To determine whether CASZ1 directly regulates *Egfl7*, we performed *in vivo* transcriptional assays where single copies of intronic regions of *Egfl7* corresponding to the putative CASZ1-bound region (introns 2-5) were placed upstream of a basal promoter driving luciferase activity. Of these intronic regions, only the 5' half of intron 3 (*E1*) resulted in a dose-dependent, reproducible increase in transcriptional activity in response to CASZ1 (Figures A1.4L-4M). To determine if CASZ1 endogenously binds to this element *in vivo* and to further refine the region within *E1*, we performed ChIP of endogenous CASZ1 from early embryos (stage 32), a time point when CASZ1 is required for *Egfl7* expression. Results showed CASZ1 binds to nucleotides 59-173 of intron 3 (*E1.2*) but not the most 5' end of *E1* (*E1.1*)(Figure A1.4N, data not shown). Thus, CASZ1 directly binds to the *Egfl7* locus *in vivo* and can activate *Egfl7* transcription through a regulatory element within intron 3 of the *Egfl7* locus.

EGFL7 Functions Downstream of CASZ1 to Control Vascular Morphogenesis

To determine if CASZ1 acts through EGFL7 to regulate EC development, we depleted *Egfl7* in embryos using a morpholino that left miR-126 expression intact (Figures SA1.4A-SA1.4E). Strikingly, EGFL7-depletion resulted in vascular phenotypes that phenocopied CASZ1-depletion (Figures A1.5A-5H, SA1.4F-SA1.4S). As with CASZ1-depleted embryos, we found a reduction in density of ECs within the vitelline vein network (stage 32)(Figures A1.5A-5D, SA1.4F-SA1.4G, SA1.4J-SA1.4M). Furthermore, while blood vessels did form in EGFL7-depleted embryos, there was

significantly reduced branching and intersomitic vessel sprouting at later stages (Figures A1.5E-5H, SA1.4H-SA1.41, SA1.4N-SA1.4Q). Quantification of vitelline vein networks at stage 36 revealed results similar to CASZ1-depletion whereby the total length of the vasculature and number of branch points and intersomitic vessels of EGFL7-depleted embryos was significantly decreased compared to controls (Figure A1.5I). Furthermore, like CASZ1-depleted embryos, and in accordance with reports of EGFL7-depletion in zebrafish (Parker et al., 2004), lumens of posterior cardinal veins of EGFL7-depleted embryos failed to form (Figures A1.5J-5M). Morpholinos targeting the Dicer cleavage site of *Xenopus* pri-miR-126 had no effect on *Egfl7* expression (Figures SA1.5A-SA1.5E) and did not result in gross defects in vessel morphology or patterning, in accordance with reports in zebrafish (Figures SA1.5F-SA1.5U)(Fish et al., 2008). Consistently, lumens of posterior cardinal veins of miR-126-depleted embryos were indistinguishable from controls (Figures SA1.5V-SA1.5Y). Taken together these results imply EGFL7 functions downstream of CASZ1 to regulate angiogenesis and vascular remodeling.

Similar to our studies in *Xenopus*, time-lapse imaging of HUVECs revealed depletion of EGFL7 by shRNA (shEgfl7, 11-fold decrease in mRNA; Figure A1.5N) phenocopied CASZ1-depletion. Most notably, EGFL7-depleted cells demonstrated similar adhesion and proliferation defects as those of CASZ1-depleted cells (Figure A1.5O, Movie SA1.2) and also displayed an elongated morphology similar to but not as extensive as observed in CASZ1-depleted cells. The sprouting angiogenesis assay further demonstrated similar defects to CASZ1-depleted cells whereby the total length of sprouts and number of branch points were significantly decreased in EGFL7-depleted

cells compared to controls (Figure A1.5P). Live imaging showed failure to sprout was due to the inability of EGFL7-depleted cells to maintain adhesion (Movie SA1.5). Results were specific since we observed minimal effect on expression of *Casz1* or *Flk1* (Figure A1.5N). Collectively, these studies show *Egfl7* functions downstream of CASZ1 to control vascular morphogenesis in *Xenopus* and humans. In addition, miR-126 does not function downstream of CASZ1 in *Xenopus* vascular development.

Egfl7 and miR-126 Function Downstream of CASZ1 to Regulate Cell Adhesion and Shape

To test if CASZ1 functions through *Egfl7* or miR-126 to regulate vascular development and morphogenesis in human ECs, we assessed if restoration of *Egfl7* or miR-126 levels rescues defects associated with CASZ1-depletion. While 29% of cells infected with shCasz1 rounded up and detached compared to 3% of control cells, infection of CASZ1-depleted cells with adenoviral constructs expressing either human *Egfl7* (Ad-Egfl7) or miR-126 (Ad-miR-126) recovered proper adhesion as only 7.6% and 1% of cells detached, respectively (Figures A1.6A, SA1.6A-SA1.6B, Movie SA1.3). However, restoration of *Egfl7,* but not miR-126, partially rescued EC morphology associated with CASZ1-depletion as measured by length-to-width ratio (L:W)(Figures A1.6B, SA1.6C). Restoration of either *Egfl7* or miR-126 failed to rescue proliferation defects (data not shown). Taken together, these studies demonstrate that CASZ1 acts to control EC adhesion through direct transcriptional regulation of *Egfl7* and miR-126. These data further indicate EGFL7 and miR-126 have distinct functions in regards to

cell morphology since EGFL7 but not miR-126 can rescue cell shape changes, and further imply CASZ1 control of G1/S progression occurs by *Egfl7*- and miR-126-independent pathways.

CASZ1 and EGFL7 Regulate RhoA

Past studies have provided evidence that two of the physiological outputs of the CASZ1/EGFL7 pathway, cell adhesion and morphology, are directly controlled by activation of Rho GTPases. Specifically, RhoA is required for actomyosin-dependent cell contractility and formation of focal adhesions (FA)(Burridge and Wennerberg, 2004; Parsons et al., 2010; Katoh et al., 2011). To identify mechanisms that mediate the physiological function of the CASZ1/EGFL7 pathway, we aimed to determine the relationship between CASZ1/EGFL7 and RhoA. We found RhoA activity and levels were dramatically diminished in CASZ1 and EGFL7-depleted cells, however, levels of other Rho proteins such as RhoC were unaltered (Figure A1.6C, SA1.6D-SA1.6E). The decrease in RhoA protein occurred at the transcriptional level as RhoA but not RhoC mRNA levels were markedly diminished in both CASZ1 and EGFL7-depleted ECs (Figure A1.6D). However, RhoB levels were slightly increased possibly indicating a compensatory mechanism for loss of RhoA (Figure A1.6D).

We reasoned reduction of RhoA expression in CASZ1- and EGFL7-depleted cells would result in concomitant impaired downstream activity. Consistently, phosphorylation of regulatory subunit of myosin light chain (p-MLC) was decreased in CASZ1-depleted cells (Figure SA1.6F). To further assess whether decreased RhoA

activity directly plays a role in the adhesion and cell shape defects we observe in CASZ1-depleted cells, we analyzed a panel of cytoskeletal and FA markers. Control cells displayed discrete bundles of F-actin stress fibers, as assayed by phalloidin staining, that contained short or punctate bands of FA markers vinculin and phosphorylated paxillin (Figure 6E, left panels). However, CASZ1-depletion mimicked treatment with the Rho kinase (ROCK) inhibitor Y-27632 resulting in diffuse actin networks devoid of stress fibers and failure of vinculin and phosphorylated paxillin to properly localize to adhesion sites on the periphery of the cell (Figure A1.6E, middle panels)(Narumiya et al., 2000). This phenotype was partially rescued by restoration of *Egfl7* levels in CASZ1-depleted cells (Figure A1.6E, right panels). Taken together these studies show CASZ1 acts through the direct transcriptional regulation of EGFL7 to control EC adhesion and shape via the RhoA pathway.

DISCUSSION

In this work we demonstrate an essential and conserved role for the CASZ1/EGFL7/RhoA pathway in vascular patterning. Collectively, these data support a mechanism whereby CASZ1 directly binds to and maintains expression of *Egfl7* in ECs. EGFL7 is then localized extracellularly where it modulates signals between ECs and the underlying ECM. This in turn is responsible for transcriptional upregulation and activity of the RhoA GTPase which ultimately mediates EC contractility and adhesive properties to promote assembly, lumen formation, and functionality of the vasculature (Figure A1.7).

CASZ1 Regulates EC Behavior Via EGFL7/RhoA to Promote Assembly of a Well-Branched Vascular Network

During embryogenesis, ECs assemble into cord-like structures that undergo further remodeling to form the primary vascular plexus. We have shown CASZ1 acts through the direct transcriptional regulation of EGFL7 to promote two critical processes during this period of embryogenesis: sprouting angiogenesis and lumen morphogenesis. The presence of thickened cords lacking lumens in CASZ1-depleted embryos, together with the observation that CASZ1-depleted ECs fail to sprout properly or adhere to extracellular substrates, strongly implies that CASZ1 functions through the EGFL7/RhoA pathway to maintain proper EC adhesion during vessel assembly.

Casz1 and RhoA

RhoA has been shown to be a central component of pathways which facilitate vascular remodeling. In this regard, RhoA has been demonstrated to be required for stress fiber formation, acting through the actomyosin contractile machinery, and for FA formation (Nobes and Hall, 1995; Chrzanowska-Wodnicka and Burridge, 1996; Burridge and Wennerberg, 2004; Katoh et al., 2011). In accordance with CASZ1 acting through RhoA to promote proper EC adhesion, we find that depleting CASZ1 phenocopies inhibition of RhoA and leads to a lack of discrete stress fibers, decreased myosin II activity, and strikingly, the absence of FA markers at sites of substrate contact. Moreover, these alterations in EC adherence can all be rescued in a CASZ1-depleted background by restoration of *Egfl7*.

The role of RhoA in tubulogenesis has been controversial. While reports have demonstrated RhoA activity is central for lumen formation, for example in the formation of the mouse dorsal aorta (Strilic et al., 2009), other reports have shown that in culture RhoA is not required for lumen formation but rather, for maintenance of patent vessels (Bayless and Davis, 2002). However, the *in vivo* relevance of the latter observation is yet to be determined since the mechanism by which lumens arise in 3D collagen culture differs significantly from that of cord hollowing *in vivo* (Davis et al., 2007; Strilic et al., 2009). Paradoxically, it has been recently demonstrated RhoA and myosin II activity must be suppressed to promote lumen formation of mouse vessels via negative regulation by Ras interacting protein 1 (RASIP1) (Xu et al., 2011). Collectively these studies along with our present findings imply that a precise level of RhoA activity is required for lumen formation with either too low or too high activity leading to failure of vascular cords to hollow and form lumens.

The finding that RhoA protein and mRNA expression are significantly diminished in CASZ1 and EGFL7-depleted HUVECs indicates transcriptional control of RhoA is impaired. Very few studies to date have focused on how RhoA transcription is controlled. While EGFL7 has been shown to interact with lysyl oxidases responsible for vascular elastogenesis as well as some Notch receptors on both ECs and neural stem cells, it is still unclear how these interactions may be influencing RhoA transcription or activity (Lelievre et al., 2008; Schmidt et al., 2009; Nichol et al., 2010). However, our results would support a mechanism by which CASZ1 modulates RhoA signaling through EGFL7 as restoration of *Egfl7* levels in CASZ1-depleted cells rescues adhesion, proper FA marker localization, and stress fiber formation. It was recently shown that RhoA is

directly activated by the Myc-Skp2-Miz1-p300 transcriptional complex (Chan et al., 2010). Given a role for c-Myc in embryonic vascular development and later angiogenic remodeling (Baudino et al., 2002; Rodrigues et al., 2008; Kokai et al., 2009), it will be interesting to investigate whether CASZ1 transcriptional regulation of *Egfl7* directly plays into Myc-mediated transcriptional control of RhoA.

Transcriptional Regulation of *Egfl7* and miR-126

Studies on *Egfl7* and miR-126 have identified a 5.4Kb upstream sequence that is sufficient to drive EC-specific expression of a reporter gene in mouse, and mutation of two evolutionarily conserved Ets binding sites within this element eliminated expression in culture (Wang et al., 2008). We have demonstrated CASZ1 is required for expression of *Egfl7* where CASZ1 is endogenously bound to intron 3 of the *Egfl7* locus in developing embryos and depletion of EGFL7 phenocopies CASZ1-depletion in embryos and HUVEC. Consistently, we note CASZ1 is not required for onset of *Egfl7* expression in embryos but rather its maintenance. Based on our studies, we favor a model by which Ets factors activate *Egfl7* via an upstream element and CASZ1 binds to intron 3 and functions to maintain *Egfl7* levels. This model is complementary to findings for the role of Ets factors in regulating the spatial pattern of *Egfl7* in mouse (Wang et al., 2008).

Our finding that EGFL7 and miR-126 are both regulated in a CASZ1-dependent manner in humans is congruent with reports in mouse. However, despite complete conservation of miR-126 across species, we also demonstrate miR-126 has undergone an evolutionarily divergent and unique means of regulation exemplified by our findings

that *Xenopus* miR-126 is expressed in domains mutually exclusive to *Egfl7* (i.e. somites) and expression of *Xenopus* miR-126 in the vasculature is CASZ1-independent. These observations are broadly consistent with recent reports that miR-126 transcription can occur independently of host gene transcription through differential intronic promoters (Monteys et al., 2010).

Conclusions

The vascular system arises via concerted efforts of individual ECs to harness their unique behaviors to assemble into tubular structures. The molecular and cellular mechanisms by which the vasculature arises are still unclear but we have identified previously unknown roles for CASZ1 in regulating sprouting and morphogenesis. While endothelium becomes stabilized and quiescent after embryonic development, vessels retain sensitivity to changes in environment due to injury, inflammation, or improper cardiac output thus making them susceptible to vascular dysfunction. In this regard, it is interesting that human CASZ1 has been linked to adult vascular diseases such as hypertension (Takeuchi et al., 2010). Events resulting in vascular dysfunction during this disease are associated with aberrant ECM remodeling, proliferation, and adhesion, all of which we have demonstrated to also be dysregulated upon depletion of CASZ1 (Lemarie et al., 2010). Therefore it will be intriguing to examine mechanisms by which CASZ1 itself is regulated and identify additional transcriptional targets that could trigger development of innovative therapeutic strategies in cardiovascular disease.

Figure A1.1. CASZ1 Expression in Vascular ECs is Evolutionarily Conserved

(A) *In situ* analysis of *Casz1 Xenopus* embryos (stage 41). Lateral view with anterior to left. *Casz1* is expressed in vascular structures including vitelline vein network (vvn, enlarged panel on right). (B) CASZ1 co-localizes with PECAM (red) in neural blood vessels of E14.5 mouse embryos. (C) RT-PCR analysis of human *Casz1* in HUVEC cDNA. *Gapdh* was used as loading control. (D) Immunoprecipitation (IP) of CASZ1 from HUVECs. Control lane (left) represents IP with no antibody (Ab). Arrowhead represents 125kD human CASZ1.

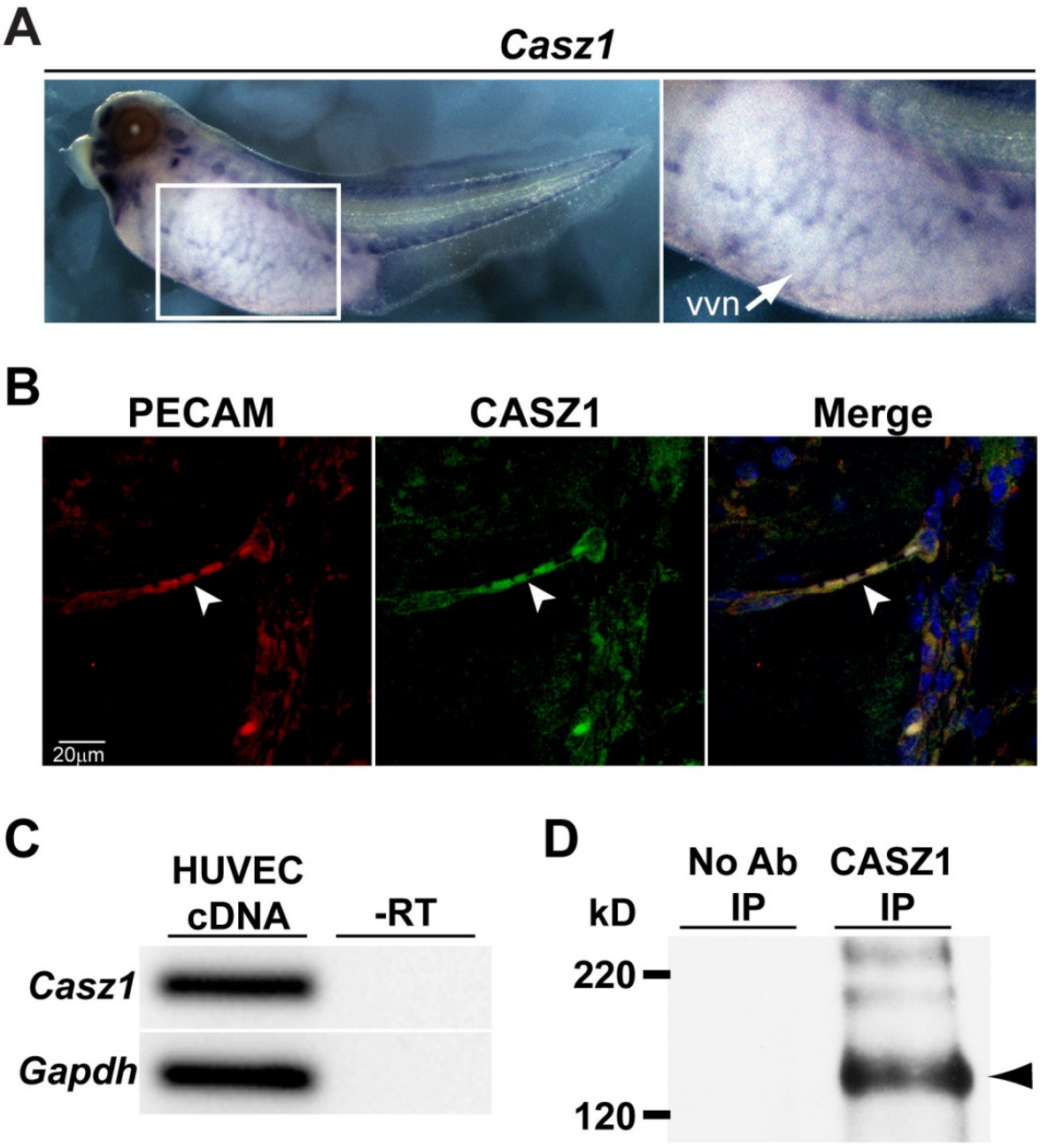
A
Casz1
vvn
B
PECAM
CASZ1
Merge
20μm
C
HUVEC cDNA
-RT
Casz1
Gapdh
D
kD
No Ab IP
CASZ1 IP
220
120

Figure A1.2. CASZ1 is Required for Vascular Development and Lumen Formation

In situ analysis with EC marker *Msr* control and CASZ1-depleted embryos (stages 32-36; lateral view with anterior to left). Vessel patterning and branching within vitelline vein network (vvn) are severely compromised at stage 32 in CASZ1-depleted embryos (A,C high magnification of vvn in B,D) and stage 36 (E,G high magnification of vvn in F,H). Note poor sprouting of intersomitic vessels (isv) in CASZ1-depleted embryos at both stages (enlarged box in A,C,E,G). (*n*=10 embryos/condition/stage, 3 independent experiments). (I) Quantification of vascular defects in control and CASZ1-depleted embryos (stage 36) representing combined total length of vessels, number of branch points within vvn, and number of isvs/embryo, respectively. Data represent mean ± SEM. (*n*=7 control and 10 Casz1 MO embryos). *: $p<0.05$; **:$p<0.01$; ***:$p<0.001$. (J-Q) Histological analysis illustrates time course of lumen formation in *Xenopus* from stages 29-39 (J-M). Note posterior cardinal vein (pcv) lumens begin to open between stages 32 and 36 in control embryos (K,L) but fail to form in CASZ1-depleted embryos (N-Q). Dorsal is top, ventral is bottom. Arrowheads correspond to positions of pcv which are enlarged in lower panels (*n*=2-5 embryos/ condition/stage). See also Figure S1.

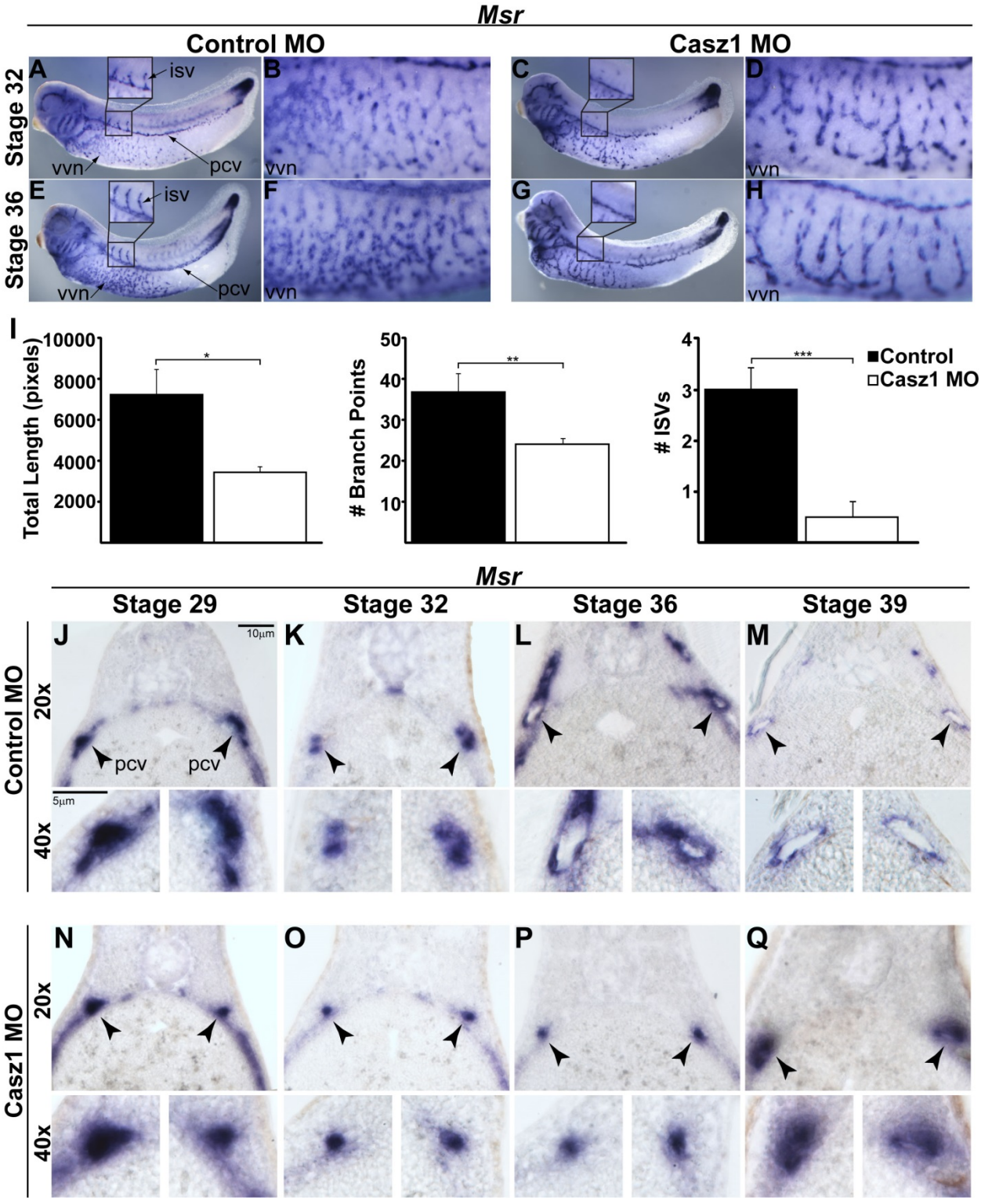
Msr
Control MO
Casz1 MO
Stage 32
Stage 36
A
B
C
D
E
F
G
H
isv
vvn
pcv
I
Total Length (pixels)
Branch Points
ISVs
Control
Casz1 MO
Msr
Stage 29
Stage 32
Stage 36
Stage 39
Control MO
Casz1 MO
20x
40x
J
K
L
M
N
O
P
Q
10μm
5μm

Figure A1.3. CASZ1 Regulates EC Behavior

(A) mRNA levels of *Casz1* after infection of HUVECs with shCasz1. *Casz1* is decreased by 16-fold. mRNA levels relative to *Rps29* ± SEM. ***: p<0.001. (B) Phase contrast images of control and shCasz1 HUVECs. Controls display cobblestone-like morphology while CASZ1-depleted cells are thin and elongated (red arrowheads for examples of each). (C) Time-lapse images of control and shCasz1 cells. Red arrowheads represent dividing control cell and rounded up CASZ1-depleted cell. Minutes elapsed presented at bottom right, taken every 5 min for 24 hr. Red arrow refers to elongated shCasz1 cell with trailing edge defects. Graph represents quantification of cells that round up and detach during imaging. Data represent mean ± SEM of 3 experiments conducted on independent batches of shRNA-infected cells (*n*=200 cells). **:p<0.01. (D) Sprouting angiogenesis assay was performed with control and CASZ1-depleted HUVEC. On day 6, cultures were fixed and stained for phalloidin and DRAQ5 (blue). Graphs represent mean ± SEM of total sprout length and number of branch points/bead (*n*=11 beads/condition). Experiments were repeated twice on independent batches of shRNA-infected cells. **:p<0.01; ***p<0.001. See also Figure S2, Movies SA1.1 and SA1.4.

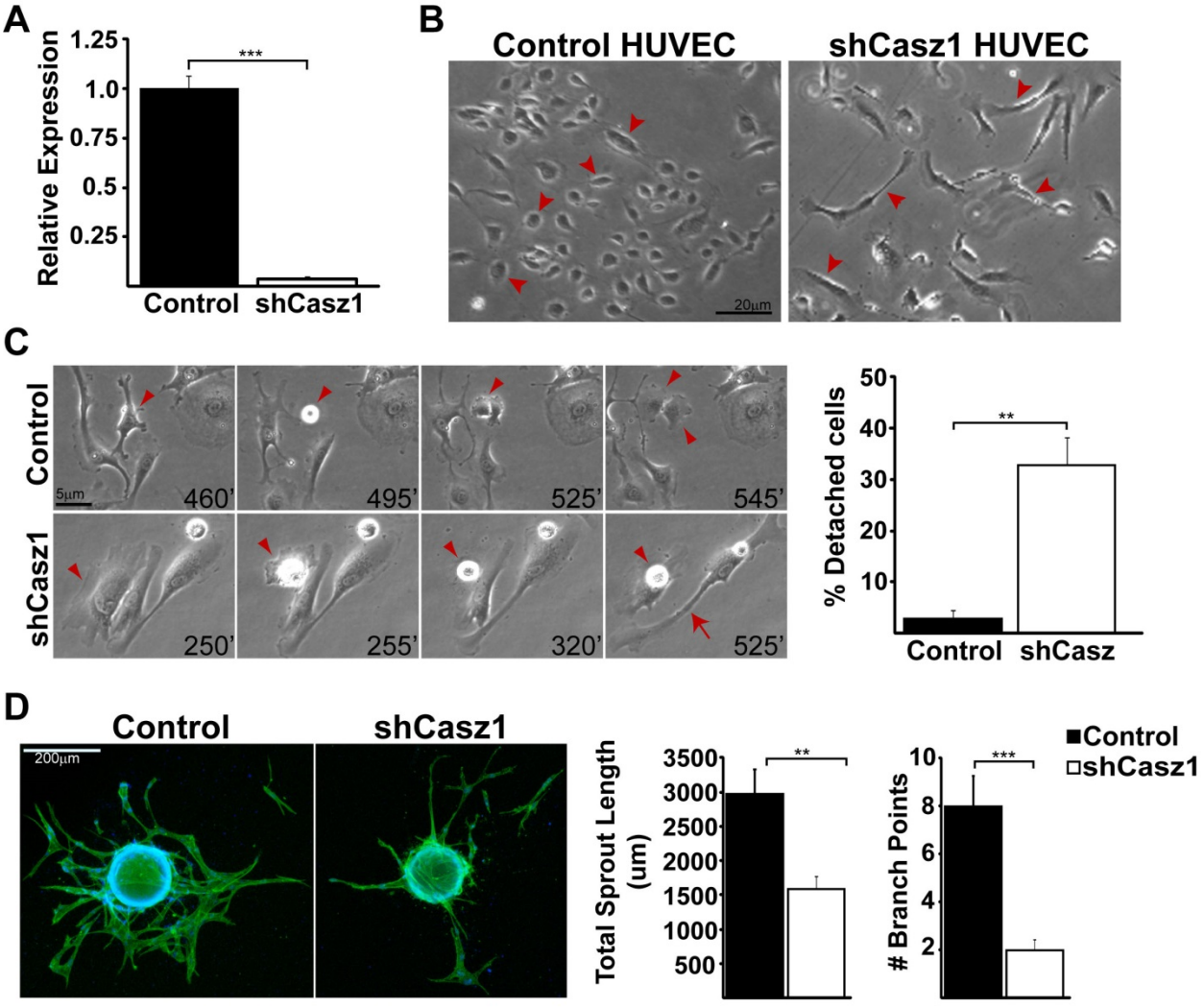
A
Relative Expression
1.25
1.0
0.75
0.5
0.25
***
Control
shCasz1
B
Control HUVEC
shCasz1 HUVEC
20μm
C
Control
shCasz1
5μm
460'
495'
525'
545'
250'
255'
320'
525'
% Detached cells
50
40
30
20
10
**
Control
shCasz
D
Control
shCasz1
200μm
Total Sprout Length (um)
3500
3000
2500
2000
1500
1000
500
**
Branch Points
10
8
6
4
2
***
Control
shCasz1

Figure A1.4. CASZ1 Directly Activates *Egfl7* Transcription

(A) Illustration of cardiovascular-enriched region dissected from *X. tropicalis* for chromatin immunoprecipitation (ChIP). (B) Genomic structure of *Xenopus Egfl7* locus denoting CASZ1 ChIP fragment. White boxes: exons; shaded boxes, miR-126 in intron 7 and intronic region potentially containing CASZ1 element (+/- 4kb). (C-J) *In situ* analysis of *Egfl7* of stages 29-39 control and CASZ1-depleted embryos (lateral view with anterior to left). Note downregulation of *Egfl7* in vitelline vein network (vvn) and intersomitic vessels (isv) in CASZ1-depleted embryos. Pcv-posterior cardinal vein. (K) Relative mRNA expression of *Egfl7*, miR-126, and *Flk1* after infection of HUVECs with shCasz1. mRNA levels relative to *Rps29* ± SEM. ***:p<0.001; NS: not significant. (L) Schematic demarcating *Egfl7* genomic DNA regions (in bp) tested for transcriptional activation. *E1* (-55–1614) within intron 3 but not *E2* (1773–3840) resulted in increased luciferase (Ying et al.) activity. (M) *Egfl7* genomic region *E1* in presence or absence of *Casz1*. Bars represent fold increase in activity relative to control ± SEM. Experiments were repeated twice on independent batches of embryos, **:p<0.01. (N) Identification of 90bp region endogenously bound by CASZ1located within non-overlapping region of *E1.2* (113-227) PCR amplicon. See also Figure S3.

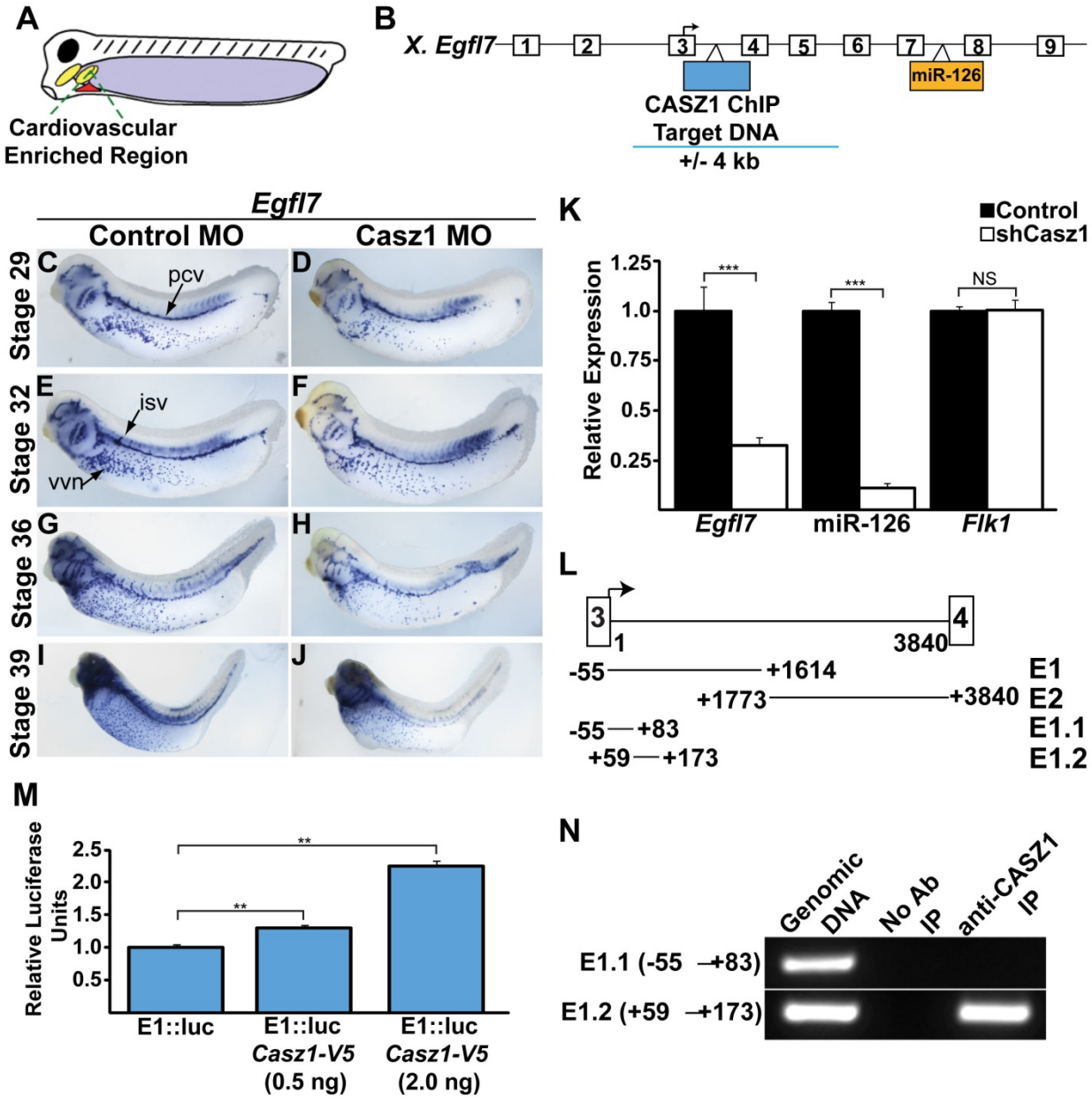
A
Cardiovascular
Enriched Region
B
X. Egfl7
1
2
3
4
5
6
7
8
9
miR-126
CASZ1 ChIP
Target DNA
+/- 4 kb
Egfl7
Control MO
Casz1 MO
Stage 29
Stage 32
Stage 36
Stage 39
C
D
E
F
G
H
I
J
pcv
isv
vvn
K
Control
shCasz1
Relative Expression
1.25
1.0
0.75
0.5
0.25
***
***
NS
Egfl7
miR-126
Flk1
L
3
4
1
3840
-55
+1614
+1773
+3840
E1
E2
-55
+83
E1.1
+59
+173
E1.2
M
Relative Luciferase Units
2.5
2.0
1.5
1.0
0.5
**
**
E1::luc
E1::luc
Casz1-V5
(0.5 ng)
E1::luc
Casz1-V5
(2.0 ng)
N
Genomic DNA
No Ab IP
anti-CASZ1 IP
E1.1 (-55 →+83)
E1.2 (+59 →+173)

Figure A1.5. EGFL7-Depletion in Embryos and HUVECs Phenocopies CASZ1-Depletion

In situ analysis with EC marker *Msr* control and EGFL7-depleted embryos (stages 32-36, lateral view with anterior to left). Note lack of branching in vitelline vein network (vvn) at stage 32 (A,C high magnification of vvn in B,D) and stage 36 (E,G high magnification of vvn in F,H). Intersomitic vessel (isv) sprouting is also impaired (A,C,E,G). (*n*=10 embryos/condition/stage, 3 independent experiments). (I) Quantification of vascular defects control and EGFL7-depleted embryos (stage 36) representing total vessel length, number of branch points within vvn, and number of isvs/embryo. Data represent mean ± SEM. (*n*=7 control and 10 Egfl7 MO embryos). *: $p<0.05$; **:$p<0.01$; ****:$p<0.0005$. (J-M) Histological analysis reveals lumenless posterior cardinal veins (pcv) in stage 36 (K) and stage 39 (M) Control and EGFL7-depleted embryos (J,L), dorsal top, ventral bottom, arrowheads correspond to pcv positions enlarged in lower panels (*n*=3 embryos/condition/stage). (N) mRNA expression of *Egfl7,* miR-126, *Casz1, and Flk1* after infection of HUVECs with shEgfl7. *Egfl7* is decreased 11-fold. mRNA levels relative to *Rps29* ± SEM. ***:$p<0.001$; NS: not significant. (O) Quantification of cells that round up and detach during imaging. Data represent mean ± SEM of 2 experiments conducted on independent batches of shRNA-infected cells. (*n*=100 cells). **:$p<0.01$. (P) Sprouting angiogenesis assay was performed with control and EGFL7-depleted HUVEC. On day 6, cultures were fixed and stained for phalloidin and DRAQ5 (blue). Graphs represent mean ± SEM of total sprout length and number of branch points/bead (*n*=11 beads/condition). Experiments were repeated twice on

independent batches of shRNA-infected cells. **:p<0.01; ***p<0.001. See also Figures S4-S5 and Movies SA1.2 and SA1.5.

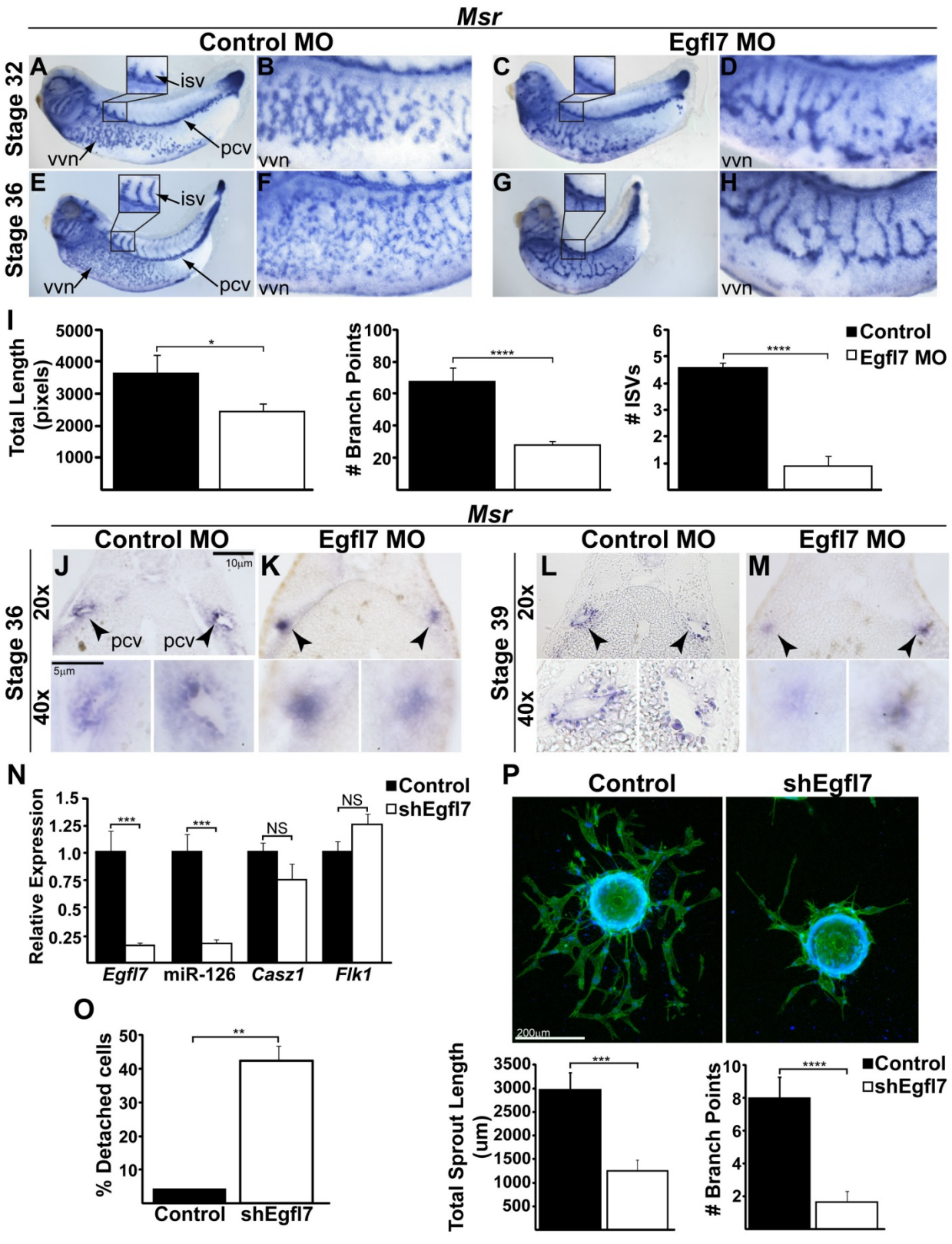
Msr
Control MO
Egfl7 MO
Stage 32
Stage 36
A
B
C
D
E
F
G
H
isv
pcv
vvn
I
Total Length (pixels)
Branch Points
ISVs
Control
Egfl7 MO
Msr
Stage 36
Stage 39
20x
40x
J
K
L
M
10μm
5μm
N
Relative Expression
Egfl7
miR-126
Casz1
Flk1
NS
O
% Detached cells
P
shEgfl7
200μm
Total Sprout Length (um)

Figure A1.6. EGFL7 and miR-126 Play Distinct Roles Downstream of CASZ1

(A) Quantification of cells co-infected with shCasz1 and Ad-Egfl7 or Ad-miR-126 that round up and detach versus shCasz1 or control shRNA alone. Data represent mean ± SEM of 2 average experiments conducted on independent batches of shRNA-infected cells. (*n*=100 cells). **:p<0.01; ****:p<0.0005. (B) Quantification of cell morphology determined by measuring length-to-width (L:W) ratio. Morphology was improved in cells co-infected with shCasz1 and Ad-Egfl7 but not in cells co-infected with Ad-miR-126. Data represent mean ± SEM of 3 experiments conducted on independent batches of shRNA-infected cells. (*n*=300-600 cells). **:p<0.01; ****:p<0.0005. (C) RhoA protein expression in shRNA-infected HUVECs. RhoA levels were markedly decreased by depletion of CASZ1 and EGFL7. Graph of densitometry of RhoA levels relative to GAPDH. (D) Relative *RhoA*, *RhoB*, and *RhoC* mRNA expression after shRNA infection. mRNA levels relative to *Rps29* ± SEM. *:p<0.05; ***:p<0.001; NS: not significant. (E) Stress fibers and FAs disrupted in CASZ1-depleted HUVECs resemble cells treated with ROCK inhibitor Y-27632 (10μM). Restoration of *Egfl7* in CASZ1-depleted cells rescues proper FA localization. Phalloidin marks F-actin filaments, vinculin (red) and phosphorylated paxillin (yellow) mark FAs. See also Figure S6 and Movie SA1.3.

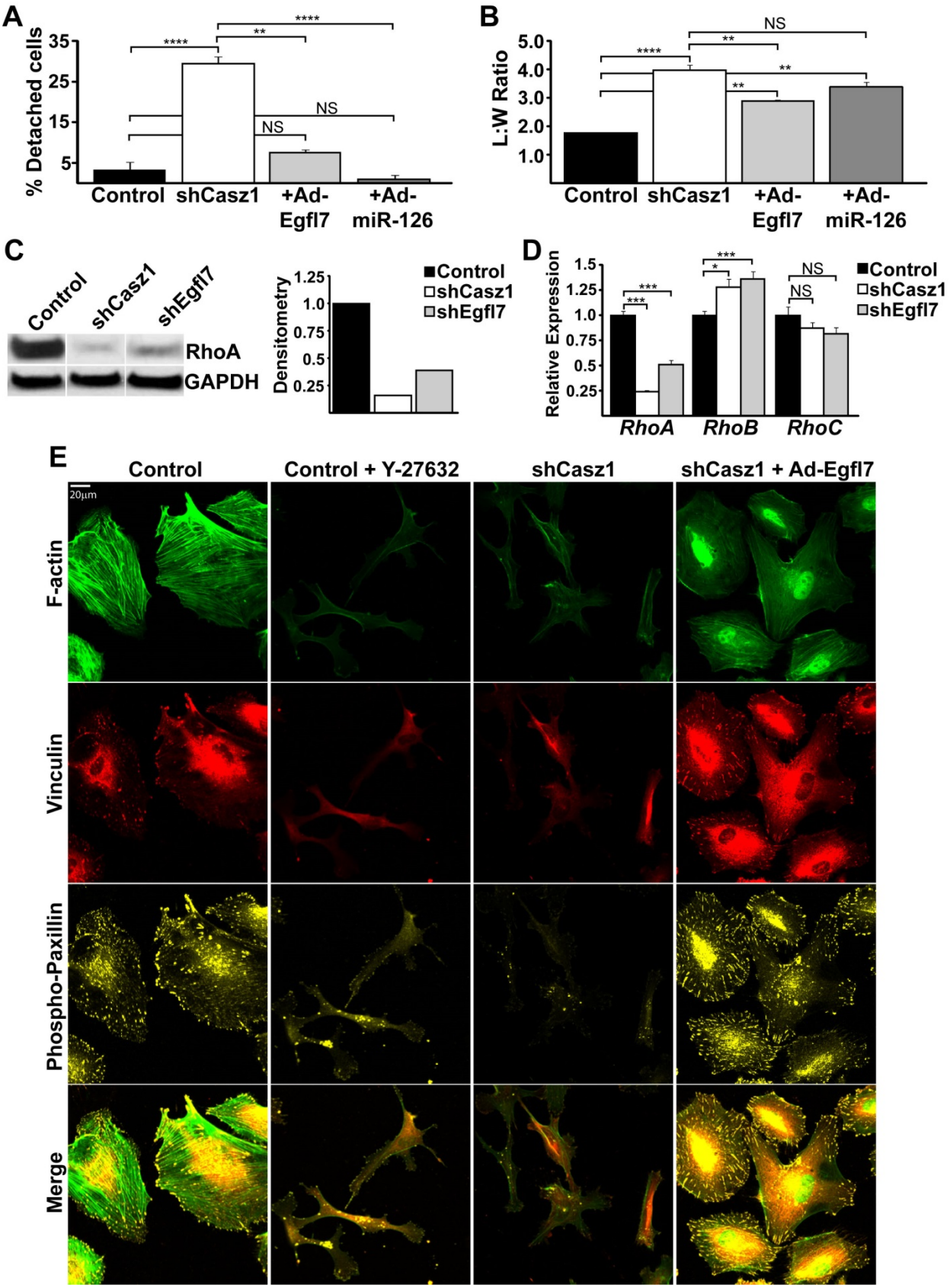
A
% Detached cells
35
25
15
5
****
**
****
NS
NS
Control
shCasz1
+Ad-Egfl7
+Ad-miR-126
B
L:W Ratio
5.0
4.0
3.0
2.0
1.0
NS
**
****
**
**
Control
shCasz1
+Ad-Egfl7
+Ad-miR-126
C
Control
shCasz1
shEgfl7
RhoA
GAPDH
Densitometry
1.25
1.0
0.75
0.5
0.25
Control
shCasz1
shEgfl7
D
Relative Expression
1.5
1.25
1.0
0.75
0.5
0.25
***
***
*
***
NS
NS
Control
shCasz1
shEgfl7
RhoA
RhoB
RhoC
E
Control
Control + Y-27632
shCasz1
shCasz1 + Ad-Egfl7
20μm
F-actin
Vinculin
Phospho-Paxillin
Merge

Figure A1.7. A model describing CASZ1 function in endothelial cells

CASZ1 functions by binding to an intronic element within the Egfl7 locus to activate proper levels of Egfl7 in endothelial cells. EGFL7 is then secreted to the extracellular matrix (ECM) where it likely binds cell-surface receptors which signal downstream to activate RhoA expression. Consequently, RhoA signaling modulates endothelial cell behaviors such as adhesion and contractility to promote vessel assembly and morphogenesis.

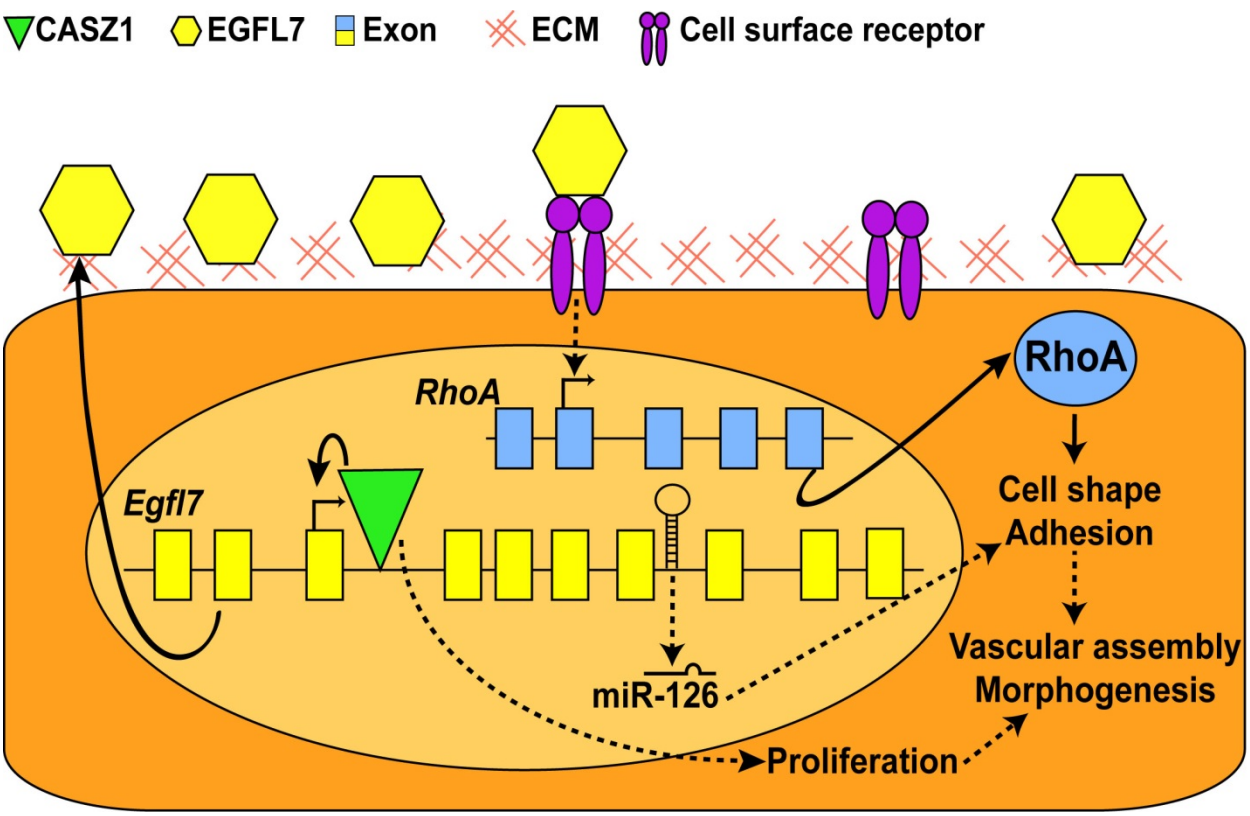

Supplemental Figure A1.1. CASZ1 is Required for Vascular Development

(A) Vascular explants excluding the head, heart, and somitic region were dissected from stage 32 embryos for RNA isolation and cDNA synthesis. RT-PCR showed that *Casz1* is co-expressed in this region with other vascular markers, *Msr* and *Erg*. *Eomesodermin* (*Eomes*), a marker of the forebrain and primitive mesendoderm, was a negative control while *Ef1*α was a loading control. (B-I) Whole-mount *in situ* analysis with EC marker *Erg* of stages 29-39 control and CASZ1-depleted embryos (lateral view with anterior to left). *Erg* was a secondary marker used to confirm vascular defects were not specific to *Msr.* Vessel branching and patterning were severely compromised in CASZ1-depleted embryos. Note lack of branching within vitelline vein network (vvn) as well as reduced sprouting of intersomitic vessels (isv). Posterior cardinal vein (pcv). (*n*=10 embryos/condition/stage, 3 independent experiments). (J-M) Whole-mount in situ analysis with EC marker *Msr* of stage 29 and 39 control and CASZ1-depleted embryos. (*n*=10 embryos/condition/stage, 3 independent experiments). (N-Q) The anterior-most region including the cardiac portion was dissected from early tailbud stage 29 control and CASZ1-depleted embryos prior to heart tube formation and therefore circulation. Explants were cultured until early tadpole stage 36 when the embryo has an established circulation and assayed by *in situ* hybridization with the endothelial marker *Ami*. (N,P) In the absence of functional circulation, control explants form a dense grossly normal vascular network similar to un-manipulated embryos (lateral view with anterior to the left). (O,Q) In the absence of CASZ1-depleted cardiac tissue and circulation, we observe an identical vascular phenotype in the trunk explants as we do in the un-

manipulated embryo indicating the vascular defects in the CASZ1-depleted embryos are independent of the cardiac defects.

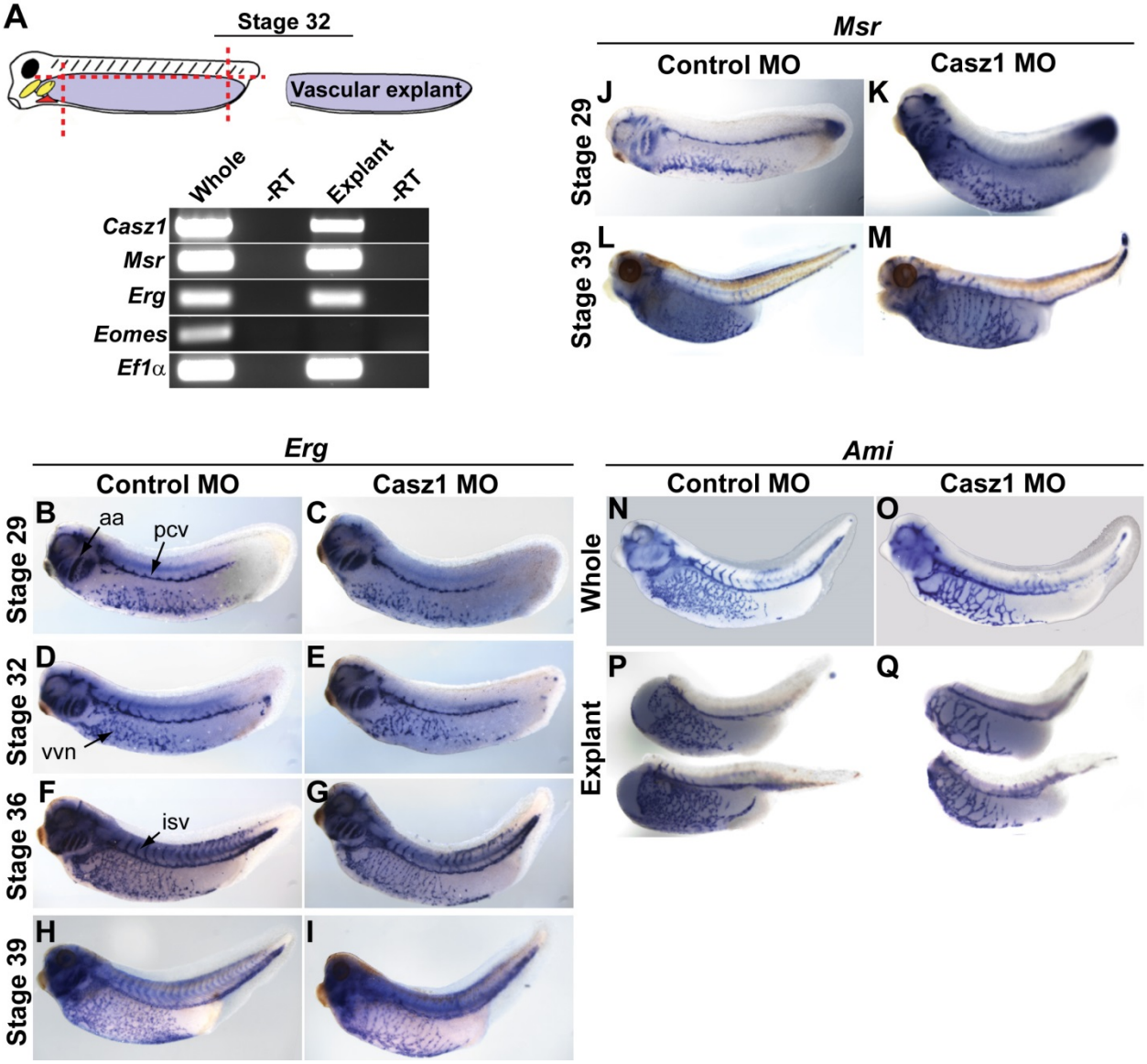

Supplemental Figure A1.2. CASZ1 is Required for EC Proliferation

(A) Control and shCasz1 cells were stained with anti-phospho-histone H3 (pH3-red) and DAPI (blue) to identify mitotic cells. Images were taken at 25x magnification while far right panels were taken at 63x. White arrowheads indicate pH3-positive cells. Graph represents quantification of pH3-positive cells. Data represent mean ± SEM of 3 independent experiments. (*n*=1000-2500 cells). (B) FACS analysis showing CASZ1-depleted cells arrest at G1/S with reduced proportion of cells in S phase compared to controls. (C) Control and CASZ1-depleted HUVECs were stained with anti-cleaved caspase-3 (red) and DAPI (blue) to identify apoptotic cells (top two panels). As a positive control, wildtype HUVECs were serum starved for 24 hr to induce apoptosis (lower panels). Images were taken at 25x magnification while far left panels were taken at 63x magnification. White arrowheads indicate cleaved caspase-3-positive cells. Graph represents quantification of cleaved caspase-3-positive cells. Data represent mean ± SEM of 2 independent experiments. (*n*=200-1000 cells).

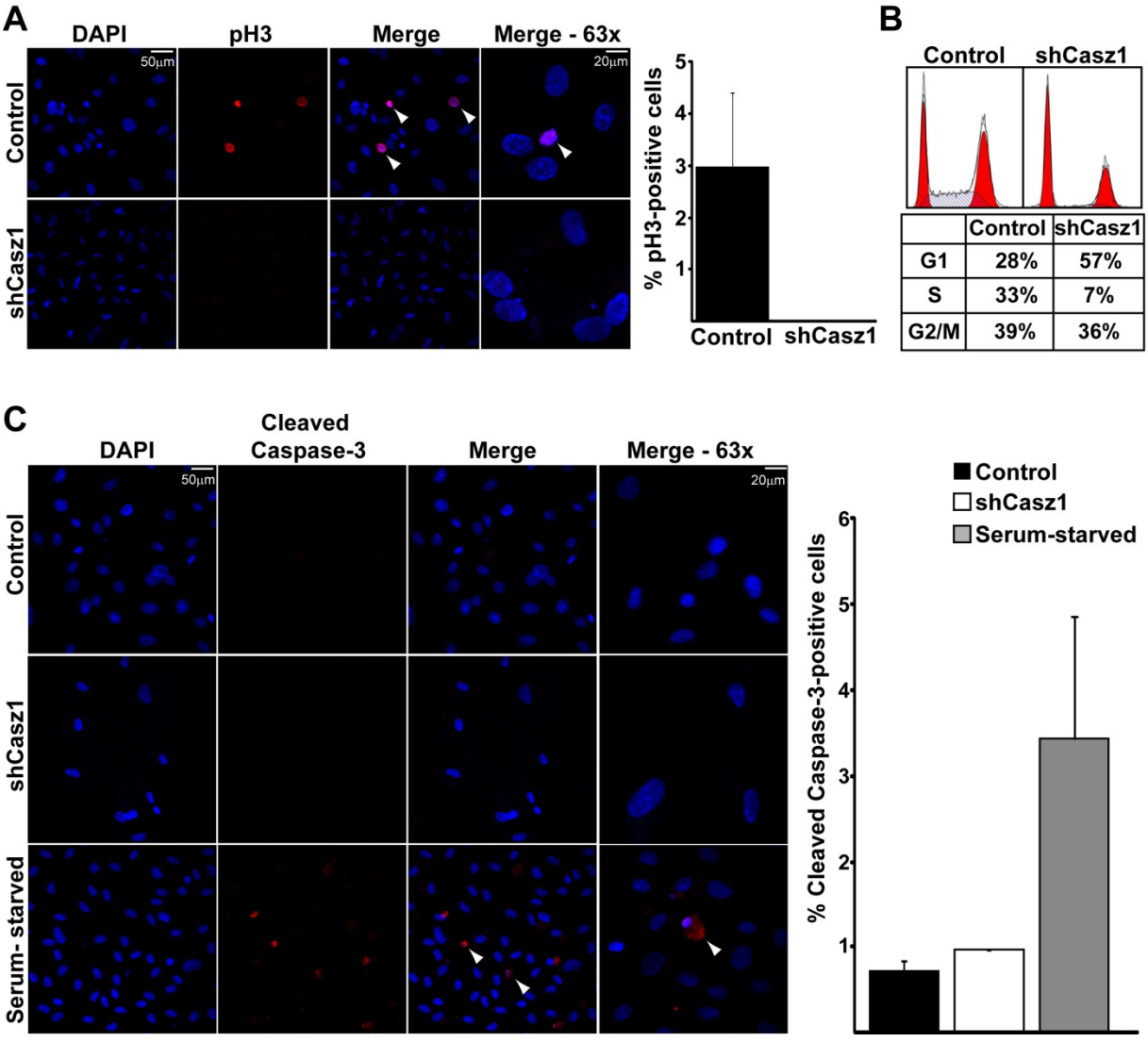
A
DAPI
pH3
Merge
Merge - 63x
Control
shCasz1
50μm
20μm
% pH3-positive cells
Control
shCasz1
B
Control
shCasz1
Control
shCasz1
G1
28%
57%
S
33%
7%
G2/M
39%
36%
C
DAPI
Cleaved Caspase-3
Merge
Merge - 63x
Control
shCasz1
Serum- starved
% Cleaved Caspase-3-positive cells
Control
shCasz1
Serum-starved

Supplemental Figure A1.3. Sequence Alignment of miR-126 and Expression of miR-126 in CASZ1-Depleted Embryos

(A) *Xenopus* miR-126 was cloned from genomic DNA and confirmed to be located in *Egfl7* intron 7. Evolutionary conservation of mature miR-126 is shown. (B-I) Whole mount *in situ* analysis of miR-126 of stage 29-39 control and CASZ1-depleted embryos (lateral view with anterior to the left). miR-126 expression commences in the vasculature including the vitelline vein network (vvn) at stage 32 (D,E) and remains intact at all stages thereafter even in the absence of CASZ1 suggesting that it may be differentially regulated than its host gene. Note the robust expression of miR-126 in somites (s). (*n*=10 embryos/condition/stage, 3 independent experiments).

A

	5′	3′
H.sapiens	UCGUACCGUGAGUAAUAAUGCG	
M.musculus	UCGUACCGUGAGUAAUAAUGCG	
D.rerio	UCGUACCGUGAGUAAUAAUGCG	
X.tropicalis	UCGUACCGUGAGUAAUAAUGCG	
X.laevis	UCGUACCGUGAGUAAUAAUGCG	

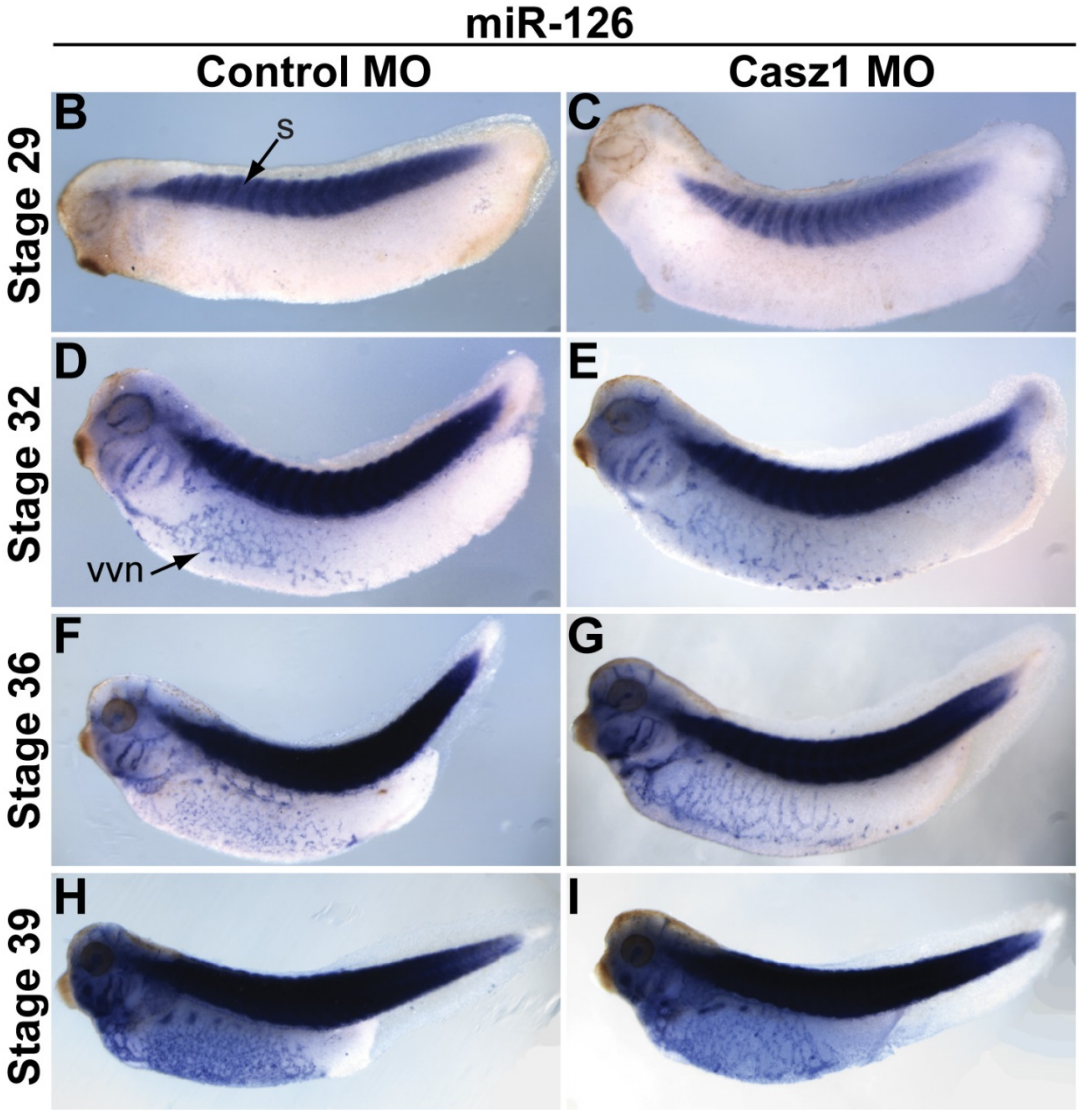

Supplemental Figure A1.4. EGFL7-Depletion Phenocopies CASZ1-Depletion During Vascular Development

(A) RT-PCR analysis of early tailbud stage 29 embryos injected at the one-cell stage with 40 ng Egfl7 MO demonstrating inhibition of proper splicing of *Egfl7* pre-mRNA. Control MO-injected embryos are negative controls and genomic DNA is a positive control for PCR amplification. (B-C) Whole mount *in situ* analysis of miR-126 expression in control and EGFL7-depleted early tadpole stage 36 embryos. There are no detectable alterations in miR-126 expression in EGFL7-depleted embryos. (D-E) Whole mount *in situ* analysis of *Casz1* expression in control and miR-126-depleted early tadpole stage 36 embryos. There are no detectable changes in *Casz1* expression in miR-126-depleted embryos. (F-I) Whole-mount in situ analysis with EC marker *Msr* of stage 29 and 39 control and EGFL7-depleted embryos. (*n*=10 embryos/condition/stage, 3 independent experiments). (J-Q) Whole-mount *in situ* analysis with EC marker *Erg* of stages 29-39 control and EGFL7-depleted embryos (lateral view with anterior to left). Vascular branching and patterning were severely disrupted in EGFL7-depleted embryos. Vitelline vein network-vvn, posterior cardinal vein- pcv, intersomitic vessels-isv. (*n*=10 embryos/condition/stage, 3 independent experiments).

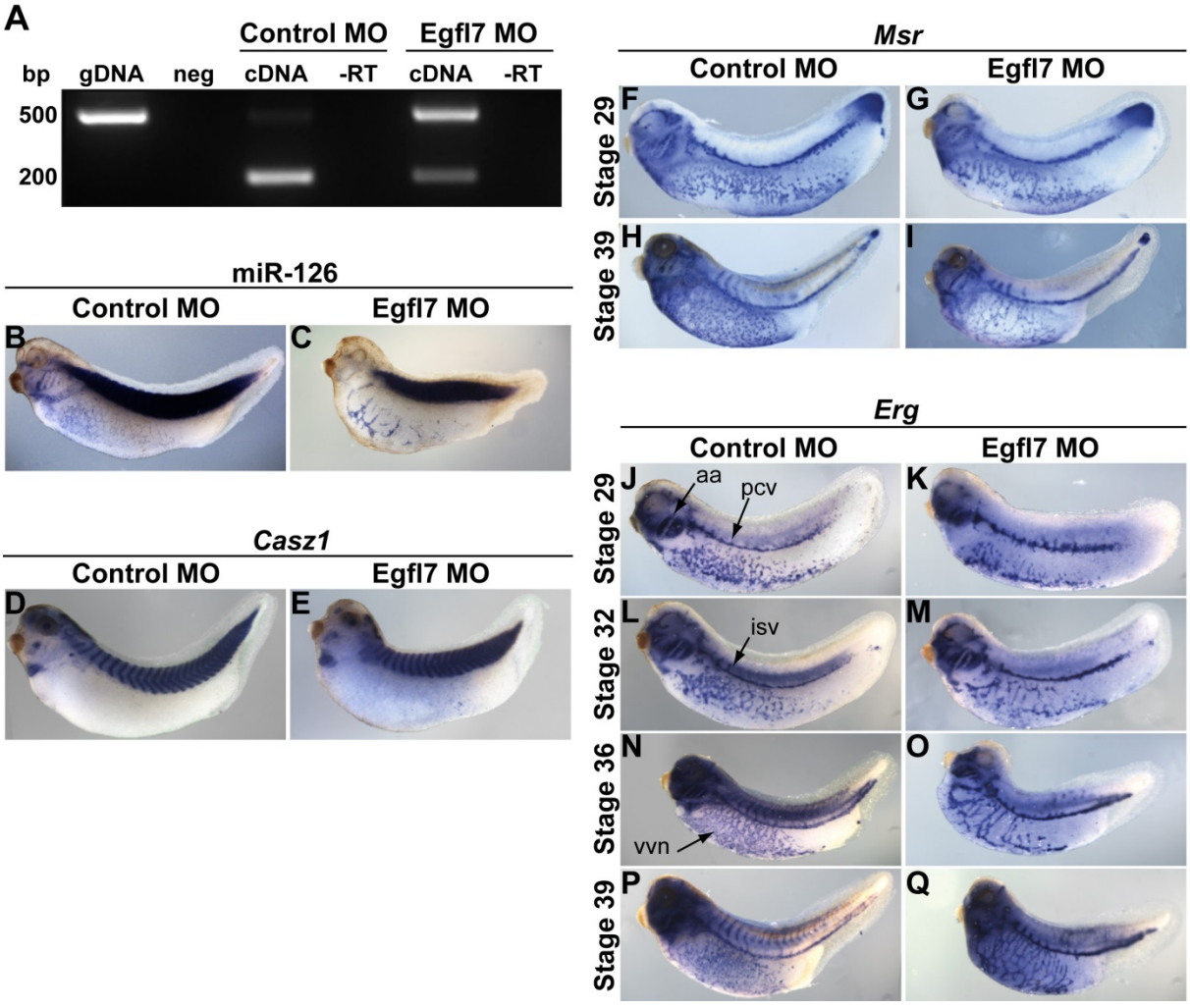
A
Control MO
Egfl7 MO
bp
gDNA
neg
cDNA
-RT
cDNA
-RT
500
200
miR-126
Control MO
Egfl7 MO
B
C
Casz1
Control MO
Egfl7 MO
D
E
Msr
Control MO
Egfl7 MO
Stage 29
F
G
Stage 39
H
I
Erg
Control MO
Egfl7 MO
Stage 29
J
aa
pcv
K
Stage 32
L
isv
M
Stage 36
N
vvn
O
Stage 39
P
Q

Supplemental Figure A1.5. miR-126 Depletion Does Not Phenocopy CASZ1-Depletion During Vascular Development

(A) Relative expression of miR-126 in embryos injected with miR-126 MO compared to control. Bars represent expression relative to miR-16 ± SEM. *:p<0.05. (B-C). Whole mount *in situ* analysis of *Egfl7* expression in control and miR-126-depleted early tadpole stage 36 embryos. There are no detectable alterations in *Egfl7* expression in miR-126-depleted embryos. (D-E) Whole mount *in situ* analysis of *Casz1* expression in control and miR-126-depleted early tadpole stage 36 embryos. There are no detectable changes in *Casz1* expression in miR-126-depleted embryos. (F-U) Whole mount *in situ* analysis of *Msr* (F,G,J,K,N,O,R,S) *and Erg* (H,I,L,M,P,Q,T,U) of stages 29-39 control and miR-126-depleted embryos (lateral view with anterior to the left). The vasculature forms normally in miR-126-depleted embryos with no apparent disruptions in vascular patterning or assembly. Vitelline vein network- vvn, posterior cardinal vein- pcv, intersomitic vessels- isv. (*n*=10 embryos/condition/stage, 3 independent experiments). (V-Y) Histological analysis shows normal lumens of pcv in stage 36 (W) and stage 39 (Y) miR-126-depleted embryos compared to controls (V,X). Dorsal is top, ventral is bottom. Arrowheads correspond to positions of pcv which are enlarged in lower panels. (*n*=2 embryos/condition/stage).

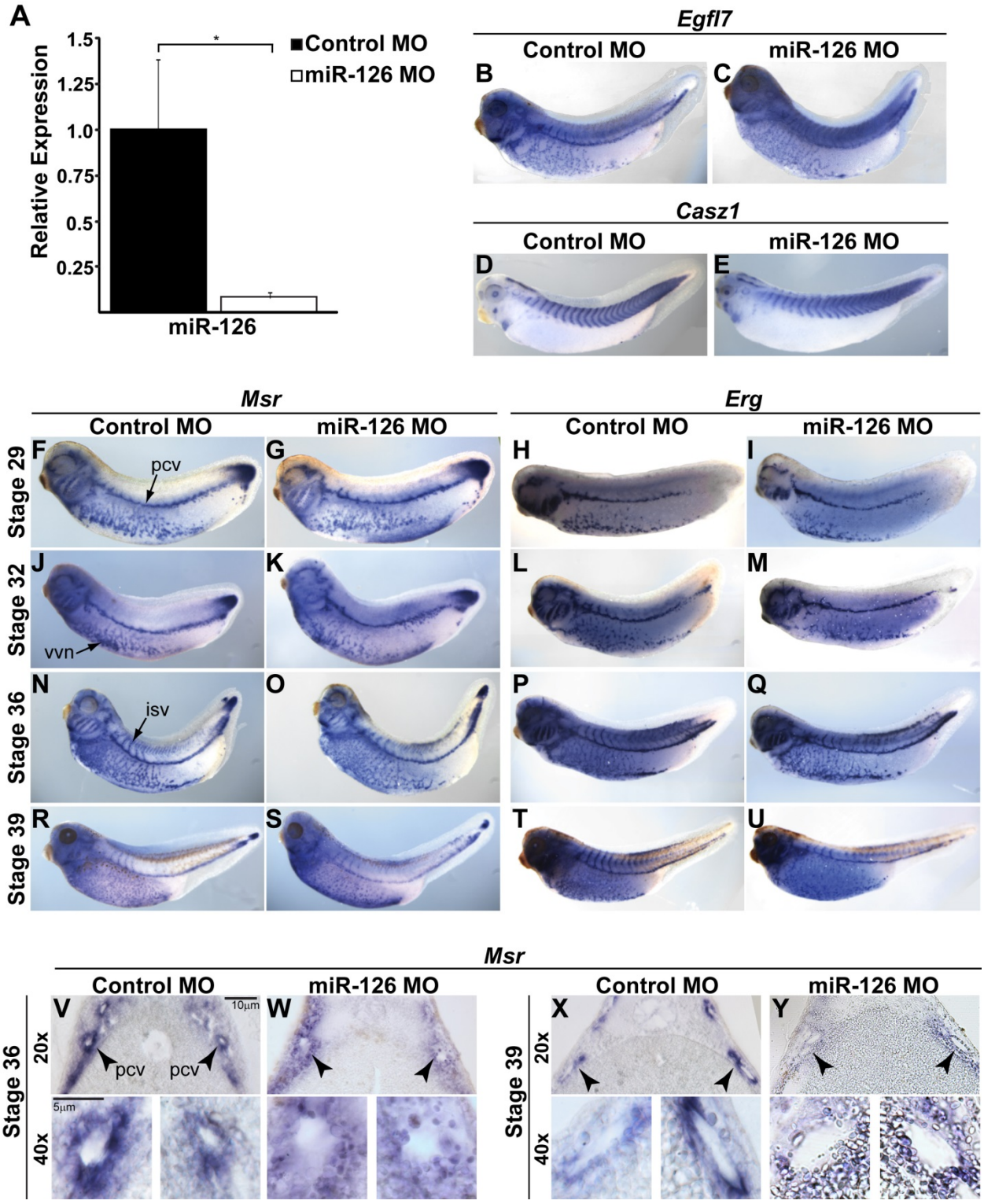
A
Relative Expression
1.5
1.25
1.0
0.75
0.5
0.25
*
Control MO
miR-126 MO
miR-126
Egfl7
Control MO
miR-126 MO
B
C
Casz1
Control MO
miR-126 MO
D
E
Msr
Control MO
miR-126 MO
Erg
Control MO
miR-126 MO
Stage 29
Stage 32
Stage 36
Stage 39
F
G
H
I
J
K
L
M
N
O
P
Q
R
S
T
U
pcv
vvn
isv
Msr
Control MO
miR-126 MO
Control MO
miR-126 MO
Stage 36
Stage 39
20x
40x
V
W
X
Y
10μm
5μm
pcv
pcv

Supplemental Figure A1.6. Efficacy of Ad-Egfl7 and Ad-miR-126

(A) Western blot of EGFL7 protein in HUVECs infected with control shRNA alone or co-infected with 25 MOI (multiplicity of infection) Ad-Egfl7. (B) Relative expression of miR-126 in HUVECs co-infected with shCasz1 and 25 MOI Ad-miR-126 compared to shCasz1 alone. mRNA levels are relative to miR-16 ± SEM. *:$p<0.05$. (C) Phase contrast images demonstrate elongated shCasz1-infected cells become more uniform in length and width after co-infection with Ad-Egfl7 but remain thin and elongated after co-infection with Ad-miR-126. (D) RhoA activity in un-stimulated (-) and Thrombin-stimulated (Thr) shRNA-infected HUVECs. RhoA activity was markedly decreased by depletion of CASZ1 and EGFL7. (E) Western blot representing unaltered RhoC protein levels in HUVECs infected with shCasz1, shEgfl7, or control shRNA. (F) Western blot showing decreased phosphorylation of myosin light chain (p-MLC) in CASZ1-depleted HUVECs versus control. Graph represents densitometry of p-MLC relative to GAPDH.

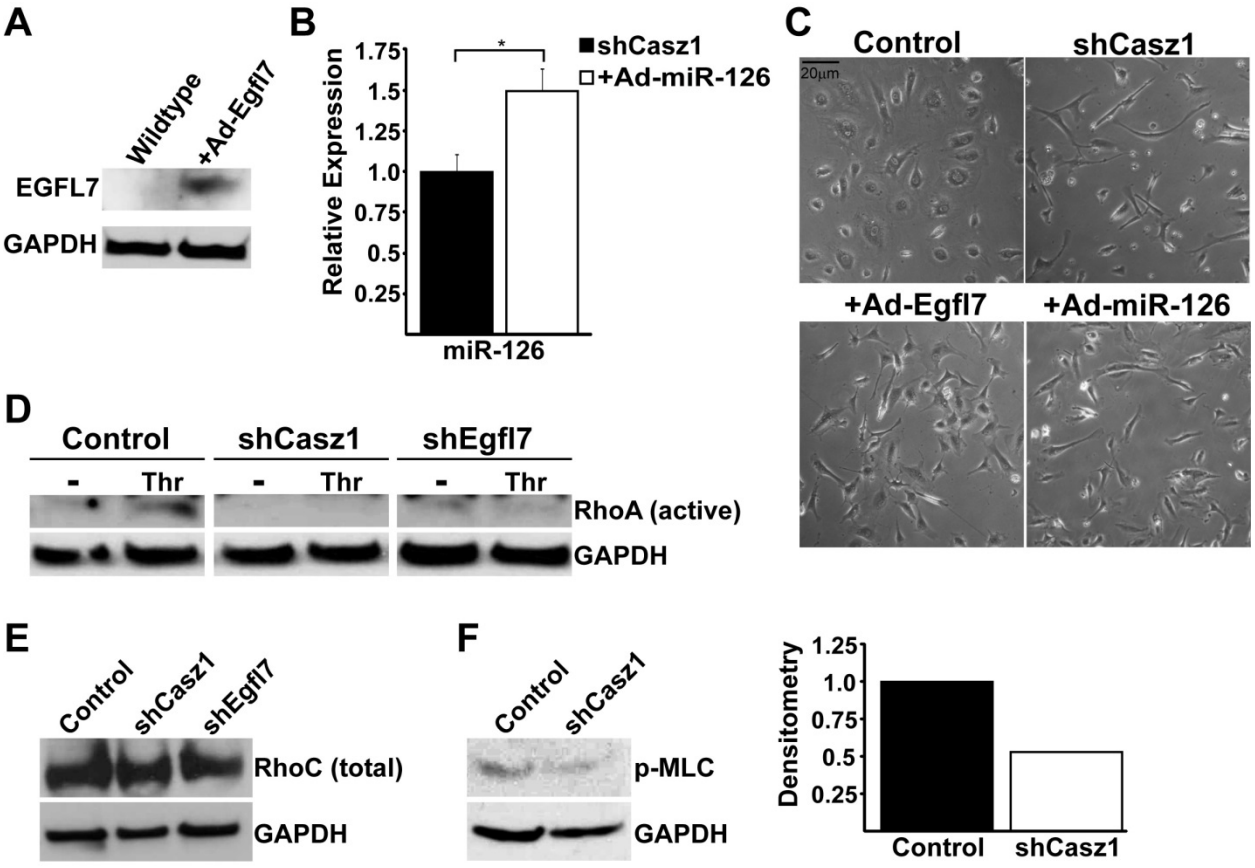
A
Wildtype
+Ad-Egfl7
EGFL7
GAPDH
B
Relative Expression
1.75
1.5
1.25
1.0
0.75
0.5
0.25
*
shCasz1
+Ad-miR-126
miR-126
C
Control
shCasz1
20μm
+Ad-Egfl7
+Ad-miR-126
D
Control
shCasz1
shEgfl7
-
Thr
-
Thr
-
Thr
RhoA (active)
GAPDH
E
Control
shCasz1
shEgfl7
RhoC (total)
GAPDH
F
Control
shCasz1
p-MLC
GAPDH
Densitometry
1.25
1.0
0.75
0.5
0.25
Control
shCasz1

Movie SA1.1. Time-lapse imaging of control and shCasz1 HUVECs

HUVECs infected with lentivirus encoding scrambled sequence shRNA (control) readily establish adhesion to the substrate and display very dynamic motility. In addition, cell divisions are frequently observed over a 24 hr time period. However, shCasz1-infected HUVECs initially adhere to the substrate but round up and detach (33%). Furthermore cells display defects in contractility as the trailing edge fails to properly retract resulting in thin, elongated cells. In over three independent experiments, a dividing CASZ1-depleted cell has never been observed. Imaging was performed at 20x magnification with images taken every 5 min.

Movie SA1.2. EGFL7-depletion phenocopies CASZ1-depletion in HUVECs

Depletion of EGFL7 phenocopies adhesion and proliferation defects of CASZ1-depleted cells. 43% of shEgfl7-infected cells fail to remain attached to the substrate and instead round up and detach (Compare to Movie SA1.1). In over 3 independent experiments, a dividing EGFL7-depleted cell has never been observed.

Movie SA1.3. Restoration of *Egfl7* or miR-126 levels rescues the adhesion defects of CASZ1-depletion

Co-infection of shCasz1 and an Egfl7-expressing adenovirus (Ad-Egfl7) results in cells that maintain adhesion to the substrate and no longer round up (compare to shCasz1 in Movie SA1.1). Cells also appear more rounded and spread compared to thin, elongated shCasz1-infected alone cells. Co-infection of shCasz1 and a miR-126-expressing adenovirus (Ad-miR-126) also results in cells that maintain adhesion to the substrate

and no longer round up (compare to shCasz1 in Movie SA1.1). Note that while adhesion is rescued, cells still display trailing edge contractility defects thus maintaining a thin, elongated appearance.

Movie SA1.4. Time-lapse imaging of sprouting control and shCasz1 HUVECs

HUVECs infected with control shRNA and embedded in fibrin gels extend from the beads to form sprouts and branches with neighboring vessels. However, shCasz1-infected HUVECs initially extend out from the bead but are unable to remain attached to the substrate subsequently detaching and preventing sprout formation. Imaging was performed over the course of 24 hr between Days 2 and 3 of the assay.

Movie SA1.5. EGFL7-depletion phenocopies CASZ1-depletion in the sprouting angiogenesis assay

shEgfl7-infected HUVECs also fail to properly sprout from the bead due to the inability to maintain adhesion to the fibrin gel (Compare to Movie SA1.1).

Supplemental Table A1.1. Putative direct targets of CASZ1

Table represents additional putative CASZ1 direct transcriptional targets that were identified through the cloning ChIP screen.

Putative CASZ1 Targets	Target DNA Location	General Function
N-myc Downregulated Gene 1 (Ndrg1)	3743 bp 3'	Cell Growth Pathway
Jumonji Domain Containing 1A	Internal	Cell Growth Pathway
Cyld	8075 bp 5'	Cell Growth Pathway
MDM2	4868 bp 3'	Cell Growth Pathway
MDM4	Internal	Cell Growth Pathway
Cyclin L2	16 bp 3'	Cell Growth Pathway
Inhibitor of Growth 1 (Ing1)	309 bp 5'	Cell Growth Pathway
Gli2	3680 bp 3'	Cell Growth Pathway
Plexin A2	Internal	Migration/Adhesion
Neurexin 3	Internal	Migration/Adhesion
FAT-J	Internal	Migration/Adhesion
Wnt1 Induced Secreted Pathway 1 (Wisp1)	Internal and 2867 bp 3'	Wnt Signaling Pathway
Novel Band 4.1-like Protein 4 (NBL4)	6788 bp 5'	Wnt Signaling Pathway
Shisa2	Internal	Wnt Signaling Pathway
Prickle1	Internal	Wnt Signaling Pathway
Msx1	8775 bp 5'	Patterning
Alk2/ACVR1	9351 bp 5'	Patterning
Troponin T Type 3 (Tnnt3)	4654 bp 5'	Structural
Myosin 5C	internal	Structural
Cytochrome b5	internal	Metabolism
Cytochrome b5 reductase isoform 2	10,000 bp 3'	Metabolism
Cytochrome C Oxidase Subunit VIII-Heart specific isoform	3859 bp 3'	Metabolism

Supplemental Table A1.2. Oligonucleotides Used for Quantitative Real-Time PCR

Gene Name	Species	Forward	Reverse
Egfl7	Human	GGGATGACTGATTCTCCTCC	CACCAGAAGCCACATCAGCAG
Casz1	Human	CCTTCTCCAAAACAGACTCC	GTTTACATCTTCAGTGACGGC
miR-126	Human/Xenopus	TCGTACCGTGAGTAATAATGCG	GCGAGCACAGAATTAATACGAC
Flk1	Human	GAAACTGACTTGGCCTCGG	GACCCGAGACATGGAATCAC
RhoA	Human	CAGTTCCCAGAGGTGTATGTG	GCGATCATAATCTTCCTGCC
RhoB	Human	GACACCGACGTCATTCTCATG	GATGATGGGCACATTGGGAC
RhoC	Human	CTACGTCCCTACTGTCTTTG	GCAGTCGATCATAGTCTTCC
RPS29	Human	CGGTCTGATCCGGAAATATG	CCCGGATAATCCTCTGAAGG

REFERENCES

Baltzinger, M., Mager-Heckel, A. M. and Remy, P. (1999). Xl erg: expression pattern and overexpression during development plead for a role in endothelial cell differentiation. *Dev Dyn* **216**, 420-433.

Barton, K., Muthusamy, N., Fischer, C., Ting, C. N., Walunas, T. L., Lanier, L. L. and Leiden, J. M. (1998). The Ets-1 transcription factor is required for the development of natural killer cells in mice. *Immunity* **9**, 555-563.

Baudino, T. A., McKay, C., Pendeville-Samain, H., Nilsson, J. A., Maclean, K. H., White, E. L., Davis, A. C., Ihle, J. N. and Cleveland, J. L. (2002). c-Myc is essential for vasculogenesis and angiogenesis during development and tumor progression. *Genes Dev* **16**, 2530-2543.

Bayless, K. J. and Davis, G. E. (2002). The Cdc42 and Rac1 GTPases are required for capillary lumen formation in three-dimensional extracellular matrices. *J Cell Sci* **115**, 1123-1136.

Burridge, K. and Wennerberg, K. (2004). Rho and Rac take center stage. *Cell* **116**, 167-179.

Campagnolo, L., Leahy, A., Chitnis, S., Koschnick, S., Fitch, M. J., Fallon, J. T., Loskutoff, D., Taubman, M. B. and Stuhlmann, H. (2005). EGFL7 is a chemoattractant for endothelial cells and is up-regulated in angiogenesis and arterial injury. *Am J Pathol* **167**, 275-284.

Carmeliet, P. (2003). Angiogenesis in health and disease. *Nat Med* **9**, 653-660.

Carmeliet, P. and Jain, R. K. (2011). Molecular mechanisms and clinical applications of angiogenesis. *Nature* **473**, 298-307.

Chan, C. H., Lee, S. W., Li, C. F., Wang, J., Yang, W. L., Wu, C. Y., Wu, J., Nakayama, K. I., Kang, H. Y., Huang, H. Y. et al. (2010). Deciphering the transcriptional complex critical for RhoA gene expression and cancer metastasis. *Nat Cell Biol* **12**, 457-467.

Christine, K. S. and Conlon, F. L. (2008). Vertebrate CASTOR is required for differentiation of cardiac precursor cells at the ventral midline. *Developmental cell* **14**, 616-623.

Chrzanowska-Wodnicka, M. and Burridge, K. (1996). Rho-stimulated contractility drives the formation of stress fibers and focal adhesions. *J Cell Biol* **133**, 1403-1415.

Cleaver, O., Tonissen, K. F., Saha, M. S. and Krieg, P. A. (1997). Neovascularization of the Xenopus embryo. *Dev Dyn* **210**, 66-77.

Cox, C. M., D'Agostino, S. L., Miller, M. K., Heimark, R. L. and Krieg, P. A. (2006). Apelin, the ligand for the endothelial G-protein-coupled receptor, APJ, is a potent angiogenic factor required for normal vascular development of the frog embryo. *Dev Biol* **296**, 177-189.

Davis, G. E., Koh, W. and Stratman, A. N. (2007). Mechanisms controlling human endothelial lumen formation and tube assembly in three-dimensional extracellular matrices. *Birth Defects Res C Embryo Today* **81**, 270-285.

De Val, S. (2011). Key transcriptional regulators of early vascular development. *Arterioscler Thromb Vasc Biol* **31**, 1469-1475.

De Val, S. and Black, B. L. (2009). Transcriptional control of endothelial cell development. *Dev Cell* **16**, 180-195.

Delgado-Esteban, M., Garcia-Higuera, I., Maestre, C., Moreno, S. and Almeida, A. (2013). APC/C-Cdh1 coordinates neurogenesis and cortical size during development. *Nature communications* **4**, 2879.

Devic, E., Paquereau, L., Vernier, P., Knibiehler, B., Audigier, Y., . (1996). Expression of a new G protein-coupled receptor X-msr is associated with an endothelial lineage in *Xenopus laevis*. . *Mechanisms of Development* **59**, 129-140.

Dowell, R. T. and McManus, R. E., 3rd. (1978). Pressure-induced cardiac enlargement in neonatal and adult rats. Left ventricular functional characteristics and evidence of cardiac muscle cell proliferation in the neonate. *Circulation research* **42**, 303-310.

Fish, J. E., Santoro, M. M., Morton, S. U., Yu, S., Yeh, R. F., Wythe, J. D., Ivey, K. N., Bruneau, B. G., Stainier, D. Y. and Srivastava, D. (2008). miR-126 regulates angiogenic signaling and vascular integrity. *Dev Cell* **15**, 272-284.

Fitch, M. J., Campagnolo, L., Kuhnert, F. and Stuhlmann, H. (2004). Egfl7, a novel epidermal growth factor-domain gene expressed in endothelial cells. *Dev Dyn* **230**, 316-324.

Harland, R. M. (1991). In situ hybridization: an improved whole mount method for Xenopus embryos. *Meth. Cell Biol.* **36**, 675-685.

Inui, M. and Asashima, M. (2006). A novel gene, Ami is expressed in vascular tissue in Xenopus laevis. *Gene Expr Patterns* **6**, 613-619.

Katoh, K., Kano, Y. and Noda, Y. (2011). Rho-associated kinase-dependent contraction of stress fibres and the organization of focal adhesions. *J R Soc Interface* **8**, 305-311.

Kokai, E., Voss, F., Fleischer, F., Kempe, S., Marinkovic, D., Wolburg, H., Leithauser, F., Schmidt, V., Deutsch, U. and Wirth, T. (2009). Myc regulates embryonic vascular permeability and remodeling. *Circ Res* **104**, 1151-1159.

Kuhnert, F., Mancuso, M. R., Hampton, J., Stankunas, K., Asano, T., Chen, C. Z. and Kuo, C. J. (2008). Attribution of vascular phenotypes of the murine Egfl7 locus to the microRNA miR-126. *Development* **135**, 3989-3993.

Lelievre, E., Lionneton, F., Soncin, F. and Vandenbunder, B. (2001). The Ets family contains transcriptional activators and repressors involved in angiogenesis. *Int J Biochem Cell Biol* **33**, 391-407.

Lelievre, E., Hinek, A., Lupu, F., Buquet, C., Soncin, F. and Mattot, V. (2008). VE-statin/egfl7 regulates vascular elastogenesis by interacting with lysyl oxidases. *EMBO J* **27**, 1658-1670.

Lemarie, C. A., Tharaux, P. L. and Lehoux, S. (2010). Extracellular matrix alterations in hypertensive vascular remodeling. *J Mol Cell Cardiol* **48**, 433-439.

Levine, A. J., Munoz-Sanjuan, I., Bell, E., North, A. J. and Brivanlou, A. H. (2003). Fluorescent labeling of endothelial cells allows in vivo, continuous characterization of the vascular development of Xenopus laevis. *Dev Biol* **254**, 50-67.

Levy, D., Ehret, G. B., Rice, K., Verwoert, G. C., Launer, L. J., Dehghan, A., Glazer, N. L., Morrison, A. C., Johnson, A. D., Aspelund, T. et al. (2009). Genome-wide association study of blood pressure and hypertension. *Nature genetics* **41**, 677-687.

Mandel, E. M., Kaltenbrun, E., Callis, T. E., Zeng, X. X., Marques, S. R., Yelon, D., Wang, D. Z. and Conlon, F. L. (2010). The BMP pathway acts to directly regulate Tbx20 in the developing heart. *Development* **137**, 1919-1929.

Monteys, A. M., Spengler, R. M., Wan, J., Tecedor, L., Lennox, K. A., Xing, Y. and Davidson, B. L. (2010). Structure and activity of putative intronic miRNA promoters. *RNA* **16**, 495-505.

Nakatsu, M. N., Sainson, R. C., Aoto, J. N., Taylor, K. L., Aitkenhead, M., Perez-del-Pulgar, S., Carpenter, P. M. and Hughes, C. C. (2003). Angiogenic sprouting and capillary lumen formation modeled by human umbilical vein endothelial cells (HUVEC) in fibrin gels: the role of fibroblasts and Angiopoietin-1. *Microvasc Res* **66**, 102-112.

Narumiya, S., Ishizaki, T. and Ufhata, M. (2000). Use and properties of ROCK-specific inhibitor Y-27632. *Methods in Enzymology* **325**, 273-284.

Nichol, D., Shawber, C., Fitch, M. J., Bambino, K., Sharma, A., Kitajewski, J. and Stuhlmann, H. (2010). Impaired angiogenesis and altered Notch signaling in mice overexpressing endothelial Egfl7. *Blood* **116**, 6133-6143.

Nieuwkoop, P. D. and Faber, J. (1967). Normal Table of *Xenopus laevis* (Daudin). Amsterdam: North Holland.

Nikolic, I., Plate, K. H. and Schmidt, M. H. (2010). EGFL7 meets miRNA-126: an angiogenesis alliance. *J Angiogenes Res* **2**, 9.

Nobes, C. D. and Hall, A. (1995). Rho, rac, and cdc42 GTPases regulate the assembly of multimolecular focal complexes associated with actin stress fibers, lamellipodia, and filopodia. *Cell* **81**, 53-62.

Parker, L. H., Schmidt, M., Jin, S. W., Gray, A. M., Beis, D., Pham, T., Frantz, G., Palmieri, S., Hillan, K., Stainier, D. Y. et al. (2004). The endothelial-cell-derived secreted factor Egfl7 regulates vascular tube formation. *Nature* **428**, 754-758.

Parsons, J. T., Horwitz, A. R. and Schwartz, M. A. (2010). Cell adhesion: integrating cytoskeletal dynamics and cellular tension. *Nat Rev Mol Cell Biol* **11**, 633-643.

Patan, S. (2000). Vasculogenesis and angiogenesis as mechanisms of vascular network formation, growth and remodeling. *J Neurooncol* **50**, 1-15.

Porrello, E. R., Johnson, B. A., Aurora, A. B., Simpson, E., Nam, Y. J., Matkovich, S. J., Dorn, G. W., 2nd, van Rooij, E. and Olson, E. N. (2011). MiR-15 family regulates postnatal mitotic arrest of cardiomyocytes. *Circulation research* **109**, 670-679.

Potente, M., Gerhardt, H. and Carmeliet, P. (2011). Basic and therapeutic aspects of angiogenesis. *Cell* **146**, 873-887.

Rodrigues, C. O., Nerlick, S. T., White, E. L., Cleveland, J. L. and King, M. L. (2008). A Myc-Slug (Snail2)/Twist regulatory circuit directs vascular development. *Development* **135**, 1903-1911.

Schmidt, M. H., Bicker, F., Nikolic, I., Meister, J., Babuke, T., Picuric, S., Muller-Esterl, W., Plate, K. H. and Dikic, I. (2009). Epidermal growth factor-like domain 7 (EGFL7) modulates Notch signalling and affects neural stem cell renewal. *Nat Cell Biol* **11**, 873-880.

Showell, C., Christine, K. S., Mandel, E. M. and Conlon, F. L. (2006). Developmental expression patterns of Tbx1, Tbx2, Tbx5, and Tbx20 in Xenopus tropicalis. *Dev Dyn* **235**, 1623-1630.

Strilic, B., Kucera, T., Eglinger, J., Hughes, M. R., McNagny, K. M., Tsukita, S., Dejana, E., Ferrara, N. and Lammert, E. (2009). The molecular basis of vascular lumen formation in the developing mouse aorta. *Dev Cell* **17**, 505-515.

Sweet, D. T., Chen, Z., Wiley, D. M., Bautch, V. L. and Tzima, E. (2012). The adaptor protein Shc integrates growth factor and ECM signaling during postnatal angiogenesis. *Blood* **119**, 1946-1955.

Takeuchi, F., Isono, M., Katsuya, T., Yamamoto, K., Yokota, M., Sugiyama, T., Nabika, T., Fujioka, A., Ohnaka, K., Asano, H. et al. (2010). Blood pressure and hypertension are associated with 7 loci in the Japanese population. *Circulation* **121**, 2302-2309.

Taranova, O. V., Magness, S. T., Fagan, B. M., Wu, Y., Surzenko, N., Hutton, S. R. and Pevny, L. H. (2006). SOX2 is a dose-dependent regulator of retinal neural progenitor competence. *Genes Dev* **20**, 1187-1202.

Wang, S., Aurora, A. B., Johnson, B. A., Qi, X., McAnally, J., Hill, J. A., Richardson, J. A., Bassel-Duby, R. and Olson, E. N. (2008). The endothelial-specific microRNA miR-126 governs vascular integrity and angiogenesis. *Dev Cell* **15**, 261-271.

Warkman, A. S., Zheng, L., Qadir, M. A. and Atkinson, B. G. (2005). Organization and developmental expression of an amphibian vascular smooth muscle alpha-actin gene. *Dev Dyn* **233**, 1546-1553.

Weinmann, A. S. and Farnham, P. J. (2002). Identification of unknown target genes of human transcription factors using chromatin immunoprecipitation. *Methods* **26**, 37-47.

Xu, K., Sacharidou, A., Fu, S., Chong, D. C., Skaug, B., Chen, Z. J., Davis, G. E. and Cleaver, O. (2011). Blood Vessel Tubulogenesis Requires Rasip1 Regulation of GTPase Signaling. *Dev Cell* **20**, 526-539.

Ying, C. Y., Dominguez-Sola, D., Fabi, M., Lorenz, I. C., Hussein, S., Bansal, M., Califano, A., Pasqualucci, L., Basso, K. and Dalla-Favera, R. (2013). MEF2B mutations lead to deregulated expression of the oncogene BCL6 in diffuse large B cell lymphoma. *Nature immunology* **14**, 1084-1092.

Appendix 2: Transcriptional regulation of blood vessel formation: The role of the CASZ1/*Egfl7*/RhoA pathway[3]

INTRODUCTION

Formation of a functional vascular system is critical for the delivery of nutrients, the removal of waste, and gas exchange. During vasculogenesis, the *de novo* formation of blood vessels, mesodermal cells differentiate into endothelial cell precursors that proliferate and migrate to specified locations in the embryo before assembling into cord-like structures to form the primary vascular plexus (Herbert and D.Y., 2011). Redistribution of junctional molecules, establishment of apicobasal polarity, and cell morphology changes all facilitate the opening of vessel lumens. These primitive blood vessels are further pruned and remodeled by angiogenesis when new vascular branches form by sprouting from pre-existing vessels. Additionally, endothelial cells become specified to contribute to either the venous or arterial vasculature (Herbert and D.Y., 2011). Understanding the molecular and cellular mechanisms underlying endothelial cell behavior will enable us to develop more efficacious therapies for diseases, such as atherosclerosis, rheumatoid arthritis, and tumorigenesis.

The specification of the cardiovascular lineage and the subsequent morphogenesis of the heart and vessels depend on the combined activities of a number

---

[3]This chapter previously appeared as an article in the journal *Developmental Cell*. The original citation is as follows: Charpentier, M.S., Dorr, and Conlon, F.L. Transcriptional regulation of blood vessel formation: The role of the CASZ1/Egfl7/RhoA-mediated pathway. *Cell Cycle* 12, no.14 (July 2013): 2165.

of transcription factors. Work within our lab revealed a novel role for the transcription factor CASZ1 in *Xenopus* cardiogenesis by regulating cardiomyocyte differentiation (Christine and Conlon, 2008). In a recent study, we also showed that CASZ1 is required for blood vessel branching and lumen formation in *Xenopus* embryos, independent of its role in cardiac development (Charpentier et al., 2013). At the cellular level, depletion of CASZ1 in primary human endothelial cells results in impaired adhesion to the underlying substrate, aberrant contractility, and G1/S cell cycle arrest, indicating that CASZ1 is necessary for promoting endothelial cell behaviors associated with proper vascular assembly (Charpentier et al., 2013). Utilizing a chromatin immunoprecipitation-cloning screen, we found that CASZ1 modulates these endothelial cell behaviors by activating the expression of its direct transcriptional target, epidermal growth factor-like domain 7 (*EGFL7*). Depletion of EGFL7, an endothelial-secreted extracellular matrix (ECM) protein, resulted in poorly arborized vascular networks that were devoid of vessel lumens, indicating a requirement for EGFL7 in angiogenesis and lumen morphogenesis in accordance with previous reports (Nichol and Stuhlmann, 2012; Nikolic et al., 2013). Moreover, the EGFL7-deficient vascular networks were similar to those in CASZ1-depleted embryos. We linked this CASZ1/*EGFL7* transcriptional hierarchy to the RhoA GTPase signaling pathway, which directly controls the cellular outputs we observed to be defective under CASZ1 and EGFL7-depleted conditions. RhoA transcript levels and activity were significantly diminished in the absence of either CASZ1 or EGFL7. Consequently, formation of actin-based stress fibers and localization of focal adhesion markers at sites of substrate contact were aberrant in CASZ1-depleted cells, but these defects were rescued by reintroduction of EGFL7.

From these results, we propose a model whereby CASZ1 binds to and activates *EGFL7* gene expression in endothelial cells in order to release EGFL7 into the ECM. Through yet unknown mechanisms, we hypothesize that EGFL7 binds to cell-surface receptors, such as integrins, to activate a signaling cascade necessary for RhoA transcription and its subsequent activity. RhoA then directly modulates endothelial cell behaviors, such as adhesion and contractility, to promote the proper assembly of vascular networks (Figure A2.1). While we have shown that activation of this pathway is necessary for the formation of a functional vascular system from a developmental standpoint, it is not surprising that improper activation of such a pathway could lead to pathological vascular remodeling in adult tissues, such as during tumorigenesis. While highly expressed in developing vessels, EGFL7 is downregulated in the quiescent vasculature of the adult, but is upregulated again in response to injury or cellular stress (Nichol and Stuhlmann, 2012). Indeed, high EGFL7 levels are correlated with several tumors and cancer cell lines, and EGFL7 monoclonal antibodies are currently being tested in clinical trials for use in vascular tumor therapies (http://www.gene.com/medical-professionals/pipeline) (Nichol and Stuhlmann, 2012). RhoA has been shown to be required for lumen formation, but increased RhoA activity also induces vascular permeability, which potentially associates RhoA with the unstable, leaky vasculature characteristic of tumors (Karlsson et al., 2009). Therefore, uncovering the molecular networks underlying embryonic development may provide novel targets for the design of therapeutics to treat patients with cancer.

There have been limited studies on mammalian CASZ1 in both development and disease. Recently, the human ortholog of *Casz1* was identified and shown to be highly

expressed in adult heart tissue (Liu et al., 2006). The evolutionary role of CASZ1 in cardiovascular development is further emphasized by a recent genome-wide association study, demonstrating a genetic association between the *Casz1* locus and both blood pressure and hypertension (Takeuchi et al., 2010). However, despite the essential role of CASZ1 in cardiovascular development and human disease, the cellular requirements and molecular mechanisms by which CASZ1 regulates cardiac development remain unknown. To address these issues, we generated a *Casz1* knockout mouse that will provide a means to understand mechanistically how this transcription factor functions in cardiovascular disease. Future studies include identifying additional transcriptional targets of CASZ1 in the heart and vasculature and investigating how CASZ1 regulates transcription. To that end, we are undertaking a number of proteomics-based approaches to determine how CASZ1 itself is regulated, to identify cardiac and/or vascular-specific co-factors with which CASZ1 interacts to regulate transcription, and to uncover novel downstream pathways dependent on CASZ1 function.

Figure A2.1. Function of CASZ1 in endothelial cells.

(A) Proper expression and activity of CASZ1 in endothelial cells results in transcriptional activation of *Egfl7* and subsequent RhoA activity thereby promoting the assembly of a well-branched, lumenized vascular system. (B) Disruption of CASZ1 function results in cords of endothelial cells lacking a central lumen and angiogenic sprouts. Branches that are apparent consist of thin, elongated cells that are unable to maintain adhesion to the underlying matrix or existing vasculature.

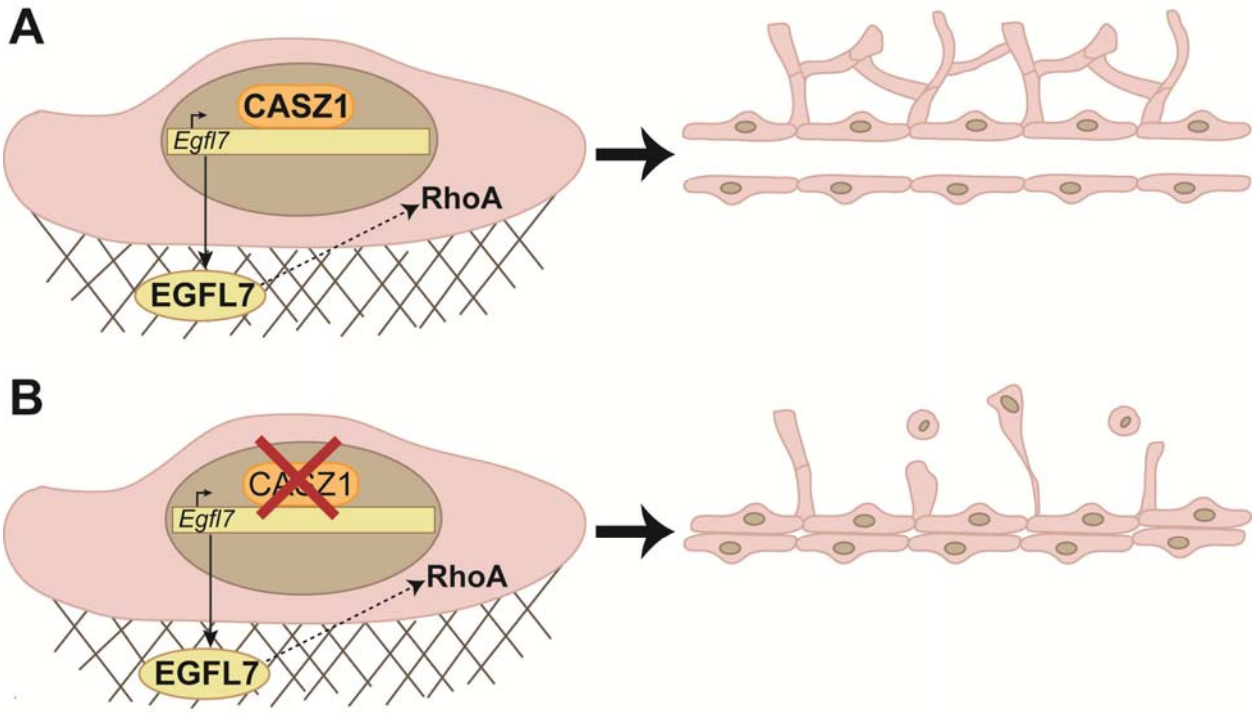

REFERENCES

Charpentier, M. S., Christine, K. S., Amin, N. M., Dorr, K. M., Kushner, E. J., Bautch, V. L., Taylor, J. M. and Conlon, F. L. (2013). CASZ1 promotes vascular assembly and morphogenesis through the direct regulation of an EGFL7/RhoA-mediated pathway. *Developmental cell* **25**, 132-143.

Christine, K. S. and Conlon, F. L. (2008). Vertebrate CASTOR is required for differentiation of cardiac precursor cells at the ventral midline. *Developmental cell* **14**, 616-623.

Herbert, S. P. and D.Y., S. (2011). Molecular control of endothelial cell behaviour during blood vessel morphogenesis. *Nat Rev Mol Cell Biol* **12**, 551-564.

Karlsson, R., Pedersen, E. D., Wang, Z. and Brakebusch, C. (2009). Rho GTPase function in tumorigenesis. *Biochim Biophys Acta* **1796**, 91-98.

Liu, Z., Yang, X., Tan, F., Cullion, K. and Thiele, C. J. (2006). Molecular cloning and characterization of human Castor, a novel human gene upregulated during cell differentiation. *Biochemical and biophysical research communications* **344**, 834-844.

Nichol, D. and Stuhlmann, H. (2012). EGFL7: a unique angiogenic signaling factor in vascular development and disease. *Blood* **119**, 1345-1352.

Nikolic, I., Stankovic, N. D., Bicker, F., Meister, J., Braun, H., Awwad, K., Baumgart, J., Simon, K., Thal, S. C., Patra, C. et al. (2013). EGFL7 ligates alphavbeta3 integrin to enhance vessel formation. *Blood* **121**, 3041-3050.

Takeuchi, F., Isono, M., Katsuya, T., Yamamoto, K., Yokota, M., Sugiyama, T., Nabika, T., Fujioka, A., Ohnaka, K., Asano, H. et al. (2010). Blood pressure and hypertension are associated with 7 loci in the Japanese population. *Circulation* **121**, 2302-2309.

APPENDIX 3: The cardiac TBX5 interactome reveals a chromatin remodeling network essential for atrial septation[4]

INTRODUCTION

Congenital malformations, or structural birth defects, are the leading cause of infant mortality in the US and Europe (Dolk et al., 2010) (Heron et al., 2009). Congenital heart disease (CHD) remains the most common congenital malformation, with atrial septal defects present in 56 per 100,000 live births. The health problem is compounded by the fact that most children are otherwise asymptomatic and that the disease, in most instances, has with no identifiable cause. Holt Oram Syndrome (HOS) is an autosomal disorder associated with cardiac septal defects and is caused by dominant mutations in the T-box transcription factor *Tbx5* (Basson et al., 1997; Li et al., 1997). Mice heterozygous for a null mutation in *Tbx5* display many of the phenotypic abnormalities of HOS, while mice homozygous null for a mutation in *Tbx5* die by E10.5 due to cardiac defects (Bruneau et al., 2001; Moskowitz et al., 2004; Moskowitz et al., 2007). In addition to its role in cardiogenesis, *Tbx5* is one of the key factors for cellular reprogramming of fibroblasts into induced cardiomyocytes (Qian et al., 2012).

[4]This chapter is an article currently in review in the *Journal of Clinical Investigation*. The original citation is as follows: Waldron, L., Kweon, J., Greco, T., Dorr, K.M., Steimle, J.D., Yang, X.H., Temple, B., Cristea, I.L., Moskowitz, I.P., and Conlon, F.L. The cardiac TBX5 interactome reveals a chromatin remodeling network essential for atrial septation (2015). *Journal of Clinical Investigation* (in review).

Whilst *Tbx5* is an essential transcription factor for heart development and reprogramming, and its disease relevance is well established, there are many critical questions unanswered about the mechanism of TBX5 function. It is not understood what proteins complex with TBX5 during different stages of cardiac development and homeostasis, how these interactions regulate TBX5's choice of distinct transcriptional targets, or how these interactions function to activate and/or repress target gene transcription. Nor is it known how these events, when disrupted, manifest into CHD. To these ends, we initiated a directed proteomic-based approach to identify endogenous cardiac proteins that function in association with TBX5.

MATERIALS AND METHODS

Generation of *Tbx5^{Avi}* mice

The targeting construct used to create a conditional knock-in allele of *Tbx5^{Avi}* was created in collaboration with the UNC Animal Models Core and the UNC BAC Core (Chapel Hill). Briefly, the biotin acceptor peptide (Avi) targeting cassette was inserted in frame to the terminal exon of the *Tbx5* gene. Targeted ES cells were selected and introduced into B6 mouse blastocysts. High-chimera males were mated with B6 females to produce F1 heterozygotes (*Tbx5$^{Avi\text{-}Neo/+}$*). Incorporation of the *Tbx5^{Avi}* construct was confirmed by PCR and Southern analysis (Supplemental Figure A3.1b), while presence of *Tbx5^{Avi}* mRNA was confirmed by RT-PCR (Supplemental Figure A3.1d). F1 heterozygotes were crossed with *Sox2-Cre* mice (Hayashi et al., 2002) to remove the neomycin selection cassette in the F2 generation (Supplemental Figure A3.1c). F2

compound heterozygous mice were intercrossed to remove the *Sox2-Cre* allele and establish $Tbx5^{Avi/Avi}$ homozygous lines. $Tbx5^{Avi/Avi}$ mice were crossed to $Rosa26^{BirA}$ mice (JAX), which have been previously described (Driegen et al., 2005), and intercrossed to obtain compound homozygotes. Genotyping was performed by PCR. Genotyping primers can be found in Supplemental Table A3.4. Southern probe was designed to *Tbx5* intron 8. Genomic DNA was digested with EcoRV or BamHI. Animal care and animal experiments were conducted in accordance with the Animal Care Committee at the University of North Carolina, Chapel Hill.

Preparation of cardiac nuclei

Frozen hearts from 4 week old $Tbx5^{Avi/Avi}$; $Rosa26^{BirA/BirA}$ (n=3, 2 replicates) and control mice (n=3) were homogenized using a mortar and pestle in liquid nitrogen. Nuclei were prepared as previously described (Franklin et al., 2011) and snap frozen in liquid N_2.

Solubilization of protein complexes

Plasmids were transfected into HEK-293 cells, harvested, and lysed as previously described (Kaltenbrun et al., 2013). Cells and nuclear pellets were resuspended in lysis buffer (200mM K-HEPES pH 7.4, 1.1M KOAc, 20mM $MgCl_2$, 1% Tween-20, 10μM $ZnCl_2$, 10mM $CaCl_2$, 0.5% Triton X-100, 500 mM NaCl, 1X protease inhibitors (Roche), 1X phosphatase inhibitors (Sigma), optimized for TBX5 complexes. Nuclei were then homogenized using a Polytron (Kinematica), and processed for immunoprecipitation as previously described (Kaltenbrun et al., 2013).

Conjugation of magnetic beads and immunoaffinity purification

Conjugation of V5 antibody to magnetic beads (Invitrogen), and immunoisolation of protein complexes was performed as previously described, (Cristea et al., 2005; Kaltenbrun et al., 2013) but modified as follows for streptavidin IPs. Immunoaffinity purifications were performed using streptavidin conjugated Dynabeads (Invitrogen) by slow rocking at RT for 30 minutes. The isolated protein complex was eluted from the beads for 20 min at 95°C in 40μL elution buffer (80mM NaOAc pH 9.0, 95% formamide). Western blots were probed with mV5 (1:5000, Invitrogen), rCHD4 (1:500, Active Motif), mHDAC2 (1:1000, Abcam), rMTA1 (1:5000, Bethyl), rTBX5 (1:1000, Aviva), gTBX5 (1:500, Santa Cruz) mGFP (1:10000, Clontech).

Mass spectrometry

Immunoisolated proteins were analyzed by mass spectrometry as previously described (Kaltenbrun et al., 2013). Briefly, tandem mass spectra were extracted by Proteome Discoverer (Thermo Fisher Scientific), and all MS/MS samples were analyzed with SEQUEST (Thermo Fisher Scientific; version 1.2.0.208), set up to search the human and mouse UniProt-SwissProt protein sequence database, assuming digestion pattern with trypsin. Scaffold (version Scaffold_3_00_06, Proteome Software Inc., Portland, OR) was used to validate MS/MS-based peptide and protein identifications. Peptide sequences were deemed a match if they could be established at >95.0% probability as specified by the Peptide Prophet algorithm (Keller et al., 2002). In turn, protein identifications were deemed a match if they could be established at >99.0% probability by the ProteinProphet algorithm and have at least two sequenced peptides.

Protein identifications and associated spectral counts were exported to Excel for further data processing.

Interaction bioinformatics analysis

Protein identifications were filtered to exclude non-specific associations. Proteins were retained as specific candidates if they (1) had at least two spectral counts in both *Tbx5*$^{Avi/Avi}$*; Rosa26*$^{BirA/BirA}$ replicates with at least 4 spectral counts in one replicate, and were uniquely identified or had at least a 2.5-fold spectral count enrichment in the *Tbx5*$^{Avi/Avi}$*; Rosa26*$^{BirA/BirA}$ condition versus the control. Candidates were assigned GO ontology classification using the UniProt GOA annotations from within the Cytoscape (v3.2) platform (Cline et al., 2007). Gene symbols were submitted to the web-based STRING database (Franceschini et al., 2013) for interaction network analysis. Interactions with a combined STRING score of > 0.4 (medium confidence) were retained, exported, and further visualized in Cytoscape.

Transcriptional assays

ChIP peak regions from our candidate genes of interest were amplified from mouse genomic DNA and subcloned into the PGL3-Promoter Luciferase vector (Promega). Primer sequences for each candidate gene are provided in Supplemental Table 5. HEK-293 cells were transfected with 600ng total DNA in 12 well plates using FuGene6 (Promega) and harvested 48 hours later for transcription assay. Transcriptional assays were performed using Dual Reporter Assay System (Promega) according to the manufacturer's protocol.

DNA constructs

Generation of the *Tbx5*^{Avi} targeting construct for embryonic stem cells and generation of chimeric mice was performed by JrGang Chen (UNC BAC Core-Chapel Hill). *Tbx5-Avi-V5* was generated by synthesizing an oligo encoding the Avi tag (5' ggc ctg aac gac atc ttc gag gct cag aaa atc gaa tgg cac gaa 3') and subcloning it into the pcDNA3.1/V5-His TOPO vector (Invitrogen). *Tbx5* full length and truncations were then subcloned into pcDNA3.1-Avi-V5. pEF1α-BirA-V5-Neo was generously provided by Stuart Orkin (Harvard University) (Kim et al., 2009). GFP tagged full length, C-terminal, and N-terminal CHD4 constructs were generously provided by Stephen Jackson (Cambridge) (Polo et al., 2010). Site-directed mutagenesis primers are available in Supplemental Table A3.6.

Genetic interaction and histology

Tbx5$^{fl/fl}$ mice were generously provided by Jon and Christine Seidman (Harvard Medical School) (Bruneau et al., 2001). The *Tbx5*$^{+/-}$ mouse has been previously reported (Bruneau et al., 2001). The *Mta1*$^{+/-}$ mouse line was generated by Harold Olivey (Indiana University Northwest) and generously provided by Eric Svensson (Novartis Institutes for Biomedial Research). All mice are in a mixed B6/129/SvEv/CD-1 background and all mouse experiments were performed according to a protocol reviewed and approved by the Institutional Animal Care and Use Committee of the University of Chicago, in compliance with the USA Public Health Service Policy on Humane Care and Use of Laboratory Animals. E13.5 wild type, *Tbx5*$^{+/-}$, *Mta1*$^{+/,-}$ and *Tbx5*$^{+/-}$;*Mta1*$^{+/-}$ compound heterozygous embryos were dissected from timed

mating between *Tbx5*$^{+/-}$ and *Mta1*$^{+/-}$ mice. Embryos were fixed in 4% PFA overnight and sent to the Human Tissue Resource Center at the University of Chicago for paraffin embedding, sectioning, and H&E staining. Slides were imaged on a Leica DM2500 microscope and QImaging Retiga 2000R 1394 Color Cooled camera.

RNA-seq

Heart tube dissections were performed as described previously (Hoffmann et al., 2014). Briefly, E9.5 *Tbx5*$^{+/+}$ and *Tbx5*$^{-/-}$ heart tubes were dissected away from the body nearest the myocardial reflections and four heart tubes were pooled to isolate sufficient RNA. Genotypes were assigned via PCR. Pools of tissue were mechanically homogenized in TRIzol Reagent (Invitrogen, Carlsbad CA) and then RNA was isolated in accordance to the manufacturer's instructions. RNA resuspended in water was further purified with 500 µl of 1-butanol (4 times) and 500 µl diethyl ether (twice) (Krebs et al., 2009). Isolated RNA underwent library preparation and 50-bp single-ended RNA sequencing at the Genomics Core Facility at The University of Chicago. Briefly, mRNA was selected for using an oligo-dT pulldown, and barcoded libraries were prepared according to Illumina's instructions accompanying the TruSeq RNA Sample prep kit v2 (Lavine et al., RS-122-2001). Library fragments of ~275 bps (insert plus adaptor and PCR primer sequences) were quantitated using the Agilent Bio-analyzer 2100 and pooled in equimolar amounts. The pooled libraries were sequenced on the HiSeq2500 in Rapid Run Mode following the manufacturer's protocols (Invitrogen, 2013).

To determine statistical significance of transcripts between *Tbx5*$^{+/+}$ and *Tbx5*$^{-/-}$ heart tubes, computations were made using a pipeline following quality control, genome

alignment, noise filtering, and two-group comparison. Transcripts with an FDR adjusted $P < 0.05$ and absolute fold change>1.57 were accepted as statistically significant.

Chromatin IP

HEK-293 cells were transfected with the *Kctd16-Luciferase* construct used in transcriptional assays, as well as wild type TBX5 or $TBX5^{S261C}$ (20 μg total DNA) using FuGene 6 (Promega). Cells were fixed in 1% PFA for 10 minutes at RT. 10 million cells were used per ChIP. Cells were lysed in ChIP Buffer (50mM Tris pH 7.5, 140 mM NaCl, 1mM EDTA, 1 mM EGTA, 0.1% sodium deoxycholate, 0.1% SDS), sonicated using a Branson 450d, 12 cycles, 30s/cycle (1s on, 0.5s off), 30% amplitude), and spun at top speed to isolate chromatin. Triton X-100 was added to 1% and added to Chd4-conjugated Protein G beads (Life Technologies) at 4°C O/N. ChIP was resumed using ChIP Protocol (Agilent). ChIP primer sequences are available in Supplemental Table 7.

TBX5 NID Modelling

The mouse TBX5 sequence was submitted to the DisProt PONDR-FIT disorder predictor in order to identify disordered regions in the protein. Both the entire protein and just the NID region were submitted to the fold recognition server HHpred (http://toolkit.tuebingen.mpg.de/hhpred) to determine if any suitable templates were available for structural modeling. A small coil-to-helical region involving residues 255-264 was predicted by HHpred. This region of TBX5 was modeled based on the correspondingly small region of the structure of the CRISPR-associated protein [PDB ID 3VZI].

RESULTS

Past attempts to isolate endogenous T-box protein complexes have been hampered by their relative low abundance and insolubility. Therefore, we knocked-in an Avitag epitope into the *Tbx5* locus to generate a $Tbx5^{Avi}$ allele (Supplemental Figure SA3.1). The Avitag is a small peptide tag that is biotinylated in the presence of the bacterial enzyme BirA. Thus, the Avitag/BirA system combines minimal structural invasiveness and the specificity and strength of the biotin-streptavidin interaction. This is the strongest non-covalent peptide-ligand interaction in nature, and therefore the affinity greatly exceeds that of any antibody-antigen interaction (Roesli et al., 2006; Wang et al., 2006). $Tbx5^{Avi}$ mice were mated to mice ubiquitously expressing BirA ($Rosa26^{BirA}$) (Driegen et al., 2005). The $Tbx5^{Avi}$; $Rosa26^{BirA}$ compound homozygous mice show no overt phenotype, have no cardiac phenotype, and are fertile. Thus, the Avitag appears to have no effect on TBX5 activity and expression of biotinylated $TBX5^{Avi}$ is not deleterious.

To define the TBX5 cardiac interactome, we performed mass spectrometry analysis of immnuoaffinity purified TBX5 complexes from $Tbx5^{Avi/Avi}$;$Rosa26^{BirA/BirA}$ cardiac nuclei (Figure A3.1a). We used an unbiased gene ontology-based bioinformatics classification to screen the functions of proteins associated with TBX5. This analysis defined a subset of 60 candidate interactions (Supplemental Table SA3.1). We analyzed these candidates by functional network analysis; drawing upon the STRING database of protein-protein interactions, 40 out of the 60 candidates were assigned to a single interconnected network (Figure A3.1b and Supplemental Figure SA3.2). This network contained the heterodimeric facilitates chromatin transcription

(FACT) complex and several members of the transcription initiation factor TFIID complex, both of which play roles in RNA Pol II-dependent gene transcription (Berk, 1999; Saunders et al., 2003). TBX5 has been long considered to be a cardiac transcriptional activator. Surprisingly, in our analysis we identified TBX5 in association with multiple components of the NuRD complex (Figure A3.1b, c) which in most instances functions as a chromatin modifying complex that represses gene transcription (Wade et al., 1998; Xue et al., 1998). We find TBX5 in association with six components of the NuRD transcriptional repression complex: CHD4, MTA1, RBBP4, GATAD2a, GATAD2b, and HDAC2. Since CHD3 commonly acts in a mutually exclusive manner with CHD4, RBBP7 and RBBP4 act redundantly, and an additional component of the NuRD complex, MBD3 has been suggested to be dispensable for transcription factor recruitment (e.g., by hunchback)(Kehle et al., 1998), we have therefore identified all the components required for a functional NuRD complex. We confirmed the interaction of TBX5 with multiple members of the NuRD complex in cardiac extracts (Figure A3.1c). Taken together these data show TBX5 interacts with components of the NuRD complex in heart tissue.

To further define the relationship between TBX5 and the NuRD complex, we generated mice heterozygous null for *Tbx5* and a central component of the NuRD complex, *Mta1* (Figure A3.2, Supplemental Figure SA3.3). At E13.5, $Mta1^{+/-}$ mice have no apparent cardiac defects (Figure A3.2c), whereas $Tbx5^{+/-}$ mice exhibit previously described cardiac defects, including ASD, ventricular septal defects (VSD) and atrioventricular septal defects (AVSDs) (also known as common atrioventricular canal (CAVC) defects (Fig. A3.2d) (Basson et al., 1994; Basson et al., 1999; Bruneau et al.,

1999; Bruneau et al., 2001; Baban et al., 2014). *Tbx5*$^{+/-}$; *Mta1*$^{+/-}$ heterozygous null embryos demonstrated a higher frequency of AVSDs than either heterozygote alone ($p<0.03$) (Figure A3.2e, Supplemental Figure SA3.3d). Taken together these results demonstrate TBX5 and MTA1 genetically interact.

The finding that TBX5 and components of the NuRD complex interact biochemically and genetically led us to hypothesize that TBX5 can function to repress aberrant gene expression in the heart. To test this hypothesis, we determined the gene targets of TBX5 repression. To this end, we performed RNA-seq analysis from E9.5 wild type and *Tbx5*$^{-/-}$ hearts to determine genes differentially expressed between wild type and *Tbx5* null hearts (Figure A3.3a, Supplemental Table SA3.2). We overlaid TBX5 ChIP-seq data (He et al., 2011) with genes upregulated in the *Tbx5* null heart. From this analysis, we identified 928 genes that are potentially repressed by TBX5 (Supplemental Table SA3.3).

To validate the genes putatively repressed by TBX5, we rank ordered the 928 genes based on relative change in expression between wild type and *Tbx5*$^{-/-}$ hearts and the number of reads in the ChIP-seq data set. From this list, we cloned the top 15 of the ChIP peak sequence elements from 14 genes and performed transcriptional assays (Figure A3.3b-m, Supplemental Figure SA3.4). Of the candidate genes tested, 11 were repressed by TBX5. This set of genes could be divided into two categories: *Casz1*, *Fgf11*, *Gad1, Kcne3, Kctd16, Nxph4, Plekha2, and Sncb* are expressed in neural lineages[23], while *Casz1*, *Col20a1, Fgf11*, *Gad1*, *Klf4, Mef2b,* and *Plekha2* are expressed in a divergent subset of cancers (Liu et al., 2011; Huang et al., 2013; Kimura et al., 2013; Ying et al., 2013; Hu et al., 2015). Together these data demonstrate that

TBX5 functions as a transcriptional repressor and acts in vivo to repress the ectopic expression of neural and cancer related genes in the heart.

To gain insight into the mechanisms of TBX5-NuRD mediated repression, we mapped the protein interaction domains of TBX5 and MTA1 and the catalytic core component of the NuRD complex, CHD4 (Supplemental Figure A3.5). We found an N-terminal CHD4 region was required for interaction with TBX5 (Supplemental Figure SA3.5c), while a C-terminal TBX5 region was necessary and sufficient for interaction with MTA1 and CHD4 (amino acids 238-340) (Figure A3.4a, Supplemental Figure SA3.5d,e). We find this hitherto uncharacterized region to be highly conserved across 48 TBX5 orthologues (Supplemental Figure SA3.6), and have shown that this domain is predicted to form a Coil followed by an α-Helix (Figure A3.4b). We have termed this structural-functional region of TBX5 the NuRD interaction domain ($TBX5^{NID}$).

The majority of TBX5 mutations associated with CHD are located within the T-box with most leading to a loss of TBX5 DNA binding or non-sense mediated decay (Fan et al., 2003b; Fan et al., 2003a; Mori and Bruneau, 2004). In addition, there exists a subset of CHD mutations that lie in the C-terminus of TBX5, outside the T-box, and the resulting forms of TBX5 are stable and bind DNA. The molecular basis for these CHD-associated mutations however, has been entirely unknown. We found TBX5 CHD-associated mis-sense mutations in the C-terminal region of TBX5 align to the $TBX5^{NID}$; $TBX5^{S252I}$, $TBX5^{S261C}$, $TBX5^{V263M}$, $TBX5^{K266R}$, and $TBX5^{Q292R}$ (Heinritz et al., 2005). We further show that these single TBX5 mis-sense mutations align along a single interaction surface of the $TBX5^{NID}$ α-Helix (Figure A3.4c). Thus, we hypothesized the CHD mis-sense mutations in the $TBX5^{NID}$ disrupt the TBX5-CHD4 interaction.

We tested the prediction that TBX5 mis-sense mutations in the $TBX5^{NID}$ alter the TBX5-NuRD association. Three single mis-sense mutations within the $TBX5^{NID}$ ($TBX5^{S261C}$, $TBX5^{V263M}$, and $TBX5^{K266R}$) abolished the interaction between TBX5 and both CHD4 and MTA1, and an additional two other CHD single mis-sense mutations ($TBX5^{S252I}$ and $TBX5^{Q292R}$) reduced the interaction (Figure A3.4d). These results show that disruption of the TBX5-NuRD complex in vivo leads to cardiac abnormalities associated with HOS.

Having demonstrated the TBX5-NuRD interaction is disrupted in CHD-associated mutations in the NID, we queried if repression of our TBX5 target genes was NuRD dependent. We performed transcriptional assays and observed of our targets repressed by TBX5, *Kctd16* and *Mef2b* fail to be repressed by TBX5 CHD associated mutation $TBX5^{S261C}$ (Figure A3.4e-f). Moreover, $TBX5^{S261C}$ failed to repress transcription of multiple elements of the *Mef2b* gene (Supplemental Figure SA3.7a-b). Taken together, with results showing that we were able to ChIP CHD4 in the presence of TBX5 to these elements (Supplemental Figure SA3.7c-d), these results imply the TBX5-NuRD complex is required to repress inappropriate gene expression in the heart and further suggest a subset of CHD mutants leads to the mis-expression of genes including *Mef2b* in the developing heart.

Analysis of TBX5 orthologues demonstrates there is a complete conservation of the $TBX5^{NID}$ amino acids mutated in TBX5-associated CHD in animals with a septated heart ($TBX5^{S261}$, $TBX5^{V263}$, $TBX5^{K266}$) (Figure A3.4g). In contrast, orthologues of TBX5 in vertebrates that lack a septated heart have amino acid substitutions at positions we show ablate the TBX5-NuRD interaction (Figure A3.4d). Taken together, this data

suggests the TBX5-NuRD interaction arose coincident with cardiac atrial septation. This hypothesis is further supported by our observations that *Tbx5*$^{+/-}$*; Mta1*$^{+/-}$ compound heterozygous mice have a higher frequency of AVSDs than either heterozygote alone (Supplemental Figure SA3.3d). AVSDs have been reported in 18 HOS patients, and 10 have been characterized to date (Kehle et al., 1998). Of these, 6 of the mutations lead to the introduction of a stop codon before the TBX5^{NID} and one mis-sense mutation maps within the TBX5^{NID} and ablates the TBX5-NuRD interaction (Figure A3.4d). Thus, we find a phenotypic correlation between those patients displaying AVSD and the genotype of those TBX5 patient mutations lacking or altering the TBX5^{NID}.

DISCUSSION

Our results demonstrate a functional requirement for an interaction between TBX5 and components of the NuRD complex. Our observation that only a subset of TBX5-repressed target genes failed to be repressed by the TBX5 HOS mutation TBX5^{S261C} (Figure A3.4e-f, Supplemental Figure SA3.8), strongly implies TBX5 functions in both a NuRD-dependent and NuRD-independent manner. Moreover, since we do not detect an alteration in cardiac genes in TBX5 null heart tissue, these data further suggest that the loss of the TBX5-NuRD interaction is not associated with a cell fate switch but rather demonstrate that the TBX5-NuRD interaction functions to prevent the expression of genes incompatible with normal heart development.

Our studies demonstrate that a proteomic based approach coupled with protein modeling provides a powerful predictive strategy in prioritizing patient mutations. This

type of approach should be applicable to the analysis of any protein in any cell or tissue type. The power of such an approach is underscored by recent high through-put sequencing studies that have led to the identification of a vast number of somatic mutations in coding regions of potential disease causing genes. However, exploiting such large data sets has proved problematic in that it is not been possible to prioritize which mutations are natural occurring, non-disease associated variants and which are disease causing. Results presented here demonstrate a novel proteomic-modeling based strategy that can lend itself to prioritizing mis-sense mutation and moreover, present a potential means to predict the disease associated phenotypes with specific mutations.

Figure A3.1. TBX5 interacts with the NuRD complex.

(a) Overview of the isolation and characterization of the endogenous cardiac TBX5 interactome. (**b**) Transcriptional TBX5 interaction network. Network nodes, labeled with mouse gene symbols, are candidate direct or indirect TBX5 interactions identified from affinity enrichment of biotinylated TBX5. Network edges represent known and/or predicted functional interactions in the STRING database. Edge thickness reflects the combined STRING evidence score for each binary relationship. Thicker edges represent increased interaction evidence. Selected transcriptional complexes within the network are highlighted in red dashed boxes. (**c**) Immnuo-isolation of endogenous $TBX5^{Avi}$ from cardiac nuclei confirms interaction of TBX5 with endogenous components of the NuRD complex.

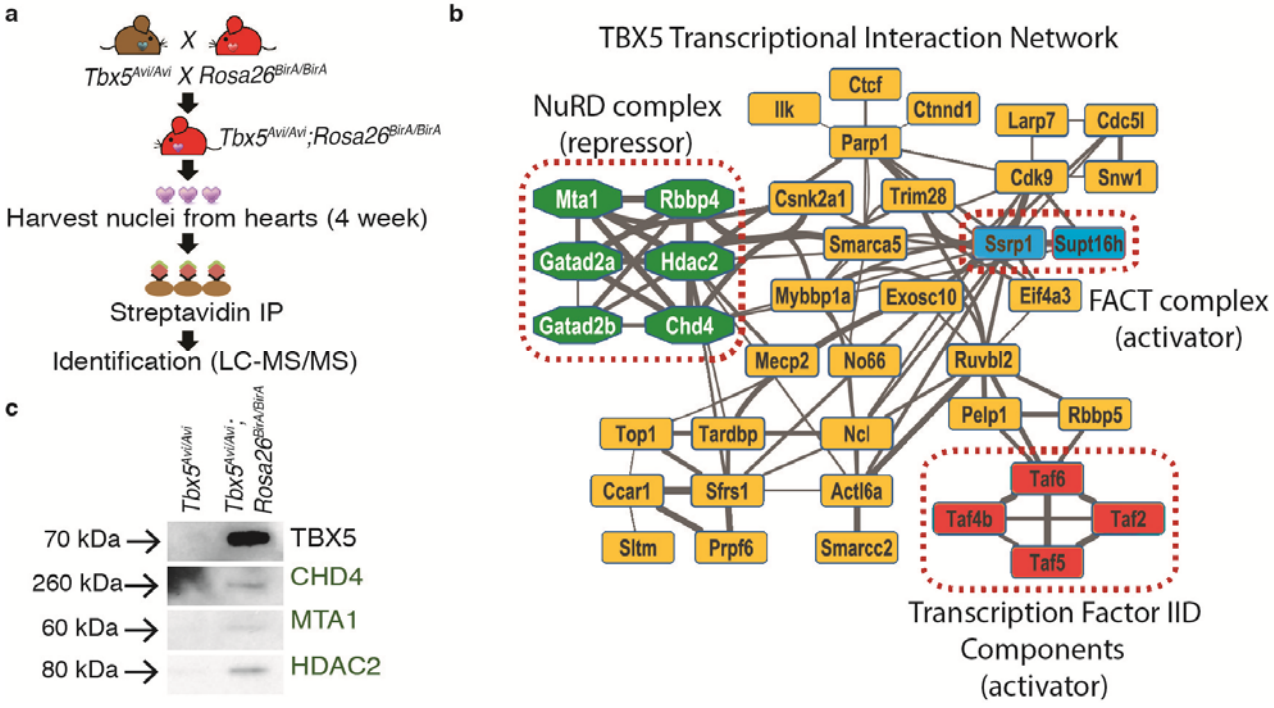

Figure A3.2. TBX5 and the NuRD complex genetically interact.

Histology staining (Hematoxylin and Eosin) of heart tissue at E13.5 (**a**) Low magnification of a wild type heart. (**b**) High magnification of a wild type, (**c**) *Mta1*$^{+/-}$, (**d**) *Tbx5*$^{+/-}$ and, (**e**) heterozygous null *Tbx5*$^{+/-}$*; Mta1*$^{+/}$ heart. Note that the *Tbx5*$^{+/-}$*; Mta1*$^{+/}$ hearts exhibited cardiac defects including ASD (asterisk) and AVSD (arrow). Cardiac defects are characterized and quantified in Supplemental Fig. 3. as = atrial septum, ivs = intervectricular septum, la = left atrium, lv = left ventricle, mv = mitral valve, ra = right atrium, rv = right ventricle, tv = tricuspid valve.

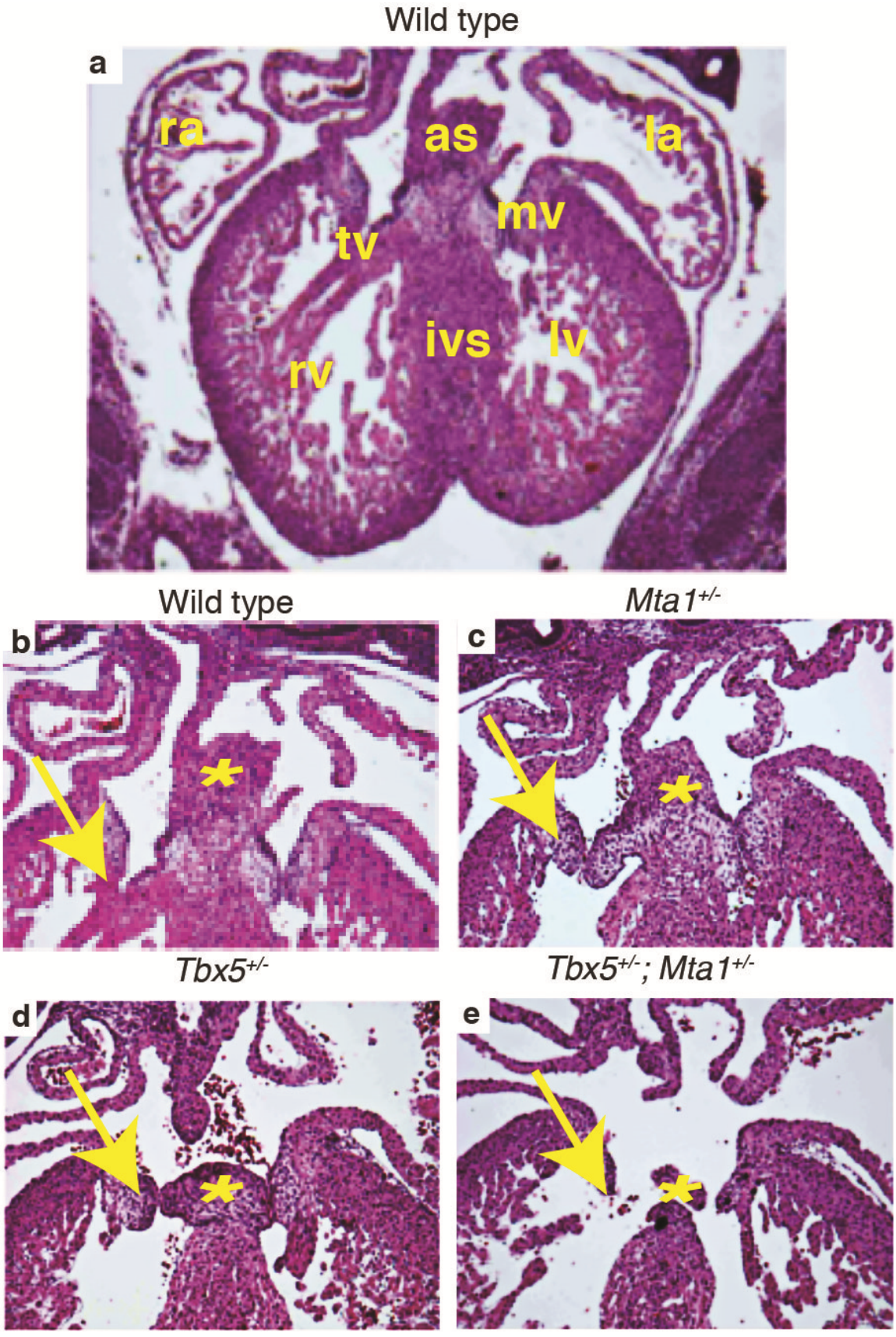
Wild type
a
ra
as
la
mv
tv
ivs
lv
rv
Wild type
Mta1+/-
b
c
Tbx5+/-
Tbx5+/-; Mta1+/-
d
e

Figure A3.3. TBX5 functions to represses neural and cancer genes in cardiac tissue.

(**a**) Schematic overlay between genes upregulated in RNA-seq between wild type and *Tbx5*$^{-/-}$ heart tissue and TBX5 ChIP-seq data[20] reveals 928 genes that are both upregulated in a *Tbx5*$^{-/-}$ null and bound by TBX5. (**b**) Summary of fold change (RNA-seq) and ChIP-seq peak values of the 15 top rank ordered genes. (**c-m**) Gene reporter elements cloned from potential TBX5 targets in the presence or absence of TBX5. Transcriptional assays of target genes show TBX5 acts as a transcriptional repressor in 11 of 15 elements tested (additional data in Supplemental Fig. 4). Genes defined as neural are shown in red, expressed in cancer as blue, or both as purple. * $p < 0.05$ *** $p < 0.001$.

a

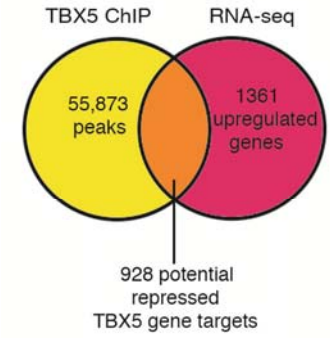

b

Gene	Log2 fold change	ChIP peak location	ChIP peak value(s)	Size of element
Casz1-1	1.26	exon 1/ intron 1	60, 29, 43	3,200 bp
Casz1-2	1.26	intron 1	32, 22, 18	2,400 bp
Col20a1	1.95	5' UTR (2.7 kb from TSS)	17, 35	1,100 bp
Fbxl20	1.37	5' UTR/ exon 1/ intron 1	25, 56, 30	1,600 bp
Fgf8	1.71	5' UTR (2.8 kb from TSS)	80	384 bp
Fgf11	3.49	intron 1	45	1,200 bp
Gad1	4.19	intron 1	17	276 bp
Kcne3	3.63	5' UTR (100bp from TSS)	23	350 bp
Kcnn2	1.23	exon 1	13	140 bp
Kctd16	4.53	5' UTR (1.4 kb from TSS)	17	426 bp
Klf4	1.74	exon 3	57, 56	3,291 bp
Mef2b	4.61	5' UTR (7.4 kb from TSS)	27	347 bp
Nxph4	4.93	5' UTR (5.7 kb from TSS)	41	490 bp
Plekha2	1.21	5' UTR (1.3 kb from TSS)	49, 33	1,700 bp
Sncb	5.01	intron 4	18	321 bp

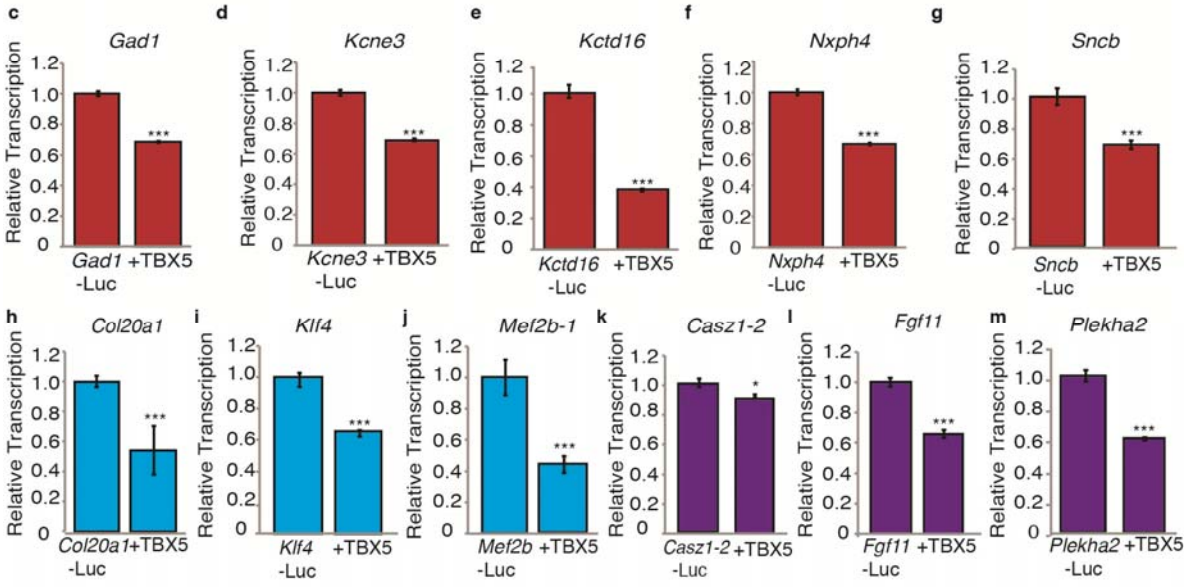

Figure A3.4. Congenital heart disease associated mutations of TBX5 disrupt TBX5-NuRD complex activity.

(**a**) Schematic of human TBX5 protein showing location of a subset of CHD associated mis-sense mutations. NID= NuRD interacting domain (aa 238-340). (**b**) Structural rendering of the $TBX5^{NID}$ shows the $TBX5^{NID}$ is comprised of a Coil region followed an α-Helix. (**c**) CHD associated mis-sense mutations align along a single surface of the α-Helix and are predicted to disrupt protein-protein interactions (representative aa $TBX5^{S261}$, $TBX5^{V263}$, and $TBX5^{K266}$ residues shown in dark blue). (**d**) IP of V5-tagged CHD associated mis-sense mutations of TBX5 probed for CHD4 and MTA1. (**e, f**) Transcription of the regulatory regions of TBX5 target genes in response to wild type TBX5 or $TBX5^{S261C}$. Additional gene targets shown in Supplemental Fig. 4 and Supplemental Fig. 8. (**g**) Phylogenetic comparison of TBX5 orthologues with boot-strap values. Sequence of core amino acid residues required for the TBX5-NuRD interaction are shown to the right. * $p< 0.05$ *** $p < 0.001$.

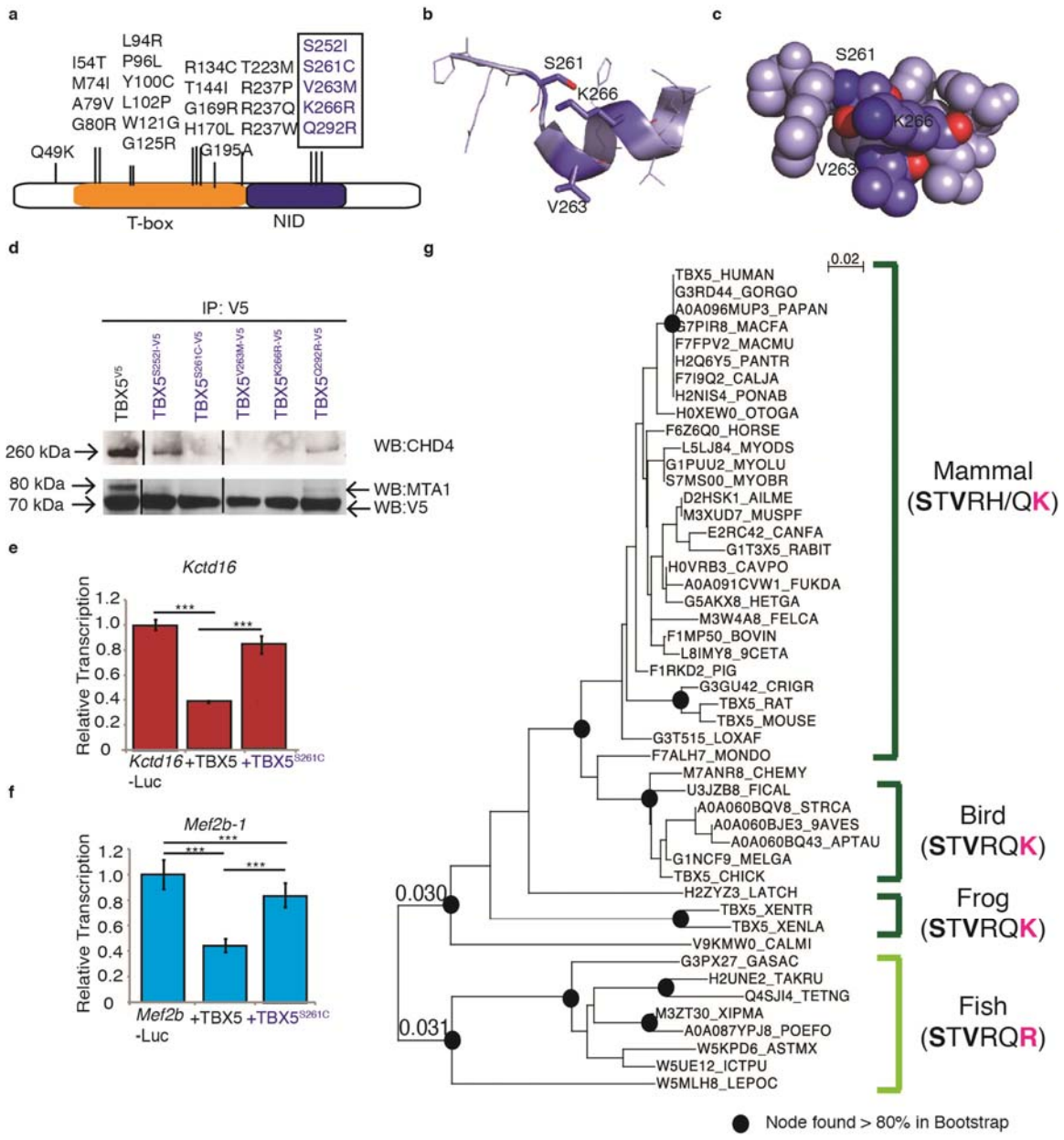
a
I54T
M74I
A79V
G80R
L94R
P96L
Y100C
L102P
W121G
G125R
R134C
T144I
G169R
H170L
T223M
R237P
R237Q
R237W
S252I
S261C
V263M
K266R
Q292R
Q49K
G195A
T-box
NID
b
S261
K266
V263
c
S261
K266
V263
d
IP: V5
TBX5V5
TBX5S252I-V5
TBX5S261C-V5
TBX5V263M-V5
TBX5K266R-V5
TBX5Q292R-V5
260 kDa
WB:CHD4
80 kDa
70 kDa
WB:MTA1
WB:V5
e
Kctd16
Relative Transcription
Kctd16 -Luc
+TBX5
+TBX5S261C
f
Mef2b-1
Relative Transcription
Mef2b -Luc
+TBX5
+TBX5S261C
g
0.02
TBX5_HUMAN
G3RD44_GORGO
A0A096MUP3_PAPAN
G7PIR8_MACFA
F7FPV2_MACMU
H2Q6Y5_PANTR
F7I9Q2_CALJA
H2NIS4_PONAB
H0XEW0_OTOGA
F6Z6Q0_HORSE
L5LJ84_MYODS
G1PUU2_MYOLU
S7MS00_MYOBR
D2HSK1_AILME
M3XUD7_MUSPF
E2RC42_CANFA
G1T3X5_RABIT
H0VRB3_CAVPO
A0A091CVW1_FUKDA
G5AKX8_HETGA
M3W4A8_FELCA
F1MP50_BOVIN
L8IMY8_9CETA
F1RKD2_PIG
G3GU42_CRIGR
TBX5_RAT
TBX5_MOUSE
G3T515_LOXAF
F7ALH7_MONDO
M7ANR8_CHEMY
U3JZB8_FICAL
A0A060BQV8_STRCA
A0A060BJE3_9AVES
A0A060BQ43_APTAU
G1NCF9_MELGA
TBX5_CHICK
H2ZYZ3_LATCH
TBX5_XENTR
TBX5_XENLA
V9KMW0_CALMI
G3PX27_GASAC
H2UNE2_TAKRU
Q4SJI4_TETNG
M3ZT30_XIPMA
A0A087YPJ8_POEFO
W5KPD6_ASTMX
W5UE12_ICTPU
W5MLH8_LEPOC
0.030
0.031
Mammal (STVRH/QK)
Bird (STVRQK)
Frog (STVRQK)
Fish (STVRQR)
Node found > 80% in Bootstrap

Supplemental Figure A3.1. Generation of the *Tbx5*^{Avi} knock-in mouse.

(**a**) (Top) The *Tbx5-Avi* targeting cassette contains the biotin acceptor peptide (Avi) fused in frame to the terminal coding exon of *Tbx5*. Neo-neomycin resistance gene. PGK- phosphoglycerate kinase-1 promoter. Amp-Ampicillan resistance gene. Exons colored brown represent untranslated exons (5' and 3' UTR). Exons colored orange represent T-box DNA binding domain. Exons colored green represent the nuclear localization signal. Exons colored pink represent the activation domain. (Middle) Schematic of the *Tbx5* recombined locus (*Tbx5*$^{Avi\text{-}Neo}$) upon homologous recombination. (Bottom) Schematic of the *Tbx5* locus upon introduction of *Cre* (*Tbx5*^{Avi}). (**b**) Southern blot of positive embryonic stem cell clone confirms homologous recombination. (**c**) Southern blot of F2 mice confirms removal of Neo cassette upon introduction of *Cre*. Samples were run on the same gel but were noncontiguous. (**d**) RT-PCR analysis of *Tbx5*$^{Avi/+}$ adult hearts demonstrates presence of *Tbx5*^{Avi} mRNA.

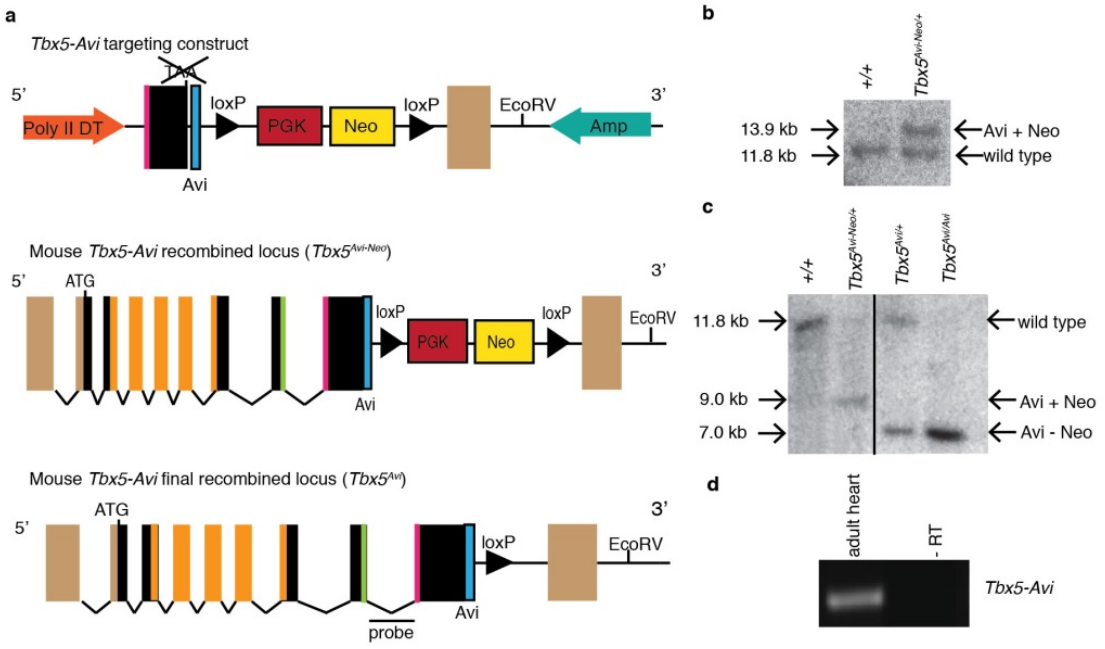

Supplemental Figure A3.2. Transcription interaction network assembled by STRING analysis.

Sixty mouse genes corresponding to TBX5 candidate interactions as identified by the gene ontology function of transcription were uploaded to the STRING database (www.string-db.org). STRING functional relationships were evaluated with default settings with text mining disabled. Forty proteins were clustered in a single network, reflecting a minimum combined STRING score of > 0.4 (medium confidence) between each binary relationship (left). This network was imported to Cytoscape for further processing (see Fig. 1). The remaining 20 nodes with scores < 0.4 are illustrated as disconnected (right).

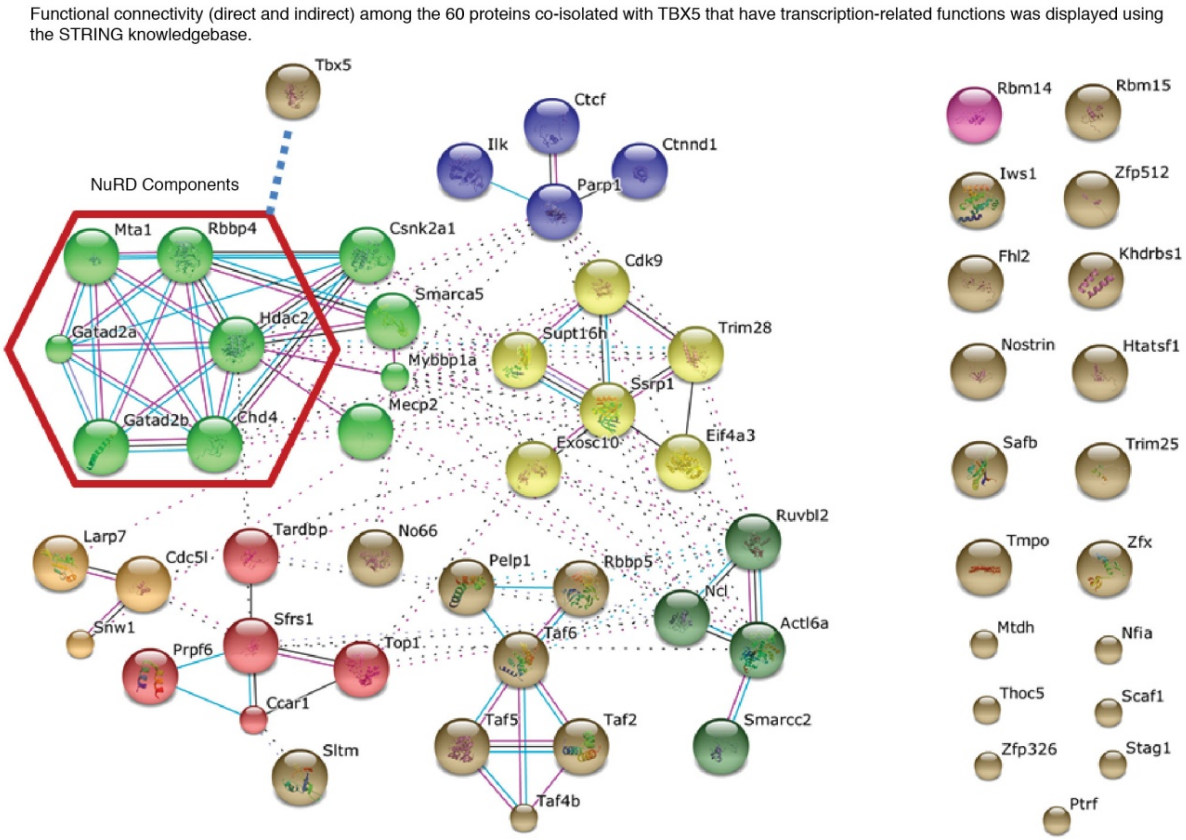

Supplemental Figure A3.3. TBX5 and the NuRD complex genetically interact.

Histology staining (Hematoxylin and Eosin) of (**a**) *Mta1*$^{+/-}$, (**b**) *Tbx5*$^{+/-}$ and, (**c**) *Tbx5*$^{+/-}$; *Mta1*$^{+/-}$ mice at E13.5. (**d**) Quantification of cardiac defects seen in all mice. Both chi-squared and Fisher's exact test show that the cardiac defects seen in *Tbx5*$^{+/-}$; *Mta1*$^{+/-}$ are significant as compared to wild type and *Tbx5*$^{+/-}$.

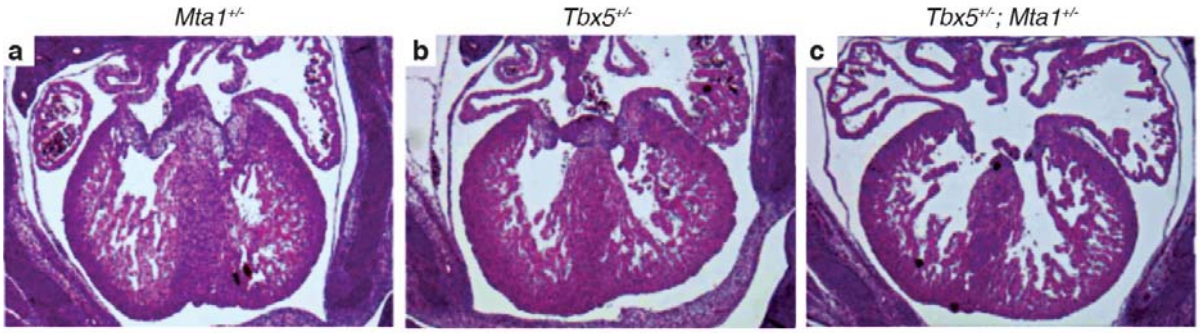

d

	Wild type	*Mta1*$^{+/-}$	*Tbx5*$^{+/-}$	*Tbx5*$^{+/-}$; *Mta1*$^{+/-}$
Intact	10	8	4	0
1° ASD	0	0	1	1
AVSD	0	0	4	12
VSD only	0	0	1	1
Total	10	8	10	14
χ^2 (vs wild type)			0.0034	0.0001
Fisher's exact test (vs wild type)		1	0.0108	0.0001
χ^2 (vs *Tbx5*$^{+/-}$)				0.0095
Fisher's exact test (vs *Tbx5*$^{+/-}$)				0.0198

Supplemental Figure A3.4. Transcriptional targets not repressed by TBX5.

(**a-d)** Gene reporter elements cloned from potential TBX5 targets in the presence or absence of TBX5. *** $p < 0.001$.

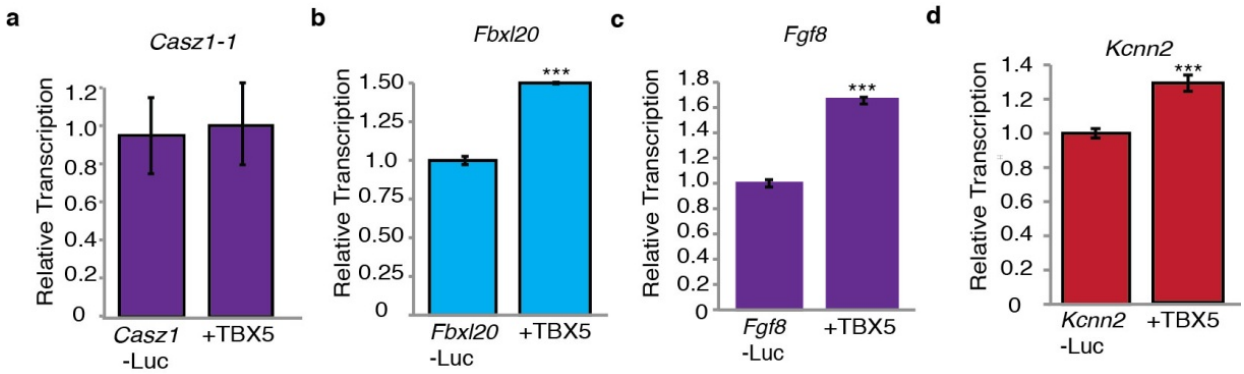

Supplemental Figure A3.5. The TBX5^{NID} is necessary and sufficient for interaction of TBX5 with CHD4.

(**a**) Schematic of CHD4 deletion constructs. Phd= Plant homeo domain. (**b**) Schematic of TBX5 deletion constructs. NLS = Nuclear Localization Signal. AD = Activation domain. (**c**) IP of full-length TBX5$^{Avi\text{-}V5}$ with GFP-tagged CHD4 deletions reveals that CHD4 interacts with TBX5 via sequences in the N-terminus of CHD4. (**d, e**) IP of CHD4 with a TBX5$^{Avi\text{-}V5}$ deletion series demonstrates TBX5 sequences aa 238-340 are both necessary and sufficient for interaction with CHD4. This region has been termed the NuRD interaction domain.

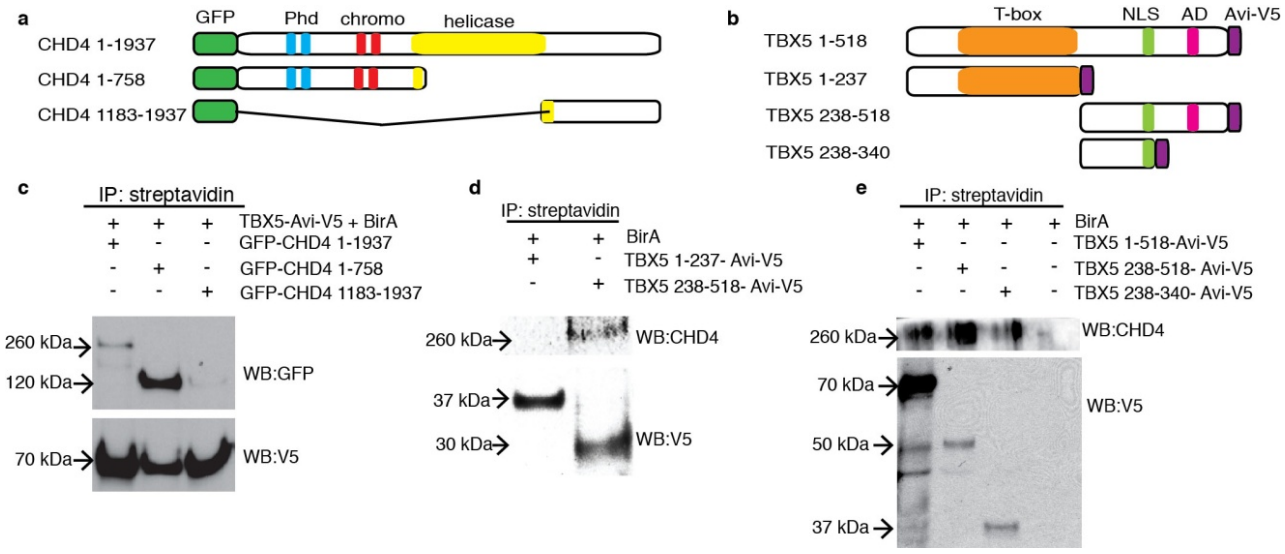

Supplemental Figure A3.6. Sequence alignment of the TBX5^{NID} from 48 TBX5 ortholgues.

Height of letters is relative conservation at that residue.

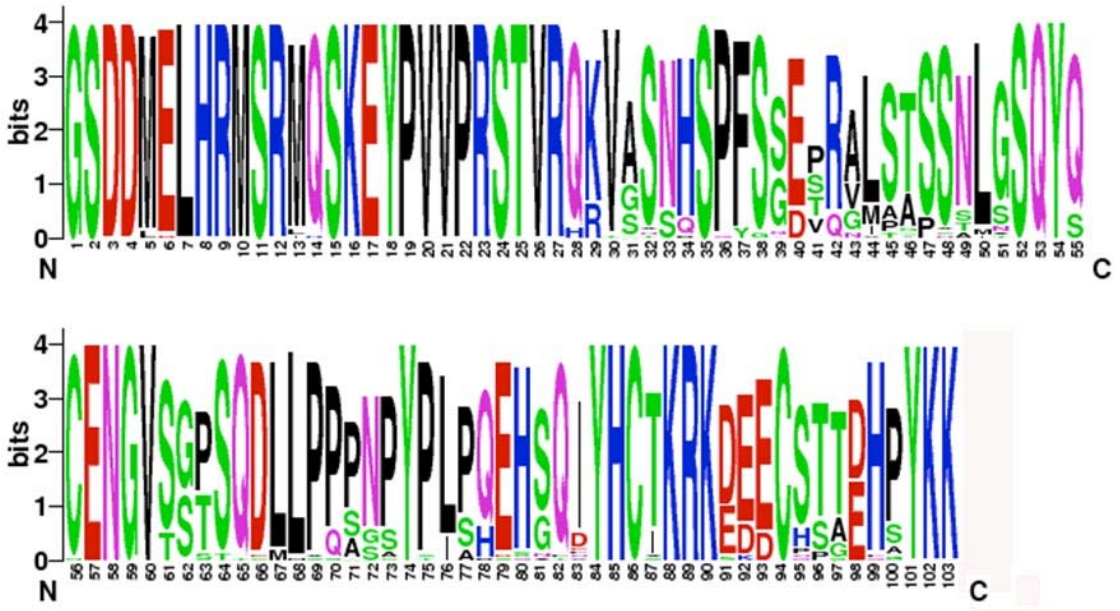

Supplemental Figure A3.7. The TBX5/NuRD complex binds to neural and cancer genes in vivo.

(a) TBX5 candidate reporter elements in the presence or absence of wild type TBX5 or $TBX5^{S261C}$. (**b**) Schematic of ChIP primer locations on *Kctd16* element. (**c**) ChIP of CHD4 from cells co-transfected with *Kctd16-Luciferase* and TBX5. *** $p < 0.001$.

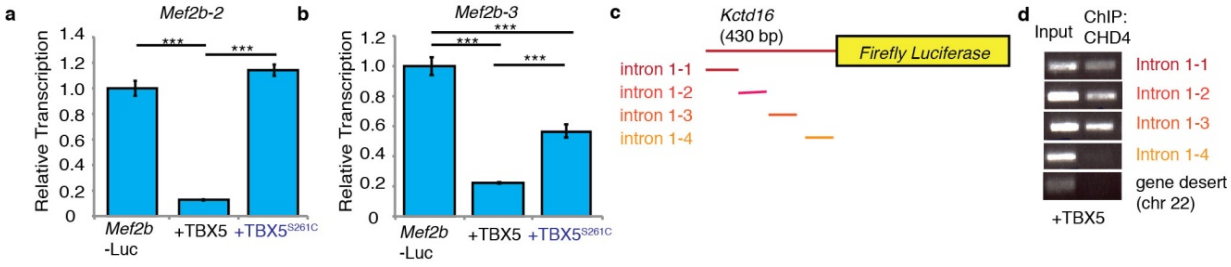

Supplemental Figure A3.8. Targets repressed by TBX5 in a NuRD independent manner.

(**a-i)** TBX5-repressed gene reporter elements and in the co-transfected with wild type TBX5 or $TBX5^{S261C}$. Genes sorted into neural (red), cancer (blue), or both (purple). * p< 0.05 *** p < 0.001.

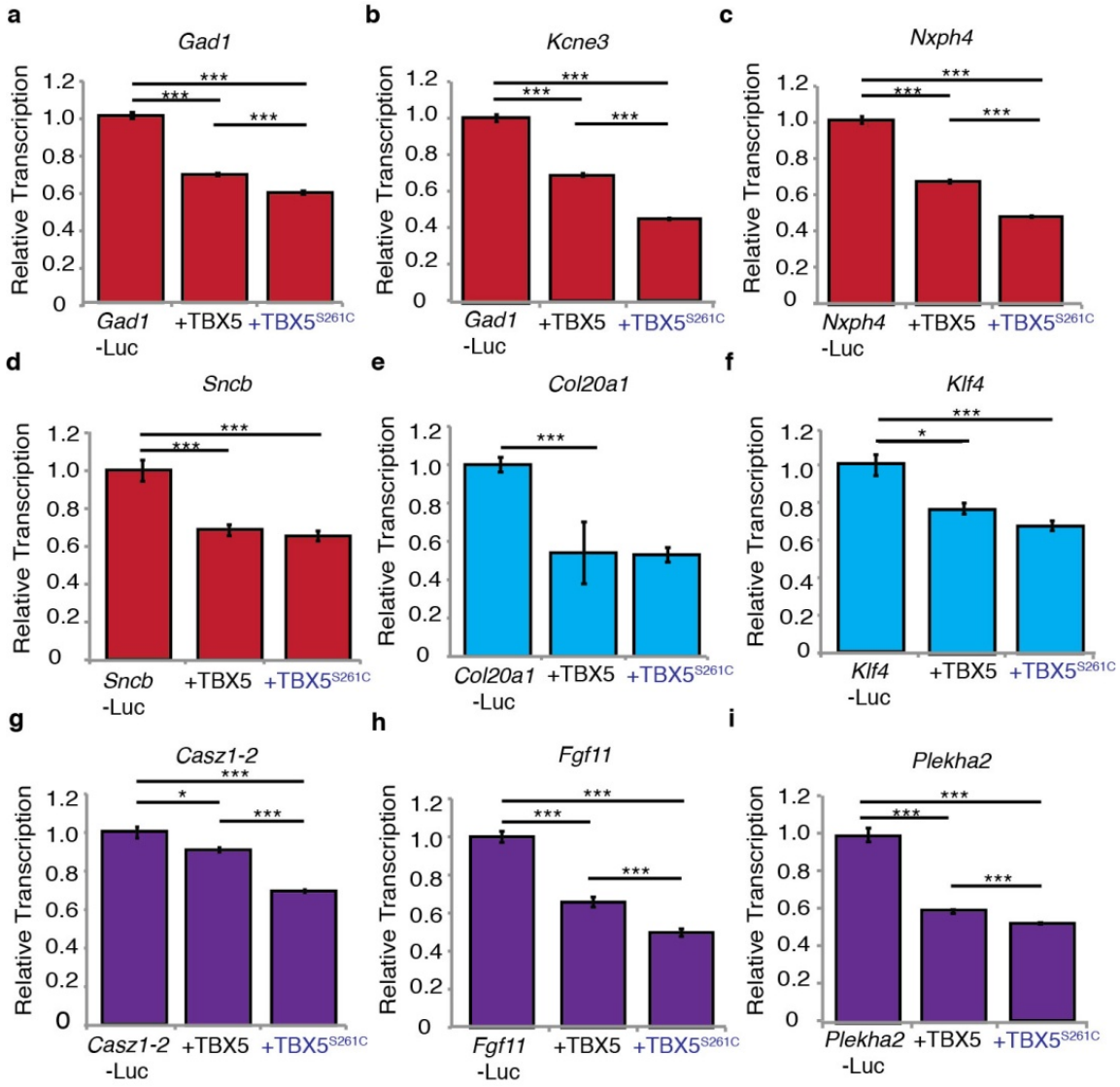

Supplemental Table A3.1. Gene-ontology analysis of candidate interactions from TBX5 complexes

Supplemental Table A3.2. Genes differentially expressed in E9.5 *Tbx5* null hearts by RNA-Seq Analysis

Supplemental Table A3.3. Genes potentially repressed by TBX5

Supplemental Table A3.4. Genotyping primers for *Tbx5*$^{Avi/Avi}$; *Rosa26*$^{BirA/BirA}$ mice.

Genotyping Primers	Sequence
Wild type *Tbx5*	F: CGGCGTGCCCAGGACCCTGT R: GGCACAGGTCAGCCTTTAGC
Tbx5^{Avi}	F: CGGCGTGCCCAGGACCCTGT R: GCGCGCCTTCGTGCCATTCGA
Sox2-Cre	F: GTCCCCTTCTCCATCTCCAG R: GCAAACGGACAGAAGCATTT
Neo	F: AGGATCTCCTGTCATCTCACCTT R: CTAGAGAATTGATCCCCTCAGAAG
Presence of BirA	F: TTACGCAAGCTGGGTGCAGA R: TTACGCAAGCTGGGTGCAGA
Absence of BirA	F: GTGTAACTGTGGACAGAGGAG R: GAACTTGATGTGTAGACCAGG

Supplemental Table A3.5. TBX5 target gene primers for transcriptional assays.

ChIP cloning PCR Primers	Sequence
Casz1-1	F: ATCGGGTACCTGTCCCTTTCTTCTGTCCCA
	R: ATCGGGTACCAGGCATAAGATCGCTGGAAA
Casz1-2	F: ATCGGGTACCACCATCCATCCTCGTGTAGC
	R: ATCGGCTAGCGCCAAAAACAGTGGCCTAAA
Col20a1	F: ATCGGCTAGCATCGAGTGTGTCAGCTGTGG
	R: ATCGAAGCTTCCGTGGTGCTGTGTTCTTAC
Fbxl20	F: GATCACGCGTGGCCCAAGGAATGGGTACT
	R: GATCACGCGTCCACAGTCGCCTCTATCGTC
Fgf8	F: CGAGGCTAGCCCAGCTCCCTCCTTCCTTTA
	R: CGAGGGTACCGGCAGCTTTCTGTCTTGGTT
Fgf11	F: GCACAGATCTGGGACTCCCTAACTGTCGTACC
	R: GCACACGCGTCCGCTGGAGCTAGTCAGG
Gad1	F: CGAGGGTACCCACTGGAATTCCTACCGTGA
	R: CGAGGCTAGCCAAGGCGTTCTGGTCTAAGG
Kcne3	F: CGCTACGCGTGTGCCACACAGCTACAATAA
	R: CGCTCTCGAGTCCGGTGAACACTGCAATAA
Kcnn2	F: GATCGGTACCCTGGTCTCCCTGCAGCTTTA
	R: GATCGCTACGGTTGTCCTGGCTCTGTTGCT
Kctd16	F: AGGACGCGTTGCTTGTGCAAACTCCAGAC
	R: GACCAGATCTAGGCAGGGCGACAGATAGAT
Klf4	F: ATCGACGCGTCTTGGCGTGAGGAACTCTCT
	R: ATCGAGATCTCGCTCAAATGGGCCTCTA
Mef2b-1	F: CGAGGTACCTCTTCTCTCGGACGGACCTA
	R: CGAGGCTAGCCACACACACTCACGGCTCTC
Mef2b-2	F: CGAGGCTAGCCTGCACAGGGACCCACAG
	R: CGAGGCTAGCCTGCACAGGGACCCACAG
Mef2b-3	F: CGAGGGTACCGCGTGCGATCACCATAACT
	R: CGAGGCTAGCAGGGGCTGCGATGTAGGT
Nxph-4	F: CGAGGGTACCGCTTGCAGAAGGGTATCTGG
	R: CGAGGCTAGCTAAGCCTCCAGGCATTCAAC
Plekha2	F: GATCGGTACCTAACTTGGAACCGACCTACG

	R: GATCGCTAGCTTTCACACCTGAGCGAACTG
Sncb	F: CACGGGTACCTCCCTCCACTGCCTCCAC R: CAGCGCTAGCGCTCCAGGGTCCTCCTAGTC

Supplemental Table A3.6. Site directed mutagenesis primer pairs. Amino acid changes are represented in bold.

S252I	F: GATGTCTCGGATGCAA**ATT**AAAGAGTATCCTGTGGTTC R: GAACCACAGGATACTCTTT**AAT**TTGCATCCGAGACATC
S261C	F: GTATCCTGTGGTTCCCAGG**TCG**ACAGTGAGGCACAAAG R: CTTTGTGCCTCACTGT**CGA**CCTGGGAACCACAGGATAC
V263M	F: GGTTCCCAGGAGCACA**ATG**AGGCACAAAGTCACCTCC R: GGAGGTGACTTTGTGCCT**CAT**TGTGCTCCTGGGAACC
K266R	F: GAGCACAGTGAGGCAC**AGA**GTCACCTCCAACCACAGC R: GCTGTGGTTGGAGGTGAC**TCT**GTGCCTCACTGTGCTC
Q292R	F: CAATTTAGGGTCCCAGTAC**CGG**TGTGAGAATGGTGTC R: GACACCATTCTCACA**CCG**GTACTGGGACCCTAAATTG

Supplemental Table A3.7. *Kctd16* intron 1 ChIP-PCR primer sequences.

Kctd16 intron 1-1	F: CAAACTCCAGACCACAGGCT R: GACAGGTTGCCAGCACTGA
Kctd16 intron 1-2	F: TCAGTGCTGGCAACCTGTC R: GAGCAGTGCAGGCAAGAAAC
Kctd16 intron 1-3	F: GTTTCTTGCCTGCACTGCT R: GAAGGAAAAGCAGCCGGGAA
Kctd16 intron 1-4	F: TGCTTTTCCTTCCCACCTGG R: GGCAGGGCGACAGATAGATG

REFERENCES

Baban, A., Pitto, L., Pulignani, S., Cresci, M., Mariani, L., Gambacciani, C., Digilio, M. C., Pongiglione, G. and Albanese, S. (2014). Holt-Oram syndrome with intermediate atrioventricular canal defect, and aortic coarctation: functional characterization of a de novo TBX5 mutation. *American journal of medical genetics. Part A* **164A**, 1419-1424.

Basson, C. T., Cowley, G. S., Solomon, S. D., Weissman, B., Poznanski, A. K., Traill, T. A., Seidman, J. G. and Seidman, C. E. (1994). The clinical and genetic spectrum of the Holt-Oram syndrome (heart-hand syndrome). *The New England journal of medicine* **330**, 885-891.

Basson, C. T., Bachinsky, D. R., Lin, R. C., Levi, T., Elkins, J. A., Soults, J., Grayzel, D., Kroumpouzou, E., Traill, T. A., Leblanc-Straceski, J. et al. (1997). Mutations in human TBX5 [corrected] cause limb and cardiac malformation in Holt-Oram syndrome. *Nature genetics* **15**, 30-35.

Basson, C. T., Huang, T., Lin, R. C., Bachinsky, D. R., Weremowicz, S., Vaglio, A., Bruzzone, R., Quadrelli, R., Lerone, M., Romeo, G. et al. (1999). Different TBX5 interactions in heart and limb defined by Holt-Oram syndrome mutations. *Proceedings of the National Academy of Sciences of the United States of America* **96**, 2919-2924.

Berk, A. J. (1999). Activation of RNA polymerase II transcription. *Current opinion in cell biology* **11**, 330-335.

Bruneau, B. G., Logan, M., Davis, N., Levi, T., Tabin, C. J., Seidman, J. G. and Seidman, C. E. (1999). Chamber-specific cardiac expression of Tbx5 and heart defects in Holt-Oram syndrome. *Developmental biology* **211**, 100-108.

Bruneau, B. G., Nemer, G., Schmitt, J. P., Charron, F., Robitaille, L., Caron, S., Conner, D. A., Gessler, M., Nemer, M., Seidman, C. E. et al. (2001). A murine model of Holt-Oram syndrome defines roles of the T-box transcription factor Tbx5 in cardiogenesis and disease. *Cell* **106**, 709-721.

Cline, M. S., Smoot, M., Cerami, E., Kuchinsky, A., Landys, N., Workman, C., Christmas, R., Avila-Campilo, I., Creech, M., Gross, B. et al. (2007). Integration of biological networks and gene expression data using Cytoscape. *Nature protocols* **2**, 2366-2382.

Cristea, I. M., Williams, R., Chait, B. T. and Rout, M. P. (2005). Fluorescent proteins as proteomic probes. *Molecular & cellular proteomics : MCP* **4**, 1933-1941.

Dolk, H., Loane, M. and Garne, E. (2010). The prevalence of congenital anomalies in Europe. *Advances in experimental medicine and biology* **686**, 349-364.

Driegen, S., Ferreira, R., van Zon, A., Strouboulis, J., Jaegle, M., Grosveld, F., Philipsen, S. and Meijer, D. (2005). A generic tool for biotinylation of tagged proteins in transgenic mice. *Transgenic research* **14**, 477-482.

Fan, C., Liu, M. and Wang, Q. (2003a). Functional analysis of TBX5 missense mutations associated with Holt-Oram syndrome. *The Journal of biological chemistry* **278**, 8780-8785.

Fan, C., Duhagon, M. A., Oberti, C., Chen, S., Hiroi, Y., Komuro, I., Duhagon, P. I., Canessa, R. and Wang, Q. (2003b). Novel TBX5 mutations and molecular mechanism for Holt-Oram syndrome. *Journal of medical genetics* **40**, e29.

Franceschini, A., Szklarczyk, D., Frankild, S., Kuhn, M., Simonovic, M., Roth, A., Lin, J., Minguez, P., Bork, P., von Mering, C. et al. (2013). STRING v9.1: protein-protein interaction networks, with increased coverage and integration. *Nucleic acids research* **41**, D808-815.

Franklin, S., Zhang, M. J., Chen, H., Paulsson, A. K., Mitchell-Jordan, S. A., Li, Y., Ping, P. and Vondriska, T. M. (2011). Specialized compartments of cardiac nuclei exhibit distinct proteomic anatomy. *Molecular & cellular proteomics : MCP* **10**, M110 000703.

Hayashi, S., Lewis, P., Pevny, L. and McMahon, A. P. (2002). Efficient gene modulation in mouse epiblast using a Sox2Cre transgenic mouse strain. *Mechanisms of development* **119 Suppl 1**, S97-S101.

He, A., Kong, S. W., Ma, Q. and Pu, W. T. (2011). Co-occupancy by multiple cardiac transcription factors identifies transcriptional enhancers active in heart. *Proceedings of the National Academy of Sciences of the United States of America* **108**, 5632-5637.

Heinritz, W., Shou, L., Moschik, A. and Froster, U. G. (2005). The human TBX5 gene mutation database. *Human mutation* **26**, 397.

Heron, M., Hoyert, D. L., Murphy, S. L., Xu, J., Kochanek, K. D. and Tejada-Vera, B. (2009). Deaths: final data for 2006. *National vital statistics reports : from the Centers for Disease Control and Prevention, National Center for Health Statistics, National Vital Statistics System* **57**, 1-134.

Hoffmann, A. D., Yang, X. H., Burnicka-Turek, O., Bosman, J. D., Ren, X., Steimle, J. D., Vokes, S. A., McMahon, A. P., Kalinichenko, V. V. and Moskowitz, I. P. (2014). Foxf genes integrate tbx5 and hedgehog pathways in the second heart field for cardiac septation. *PLoS genetics* **10**, e1004604.

Hu, S., Li, L., Yeh, S., Cui, Y., Li, X., Chang, H. C., Jin, J. and Chang, C. (2015). Infiltrating T cells promote prostate cancer metastasis via modulation of FGF11-->miRNA-541-->androgen receptor (AR)-->MMP9 signaling. *Molecular oncology* **9**, 44-57.

Huang, C. C., Tu, S. H., Lien, H. H., Jeng, J. Y., Huang, C. S., Huang, C. J., Lai, L. C. and Chuang, E. Y. (2013). Concurrent gene signatures for han chinese breast cancers. *PloS one* **8**, e76421.

Kaltenbrun, E., Greco, T. M., Slagle, C. E., Kennedy, L. M., Li, T., Cristea, I. M. and Conlon, F. L. (2013). A Gro/TLE-NuRD corepressor complex facilitates Tbx20-dependent transcriptional repression. *Journal of proteome research* **12**, 5395-5409.

Kehle, J., Beuchle, D., Treuheit, S., Christen, B., Kennison, J. A., Bienz, M. and Muller, J. (1998). dMi-2, a hunchback-interacting protein that functions in polycomb repression. *Science* **282**, 1897-1900.

Keller, A., Nesvizhskii, A. I., Kolker, E. and Aebersold, R. (2002). Empirical statistical model to estimate the accuracy of peptide identifications made by MS/MS and database search. *Analytical chemistry* **74**, 5383-5392.

Kim, J., Cantor, A. B., Orkin, S. H. and Wang, J. (2009). Use of in vivo biotinylation to study protein-protein and protein-DNA interactions in mouse embryonic stem cells. *Nature protocols* **4**, 506-517.

Kimura, R., Kasamatsu, A., Koyama, T., Fukumoto, C., Kouzu, Y., Higo, M., Endo-Sakamoto, Y., Ogawara, K., Shiiba, M., Tanzawa, H. et al. (2013). Glutamate acid decarboxylase 1 promotes metastasis of human oral cancer by beta-catenin translocation and MMP7 activation. *BMC cancer* **13**, 555.

Krebs, S., Fischaleck, M. and Blum, H. (2009). A simple and loss-free method to remove TRIzol contaminations from minute RNA samples. *Analytical biochemistry* **387**, 136-138.

Lavine, K. J., Yu, K., White, A. C., Zhang, X., Smith, C., Partanen, J. and Ornitz, D. M. (2005). Endocardial and epicardial derived FGF signals regulate myocardial proliferation and differentiation in vivo. *Developmental cell* **8**, 85-95.

Li, Q. Y., Newbury-Ecob, R. A., Terrett, J. A., Wilson, D. I., Curtis, A. R., Yi, C. H., Gebuhr, T., Bullen, P. J., Robson, S. C., Strachan, T. et al. (1997). Holt-Oram syndrome is caused by mutations in TBX5, a member of the Brachyury (T) gene family. *Nature genetics* **15**, 21-29.

Liu, Z., Yang, X., Li, Z., McMahon, C., Sizer, C., Barenboim-Stapleton, L., Bliskovsky, V., Mock, B., Ried, T., London, W. B. et al. (2011). CASZ1, a candidate tumor-suppressor gene, suppresses neuroblastoma tumor growth through reprogramming gene expression. *Cell death and differentiation* **18**, 1174-1183.

Mori, A. D. and Bruneau, B. G. (2004). TBX5 mutations and congenital heart disease: Holt-Oram syndrome revealed. *Current opinion in cardiology* **19**, 211-215.

Moskowitz, I. P., Pizard, A., Patel, V. V., Bruneau, B. G., Kim, J. B., Kupershmidt, S., Roden, D., Berul, C. I., Seidman, C. E. and Seidman, J. G. (2004). The T-Box transcription factor Tbx5 is required for the patterning and maturation of the murine cardiac conduction system. *Development* **131**, 4107-4116.

Moskowitz, I. P., Kim, J. B., Moore, M. L., Wolf, C. M., Peterson, M. A., Shendure, J., Nobrega, M. A., Yokota, Y., Berul, C., Izumo, S. et al. (2007). A molecular pathway including Id2, Tbx5, and Nkx2-5 required for cardiac conduction system development. *Cell* **129**, 1365-1376.

Polo, S. E., Kaidi, A., Baskcomb, L., Galanty, Y. and Jackson, S. P. (2010). Regulation of DNA-damage responses and cell-cycle progression by the chromatin remodelling factor CHD4. *The EMBO journal* **29**, 3130-3139.

Qian, L., Huang, Y., Spencer, C. I., Foley, A., Vedantham, V., Liu, L., Conway, S. J., Fu, J. D. and Srivastava, D. (2012). In vivo reprogramming of murine cardiac fibroblasts into induced cardiomyocytes. *Nature* **485**, 593-598.

Roesli, C., Neri, D. and Rybak, J. N. (2006). In vivo protein biotinylation and sample preparation for the proteomic identification of organ- and disease-specific antigens accessible from the vasculature. *Nature protocols* **1**, 192-199.

Saunders, A., Werner, J., Andrulis, E. D., Nakayama, T., Hirose, S., Reinberg, D. and Lis, J. T. (2003). Tracking FACT and the RNA polymerase II elongation complex through chromatin in vivo. *Science* **301**, 1094-1096.

Wade, P. A., Jones, P. L., Vermaak, D. and Wolffe, A. P. (1998). A multiple subunit Mi-2 histone deacetylase from Xenopus laevis cofractionates with an associated Snf2 superfamily ATPase. *Current biology : CB* **8**, 843-846.

Wang, J., Rao, S., Chu, J., Shen, X., Levasseur, D. N., Theunissen, T. W. and Orkin, S. H. (2006). A protein interaction network for pluripotency of embryonic stem cells. *Nature* **444**, 364-368.

Xue, Y., Wong, J., Moreno, G. T., Young, M. K., Cote, J. and Wang, W. (1998). NURD, a novel complex with both ATP-dependent chromatin-remodeling and histone deacetylase activities. *Molecular cell* **2**, 851-861.

Ying, C. Y., Dominguez-Sola, D., Fabi, M., Lorenz, I. C., Hussein, S., Bansal, M., Califano, A., Pasqualucci, L., Basso, K. and Dalla-Favera, R. (2013). MEF2B mutations lead to deregulated expression of the oncogene BCL6 in diffuse large B cell lymphoma. *Nature immunology* **14**, 1084-1092.